Above-water radiance and remote sensing reflectance measurement and analysis protocols

10 authors, including:

Robert Arnone
University of Southern Mississippi
279 PUBLICATIONS **8,386** CITATIONS

SEE PROFILE

Robert J Frouin
University of California, San Diego
331 PUBLICATIONS **12,364** CITATIONS

SEE PROFILE

Kendall Carder
SRI International
189 PUBLICATIONS **19,369** CITATIONS

SEE PROFILE

Curtis Mobley
Sequoia Scientific, Inc.
141 PUBLICATIONS **10,719** CITATIONS

SEE PROFILE

Some of the authors of this publication are also working on these related projects:

Project Maritime Advanced Geospatial Intelligence Craft View project

Project Inverse methods for estimating inherent optical properties from radiometric measurements View project

NASA/TM-2000-209966

Ocean Optics Protocols For Satellite Ocean Color Sensor Validation, Revision 2

Giulietta S. Fargion
SAIC General Sciences Corporation, Beltsville, Maryland

James L. Mueller
Center for Hydro-Optics and Remote Sensing
San Diego, State University, San Diego, California

Preface

The document stipulates protocols for measuring bio-optical and radiometric data for the Sensor Intercomparison and Merger for Biological and Interdisciplinary Oceanic Studies (SIMBIOS) Project activities and algorithm development. This document supersedes the earlier version (Mueller and Austin 1995) published as Volume 25 in the *SeaWiFS Technical Report Series.* This document is organized into four parts:

- *Part I* - Address perspectives on ocean color research and validation, and requirements for *in situ* observations (Chapter 1 and Chapter 2).
- *Part II* - Address the characteristics and performance specifications of the instruments used for *in situ* observation, and provide protocols for their calibration and characterization (Chapters 3 through 10).
- *Part II* - Provide detailed protocols describing methods for making each type of field measurement and associated data analysis (Chapters 11 through 14).
- *Part IV* - Address the methods and procedures for data archival, data synthesis and merging, and quality control (Chapter 15).

This document marks a significant departure from, and improvement on, the format and content of Mueller and Austin (1995). The authorship of the protocols has been greatly broadened to include experts specializing in some key areas. New chapters have been added to provide detailed and comprehensive protocols for stability monitoring of radiometers using portable sources (Chapter 7 by Hooker), above-water measurements of remote-sensing reflectance (Chapter 10 by Mueller et al.), spectral absorption measurements for discrete water samples (Chapter 12 by Mitchell et al.), HPLC pigment analysis (Chapter 13 by Bidigare and Trees) and fluorometric pigment analysis (Chapter 14 by Trees et al.). Protocols were included in Mueller and Austin (1995) for each of these areas, but the new treatment makes significant advances in each topic area. There are also new chapters prescribing protocols for calibration of sun photometers and sky radiance sensors (Chapter 6 by Pietras *et al*.), sun photometer and sky radiance measurements and analysis (Chapter 11 by Frouin et al.), and data archival (Chapter 15 by Werdell et al.). These topic areas were barely mentioned in Mueller and Austin (1995).

The present status of the protocols is less encouraging with respect to radiometric measurements from moored and drifting buoys, methods of inherent optical properties measurement and calibration, and airborne measurements. There have been rapid and significant advances in each of these areas over the past five years. Unfortunately, other commitments of key scientists specializing in these areas made it impractical to carry out the discussions needed to establish a consensus on draft protocols within the short time allowed for preparation and publication of this document. The status of methods in these topic areas are briefly reviewed in Chapters 3 and 10, together with protocols for computing Normalized Water-Leaving Radiance (including BRDF effects) and for measuring ancillary variables. Developing new chapters describing comprehensive, up-to-date protocols in each of these areas is a high priority for future revisions to this document.

This technical report is not meant as a substitute for scientific literature. Instead, it will provide a ready and responsive vehicle for the multitude of technical reports issued by an operational Project. The contributions are published as submitted, with the exception of minor edits to correct obvious grammatical or clerical

Table of Contents and Author List

Chapter 1

Ocean Color Radiometry and Bio-Optics

James L. Mueller[1], Roswell W. Austin[1], Giulietta S. Fargion[2] and Charles R. McClain[3]

[1]*Center for Hydro-Optics and Remote Sensing, San Diego State University, California*
[2]*SAIC General Sciences Corporation, Beltsville, Maryland*
[3]*NASA, Goddard Space Flight Center, Greenbelt, Maryland*

1.1 INTRODUCTION

The *Ocean Optics Protocols for Satellite Ocean Color Sensor Validation (Version 2.0)* are intended to provide standards, which if followed carefully and documented appropriately, will assure that any particular set of optical measurements will be acceptable for ocean color sensor validation and algorithm development. These protocols are guidelines and may be somewhat conservative. In the case of ship shadow avoidance, for example, there are some circumstances in which acceptable radiometric profiles may be acquired considerably closer to a ship than is specified here (Section 10.1). When the protocols are not followed in such cases, however, it is incumbent upon the investigator to explicitly demonstrate that the actual error levels are within tolerance. Close adherence to these protocols is the most straightforward way for an investigator to establish a measurement that is uncontaminated by artifacts, such as ship shadow, and is accurate enough to meet the requirements of satellite ocean color product validation.

Finally, having a standard set of measurement protocols is indispensible in developing consistency across the variety of international satellite ocean color missions either recently launched or scheduled for launch in the next few years. While each mission has its own validation effort, the mission validation teams should not need to define separate validation measurement requirements. In the U.S., for instance, ocean color validation support is derived from four separate funding programs, i.e., the Sea-viewing Wide Field-of-view Sensor (SeaWiFS) Project, Moderate Resolution Imaging Spectroradiometer (MODIS) validation program, the Earth Observing System (EOS) calibration and validation program, and the Sensor Intercomparison for Marine Biology and Interdisciplinary Oceanic Studies (SIMBIOS) Project (McClain and Fargion, 1999 a and b).

Continued development and refinement of these protocols help ensure coordination, collaboration, and communication between those involved.

1.2 OBJECTIVES

Immediate concerns focused previous versions of the Ocean Optics Protocols (Mueller and Austin 1992, 1995) on specific preparations for the SeaWiFS mission. In the interim, not only SeaWiFS, but the Japanese Ocean Color Temperature Sensor (OCTS), the Polarization Detection Environmental Radiometer (POLDER), and the MODIS global coverage ocean color systems have been successfully launched and brought into operation, and the near-term launch of several other such systems is anticipated (Appendix A). The SIMBIOS Program goal is to assist the international ocean color community in developing a multi-year time-series of calibrated radiances that transcends the spatial and temporal boundaries of individual missions. Specific objectives are to: (1) quantify the relative accuracies of the products from each mission, (2) work with each project to improve the level of confidence and compatibility among the products, and (3) develop methodologies for generating merged level-3 products. SIMBIOS has identified the primary instruments to be used for developing global data sets. These instruments are SeaWiFS, OCTS, POLDER [Advanced Earth Observing Satellite (ADEOS)-I and II], MODIS (Terra and Aqua), Multi-angle Imaging SpectroRadiometer MISR, Medium Resolution Imaging Spectrometer (MERIS), and Global Line Imager (GLI). The products from other missions [e.g., Ocean Color Imager (OCI), Ocean Scanning Multisprectral Imager (OSMI), and Modular Optoelectronic Scanner (MOS)] will be tracked and evaluated, but are not considered as key data sources for a combined global data set.

The scope of the present version of the protocols is, therefore, broadened to support development of bio-optical databases that meet the exapanded requirements of the SIMBIOS goals and objectives. The key objective addressed by the original working group was to recommend protocols and standards for supporting *in situ* optical measurements. The original objectives remain valid today, albeit with broader requirements for detailed measurements and sensor characteristics (e.g. wavelength characteristics). The generalized protocol objectives address the following subject areas:

1. The required and useful optical parameters to be used for validation of satellite ocean color sensor normalized water-leaving radiances and atmospheric correction algorithms, and for monitoring each satellite sensor's calibration and stability, will be defined.

2. The instrumentation requirements, and standards for measuring the parameters in item 1, including definitions of measured quantities, wavelengths, field-of-view (FOV) and band specifications, sensitivity, uncertainty and stability, will be delineated.

3. The optical instrument characterization, intercalibration standards, and related protocols will be defined. This objective includes the following subjects:
   a) laboratory calibration and characterization measurements, uncertainties, and procedures to be applied to instruments used in satellite ocean color sensor validation and algorithm development activities;
   b) pre- and post-deployment measurements and procedures to be followed with moored instrumentation; and
   c) methods for instrument calibration and characterization, and the requirements for record keeping and traceability, including intercalibrations of radiometric and optical standards between participating laboratories.

4. The at-sea optical sampling strategy and protocols will be standardized. This objective includes such considerations as:
   a) the rationale and justifications for moored, underway, drifting, shipboard, and airborne measurements;
   b) ship shadow avoidance, depth resolution in optical profiles, and total sampling depths; and
   c) time of day, sky conditions, season, and geographic considerations.

5. The analysis approaches to be used shall be refined. This objective includes procedures and methodologies recommended for generating variables from *in situ* observations, e.g., L_{WN} (z) from Lu (z), K(z), remote sensing reflectance, etc., as well as error analysis.

6. Protocols for ancillary measurements, data archiving, database population, and access to data will be standardized.

7. The required atmospheric measurements will be defined, and the degree to which standard methodologies are available will be evaluated.

Specific methods for development and validation of bio-optical algorithms for ocean color sensors are only briefly examined in this report. Nonetheless, the scope of the optics protocols includes data requirements and sampling strategies for bio-optical and radiometric measurements supporting these activities. This topic includes the following subjects:

1. Discrete chlorophyll *a* and pigment concentrations will be measured using for high performance liquid chromatography (HPLC) pigment sampling and analysis, protocols and standards for which closely follow those adopted by the Joint Global Ocean Flux Study (JGOFS) (UNESCO 1994).

2. An assessment will be made of the roles of underway, moored, and discrete fluorescence measurements, how such measurements are calibrated, and their usefulness for satellite data product validation. Protocols are included for fluorometric measurement of chlorophyll a concentration, again closely following the counterpart JGOFS protocols (UNESCO 1994).

3. The need for biogeochemical measurements of colored dissolved organic material (CDOM), coccoliths, suspended sediment, detritus, etc., will be examined on the basis of baseline product requirements. Protocols are included here for *in situ* and laboratory measurements of spectral absorption by CDOM, and by suspended particles. The other aspects of this topic are addressed in more general terms.

1.3 SENSOR CALIBRATION

The individual satellite sensor project offices, as well as the SIMBIOS Project, must make every

effort to track the sensor's performance throughout the duration of the mission. Since SeaWiFS, for example, is designed for a five-year mission, it was certain from the outset that the sensor calibration at each wavelength would change in some unpredictable manner as a function of time. Experience with Coastal Zone Color Scanner (CZCS) has shown it is very difficult to determine a sensor's calibration once it has been launched (Viollier 1982, Gordon et al. 1983, Hovis et al. 1985, Mueller 1985, Gordon 1987, and Evans and Gordon 1994). Similar problems have been encountered with other earth observing systems, such as the National Oceanic and Atmospheric Administration (NOAA) Advanced Very High Resolution Radiometer (AVHRR) (Brown and Evans 1985 and Weinreb et al. 1990). Because of the large atmospheric contribution to the total observed radiances (Gordon 1981) and the great sensitivity of the bio-optical algorithms to the estimated water-leaving radiances (Clark 1981), small errors in the calibration can induce sizable errors in derived geophysical products, rendering them useless for many applications.

By processing large quantities of so-called ``clear water'' imagery, i.e., water with pigment concentrations less than 0.25 mg m^3 (Gordon and Clark 1981), Evans and Gordon (1994) were able to develop a *vicarious* calibration that was used in the global processing of the entire CZCS data set (Esaias et al. 1986, Feldman et al. 1989 and McClain et al. 1993). The approach, however, requires assumptions that may limit the scientific utility of ocean color imagery. Specifically, the normalized clear water-leaving radiances, L_{WN} (443), L_{WN} (520), and L_{WN} (550), were assumed to be 1.40, 0.48, and 0.30 mW cm^{-2} m^{-1} sr^{-1}, respectively. The Angstrom exponents were assumed to be zero and certain geographical regions such as the Sargasso Sea were assumed to be clear water sites at all times. Under these assumptions, the clear-water (L_{WN}) values were used to calculate calibration adjustment coefficients to bring CZCS derived (L_{WN}) values into agreement for these regions. The vicarious calibration of the 443 nm band is tenuous, because of the great variability in L_{WN}(443) even in clear water. Additionally, certain command and engineering data from the NIMBUS-7 platform were not archived, so that a detailed analysis of possible effects related to the spacecraft environment and the effects of spacecraft operation on the calibration could not be performed.

Unlike CZCS, SeaWiFS and other modern ocean color sensors routinely produce geophysical fields in a near-real time, operational mode for distribution to the science community. This aspect, as well as merger of multi-satellite data sets spanning many years, necessitates constant evaluation of system performance and derived products for all of the sensors. Therefore, a consistent multifaceted approach to address problems of sensitivity degradation and sensor characterization is required on a continuing basis. The goal is to ensure that satellite derived water-leaving radiances are accurately known and meet the specifications of the individual missions and SIMBIOS.

As implemented by the SeaWiFS Project Office (SPO), for example, the validation program includes both onboard and vicarious calibration approaches (McClain et al. 1998, Barnes et al. 1999a and McClain et al. 2000a and 2000b). SeaWiFS has a solar measuring diffuser plate to reference the response to the sun and is also capable of periodically imaging the moon by maneuvering the spacecraft (Barnes et al. 1999b). MODIS and some other ocean color sensors have similar capabilities. The vicarious calibration program incorporates measurements of water-leaving radiances, and other related quantities, from ships, drifting buoys, and fixed moorings, to develop time series and geographically diverse samples of oceanic and atmospheric data. Each approach has advantages and disadvantages, but when combined, they should provide a complementary and comprehensive data set that will be sufficient to monitor short-term changes and long-term trends in the sensor's performance.

Presently, the SIMBIOS Project uses a combination of satellite and in situ observations from geographically diverse vicarious calibration test sites as a means of comparing ocean color satellite instruments. Using this vicarious calibration approach, results retrieved from different sensors can be meaningfully compared and possibly merged. More importantly, one can use the same procedure, with in situ ocean and atmospheric optical property measurements, to recalibrate satellite sensors (Fargion et al., 1999).

The SIMBIOS calibration strategy is to focus on regions and circumstances where the optical properties of the marine atmosphere and ocean are well understood and homogeneous, i.e., where the errors in the atmospheric correction and the in situ optical measurements are expected to be minimal. The Marine Optical Buoy (MOBY) (Clark et al. 1997), near the island of Lanai, Hawaii, provides the principal instrumented test site for vicarious calibration measurements. The MOBY project officially supports the validation of ocean color data that is collected by SeaWiFS and MODIS. In

addition, MOBY has been successfully used for OCTS and POLDER and indirectly for MOS (Wang and Franz, 1999) vicarious calibrations.

1.4 BIO-OPTICAL ALGORITHMS

The SPO, and each of the counterpart ocean color sensor projects, is responsible for producing a standard set of derived products. The oceanic products include chlorophyll concentration, K(490), and five normalized water-leaving radiances.

The basic quantities to be computed from the sensor radiances are the water-leaving radiances, from which all other derived products *except* the aerosol products are computed. Every effort must be made to ensure these radiances meet the specifications, ± 5% in Case-1 waters. This requires the atmospheric correction algorithms to be considerably more sophisticated than were the original CZCS algorithms.

The baseline bio-optical products must meet the SeaWiFS, MODIS, other sensors, and SIMBIOS Project accuracy requirements over a variety of water masses. The CZCS algorithms were based on a data set consisting of fewer than 50 data points (only 14 observations were available for the band-2-to-band-3 ratio algorithm) and performed poorly in regions of high concentrations of phytoplankton pigments, suspended sediment, or CDOM, and in coccolithophorid blooms (Groom and Holligan 1987). Accurate estimates of the baseline products are essential if SeaWiFS is to be useful in programs such as JGOFS [National Academy of Science (NAS) 1984] and climate change research.

SeaWiFS, and the other modern ocean color sensors, have the capability, due to improvements in the signal-to-noise ratio (SNR), digitization, dynamic range, and wavelength selection, to increase the accuracy of these products and to flag areas where anomalies or low confidence conditions exist. Clearly, a much larger database is needed for developing and validating a broader variety of bio-optical algorithms, some of which will be region specific. The radiometric, optical, and chemical field observations used in deriving bio-optical algorithms and for vicarious calibration of the sensor must, therefore, conform to stringent, uniform requirements with respect to instrument calibration and characterization, and methods of observation.

The SeaWiFS and SIMBIOS Projects manage a program to compare the various atmospheric correction and bio-optical algorithms proposed by the science community (Wang and Bailey 2000, McClain et al. 2000a and b, O'Reilly et al., 2000). The purpose of this program is to independently evaluate suggested improvements, or additions, to the SeaWiFS and merged products. This component of the calibration and algorithm development program runs in parallel with, but off-line from, operational processing and provides an essential mechanism for incorporating data and analyses from the community at large.

1.5 VICARIOUS CALIBRATION

For ocean observations, it is easy to show (Gordon 1987 and Gordon 1988) that satellite sensor calibration requirements based on the quality of the existing CZCS pigment algorithms exceed currently available capabilities. Furthermore, the sensor calibration is unlikely to remain unchanged through launch and five years of operation in orbit. The only foreseeable way of approaching the ocean calibration needs is through vicarious calibration, i.e., fine tuning the calibration in orbit.

The methodology used to achieve vicarious calibration for CZCS was described in detail by Gordon (1987). First, the calibration was initialized after launch by forcing agreement between the sensor-determined radiance and the expected radiance based on radiometric measurements made at the surface under clear atmospheric conditions. Next, since the CZCS responsivity was observed to be time dependent, the algorithms were applied to other scenes characterized by bio-optical surface measurements and more typical atmospheres, and the calibration was adjusted until the measured water-leaving radiances were reproduced. Finally, the surface measurements of pigments were combined with satellite pigment estimates for a wide variety of atmospheric conditions, and the radiance calibration was fine tuned until the best agreement was obtained between the retrieved and true pigments.

The CZCS vicarious calibration was not radiometric. It was a calibration of the entire system-sensor plus algorithms. To predict the radiance measured at the satellite, I_t, the water-leaving radiance, the aerosol optical thickness, and the aerosol phase function are all required. Also needed are ancillary data such as the surface pressure, wind speed, and ozone optical thickness. These data for vicarious calibration and validation will be obtained by measuring the upwelling radiance distribution just beneath the surface, along with the aerosol optical thickness and the sky radiance, at the time of the satellite overpass (Clark

et al. 1997). The sky radiance will be used to deduce the required information about the aerosol phase function (Voss and Zibordi 1989). The data set will be used to deduce L_t, at the top of the atmosphere, coincident with a SeaWiFS overpass from which the calibration will be initialized.

The present approach used by the SIMBIOS and SeaWiFS Projects is to develop a Level-1b to Level-2 software package (MSl12) which is capable of processing data from multiple ocean color sensors using the standard SeaWiFS atmospheric correction algorithms of Gordon and Wang (1994a, b). The integration of a new sensor into MSl12 involves the development of a set of input functions and derivation of band-pass specific quantities such as Rayleigh scattering tables and Rayleigh-aerosol transmittance tables. Once the processing capability has been established, the vicarious calibration can be tuned using match-up data from the MOBY site, and/or cross calibration with another sensor. For example, Wang and Franz (1999) used SeaWiFS normalized remote sensing reflectances and aerosol models to successfully re-calibrate the MOS spectral channels.

Using this approach, the SIMBIOS Project can provide a completely independent assessment of instrument calibration and sensor-to-sensor relative calibration. The Project also provides insight to the sensor teams on how differences in calibration techniques and atmospheric correction algorithms propagate through the processing to produce differences in retrieved optical properties of the water. It must be stressed that this exercise is absolutely essential for calibrating the ocean color systems, i.e., sensors plus algorithms, and that it cannot be implemented without a high quality surface data set obtained simultaneously with the satellite imagery.

1.6 AEROSOL OPTICAL THICKNESS VALIDATION

Aerosol optical thickness products determined from the satellite ocean color data itself are critical factors in the uncertainty budgets of atmospheric correction algorithms (Gordon and Wang 1994a) and results of vicarious calibrations (Clark et al. 1997; Gordon 1981, 1987, 1988). The SIMBIOS Project is validating the SeaWiFS aerosol optical products by comparing them to *in situ* measurements (Wang et al., 2000). A second, related objective of these comparisons is to determine the validity of the aerosol models currently used by SeaWiFS for atmospheric correction.

The principal source of *in situ* aerosol observations is the Aerosol Robotic Network (AERONET). AERONET is a network of ground-based automated sun photometers owned by national agencies and universities (Holben et al. 1998). AERONET data provides globally distributed, near-real time observations of aerosol spectral optical depths, aerosol size distributions, and precipitable water. Because the majority of the AERONET stations are at continental locations, SIMBIOS augmented the network with 12 additional island and coastal sites, including Lanai and Oahu Hawaii, Ascension Island, Bahrain, Tahiti, Wallops Island, South Korea, Turkey, Argentina, Azores and Perth. SIMBIOS Project also has shipboard hand-held sun photometers (MicroTops, PREDE, SIMBAD and Lidar). These instruments are calibrated in collaboration with the AERONET Program at NASA Goddard Space Flight Center (GSFC) and loaned to investigators staging SIMBIOS sponsored research expeditions.

1.7 COMMUNITY PARTICIPATION

The SeaWiFS and SIMBIOS Project Offices rely on the oceanographic community to perform field research for atmospheric and bio-optical algorithm development, and for all of the *in situ* data collection for the vicarious sensor calibration. The SIMBIOS Project sponsors a subset of these observations, but many projects sponsored by the NASA Research and Application Program, other government agencies and the international ocean color research community all make major contributions to the global multi-year effort.

The SIMBIOS Project has undertaken the challenge of coordinating the in situ observations contributed by these various programs, linking it to ocean color imagery from the international ensemble of satellite sensors, and making the overall data sets available to the ocean color research community (McClain and Fargion 1999a,b). A workable strategy to meet those challenges first requires a clear definition of the observations, uncertainties, and data collection protocols associated with each type of activity. The purpose of this document is to clarify these requirements.

1.8 PROTOCOL DOCUMENT ORGANIZATION

The chapters of this document are organized into four parts. Chapters 1 and 2 address perspectives on ocean color research and validation, and requirements for *in situ* observations. Chapters 3 through 10 address the characteristics and performance specifications of the instruments used for in situ observation, and provide protocols for their calibration and characterization. Chapters 11 through 14 provide detailed protocols describing methods for making each type of field measurement and associated data analysis. Finally, Chapter 15 address the methods and procedures for data archival, data synthesis and merging, and quality control.

REFERENCES

Barnes, R. A., R. E. Eplee, F. S. Patt, and C. R. McClain 1999a: Changes in the radiometric sensitivity of SeaWiFS determined from lunar and solar-based Measurements. *Applied Optics*, **38**, 4649-4669.

Barnes, R.A., R.E. Eplee, Jr., S.F. Biggar, K.J. Thome, E.F. Zalewski, P.N. Slater, and A.W. Holmes 1999b: The SeaWiFS Solar Radiation-Based Calibration and the Transfer-to-Orbit Experiment. *NASA Tech. Memo. 1999--206892, Vol. 5*, S.B. Hooker and E.R. Firestone, Eds., NASA Goddard Space Flight Center, 28 pp.

Brown, O. B., and R. H. Evans 1985: Calibration of Advanced Very High Resolution Radiometer infrared observations. *J .Geophys. Res.*, **90**, 11,667-11,677.

Clark, D. K., 1981: Phytoplankton pigment algorithms for the Nimbus-7 CZCS. *Oceanography from Space*, J.F.R. Gower Ed., Plenum Press, 227-238.

Clark, D.K., H.R. Gordon, K.J. Voss, Y. Ge, W. Broenkow, and C.C. Trees, 1997: Validation of atmospheric correction over oceans. *J. Geophys. Res.*, **102,** 17,209-17217.

Esaias, W., G. Feldman, C.R. McClain, and J. Elrod, 1986: Satellite observations of oceanic primary productivity. *EOS, Trans. AGU*, **67**, 835--837.

Evans, R.H., and H.R. Gordon, 1994: Coastal zone color scanner system calibration: A retrospective examination. *J. Geophys. Res.,* **99**, 7,293--7,307.

Fargion G.S., C.R. McClain, H. Fukushima, J.M. Nicolas and R.A. Barnes, 1999: Ocean color instrument intercomparisons and cross-calibrations by the SIMBIOS Project. *SPIE* Vol. **3870**,397-403.

Feldman, G., N. Kuring, C. Ng, W. Esaias, C. McClain, J. Elrod, N. Maynard, D. Endres, R. Evans, J. Brown, S. Walsh, M. Carle, and G. Podesta, 1989: Ocean Color: Availability of the global data set. *EOS*, *Trans. AGU*, **70**, 634.

Groom, S.B., and P.M. Holligan, 1987: Remote sensing of coccolithophorid blooms. *Adv. Space Res*., **7**, 73--78.

Gordon, H.R. and D.K. Clark, 1981: Clear water radiance for atmospheric correction of coastal zone color scanner imagery. *Appl. Opt.,***20**,4,175-4,180.

Gordon, H.R., 1981: Reduction of error introduced in the processing of coastal zone color scanner-type imagery resulting from sensor calibration and solar irradiance uncertainty. *Appl. Opt*., **20**, 207--210.

Gordon H.R., J.W. Brown, O.B. Brown, R.H. Evans, and D.K. Clark 1983: Nimbus-7 CZCS: Reduction of its radiometric sensitivity with time. *Appl.Opt*., **24**, 3,929-3,931.

Gordon H.R., 1987: Calibration requirements and methodology for remote sensors viewing the ocean in the visible. *Remote Sens. Environ.,***22**,103-126

Gordon H.R., 1988: Ocean color remote sensing systems: radiometric requirements. *Recent Advances in Sensors, Radiometry, and Data Processing for Remote Sensing*, P.N. Slater, Ed. SPIE, **924**, 151-157.

Gordon, H.R. and M. Wang, 1994a: Retrieval of water-leaving radiance and aerosol optical thickness over the oceans with SeaWiFS: A preliminary algorithm, *Appl. Opt*., **33**, 443-452.

Gordon, H.R. and M. Wang, 1994b: Influence of oceanic whitecaps on atmospheric correction of ocean color sensors, *Appl. Opt*., **33**, 7,754-7,763.

Holben, B.N., T.F. Eck, I. Slutsker, D. Tanre, J.P. Buis, A. Setzer, E. Vermote, J.A. Reagan, Y.J. Kaufman, T. Nakajima, F. Leaven, I.

Jankowiak, and A. Smirnov, 1998: AERONET – a federated instrument network and data archive for aerosol characterization. *Remote Sens. Environ*., **66**, 1-16.

Hovis W.A., J.S. Knoll, and G.R. Smith, 1985: Aircraft measurements for calibration of a orbiting spacecraft sensor. *Appl.Opt.,* **24**,407-410.

McClain, C.R., G. Feldman and W.Esaic, 1993: Biological Oceanic Productivity, in *Atlas of Satellite Observations Related to Global Change*, R.Gurney, J.L.Foster (Eds.), Cambridge Press, NY, 251-263, 470 pp.

McClain, C.R., M. Cleave, G. Feldaman, W. Gregg and S.B. Hooker, 1998: Science quality SeaWiFS Data for global biosphere research. *Sea Technology*, **39**, 10-16.

McClain, C.R. and G.S. Fargion, 1999a: SIMBIOS Project 1998 Annual Report, *NASA Tech. Memo. 1999-208645*, NASA Goddard Space Flight Center, Greenbelt, Maryland, 105 pp.

McClain, C.R. and G.S. Fargion, 1999b: SIMBIOS Project 1999 Annual Report, *NASA Tech. Memo. 1999-209486,* NASA Goddard Space Flight Center, Greenbelt, Maryland, 128 pp.

McClain R.C., E. Ainsworth, R. Barnes, R. Eppley et al. , 2000: SeaWiFS Postlaunch Calibration and Validation Part 1, *NASA TM 2000-206892, Vol. 9, NASA Tech. Memo. 104566,* S.B. Hooker and E.R. Firestone, Eds., NASA Goddard Space flight center, Greenbelt, Maryland (in press).

McClain R.C., R. A. Barnes, R. E. Eplee, Jr., B. A. Franz, et al., 2000b: SeaWiFS Postlaunch Calibration and Validation Part 2, *NASA TM 2000-206892, Vol 10*, *NASA Tech. Memo. 104566,* S.B. Hooker and E.R. Firestone, Eds., NASA Goddard Space flight center, Greenbelt, Maryland (in press).

Mueller, J.L. 1985: Nimbus-7 CZCS: electronic overshoot due to cloud reflectance. *Appl. Opt.,* **27**,438-440.

Mueller, J.L. and R.W. Austin, 1992: Ocean optics protocols. *NASA Tech. Memo. 104566, Vol. 5,* S.B. Hooker and E.R. Firestone, Eds., NASA Goddard Space flight center, Greenbelt, Maryland, 45 pp.

Mueller, J.L. and R.W. Austin, 1995: Ocean Optics Protocols for SeaWiFS Validation, Revision 1. *NASA Tech. Memo. 104566, Vol 25,* S.B. Hooker and E.R. Firestone, Eds., NASA Goddard Space flight center, Greenbelt, Maryland, 66 pp.

O'Reilly J. E., S. Maritorena, D. Siegel et al., 2000 SeaWiFS Postlaunch Calibration and Validation Part 3, *NASA TM 2000-206892, Vol. 11, NASA Tech. Memo. 104566,* S.B. Hooker and E.R. Firestone, Eds., NASA Goddard Space flight center, Greenbelt, Maryland (in press).

UNESCO, 1994: Protocols for the Joint Global Ocean Flux Study (JGOFS) Core Measurements, *Manual and Guides 29*, 170pp.

Viollier, M., 1982: Radiance calibration of the Coastal Zone Color Scanner: a proposed adjustment. *Appl. Opt*., **21**, 1,142--1,145.

Voss, K. J. and G. Zibordi, 1989: Radiometric and geometric calibration of a spectral electro-optic "fisheye' camera radiance distribution system. *J. Atmos. Ocean. Tech*.., **6**, 652-662.

Wang, M. and B.A. Franz, 1999: Comparing the ocean color measurements between MOS and SeaWiFS. *IEEE Trans. Geosci. Remote Sens.*, in press.

Wang, M., S. Bailey, C. Pietras and C. R. McClain, 2000: Correction of Sun Glint Contamination on the SeaWiFS Aerosol Optical Thickness Retrievals, in McClain et al., SeaWiFS Postlaunch Calibration and Validation Analyses, Part 1*, NASA TM 2000-206892, Vol 9*, in press.

Weinreb, M.P., G. Hamilton, S. Brown, and R.J. Koczor, 1990: Nonlinear corrections in calibration of Advanced Very High Resolution Radiometer infrared channels. *J. Geophys. Res*., **95**, 7,381--7,388.

Chapter 2

Data Requirements for Ocean Color Algorithms and Validation

James L. Mueller[1], Giulietta S. Fargion[2] and Charles R. McClain[3]

[1]*Center for Hydro-Optics and Remote Sensing, San Diego State University, California*
[2]*SAIC General Sciences Corporation, Beltsville, Maryland*
[3]*NASA, Goddard Space Flight Center, Greenbelt, Maryland*

2.1 INTRODUCTION

The principal *in situ* variables to be measured, or derived from measurements, for satellite ocean color sensor validation, and algorithm development and validation, are listed in Table 2.1. The variables are grouped, in Table 2.1, into four related groups: Radiometric Quantities (both oceanic and atmospheric), Inherent Optical Properties (IOP) of sea water, Biogeochemical and Bio-Optical Properties of sea water, and Ancillary Data and Metadata required to support the use, analysis, interpretation, and quality assessment of the other data. Those *in situ* variables that are measured are classified into three categories of descending priority.

The first category of measurements, flagged "Required" in Table 2.1, is the minimum subset required for validating a satellite sensor's radiometric performance, normalized water-leaving radiances, and fundamental derived products, including chlorophyll a concentration, aerosol optical thickness, and K(490), and for associated algorithm development and validation.

The second category, flagged "Highly Desired" in Table 2.1, are measurements that supplement the minimum subset and are needed for investigations focused on atmospheric correction algorithms and aerosols, relationships between IOP and remote sensing reflectance, and/or Case 2 algorithms.

The third category, flagged "Specialized Measurement" in Table 2.1, are measurements which either address aspects of ocean bio-optics that are secondary to satellite remote sensing, or require highly specialized equipment that is not readily available to the community at large.

A fourth category, flagged as "Derived", comprises key quantities that are either calculated from the *in situ* measurements, or are derived from models. The above set of variables is also listed in Table 2.2, to identify the satellite ocean color

sensor application for which each measurement is needed. Table 2.2 also provides an index of the protocol chapters addressing each *in situ* measurement.

2.2 RADIOMETRIC QUANTITIES

Surface incident spectral irradiance in air, $E_s(\lambda) = E_d(0^+, \lambda)$, downwelled spectral irradiance, $E_d(z, \lambda)$, and upwelled spectral radiance, $L_u(z, \lambda)$, are the fundamental measurable quantities needed to derive normalized water-leaving radiances (or equivalently remote sensing reflectance) in most circumstances. Other radiometric properties listed in Table 2.1, including sky radiance and normal solar irradiance, are also important *in situ* measurements in the SIMBIOS ocean color validation program. Also listed are critical radiometric quantities that are calculated, or derived, from *in situ* measurements. In some cases, listed radiometric quantities may be derived, wholly or in part, from other non-radiometric measurements listed in the table. For example, remote sensing reflectance may either be calculated directly as the ratio $L_W(\lambda):E_s(\lambda)$, or it may be modeled as a function of the IOP ratio $b_b(\lambda):a(\lambda)$ and the BRDF.

Downwelled spectral irradiance, $E_d(z, \lambda)$, is required to compute the diffuse attenuation coefficient, $K_d(z, \lambda)$, which in turn, is needed for diffuse attenuation coefficient algorithm development (Austin and Petzold 1981; Mueller and Trees 1997; Mueller 2000), and for optically weighting the pigment concentrations to be estimated from remotely sensed ocean color (Gordon and Clark 1980). As with $L_u(0^-, \lambda)$, $E_d(0^-, \lambda)$, must be determined by extrapolation from a profile of $E_d(z, \lambda)$, over the upper few diffuse attenuation lengths and reconciled with the direct surface measurement above the water of $E_s(\lambda)$.

Upwelled spectral radiance, $L_u(0^-, \lambda)$ is the in-water variable which, when propagated upward through the sea surface, leads to the *measured* value of $L_W(\lambda)$. $L_W(\lambda)$ is, in turn, adjusted using $E_s(\lambda)$ to derive the normalized water-leaving radiance, $L_{WN}(\lambda)$, for a no-atmosphere, zenith sun at the mean Earth-sun distance. Unfortunately, it is not practical to measure $L_u(0^-, \lambda)$ precisely at an infinitesimal depth below the surface. Therefore, the profile of $L_u(z, \lambda)$, must be measured over the upper few optical depths with sufficient accuracy to determine $K_L(z, \lambda)$ for $L_u(z, \lambda)$, and to propagate $L_u(z, \lambda)$ to the surface. At near-infrared (NIR) wavelengths, the first optical attenuation length is confined to the upper few tens of centimeters. Determination of $L_u(0^-, \lambda)$, in this situation is more challenging and will require special instruments and experiment designs to accommodate the effects of instrument self-shading, wave focusing, small-scale variability, possible fluorescence, Raman scattering, and extremely small working volumes. Similar complications arise at all wavelengths in Case-2 waters. For algorithm development and validation in these difficult cases, measurements of inherent optical properties (IOPs), including $a(z, \lambda)$, $c(z, \lambda)$ and $b_b(z, \lambda)$, and spectral fluorescence, may be usefully combined with $E_d(z, \lambda)$, and $L_u(z, \lambda)$ measured with specially designed radiometers and $L_{sfc}(\lambda,\theta,\phi,\theta_o,\phi_o)$ and $Lsky(\lambda,\theta,\phi,\theta_o,\phi_o)$ measured above-water.

Upwelled spectral irradiance, $E_u(z, \lambda)$, is a useful measurement, in addition to E_d and L_u, because there exist both empirical and theoretical relationships between IOPs, phytoplankton pigments, TSM, and irradiance reflectance. $L_u(0^-, \lambda)$ and $E_u(0^-, \lambda)$ are related by the factor $Q(\lambda)$, which is not well determined at present, and has been shown to vary with solar zenith angle (Morel and Gentili 1993, 1996; Morel, Voss and Gentili 1995). Combined measurements of $L_u(0^-, \lambda)$ and $E_u(0^-, \lambda)$ will be extremely useful in determining $Q(\lambda)$ which will, in turn, allow traceability of the measurements by the SIMBIOS ensemble of satellite ocean color sensors to previously derived irradiance reflectance relationships and algorithms.

Radiance distribution measurements $L(z,\lambda,\theta,\phi)$ just beneath the sea surface will be required for quantifying the angular distribution of water-leaving radiance at stations used for system calibration initialization and long-term system characterization. These measurements will also necessary to determine the Bidirectional Reflectance Distribution Function (BRDF) of the water and verify the models used to normalize water-leaving radiance for variations in viewing and solar zenith angles (Morel and Gentili 1996).

Water Surface Radiance (in air), $L_{sfc}(\lambda,\theta,\phi,\theta_o,\phi_o)$, measured from the deck of a ship (or a low-flying aircraft) is a potentially useful substitute for $L_W(\lambda)$ determined from in-water $L_u(0^-, \lambda)$. The measured surface radiance is the sum of water-leaving radiance and sky radiance reflected from the wave-roughened sea surface. The principal, and significant, source of uncertainty in this approach is associated with removal of reflected sky radiance from the total signal.

Surface incident spectral irradiance, $E_s(\lambda)$, is usually measured on a ship well above the water. In the previous versions of these protocols (Mueller and Austin 1992, 1995), it was suggested that $E_s(\lambda)$ might alternatively be determined from measurements of $E_d(0^-, \lambda)$ made some distance from the ship using a radiometer floated just beneath the surface. The community has gained experience with this approach and found that wave-induced fluctuations in near-surface irradiance produce an uncertainty in $E_d(0^-, \lambda)$ approaching 10% in even ideal cases (Siegel *et al.* 1995). $E_s(\lambda)$ varies due to fluctuations in cloud cover and aerosols, and with time of day, i.e., solar zenith angle. Profiles of $E_d(z, \lambda)$, and $L_u(z, \lambda)$, must be normalized to account for such variabilities during a cast.

Normal Solar Irradiance spectra $E_N(\lambda,\theta_o,\phi_o)$ should be measured using a sun photometer in order to determine atmospheric transmittance and aerosol optical depths at each station. These data are particularly needed to verify the atmospheric corrections in direct match-up comparisons between satellite ocean color sensor $L_W(\lambda)$ estimates and those determined from in-water measurements of $L_u(z, \lambda)$.

Sky radiance, $Lsky(\lambda,\theta,\phi,\theta_o,\phi_o)$, is required to enable estimation of the aerosol phase function through inversion of the radiative transfer equation. It is also useful for estimating the mean cosine of the transmitted light field in the water. The sky radiance should be measured directly; for the latter application, however, it need only be estimated by occulting the sun's image on a deck cell measuring the incident spectral radiance from the sun and sky. The mean cosine at the surface can be used with profile measurements of $E_d(\lambda)$, $E_u(\lambda)$, and $c(\lambda)$ to estimate $b_b(\lambda)$ (Gordon 1991). An ability to exploit this and similar relationships will greatly enhance both development and verification of bio-optical algorithms. The spectral sky radiance distribution over zenith and azimuth angles is required to determine the aerosol scattering phase functions at radiometric comparison stations during system initialization cruises. It is also measured routinely

9

at a network of fixed island and coastal sites distributed around the world. Finally, $L_{sky}(\lambda,\theta,\phi,\theta_o,\phi_o)$ is measured and multiplied by the reflectance of the sea surface to derive $L_W(\lambda,\theta,\phi,\theta_o,\phi_o)$ from $L_{sfc}(\lambda,\theta,\phi,\theta_o,\phi_o)$ measurements.

Diffuse Sky Irradiance, $E_{sky}(\ )$, may be measured using a fast-rotating, shipboard version of a Shadowband Radiometer, or by manually obscuring the direct solar irradiance, $E_{sun}(\ )$, component of $E_s(\ )$. This measurement is extremely useful for determining the ratio $E_{sun}(\ ){:}E_{sky}(\ )$, which is a critical factor in self-shading corrections to $L_u(z,\ )$ and $E_u(z,\ )$ measurements (Gordon and Ding 1992).

2.3 INHERENT OPTICAL PROPERTIES

Inherent Optical Properties (IOP) must be measured for development and validation of the ocean color semi-analytic Case-2 chlorophyll a algorithm. This algorithm is based on an explicit theoretical function of the ratio of backscattering to absorption, $b_b(\ ){:}a(\ )$. This ratio is also an important factor in the BRDF models underlying the Morel and Gentili (1996) normalization for solar and viewing azimuth and zenith angles. Due to recent advances in instrumentation, it is now practical to routinely measure in situ profiles of *absorption* $a(z,\ )$, *beam attenuation* $c(z,\ )$ and *backscattering* $b_b(z,\ )$ coefficients. The scattering coefficient may therefore also be obtained as $b(z,\ ) = c(z,\ ) - a(z,\ )$. The IOP's also provide critical factors in the Gordon and Ding (1992) model used to correct upwelled radiance and irradiance measurements for instrument self shading. Future algorithm development and validation experiments involving these algorithms must, therefore, include absorption, beam attenuation, and backscattering measurements. It is anticipated that new instruments, now under development and testing, will allow in situ measurements of the volume scattering function $\beta(z, \lambda,\theta,\phi,\theta',\phi')$. Measurements of $\beta(z, \lambda,\theta,\phi,\theta',\phi')$ will be very useful in advancing remote sensing reflectance models and algorithms involving the BRDF.

The *particle absorption coefficient*, $a_p(z,\ )$, which is comprised of absorption by living, dead, and inorganic particles, is a useful variable for modeling the portion of solar energy that is absorbed by phytoplankton and bacteria. A laboratory spectrophotometer may be used to measure $a_p(z,\ )$ of particles filtered from seawater

samples collected at depth z, or it may be computed as the difference between *in situ* measurements with a pair of filtered (CDOM absorption) and unfiltered (total absorption) instruments.

The *colored dissolved material (CDOM) absorption coefficient,* $a_g(z,\ )$, is an important contributor to total absorption in many coastal waters. Because CDOM, variously referred to as *gelbstoffe, gilvin,* or *yellow-matter*, absorbs very strongly in the blue, its undetected presence can create large regional uncertainties in chlorophyll a retrievals from ocean color image data. The CDOM absorption coefficient $a_g(z,\ )$ may either be measured *in situ* by installing a 0.2 μm in the water intake port of an absorption and beam attenuation meter, or in the laboratory using a spectrophotometer to measure absorption by filtered seawater, typically over a 10 cm path.

The non-pigmented particle absorption coefficient, $a_d(z,\ )$, accounting for absorption of light by detritus (or tripton), represents a major loss of light which would otherwise be available to the phytoplankton component of the marine hydrosol. In many cases, absorption by detritus is a significant term in the marine radiative transfer processes, and its determination is useful for phytoplankton production models and for modeling the light field. The spectral absorption coefficient $a_d(z,\ )$ using the $a_p(z,\ )$ filters, after they are washed with hot methanol to remove phytoplankton pigments (Kishino *et al.* 1985).

2.4 BIOGEOCHEMICAL AND BIO-OPTICAL QUANTITIES

Phytoplankton pigment composition will be determined using the *HPLC* method to develop and validate ocean color pigment algorithms, and to assess the effects of accessory pigment concentrations on water-leaving spectral radiances. These data may also be used to calibrate continuous profiles of *in situ* fluorescence. *Chlorophyll a and pheopigment concentrations* will also be determined using the *fluorometric method.* The HPLC chlorophyll a concentrations are more accurate than fluorometric concentrations, which are often biased systematically throughout a particular geographic region and time of year. On the other hand, fluorometric measurements of chlorophyll a concentration are both far easier and less expensive to perform, allowing a far greater number of pigment validation samples to be acquired on a given cruise than if HPLC sampling were used alone. If a well-distributed subset of

pigment filter samples from each validation cruise are reserved for HPLC measurements, it is possible and operationally effective to derive regional and temporal corrections to scale fluorometric and HPLC chlorophyll a concentrations into close agreement.

Phycobilipigments, present in cyanobacteria and cryptophytes, are treated separately from the HPLC fat-soluble pigments. Phycoerythrin and phycocyanin are the two major groups of phycobilipigments found in the marine environment. The concentration of these water-soluble pigments is important due to the contribution of solar stimulated phycoerythrin fluorescence to the underwater light field, and also to characterize the phytoplankton population. At times, species that contain phycobilipigment can account for a large fraction of the primary productivity (especially in oligotrophic waters) and have been difficult to quantify due to their small size. Although neither SeaWiFS nor MODIS contains bands at the absorption or fluorescence peaks of phycobilipigments, future satellite ocean color sensors, including GLI and MERIS will have appropriate bands. The present protocols do not specify methods for measuring phycobilipigments, but qualitative concentrations may be obtained today using a fluorometric approach, and a new capillary electrophoresis method is currently under development. We anticipate that a chapter giving protocols for measuring this important group of phytoplankton pigments will emerge in the near future.

Coccolith concentration, which is the number density of small plates (coccoliths) composed of calcium carbonate ($CaCO_3$), is very important to light scattering. Coccoliths are produced in copious amounts by marine phytoplankton called coccolithophorids. Scattering of light by coccoliths is highly apparent in visible wavelength satellite imagery, because they perturb the usual relationships between water-leaving radiances and pigment concentration, and therefore, adversely impact atmospheric corrections (Balch et al. 1991, Voss et al.,1998). Additionally, coccolith formation, sinking, and dissolution are significant factors in the ocean carbon flux budget. It is, therefore, necessary to measure coccolith concentration, both as number density and $CaCO_3$ concentration, to aid in 1) the correction of chlorophyll a concentration algorithms, 2) coccolith algorithm development, and 3) atmospheric correction development and validation. This present version (2.0) of the ocean optics protocols does not cover methods for measuring coccolith

concentration. Such protocols may be included in a future revision.

Total Suspended Matter (TSM) measurements are required to assess the effect of suspended sediment on the derived products. TSM is of primary importance in coastal waters, where simple radiance ratio algorithms for TSM have uncertainties equivalent to, or greater than, those for estimating chlorophyll-like pigment concentration. Organic suspended matter and inorganic suspended matter concentrations are subfractions of TSM; this partitioning of TSM is particularly useful in process studies.

Continuous profile measurements of *in situ chlorophyll a fluorescence intensity* are exceptionally useful as guidance in analyzing profiles of $E_d(z)$, $L_u(z)$, and $E_u(z)$ to derive profiles of $K_d(z)$, $K_L(z)$, and $K_u(z)$, respectively. Moreover if these profiles are viewed in real time, they are also useful guides for taking water samples at depths that allow the vertical structure of pigment concentration profiles to be accurately resolved in the top optical depth and subsurface chlorophyll maxima. Finally, the continuous *in situ* chlorophyll a fluorescence profile may be used to interpolate HPLC, or extracted fluorescence, measurements of chlorophyll a concentrations from water samples at discrete depths. It is desirable to make these measurements simultaneously with IOP profiles, and also those of irradiance and radiance if it can be done in a way to avoid self-shading of the radiometers.

2.5 ANCILLARY DATA AND METADATA

The geographic location and time at which *in situ* validation data are acquired are essential information that must be included in every data submission under the SIMBIOS program. The obvious metadata items in this context are *latitude, longitude, date and time (UTC)*. Expressing date and time in UTC is also essential, even though it may be helpful to also list local date and time with a validation station's metadata. Too often, field investigators neglect to identify (or possibly even keep track of) the time zone used by a PC to enter time into data records.

Sea state, expressed as significant wave height in m, must be reported with in situ validation measurements. Whitecap conditions, expressed as the estimated fractional aereal coverage are also useful and highly desired. Digital photographs documenting surface wave and whitecap conditions during radiometric measurements are also helpful.

This information is essential for identifying measurements made under questionable environmental conditions.

Wind speed and direction are required to generate, through models, estimates of the surface wave slope distribution, which will be used to calculate reflected skylight and sun glint in radiative transfer models (Cox and Munk 1954). Surface wave models driven by wind velocity may also be used to provide quantitative estimates of surface wave induced radiometric fluctuations. Qualitatively, wind velocity, and photographs or videotape recordings of sea state, will be useful for assessing station data quality.

Surface barometric pressure measurements are required to validate both atmospheric correction algorithms and the surface pressures derived from operational weather analyses for use in processing satellite ocean color data

Cloud cover (expressed as fractional coverage in octals, or percent) is essential metadata used for assessing data quality and screening questionable cases from algorithm development and validation analyses. A description of sky conditions near the sun and satellite zenith and azimuth angles, including whether the sun is obscured during observations, is also important information. Cloud type information is also useful, as are photographs of sky conditions.

Secchi depth measurements are required for real-time assessment of water transparency during a station and as a quality check during analysis of radiometric profiles.

Water depth, in m, is important information for screening data from shallow water cases where bottom reflections may be present in water-leaving radiance measurements.

Hydrographic data, *water temperature (T), and salinity (S)*, derived from *conductivity, temperature, and depth (CTD)* profiles, are useful for characterizing the physical water mass regime in which an optical profile is measured. A T-S characterization is especially important near ocean fronts and eddies where interleaving water masses of very different biogeochemical composition, and therefore fundamentally different bio-optical properties, can produce complex spatial and temporal patterns of near-surface optical properties. In these circumstances, T-S profiles can provide an indication of whether a station location is suitable for reliable remote sensing validation and algorithm development comparisons. The T(z) and S(z) measurements are also needed for corrections to pure water absorption in processing IOP measurements.

2.6 PROCESS MODEL RELATED DATA

Other types of in situ measurements are also important in the context of ocean color validation, because they are needed either to support, or validate, process models that are derived with the aid of ocean color image data. Primary productivity models are, perhaps, the foremost example of these secondary products of satellite ocean color measurements. The *in situ* measurements needed to support such models, and other scientific investigations and applications that may exploit ocean color data products, are undeniably important and closely related to the quantities listed in Table 2.1. These measurements are not, however, essential to algorithm development and validation of products derived from the ocean color data directly. In the future, the scope of the ocean optics protocols may be expanded to embrace methods for measuring and/or analyzing some of these variables, but at present they are not included. Some of the more important measurements of this class are briefly described in this section, but none of them are discussed in detail.

Aerosol concentration samples using high volume techniques will be useful, in conjunction with aerosol optical depth spectra determined from sun photometer measurements, for chemical, size, and absorption characterization of aerosols, especially in studies of the effects of Saharan and Asian dust clouds on atmospheric corrections.

Particulates, both POC and PON, are required for process studies to help characterize the adaptive state of phytoplankton and to inventory critical biogeochemical elements.

DOC has been shown to be a major pool of carbon in the oceans. Quantification of the transformations of this pool is crucial to understanding the marine carbon cycle. The colored fraction, CDOM, of the DOC is highly absorbent in the blue range, thus decreasing blue water-leaving radiances, and it must be taken into consideration for pigment concentration algorithms. DOC measurements are needed to develop robust relationships between CDOM and DOC, which are needed to evaluate the usefulness of ocean color observations for estimating DOC concentrations.

CDOM concentrations are required to assess the effect of Gelbstoff on blue water-leaving radiances and chlorophyll concentration. This is of primary importance in Case-2 waters, but is also relevant to phytoplankton degradation products in Case-2 waters.

Humic and fulvic acids comprise the bulk of CDOM and have different specific spectral absorption coefficients. Their concentrations are useful for determining the correction used for phytoplankton pigment concentration algorithms in Case-2 waters and for estimating CDOM from ocean color observations.

Particle size spectra are very useful for in-water radiative transfer calculations, particularly if measurements include particles smaller than 1 m.

Particle fluorescence, measured using laser sources on single-cell flow systems, may be used to calculate particle scattering-to-fluorescence ratios for evaluating the population structure of the plankton (both phyto- and zooplankton).

Phytoplankton species counts are important because species-to-species variability in optical and physiological properties represents a major source of variability in bio-optical algorithms and primary productivity models. This has been recognized, but it is generally ignored in remote sensing algorithms due to the tedious nature of species enumeration, the small sizes of many species, and the large number of species involved. This information, however, at various levels of rigor, is useful in evaluating the population and pigment composition. This is especially important for some groups, such as coccolithophorids.

Primary productivity, using the radioactive isotope ^{14}C estimation method, is not strictly required for validation of water-leaving radiances or system initialization. It is a MODIS product and will be a SeaWiFS production in the future. It will, however, be extremely useful for process study applications of ocean color data if these measurements are made at the same time that the water column optical properties are determined. These data will aid in the development of models of primary production using satellite ocean color observations, a goal which is central to all global ocean color mission. Of special importance are determinations of key photo-physiological parameters derived from production measurements as functions of irradiance. If ^{14}C productivity measurements are made, they should conform to the *JGOFS Core Measurements Protocols* (JGOFS 1991).

REFERENCES

Austin, R.W., and T.J. Petzold, 1981: The determination of diffuse attenuation coefficient of sea water using the Coastal Zone Color Scanner. *Oceanography from Space*, J.F.R. Gower, Ed., Plenum Press, 239-256.

Balch, W.M., P.M. Holligan, S.G. Ackleson, and K.J. Voss, 1991: Biological and optical properties of mesoscale coccolithophore blooms in the Gulf of Maine. *Limnol. Oceanogr.*, **36**, 629-643.

Cox, C., and W. Munk, 1954: Measurements of the roughness of the sea surface from photographs of the sun's glitter. *J. Opt. Soc. Am.,* 44, 838--850.

Gordon, H.R., 1991: Absorption and scattering estimates from irradiance measurements: Monte Carlo simulations. *Limnol. Oceanogr.*, **36**: 769--777.

Gordon, H.R., and D.K. Clark, 1980: Remote sensing optical properties of a stratified ocean: an improved interpretation. *Appl. Optics*,**19**: 3,428--3,430.

Joint Global Ocean Flux Study, 1991: JGOFS Core Measurements Protocols. *JGOFS Report No. 6*, Scientific Committee on Oceanic Research, 40 p.

Kishino, M., N. Okami, and S. Ichimura, 1985: Estimation of the spectral absorption coefficients of phytoplankton in the sea. *Bull. Mar. Sci.,*37, 634--642.

Morel, A., and B. Gentili, 1993: Diffuse reflectance of oceanic waters. II. Bidirectional aspects. *Appl. Opt.*, **32**: 6,864--6,879.

Morel, A., and B. Gentili, 1996: Diffuse reflectance of oceanic waters. III. Implication of bidirectionality for the remote-sensing problem. *Appl. Optics*, **35**: 4850-4862.

Morel, A., K.J. Voss, and B. Gentili, 1995: Bidirectional reflectance of oceanic waters: a comparison of modeled and measured upward radiance fields. *J. Geophys. Res.***100**: 13,143-13,151.

Mueller, J.L., and R.W. Austin, 1992: Ocean Optics Protocols for SeaWiFS Validation. *NASA Tech. Memo. 104566, Vol. 5,* S.B. Hooker and E.R. Firestone, Eds., NASA Goddard Space Flight Center, Greenbelt, Maryland, 43 pp.

Mueller, J.L., and R.W. Austin, 1995: Ocean Optics Protocols for SeaWiFS Validation, Revision 1. *NASA Tech. Memo. 104566, Vol. 25,* S.B. Hooker, E.R. Firestone and J.G. Acker, Eds.,

NASA Goddard Space Flight Center, Greenbelt, Maryland, 67 pp.

Mueller, J.L. and C.C. Trees, 1997: Revised SeaWiFS prelaunch algorithm for the diffuse attenuations coefficient K(490). In: Yeh, et al. Case Studies for SeaWiFS Calibration and Validation, Part 4. *NASA Tech. Memo. 104566, Vol. 41,* S.B. Hooker, E.R. Firestone and J.G. Acker, Eds., NASA Goddard Space Flight Center, Greenbelt, Maryland, 18-21.

Voss, K.J., W.M. Balch and K.A. Kilpatrick, 1998: Scattering and attenuation properties of

Emiliania huxleyi cells and their detached coccoliths, *Limnol. Oceangr.,* **43**(5): 870-876.

Siegel, D.A., M.C. O'Brien, J.C. Sorensen, D.A. Konnoff, E.A. Brody, J.L. Mueller, C.O. Davis, W.J. Rhea, and S.B. Hooker, 1995. Results of the SeaWiFS Data Analysis Round-Robin, July 1994 (DARR-94). *NASA Tech. Memo. 104566, Vol. 26*, S.B. Hooker and E.R. Firestone, Eds., NASA Goddard Space Flight Center, Greenbelt, MD. 58pp.

Table 2.1 Principal *in situ* observations for satellite ocean color system validation, and algorithm development and validation. The right-hand column identifies and classifies measurements as: (a) required for minimal validation match-ups; (b) highly desired and important for general algorithm development and validation ; (c) specialized measurements of important, but restricted, applicability to algorithm development and validation (for the present); and (d) calculated or derived quantities.

	Required	Highly Desired	Specialized Measurement	Derived
Radiometric Quantities				
Downwelled Irradiance $E_d(z,\lambda)$	✓			
Upwelled Radiance $L_u(z,\lambda) = L(z, \lambda,0,0)$	✓			
Upwelled Irradiance $E_u(z,\lambda)$			✓	
Radiance Distribution in water $L(z, \lambda,\theta,\phi)$			✓	
Water Surface Radiance in air $L_{sfc}(\lambda,\theta,\phi)$		✓		
Incident Irradiance in air $E_s(\lambda) = E_d(0^+,\lambda)$	✓			
Normal Solar Irradiance $E_N(z,\lambda)$	✓			
Sky Radiance $L_{sky}(\lambda,\theta,\phi)$		✓		
Diffuse Sky Irradiance $E_{sky}(\lambda)$		✓		
Direct Sun Irradiance $E_{sun}(\lambda) = E_s(\lambda) - E_{sky}(\lambda)$				✓
Water-Leaving Radiance $L_w(\lambda,\theta,\phi,\theta_o,\phi_o)$				✓
Remote Sensing Reflectance $R_{RS}(\lambda,\theta,\phi,\theta_o,\phi_o)$				✓
Attenuation Coefficient $K(z,\lambda)$ for $E_d(z,\lambda)$ and $L_u(z,\lambda)$				✓
Ocean Bidirectional Reflectance Distribution Function BRDF				✓
Aerosol Optical Depth $\tau_a(\lambda)$	✓			
Aerosol Phase Function $P_a(\lambda,\theta,\phi,\theta',\phi)$				✓
Absorbing Aerosol Height Profiles (LIDAR Profilometer)			✓	
Inherent Optical Properties				
Beam Attenuation Coefficient $c(z,\lambda)$		✓		
Absorption Coefficient $a(z,\lambda)$		✓		
Backscattering Coefficient $b_b(z,\lambda)$		✓		
Scattering Coefficient $b(z,\lambda) = c(z,\lambda) - a(z,\lambda)$				✓
Volume Scattering Function $\beta(z, \lambda,\theta,\phi,\theta',\phi')$			✓	
Particle Absorption Coefficient $a_p(z,\lambda)$		✓		✓
Dissolved Material (CDOM) Absorption Coefficient $a_g(z,\lambda)$		✓		
Non-Pigmented Particle Absorption Coefficient $a_d(z,\lambda)$		✓		
Phytoplankton Absorption Coefficient $a_\phi(z,\lambda)$		✓		
Biogeochemical and Bio-Optical Quantities				
Phytoplankton Pigment Composition (HPLC method)	✓			
Chlorophyll a and Phaepigments Conc. (Fluorometric method)	✓			
Phycobiliprotein Concentrations			✓	
Coccolith Concentrations			✓	
Total Suspended Particulate Material (SPM)			✓	
Fluorescence Intensity, *in situ* profile $F(z)$		✓		
Ancillary Data and Metadata				
Latitude and Longitude	✓			
Date and Time (UTC)	✓			
Wave Height	✓			
Whitecap Conditions (fractional amount of surface)		✓		
Wind Speed and Direction	✓			
Surface Barometric Pressure	✓			
Cloud Cover (amount, and sun obscuration information)	✓			
Cloud Type		✓		
Secchi Depth	✓			
Water Depth	✓			
Conductivity and Temperature over Depth (CTD) $T(z)$, $S(z)$		✓		

Table 2.2   Principal *in situ* observations for satellite ocean color system validation, and algorithm development and validation.   The right-hand column identifies the protocol chapters and suggested applications. The application keys are: System Validation (1); Radiometric System Performance Validation and Vicarious Calibration (2); Atmospheric Correction Validation (3); Atmospheric Product Validation (4); Bio-Optical Product Validation (5); Algorithm Development and Validation (6); Atmospheric Property and Correction Algorithms (7); Bio-Optical Algorithms (8); IOP Algorithms and Semi-Analytic IOP-Based Algorithms (9); Normalized $L_w(\lambda)$ and $R_{RS}(\lambda)$ Algorithms (10); Metadata (all applications) (11) ; Quality Control (12); and All Above Applications (13).

	Protocol Chapters	*Applications Keys*
Radiometric Quantities		
Downwelled Irradiance $E_d(z,\lambda)$	9	1,5,6,8-10
Upwelled Radiance $L_u(z,\lambda) = L(z, \lambda,0,0)$	9,10	1-3,5,6,8-10
Upwelled Irradiance $E_u(z,\lambda)$	9	6,9,10
Radiance Distribution in water $L(z, \lambda,\theta,\phi)$	TBD	1,2,6,9,10
Water Surface Radiance in air $L_{sfc}(\lambda,\theta,\phi)$	10	1-3,5,6,8-10
Incident Irradiance in air $E_s(\lambda) = E_d(0^+,\lambda)$	6, 9-11	1,6,8,9,10,13
Normal Solar Irradiance $E_N(z,\lambda)$	6,11	1-4,6,7,10,12
Sky Radiance $L_{sky}(\lambda,\theta,\phi)$	10, 11	1-4,6,7,10
Diffuse Sky Irradiance $E_{sky}(\lambda)$	6, 9	1,6,13
Direct Sun Irradiance $E_{sun}(\lambda) = E_s(\lambda) - E_{sky}(\lambda)$	6, 9	1,6,13
Water-Leaving Radiance $L_w(\lambda,\theta,\phi,\theta_o,\phi_o)$	9-10	1,6,13
Remote Sensing Reflectance $R_{RS}(\lambda,\theta,\phi,\theta_o,\phi_o)$	9-10	1,6,13
Attenuation Coefficient $K(z,\lambda)$ for $E_d(z,\lambda)$ and $L_u(z,\lambda)$	9	1,5,6,8,9
Ocean Bidirectional Reflectance Distribution Function BRDF	TBD	1,6,13
Aerosol Optical Depth $\tau_a(\lambda)$	11	1-3,4,6,7
Aerosol Phase Function $P_a(\lambda,\theta,\phi,\theta',\phi)$	11	1-3,4,6,7
Absorbing Aerosol Height Profiles (LIDAR Profilometer)	TBD	1-3,6,7
Inherent Optical Properties		
Beam Attenuation Coefficient $c(z,\lambda)$	TBD	1,5,6,8-10
Absorption Coefficient $a(z,\lambda)$	TBD	1,5,6,8-10
Backscattering Coefficient $b_b(z,\lambda)$	TBD	1,5,6,8-10
Scattering Coefficient $b(z,\lambda) = c(z,\lambda) - a(z,\lambda)$	TBD	1,5,6,8-10
Volume Scattering Function $\beta(z, \lambda,\theta,\phi,\theta',\phi)$	TBD	1,5,6,8-10
Particle Absorption Coefficient $a_p(z,\lambda)$	12	1,5,6,8,9
Dissolved Material (CDOM) Absorption Coefficient $a_g(z,\lambda)$	12	1,5,6,8,9
Non-Pigmented Particle Absorption Coefficient $a_d(z,\lambda)$	12	1,5,6,8,9
Phytoplankton Absorption Coefficient $a_\phi(z,\lambda)$	12	1,5,6,8,9
Biogeochemical and Bio-Optical Quantities		
Phytoplankton Pigment Composition (HPLC method)	13	1,5,6,8,9
Chlorophyll a and Phaepigments Conc. (Fluorometric method)	14	1,5,6,8
Phycobiliprotein Concentrations	TBD	6,8
Coccolith Concentrations	TBD	1,5,6,8,9,12
Total Suspended Particulate Material (SPM)	8	5,6,8,12
Fluorescence Intensity, *in situ* profile F(z)	14	12
Ancillary Data and Metadata		
Latitude and Longitude	8	11
Date and Time (UTC)	8	11
Wave Height	8	12
Whitecap Conditions (fractional amount of surface)	8	12
Wind Speed and Direction	8	1-3,6,10,12
Surface Barometric Pressure	8	1,2,5
Cloud Cover (amount, and sun obscuration information)	8	6,10,12
Cloud Type	8	12
Secchi Depth	8	12
Water Depth	8	12
Conductivity and Temperature over Depth (CTD) T(z), S(z)	8	9,10,12

Chapter 3

Instrument Specifications, Characterization and Calibration Overview

James L. Mueller

Center for Hydro-Optics and Remote Sensing, San Diego State University, California

3.1 INTRODUCTION

A central focus of the SIMBIOS program, and of independent validation activities in the SeaWiFS and other ocean color sensor projects, is the estimation of uncertainties in satellite determinations of normalized water-leaving radiance (or equivalently, normalized remote-sensing reflectance), atmospheric correction and bio-optical algorithms, and derived products. In most cases, statistical comparisons with *in situ* measurements – or quantities derived from *in situ* measurements – play a central role in estimating the uncertainties in the satellite ocean color measurements, algorithms and derived products. The uncertainty budgets of *in situ* measurements used for comparisons are obvious critical factors in such validation analyses, as also are details and uncertainties of critical design and performance characteristics of the instruments with which they are measured.

This and the next several chapters specify appropriate instrument characteristics and describe accepted laboratory procedures for characterizing instruments to determine and verify their compliance with those specifications. Detailed characterization and calibration protocols for radiometers and sun photometers are provided in Chapters 5, 6 and 7. The status of each of these chapters, and topic areas in each where future advances and/or changes may be appropriate, are discussed briefly in sections 3.3 through 3.6. Because of the time constraints for publication of this version of the Ocean Optics Protocols, it has not been possible to provide a similar in-depth treatment for characterization and calibration of instruments used to measure inherent optical properties (IOP). The current state of the art regarding IOP instrument calibration is briefly abstracted below in Section 3.7. The SIMBIOS Project Office plans to sponsor focused workshops to prepare protocol chapters on IOP topics for a future update of the Ocean Optics Protocols. This document does not provide detailed methods for calibrating meteorological sensors, CTD instruments, pressure transducers, and other ancillary sensors. Sections 3.8 through 3.10 emphasize the importance of using properly calibrated sensors to make these important supporting measurements, but a well-established infrastructure for these calibration services exists within the general oceanographic and atmospheric communities.

3.2 EXTRATERRESTRIAL SOLAR FLUX SPECTRUM

These protocols, and SeaWiFS, MODIS and CZCS algorithms, are all predicated on using a single determination of the spectrum of extraterrestrial solar irradiance for the average distance between the earth and sun, $\overline{F}_o(1)$. Within the ocean color remote sensing and ocean optics communities, the presently accepted extraterrestrial solar flux spectrum is that of Neckel and Labs (1984). There is less unanimity in the atmospheric community, and in some segments of the international remote sensing community, in the choice of a "standard" solar spectrum.

It is absolutely essential that a single, common standard solar flux spectrum be used in every aspect of research and validation in ocean color remote sensing. The extraterrestrial solar flux enters into normalization of water leaving radiance, calibration and interpretation of atmospheric radiation measurements, and atmospheric correction algorithms for all satellite ocean color radiometers. For example, if normalized water leaving radiance were computed from *in situ* measurements using a "better" estimate of the solar flux, in lieu of Neckel and Labs (1984), a comparison with a satellite determination of normalized water-leaving radiance would be biased by the difference between the two solar spectra. There is some evidence (Biggar 1998; Schmid *et al*. 1998) that the recent measurements of Thuillier *et*

al. (1998) are more consistent with NIST traceable lamp-based irradiance and radiance sources. On the basis of such findings, it seems clear that NASA and the international ocean color community should reconsider the choice of a standard for extraterrestrial solar flux. Assuming that a change would improve the uncertainty budget of, e.g. atmospheric correction validations, the expected benefits are obvious. On the other hand, adopting a different solar spectrum would require significant changes in the software used for operational processing and validation analyses within SeaWiFS, MODIS and other ocean color satellite project offices. Any such transition must be planned and implemented comprehensively in a forum that embraces the entire international community. It would be appropriate for this task to be addressed by a working group convened under the auspices of the International Ocean Color Coordinating Group (IOCCG).

Until such time as a new standard is adopted, however, compliance with the present Ocean Optics Protocols requires that any analysis, or application, involving extraterrestrial solar irradiance $\overline{F}_o(\lambda)$ use the scale of Neckel and Labs (1984).

3.3 INSTRUMENT PERFORMANCE SPECIFICATIONS

Chapter 4 provides detailed specifications for performance-related characteristics of radiometers, and other types of instruments, that measure *in situ* variables used to validate satellite ocean color sensors, algorithms and derived products. The specifications in this revision (2.0) to the protocols are little changed from those in Mueller and Austin (1995). Most additions and changes are related to the characteristics of additional satellite instruments addressed under the SIMBIOS program.

Time constraints and conflicting schedule demands of key individuals precluded adequate community-wide review, debate and refinement of specifications in a few areas where instrument development has progressed significantly. Topic areas that should be reviewed thoroughly in preparation of this chapter for Revision 3 of the Ocean Optics Protocols (2001) include specifications of performance-related characteristics of:

1. hyperspectral radiance and irradiance spectrometers, especially those based on miniature fiber-optic monochromators; and

2. instruments used to measure IOP's (absorption, beam attenuation and backscattering) *in situ*.

3.4 CHARACTERIZATION OF OCEANOGRAPHIC AND ATMOSPHERIC RADIOMETERS

The procedures given here are essentially those from Mueller and Austin (1995). Changes and additions primarily reflect results and lessons learned from the SeaWiFS Intercomparison Round-Robin Experiment (SIRREX) series (e.g. Mueller *et al*. 1996; Johnson *et al*. 1996) and deal primarily with methods for transferring the NIST scale of spectral irradiance from an FEL lamp source to the responsivity scales of oceanographic and atmospheric radiometers. The SIMBIOS and SeaWiFS Project Offices are continuing the SIRREX series to assure maintenance of consistent radiometric calibration uncertainties throughout the community (Riley and Bailey 1998) and for better determination of, e.g., quantitative uncertaintites associated with radiance calibrations using Spectralon plaques (S. Hooker, pers. comm.).

The Chapter 5 protocols have also been changed to recommend experimental determination of immersion factors for every individual underwater irradiance collector. In Mueller and Austin (1995), it was suggested that immersion factors determined for a prototype irradiance collector could be used for other radiance collectors of the same size, design and material specifications. The results of Mueller (1995) demonstrated that individual deviations between collectors of the same design, size and materials may be as large as 8%, with a 3% RMS uncertainty for the group of such instruments tested. Using replicated tests and variations in setup configuration for each instrument tested, the experimental uncertainty associated with the immersion factor characterization procedure was shown to be less than 1% (Mueller 1995). Topic areas in Chapter 5 that should be reviewed and considered for possible inclusion in Revision 3 (2001) include:

1. Methods for applying to ocean radiometers (K. Carder and R. Steward, pers. comm.) the sun-based methods used in the atmospheric radiation community for calibrating sun photometers (Chapter 6 of these protocols (Schmid *et al*. 1998) and other radiometers (Biggar 1998). In this regard, the question of continuing to use the Neckel and Labs (1984) $\overline{F}_o(\lambda)$ spectrum, or an alternative such as that

of Thuillier *et al*. (1998), will become critically important (see the discussion in Sect. 3.2 above).

2. Uncertainty budgets associated with the use of Spectralon reflectance plaques for calibrating radiance sensors. In Revision 3, any changes in this subject area would reflect new results and conclusions from SIRREX-7 (S. Hooker, pers. comm.).

3. Improved methods for characterizing stray-light, spectral calibration, and slit responses in monochromator based hyperspectral spectrometers, which are increasingly being adopted and used within the ocean color research community.

3.5 CALIBRATION OF SUN PHOTOMETERS AND SKY RADIANCE SENSORS

Chapter 6 is a completely new addition to the protocols. The calibration and characterization of sun photometers and sky radiance sensors was covered very briefly in Mueller and Austin (1995), and no detailed method descriptions were provided. These new protocols are based on the methods developed within the atmospheric radiation community, and by the AERONET Project at GSFC and its collaborating institutions around the world. Protocols for calibrating Shadowband Radiometers are also new to the Ocean Optics Protocols. There is considerable overlap between Chapters 5 and 6, and there are some redundancies that should be reviewed carefully in preparation for Revision 3 to the Ocean Optics Protocols (in 2001).

3.6 STABILITY MONITORING OF FIELD RADIOMETERS USING PORTABLE SOURCES

Mueller and Austin (1995) recommended the development and use of portable standards to verify the stability of radiometers during deployment on research cruises, or other field deployments, of several weeks duration. These general recommendations were based on limited experience with prototype analog sources developed by Austin and his colleagues in the 1980's at the Scripps Visibility Laboratory. Since 1995, joint research by investigators at NIST and GSFC developed a much-improved prototype of a portable source, the SeaWiFS Quality Monitor (SQM), suitable for shipboard use (Johnson *et al.* 1998) and

demonstrated its ability to verify stability of radiometers with an uncertainty < 1% (Hooker and Aiken 1998). Subsequently, less expensive versions of the SQM have been developed and become commercially available. Chapter 7 provides a review of this development, detailed protocols for using SQM devices in the field, and uncertainty budgets.

3.7 CALIBRATION OF INHERENT OPTICAL PROPERTY SENSORS

Many significant improvements have been made, over the last five years, in the development and understanding of instruments used to measure inherent optical properties (IOP). Today, *in situ* profile determinations of the coefficients of absorption $a(z,\lambda)$, beam attenuation $c(z,\lambda)$ and backscattering $b_b(z,\lambda)$ – all in m^{-1} – are almost routinely made and reported by many investigators in the ocean optics and ocean color remote sensing communities. However, key members of the IOP subcommunity continue an active debate on the relative merits of alternative design characteristics of, and methods for calibrating and using, these first and second generation instruments. In the case of some instruments and measurements, e.g. the AC9 absorption and beam attenuation meters (see below), a *de facto* consensus is emerging on methods and uncertainty budgets. In these cases, it remains only to draft protocols and pass it though a critical review by the community; a focused workshop is often the surest way to do this quickly. In other cases, technical questions and valid criticisms remain to be answered before protocols can be distilled from various proposed methods; additional research to sort out uncertainties is clearly needed here.

The present version of the Ocean Optics Protocols does not provide complete protocols, or even provisional protocols, for either *in situ* measurements of IOP, or calibration of IOP instruments. It is planned to remedy that omission in a future revision of this document by including new chapters on *in situ* measurements of absorption, beam attenuation and backscattering. For the present, however, the closest thing to protocols are the methods and calibrations specified by instrument manufacturers, a few published journal articles, and informal instructions and reference materials provided via www pages by a few recognized experts in various aspects of IOP measurements.

Pure Water Absorption and Scattering Coefficients

The recommend values for the volume absorption coefficients of pure water, $a_w(\lambda)$ in m^{-1}, are those of Sogandares and Fry (1997) for wavelengths between 340 and 380 nm, Pope and Fry (1997) for wavelengths between 380 and 700 nm, and Smith and Baker (1981) for wavelengths between 700 and 800 nm. The recommended values for the volume scattering coefficients of pure water, $b_w(\lambda)$ in m^{-1}, are those of Morel (1974).

Single-Wavelenth Transmissometers

Relatively simple single-wavelength (usually near 660 nm) transmissometers have been in widespread use for two decades. Although the beam attenuation coefficients c(z,660) obtained with these devices are no longer state of the art measurements, the profiles of this variable are strongly correlated with concentrations of suspended particles. Protocols for using these instruments are unchanged from those in Mueller and Austin (1995).

The manufacturer first calibrates a transmissometer of this type by measuring its response in pure water. He also measures the open and blocked (dark) sensor responses in air and records these as *factory air calibration* coefficients. The user must perform air calibrations in the field. When transmissometer profiles are analysed (Chapter 8), the field and factory air calibrations are used to compensate for drift in the instrument's sensitivity over time.

The windows on the beam transmissometer must be cleaned with lens cleaner or a mild detergent solution and a soft cloth or tissue, rinsed with distilled water, then rinsed with isopropyl alcohol and wiped dry. An approximate *air calibration* reading should be made before every cast to verify that the windows are clean. A transmissometer *dark voltage* should also be measured at this time. These *on-deck air calibrations* are not, however, very reliable measures of temporal drift or degradation in the instrument's source or detector. In the humid, or even wet, environment on the deck of a ship, the windows are often quickly obscured by condensation, and the glass also tends to absorb enough water to affect transmission slightly (Zaneveld pers. comm.). A very careful air calibration should be performed before and after each cruise under dry laboratory conditions. During an extended cruise, it is also recommended to remove the instrument to a dry location in a

shipboard laboratory, and after allowing several hours for the windows to dehydrate, a careful air calibration should be performed. Only the laboratory air calibrations should be used in the final processing of beam transmissometer data.

Both the laboratory condition air calibration and dark voltages, and the factory calibration voltages, assume the data acquisition system measures instrument response as true volts. It is imperative, therefore, to calibrate the end-to-end analog-to-digital (A/D) data acquisition system and characterize its response $\tilde{V}$ to known input voltages $\hat{V}$. Corrections in the form of a linear function

$$\hat{V} = g(T)\tilde{V} + f(T), \qquad (3.1)$$

where T is temperature, must usually be applied to external voltage inputs recorded with the A/D circuits of CTDs or profiling radiometer systems. The range dependent A/D bias coefficients should be determined at approximately 5^0 C intervals, over the range from 0--25^0 C, to characterize the temperature sensitivity of the data acquisition system.

Absorption and Beam Attenuation Meters

The discussion in this section pertains only to instruments and calibration for *in situ* measurements of absorption. Protocols for laboratory spectrophotometric measurements of absorption by particles filtered from water samples, and by colored dissolved organic material (CDOM) in filtrate, are contained in Chapter 12 of this document.

It is increasingly common for ocean color investigators to measure the coefficients of absorption $a(\lambda)$ and beam attenuation $c(\lambda)$ using dual path transmissometers. In the beam attenuation path, a detector measures the light transmitted over the open path from a collimated source; both absorbed and scattered photons are attenuated. In the absorption part of the instrument, a beam of light passes through the center of a tube having a reflective wall that redirects most scattered photons into the forward direction toward a large detector which fills the exit cross section; only those photons that are either absorbed, or scattered in the backward direction, are attenuated. Because the backscattering by marine particles is a small fraction of their total scattering, it is possible to model this contribution and subtract it to obtain $a(\lambda)$ within a reasonable uncertainty. These devices may also be used to measure absorption by CDOM

if a 0.4 μm filter is inserted in the instrument's intake port. Since the beam attenuation coefficient is the sum of absorption and scattering, i.e.

$$c(\lambda) = a(\lambda) + b(\lambda), \ \text{m}^{-1}, \qquad (3.2)$$

it is also possible to determine the total scattering coefficient b(λ) as the difference between the measured values of c(λ) and a(λ).

Perhaps the best known example of this class of instruments is the AC9, which uses interference filters to measure a(λ) and c(λ) at 9 wavelengths. The AC9 is manufactured by WetLABS of Philomath, OR. Alternative instrument designs are also commercially available, e.g. from HOBILABS of Moss Landing, CA and other manufacturers. These protocols make no recommendations regarding specific manufacturers or instruments, and examples of specific instruments are included here only for purposes of illustrating general characteristics and procedures.

The instrument manufacturer performs two *factory calibration* procedures to first determine the instrument's temperature dependence, and second to record its response when optically clean water is being measured. To obtain good data, it is absolutely essential to repeat this second calibration measurement frequently (typically once per day) in the field. Protocols for carrying out calibrations are provided by each instrument's manufacturer. Additional protocols for calibrating the AC9, expanding on methods described in Twardowski *et al*. (1999), and other IOP instruments have been developed by the Optical Oceanography Group at Oregon State University and may be accessed via *http://photon.oce.orst.edu/* (S. Pegau, Pers. Comm.). Perhaps the most challenging aspects of these protocols deal with methods for using reverse-osmosis filtration systems to obtain optically pure water in the field, and with procedures to verify the optical purity of the water.

Backscattering Meters

There is little historic data on the variation of the shape of the volume scattering function β(θ,λ) in the backward direction. Petzold (1972) described the scattering function for selected natural waters measured with the General Angle Scattering Meter (GASM). This reference is the one most widely used to describe shapes of β(θ,λ). Since that time, only Balch *et al*. (1994) have published new *in situ* measurements, again using GASM, describing the shape of β(θ,λ) for marine hydrosols.

The GASM, built *circa* 1970 at the Scripps Institution of Oceanography's Visibility Laboratory (Petzold 1972), consists of a lamp focused into a cylindrical beam, and a narrow field of view detector mounted to swing in an arc to view the beam at many off-axis scattering angles between approximately 10° and 170°. At each incremental angle, the instrument pauses and light scattered from the source beam into the detector's field of view is measured. The phase functions at different wavelengths are determined by changing interference filters. The next generation of instruments were designed to measure β(θ,λ) at a single wavelength (typically 532 nm) and a single angle, e.g. 150° (Maffione et al. 1991) or 170° (Smart 1992). The first commercial versions of these so-called *backscattering meters*, the HydroScat series of instruments manufactured by HOBILABS Inc. (*www.hobilabs.com*), measure scattering at a centroid angle of 140° at several fixed wavelengths (Maffione and Dana 1997). A more recent entry into this market is the ECO-VSF series of scattering meters manufactured by WETLABS (*www.wetlabs.com*), which are designed to measure scattering at a single wavelength (450, 530 or 650 nm) but at three scattering centroid angles 100°, 120° and 150°.

Any sensor designed to measure β(θ,λ), at any nominal scattering angle θ , actually measures a weighted integral of radiance scattered from a working volume defined by the intersection of the illumination source beam and angular field of view of the detector system. The source illumination is attenuated by the factor $e^{-r(\theta)c(\lambda)}$ over the slightly varying pathlength r(θ) from source to detector through each infinitesimal element of the finite working volume. If both source illumination and detector angular response functions are azimuthally symmetric about their nominal axes, and the working volume is very small, the integral may be expressed in the relatively simple conceptual form

$$\overline{\beta}\left(\overline{\theta},\overline{\lambda};c\right) = 2\pi \int_{\Delta\lambda} \int_0^\pi \beta(\theta,\lambda) W(\theta,\lambda;c)\sin\theta \, d\theta \, d\lambda,$$
$$\text{m}^{-1}\,\text{sr}^{-1}, \qquad (3.3)$$

where the weighting function W(θ,λ;c) accounts for the angular θ and wavelength λ dependencies of illumination and detector response functions, and attenuation over a variable pathlength, in each each infinitesimal subelement of the working volume. The parameters $\overline{\theta}$ and $\overline{\lambda}$ are respectively the centroid scattering angle and wavelength of the weighted integral. The functional form and

detailed parametric dependencies of the weighting function are greatly abstracted in (3.3), which is presented here only as a conceptual framework for the discussion. The weighting function can be measured by moving a Spectralon reflective target through the working volume (Maffione and Dana 1997), a procedure that also serves to calibrate the device. Alternatively, if the spectral and geometric distribution functions of the source illumination and detector response are well characterized, the weighting function can be calculated from first principles (Zaneveld and Twardowski, Pers. Comm), albeit based on a geometrically more complicated form of the integral equation abstracted here as (3.3). Given the weighting function, the scattering sensor may be calibrated by measuring its response to scattering by polystyrene spheres, the scattering functions of which may be accurately determined using Mie scattering computations (Zaneveld and Twardowski, Pers. Comm).

The scattering parameter of principal interest in the context of the Ocean Optics Protocols for Satelline Ocean Color Sensor Validation is the backscattering coefficient

$$b_b(\boldsymbol{l}) = 2\boldsymbol{p}\int_{\frac{\boldsymbol{p}}{2}}^{\boldsymbol{p}} \boldsymbol{b}(\boldsymbol{q}, \boldsymbol{l})\sin\boldsymbol{q}d\boldsymbol{q}, \ \text{m}^{-1}, \quad (3.4)$$

assuming azimuthal symmetry. Clearly none of the sensors described above measure $b_b(\lambda)$. To estimate the backscattering from measured $\overline{\boldsymbol{b}}(\overline{\boldsymbol{q}}, \overline{\boldsymbol{l}}; c)$ at a single angle, one invokes the mean value theorem to observe that there must be at least one angle θ^* for which (3.4) reduces to

$$\begin{aligned} b_b(\boldsymbol{l}) &= 2\boldsymbol{p}\boldsymbol{b}(\boldsymbol{q}^*, \boldsymbol{l})\int_{\frac{\boldsymbol{p}}{2}}^{\boldsymbol{p}}\sin\boldsymbol{q}d\boldsymbol{q} \\ &= 2\boldsymbol{p}\boldsymbol{b}(\boldsymbol{q}^*, \boldsymbol{l}). \end{aligned} \quad (3.5)$$

Clearly, θ^* will vary between volume scattering functions of differing shape in the backward direction, and measured values $\overline{\boldsymbol{b}}(\overline{\boldsymbol{q}}, \overline{\boldsymbol{l}}; c) \neq \boldsymbol{b}(\boldsymbol{q}^*, \boldsymbol{l})$ even if $\overline{\boldsymbol{q}} = \boldsymbol{q}^*$ and $\overline{\boldsymbol{l}} = \boldsymbol{l}$. Oishi (1990) carried out a series of Mie scattering calculations for polydispersions of spheres, assuming a variety of different size distributions similar to those observed for marine hydrosols. He then assumed there would be some constant θ^* at which backscattering coefficients calculated with (3.5) would be linearly related to exact values of $b_b(\lambda)$ with a reasonable level of RMS uncertainty. He therefore revised (3.5) to the form

$$\hat{b}_b(\boldsymbol{l}) = 2\boldsymbol{pc}\boldsymbol{b}(\boldsymbol{q}^*, \boldsymbol{l}) \quad (3.6)$$

and found the minimum RMS deviations at $\theta^* = 120^o$ with $\chi = 1.14$, but the smallest maximum prediction error occurred at $\theta^* = 140^o$ with $\chi = 1.08$. Maffione and Dana (1997) independently repeated an analysis similar to Oishi's (1990) and found that, for $\theta^* = 140^o$ with $\chi = 1.08$, the uncertainty in backscattering coefficients estimated with (3.6) is ~9%. This is essentially the algorithm provided with the HOBILABS HydroScat instruments. The algorithm recommended for use with the WETLABS ECO-VSF instrument uses the 3-angle scattering measurements to adjust (3.6) for variations in the shape of the phase functions, but the underlying premise and approach to estimating the backscattering coefficient are otherwise similar (Beardsley and Zaneveld 1969; Zaneveld and Twardowski, Pers. Comm.).

Measurements of backward scattering have also been made using benchtop laboratory instruments, and either discrete water samples, or water pumped in a "flow-through" mode. Tassan and Ferrari (1995), for example, used a dual-beam spectrophotometer, with an integrating sphere attachment, to measure total and backward scattering by mineral particles suspended in water. Balch et al. (1999) used a benchtop laser device manufactured by Wyatt Technologies to measure $\overline{\boldsymbol{b}}(\overline{\boldsymbol{q}}, \overline{\boldsymbol{l}}; c)$, in discrete and flow-through sampling modes, at several angles and two wavelengths. The coefficient $b_b(\lambda)$ was then estimated by fitting measurements at $\overline{\boldsymbol{q}} = 45^o$, 90° and 135° to the function recommended by Beardsley and Zaneveld (1969), and then integrating that function from 90° to 180°.

Calibration of the Wyatt Technologies volume scattering device uses a solid isotropic scattering standard provided by the manufacturer. The composition of the standard is a proprietary secret of Wyatt Technologies, and only the calibration coefficients are provided to the user. Because of the undisclosed properties of its calibration standard, the Wyatt Technologies device must be viewed as a "black box" that must be evaluated through independent comparisons with other known standards, before its use can be accepted as part of a general protocol.

3.8 CALIBRATION OF METEOROLOGICAL SENSORS

The uncertainties of several meteorological variables are significant components of uncertainty budgets associated with using *in situ* measurements to validate satellite ocean color measurements and algorithms. Uncertainty in barometric pressure can affect that of absorption terms in atmospheric correction algorithms. Uncertainty in surface wind velocity directly affects sun and sky glint reflection estimates used to correct water-leaving radiance determinations from satellites and *in situ* above-water radiometers. Anemometers, barometers, thermometers (air temperature), and hygrometers should be calibrated using methods and at intervals recommended by the World Metorological Organization (WMO). Calibration services and certification are available through the vendors who supply meteorological instruments, and in the laboratories of some academic oceanographic and/or atmospheric institutions.

3.9 CTD CALIBRATION

The conductivity probe, temperature probe, and pressure transducer of the CTD should be recalibrated before and after each major cruise by a properly equipped physical oceanographic laboratory, including those maintained by many university oceanography departments and CTD manufacturers. In addition, the conductivity probe should be independently calibrated during the course of each cruise by obtaining salinity water samples simultaneous with CTD readings. These salinity samples are to be analyzed, either at sea or ashore, with a laboratory salinometer calibrated with International Association for the Physical Sciences of the Ocean (IAPSO) Standard Seawater.

3.10 PRESSURE TRANSDUCER CALIBRATIONS

It is important to frequently calibrate pressure transducers on oceanographic profiling instruments. For purposes of these protocols, the pressure in decibars is equivalent to depth in meters. Adjustments for the density of seawater are negligible in the present context. On the other hand, inaccurate calibration of the pressure sensor will lead to artifacts and increased uncertainty in, e.g., the computation of the diffuse attenuation coefficients $K(z, \lambda)$. If an instrument's pressure transducer port is equipped with a threaded fitting, a hose filled with distilled water may be used to connect it to a hand-pump and NIST traceable dead weight tester (several models are commercially available). Another common arrangement is to immerse the instrument in a pressure chamber, which is connected in turn to the pump and pressure calibration device. In either case, water pressure is increased in steps to produce several readings spanning the operating range of the instrument under test, and a polynomial equation is fit to the data to relate transducer output to the pressures measured with the dead-weight tester. Detailed methods and a certificate of NIST traceable calibration should be obtained from the manufacturer of the pressure calibration device. Calibration services of this type are readily available, on a fee-for-service basis, at laboratories maintained by many oceanography departments and commercial vendors of oceanographic equipment.

If simultaneous deployment of the CTD with optical instruments having independent pressure transducers is practical, the two depths measured by the different instruments should be compared over the range of the cast. If depth measurements disagree significantly, these comparisons may be used to correct whichever transducer is found to be in error through analysis of pre- and post-cruise pressure transducer calibrations.

REFERENCES

Balch, W.M., D.T. Drapeau, T.L. Cucci, R.D. Vaillancourt, K.A. Kilpatrick and J.J. Fritz, 1999: Optical backscattering by calcifying algae separating the contribution by particulate inorganic and organic carbon fractions. *J. Geophys. Res*. **104**: 1541-1558.

Balch, W.M., P.M. Holligan, S.G. Ackleson, and K.J. Voss, 1991: Biological and optical properties of mesoscale coccolithophore blooms in the Gulf of Maine. *Limnol. Oceanogr.*, **36**: 629-643.

Beardsley, G.F. and J.R.V. Zaneveld, 1969: Theorectical dependence of the near-asymptotic apparaent optical properties on the inherent optical properties of sea water. *J. Optical Soc. Amer.* **59**: 373-377.

Biggar, S.F. 1998: Calibration of a visible and near-infrared portable transfer radiometer. *Metrologia*, **35**: 701-706.

Hooker, S.B. and J. Aiken, 1998: Calibration evaluation and radiometric testing of field radiometers with the SQM. *J. Atmos. Oceanic Tech.*, **15**: 995-1007.

Johnson, B.C., S.S. Bruce, E.A. Early, J.M. Houston, T.R. O'Brian, A. Thompson, S.B. Hooker and J.L. Mueller, 1996: The Forth SeaWiFS Intercalibration Round-Robin Experiment (SIRREX-4), May 1995. *NASA Tech. Memo. 104566, Vol. 37,* S.B. Hooker, E.R. Firestone and J.G. Acker, Eds., NASA GSFC, Greenbelt, Maryland, 65 pp.

Johnson, B.C., P-S. Shaw, S.B. Hooker and D. Lynch, 1998: Radiometric and engineering performance of the SeaWiFS Quality Monitor (SQM): a portable light source for field radiometers. *J. Atmos. Oceanic Tech.*, **15**: 1008-1022.

Maffione, R.A. and D.R. Dana: Instruments and methods for measuring the backward-scattering coefficient of ocean waters. *Appl. Opt.* **36**: 6057-6067.

Mueller, J.L., 1995: Comparison of irradiance immersion coefficients for several marine environmental radiometers (MERs), In: Mueller, J.L. and others, Case Studies for SeaWiFS Calibration and Validation, Part 3. *NASA TM 104566*, Vol. **27**: 3-15*,* Hooker, S.B., E.R. Firestone and J.G. Acker, Eds.

Mueller, J.L., and R.W. Austin, 1995: Ocean Optics Protocols for SeaWiFS Validation, Revision 1. *NASA Tech. Memo. 104566, Vol. 25,* S.B. Hooker, E.R. Firestone and J.G. Acker, Eds., NASA GSFC, Greenbelt, Maryland, 67 pp.

Mueller, J.L., B.C. Johnson, C.L. Cromer, S.B. Hooker, J.T. McLean and S.F. Biggar, 1996: The Third SeaWiFS Intercalibration Round-Robin Experiment (SIRREX-3), 19-30 September 1994. *NASA Tech. Memo. 104566, Vol. 34,* S.B. Hooker, E.R. Firestone and J.G. Acker, Eds., 78 pp.

Morel, A., 1974: Optical properties of pure water and pure sea water. In: *Optical Aspects of Oceanography*, N.G. Jerlov and E.S. Nielson, Eds., pp1-23.

Neckel, H., and D. Labs, 1984: The solar radiation between 3,300 and 12,500 AA. *Solar Phys.*, **90**: 205--258.

Oishi, T., 1990: Significant relationship between the backward scattering of sea water and the scatterance at 102o. *Appl. Opt.* **29**:4658-4665.

Petzold, T.J., 1972: Volume Scattering Functions for Selected Ocean Waters. *SIO Ref. No. 72--78*, Scripps Institution of Oceanography, La Jolla, California, 79 p.

Pope, R.M. and E.S. Fry. 1997: Absorption spectrum (380-700 nm) of pure water. II. Integrating cavity measurements. *Appl. Opt.* **36**: 8710-8723.

Riley, T. and S. Bailey, 1998: The Sixth SeaWiFS Intercalibration Round-Robin Experiment (SIRREX-6) August—December 1997. *NASA/TM-1998-206878*. NASA, Goddard Space Flight Center, Greenbelt, MD. 26pp.

Schmid, B., P.R. Spyak, S.F. Biggar, C. Wehrli, J. Seider, T. Ingold, C. Matzler and N. Kampfer. 1998: Evaluation of the applicability of solar and lamp radiometric calibrations of a precision Sun photometer operating between 300 and 1025 nm. *Appl. Opt.* **37**: 3923-3941.

Smith, R.C. and K.S. Baker. 1981: Optical properties of the clearest natural waters (200-800 nm). *Appl. Opt.* **20**:177-184.

Sogandares, F.M. and E.S. Fry. 1997: Absorption spectrum (340-640 nm) of pure water. I. Photothermal measurements. *Appl. Opt.* **36**: 8699-8709.

Tassan, S. and G.M. Ferrari, 1995: Proposal for the measurement of backward and total scattering by mineral particles suspended in water. *Appl. Opt.* **34**: 8345-8353.

Thuillier, G., M. Herse, P.S. Simon, D. Labs, H. Mandel, D. Gillotay and T. Foujols. 1998: The visible solar spectral irradiance from 350 to 850 nm as measured by the SOLSPEC spectrometer during the Atlas I mission. *Solar Phys.* **177**: 41-61.

Twardowski, M.S., J.M. Sullivan, P.L. Donaghay and J.R.V. Zaneveld. 1999: Microscale quantification of the absorption by dissolved and particulate material in coastal waters with an AC-9. *J. Atmos. Oceanic Tech.* **16**: 691-707.

Chapter 4

Instrument Performance Specifications

James L. Mueller and Roswell Austin

Center for Hydro-Optics and Remote Sensing, San Diego State University, California

4.1 INTRODUCTION

This report describes measurements of optical properties, and other variables, necessary for validating data obtained with satellite ocean color instruments, and for the development of in-water and atmospheric algorithms. The specifications herein are those required of instruments used on ships, or other platforms, to acquire that *in situ* data. In some cases, the specifications have been selected to allow use of instruments that are affordable and that either currently exist, or that can be developed without major improvements in today's state-of-the-art technology. In a few cases, new or improved instruments must be developed to realize the specified performance characteristics. The data uncertainty requirements for this program are more severe than those for a general ocean survey. Here, various investigators will use a variety of instruments that will be calibrated independently at a number of facilities, and contribute data to a common database which will be used to validate SeaWiFS and other satellite ocean color measurements. The resulting radiometric and bio-optical database will provide an essential means of detecting and quantifying on-orbit changes in the satellite instruments relative to their prelaunch calibrations and characterizations. This chapter specifies instrument characteristics and data uncertainties thought by the SPSWG to be necessary, as well as sufficient, for this task. The validation analysis would be significantly degraded should calibration errors or differences of even a few percent, or wavelength errors or differences of a few nanometers, occur in (between) the instruments used to acquire the validation *in situ* bio-optical database.

4.2 IN-WATER RADIOMETERS

This section specifies radiometric characteristics for instruments that are used to measure $E_d(z, \lambda)$, $E_u(z, \lambda)$ and $L_u(z, \lambda)$. The specifications are applicable to filter radiometers and to spectroradiometers based on monochromators. Minimum performance characteristics are specified for spectral resolution, radiometric responsivity and resolution, signal-to-noise ratios (SNRs), radiometric saturation and minimum detectable values, angular response, temporal sampling resolution, linearity, and stability.

Spectral Characteristics

In-water radiometers shall be capable, as a minimum, of making measurements at the wavelengths shown in Table 4-1, which refers specifically to the SeaWiFS channels. The SeaWiFS channel wavelength combination is consistent with the recommended preferred ocean radiance channel combination (C3) recommended by Morel et al. (1998), albeit with wider spectral bandwidths. For the SIMBIOS *in situ* validation database, the wavelength combinations in Table 4-1 must be expanded to provide radiance and irradiance measurements at the greater number of wavelengths represented by the full ensemble of ocean color sensors (Appendix A). For example, OCTS and POLDER each had a channel at 565 nm, rather than that at 555 nm on SeaWiFS. For purposes of these protocols, in-water radiometer channels at these additional wavelengths must match the satellite channel wavelengths and have FWHM bandwidths within the same tolerances described below with reference to Table 4-1.

Table 4-1 presumes the use of properly blocked interference filters to provide the required spectral bandpass and out-of-band rejection (10^{-6} or better). Care must also be taken to avoid possible out-of-band leakage due to fluorescence by filter, or other optical component, materials. Filter radiometers should have channels with center wavelengths, as measured in the assembled instrument, matching those given in Table 4-1 to within ± 1 nm for 410 and 443nm, and within ± 2 nm for all other spectral bands. Shifts of these magnitudes in center wavelengths will result in changes in measured radiometric values of approximately ±1% or less (Booth pers. comm.) and this specification should

be met if possible. It is recognized, however, that enforcing a ± 1 nm hard-and-fast specification could be prohibitively expensive, and this tolerance should be regarded as a goal. With knowledge, to less than 0.2 nm, of the actual center wavelengths and complete spectral response functions, corrections probably can be made to infer effective radiometric quantities for the satellite instrument channels. Bandwidths must be 10 nm ± 2 nm FWHM. They are made narrower than, for example, the SeaWiFS channels to reduce the skewing of the parameters derived from underwater irradiance, or radiance, profiles in spectral regions where absorption by natural sea water exhibits rapid variation with wavelength.

Table 4.1. Recommended spectral bands for discrete wavelengh filter radiometers using 10nm full-width at half-maximum (FWHM) bandwidths. In addition, out-of-band blocking in the tails of the instrument response functions should be at least 10^{-6}.

SeaWiFS Band	Wavelenghts [nm]	E_d, E_u, L_u [nm]	E_s [nm]
1	402-422	412[1]	412
2	433-453	443,435[2]	443
3	480-500	490	490
4	500-520	510	510
5	545-565	555	555
6	660-680	665,683	665
5	545-565	555	555
6	660-680	665,683	665[3]
7	745-785	[4]	780
8	845-885	[4]	875[5]

1. A preferred option is to replace two separate 10nm FWHM bands centered at 406 and 416nm, with a single 412 nm channel. The two channels would allow more accurate modeling of L_{WN} (412) matching SeaWiFS charactericis.
2. An optional extra band is used to improve modeling of L_{WN} (λ) radiances to match the SeaWiFS 443 nm channel.
3. E_s deck, only channel in this band is necessary.
4. Due to the specialized nature of infrared in-water measurements, specialized sensors will be needed.

To maintain the above tolerances, it is anticipated that filters will be ordered to a center wavelength with a tolerance of λ_0, ±1 nm and a FWHM bandwidth of 8.5 ±1 nm. When the filter is installed in a radiometer with a 10° (half-angle) FOV, however, the spectral bandpass will broaden by 2-3nm, and the center wavelength will shift. Furthermore, as a filter ages in use, its transmission

curve may undergo changes to further broaden the FWHM bandpass and shift the peak. The tolerances specified above include an allowance for some degradation before expensive filter and detector changes must be done. In a single instrument, all channels at a given nominal wavelength should match within 1 nm, if possible. It is desirable, therefore, to obtain all of the filters used by an investigator for measurements at any nominal wavelength (λ_n) from a single manufacturing lot when possible. If this is done, $E_s(\lambda_n)$, $E_d(\lambda_n)$, $E_u(\lambda_n)$, and $L_u(\lambda_n)$, and any atmospheric radiometric quantities measured with that investigator's systems, would all have a greater likelihood of being measured over the same range of wavelengths, for each nominal wavelength (λ_n). In any event, the actual spectral response function of each instrument channel must be measured and known with an uncertainty less than 0.2 nm.

High resolution monochromator-based spectroradiometers, with adequate sensitivity and stray light rejection characteristics, are also suitable instruments and are recommended for many algorithm development studies. Suitable specifications for such instruments are given in Table 4-2. (These instruments must also meet the specifications summarized in Tables 4-1 and 4-3.)

Table 4-2. High resolution spectroradiometric specifications

Optical Sensors	
Spectral Range:	380 to 750 / 900 nm
Spectral Resolution:	5 nm (or less FWHM)
Wavelenght Accurancy:	10% FWHM of resolution (0.5 nm)
Wavelenght Stability:	5% FWHM of resolution (0.25 nm)
Signal-to-Noise Ratio:	1,000:1 (at minimum)
Stray Light Rejection:	10^{-6}
Radiometric Accuracy:	3%
Radiometric Stability:	1%
FOV Maximum:	10° (for radiance)
Temperature Stability:	Specified for 0–35°C
Linearity:	Correctable to 0.1%
Ancillary Sensors	
Temperature:	0.2°C
Pressure:	0.1% (full scale)
Horizontal Inclination:	1° over 40° range

Responsivity, SNR, and Resolution

The expected operating limits for radiometric responsivities, SNR, and digital resolution are specified in Table 4-3, the limits for which were derived as follows:

1. An E_d saturation value of 300 μW cm^{-2} nm^{-1} is assumed at all wavelengths.
2. Implicit, but not stated, in Table 4-3 is that the minimum required E_d (0) is 20 μW cm^{-2} nm^{-1}; it will not be appropriate to occupy validation stations when illumination is less than this minimum.
3. The minimum $E_d(0)$ implies a minimum detectable $E_d(z)$ value of $1\mu W$ cm^{-2} nm^{-1} at 3 optical depths (3/K).
4. Digital resolution must be less than or equal to 0.5% of the reading to maintain a 100:1 SNR. To permit a 1% uncertainty in absolute calibration, if that goal can be met in the calibration laboratory, the instrument must digitally resolve 0.1% of the irradiance (radiance) produced by the laboratory standards used; typical irradiance (radiance) values for calibration using 1,000 W FEL standard lamps traceable to the National
5. Institute of Standards and Technology (NIST), and required digital resolutions at these signal levels, are given in Table 4-3 as ``Calibration Irradiance'' and ``Digital Resolution (cal.),'' respectively. A SNR of 100:1 requires a resolution in $E_d(z)$ at three optical depths to 0.005 μW cm^{-2} nm^{-1} per count, i.e., 2.5 digit resolution. At the surface, E_d (0) should be resolved to 0.05 μW cm^{-2} nm^{-1} per count.
6. The Case-1 saturation values of E_d (0) represent the *Instrument Specification Subgroup's* (Mueller and Austin 1992) estimate of maximum reflectances to be expected in ordinary Case-1 waters: 12.5% at 410 nm, 7.5% at 488 nm and 0.5% at 670 nm. These saturation values will be too low for measurements in Case-2 waters or coccolithophore blooms. In these situations, a maximum expected reflectance of 40% for λ <660 nm and 20% for $\lambda \geq$ 660,nm is assumed. This implies that the expected maximum irradiance in E_d (0) should be 80 μW cm^{-2} nm^{-1} for λ <660 nm and 40 μW cm^{-2} nm^{-1} for $\lambda \geq$ 660 nm.
7. The minimum required irradiances at three optical depths (as given in Table 4-3) assumes minimum reflectances of 1% at 410 nm, 2% at 488 nm, and 0.15% at 670 nm.
8. The saturation and minimum radiances, and radiance responsivity resolutions, for L_u (0) and L_u (3/K_d) are calculated as Lu/Eu = 1/Q times the corresponding specification for E_u (0) or E_u (z). In Mueller and Austin (1995) it was assumed that Q = 5, a constant, at all wavelengths and depths. Morel and Gentili

(1996) showed that Q actually varies between approximately 3.14 and 5 at 410 and 488 nm, and between approximately 3.14 and 5.7 at 670 nm. Saturation radiances, for the worst case of Q = 3.14 (very clear waters with the sun nearly overhead), are increased by a factor of 1.6 at all three wavelengths relative to Mueller and Austin (1995). Minimum radiances at 670 nm, for the worst case of Q = 5.7 (turbid waters and solar zenith angle > 60°), are decreased by a factor of 0.75, and the implied digital resolution at 670 nm was changed accordingly. Minimum expected radiances and required digital resolution at 410 and 488 nm are unchanged.

The specifications in Table 4-3 are meant as guidance to interpret the following required performance requirements:

a) The instrument must maintain a 100:1 SNR at every operating range encountered, during field measurements.
b) The data for measurements obtained in the field must be recorded with a digital resolution less than or equal to 0.5% of reading.
c) The dynamic range of the instrument's linear sensitivity must extend to include the signal levels encountered during laboratory calibrations, and the calibration signals must be recorded with a digital resolution of 0.1% of reading to permit 1% uncertainty in calibration.

In general, the above performance specifications do not pose exceptionally difficult engineering challenges, with the possible exception of the full dynamic range implied by Case-2 or coccolith saturation radiance L_u (665) to minimum expected L_u (665). In any event, this situation will require specially designed radiometers (Section 4.1.8). It is not necessary that every radiometer used for satellite ocean color sensor validation

Table 4-3.   Required instrument and sensitivities for SeaWiFS validation and algorithm development as a function of radiometric measured variable and wavelength.

Property	Variable	410 nm	488 nm	665 nm	Comment
$E_d(z, \lambda)$,	$E_d(0)_{max}$	300	300	300	Saturation Irradiance
Downwelled	$E_d\left(\dfrac{3}{K_d}\right)$	1	1	1	Minimum Expected Irradiance
Irradiance	$\dfrac{dE}{dN}$	5×10^{-3}	5×10^{-3}	5×10^{-3}	Digital Resolution (profiles)
	$\dfrac{dE}{dN}$	5×10^{-2}	5×10^{-2}	5×10^{-2}	Digital Resolution (surface unit)
$E_u(z, \lambda)$,	$E_u(0)_{max}$	120	120	60	Saturation Irradiance (Case-2/coccoliths)
Upwelled		37	22	1.5	Saturation Irradiance (Case-1)
Irradiance	$E_u\left(\dfrac{3}{K_d}\right)$	1×10^{-2}	2×10^{-2}	1.5×10^{-3}	Minimum Expected Irradiance
	$\dfrac{dE}{dN}$	5×10^{-4}	5×10^{-4}	5×10^{-5}	Digital Resolution (surface unit)
	$\dfrac{dE}{dN}$	5×10^{-5}	5×10^{-5}	5×10^{-6}	Digital Resolution (profiles)
$L_u(z, \lambda)$,	$L_u(0)_{max}$	38	38	13	Saturation Radiance (Case-2/coccoliths)
Upwelled		12.0	7.2	0.5	Saturation Radiance (Case-1)
Radiance	$L_u\left(\dfrac{3}{K_d}\right)$	2×10^{-3}	4×10^{-3}	2.25×10^{-4}	Minimum Expected Radiance
	$\dfrac{dL}{dN}$	5×10^{-4}	5×10^{-4}	5×10^{-5}	Digital Resolution (surface unit)
	$\dfrac{dL}{dN}$	5×10^{-5}	5×10^{-5}	1×10^{-6}	Digital Resolution (profiles)
E_{cal}, Source	E_{cal}	2	5	15	Calibration Irradiance
Irradiance	$\dfrac{dE}{dN}$	2×10^{-3}	5×10^{-3}	1×10^{-2}	Digital Resolution (E_d, E_s, E_u cal.)
L_{cal}, Source	L_{cal}	0.6	1.5	4.5	Calibration Radiance
Radiance	$\dfrac{dL}{dN}$	6×10^{-4}	1×10^{-3}	4×10^{-3}	Digital Resolution (L_u cal.)

Notes: 1. E_u and E_d are in units of mW cm^{-2} nm^{-1} and L_u is in units of mW cm^{-2} nm^{-1} sr^{-1}.
2. Responsivity resolution in radiometric units per digital count at the minimum required signal level.
3. Specified ranges should maintain a 100:1 SNR.

operate over the full dynamic ranges given in Table 4-3. A radiometer is merely required to maintain the above performance specifications over the dynamic ranges of irradiance and radiance existing at locations and associated illumination conditions where it is used for validation or algorithm development.

Linearity and Stability

Errors attributable to linearity or stability should be less than 0.5% of the instrumental readings over the dynamic ranges specified in Table 4-3. This is a challenging goal, but one which must be met if the equally challenging goal of achieving

1% uncertainty in absolute calibration is to be meaningful.

Sampling Resolution

Sampling frequency should be compatible with the profiling technique being used. For the preferred multispectral filter radiometers and spectroradiometric (dispersion) instruments using array sensors, the minimum sampling frequencies are determined by the profiling rate and the depth resolution required. In general, five or more samples per meter should be obtained at all wavelengths. All channels of E_d (z, λ), E_u (z, λ) and L_u (z, λ) at all wavelengths should be sampled within 10^{-2} s at each given depth.

The time response of the instrument to a full-scale (saturation to dark) step change in irradiance should be less than one second to arrive at a value within 0.1%, or one digitizing step, whichever is greater, of steady state. In addition, the electronic *e*-folding time constant of the instrument must be be consistent with the rate at which the channels are sampled, i.e., if data are to be acquired at 10 Hz, the *e*-folding time constant should be 0.2s to avoid aliasing. Individual data scans may be averaged to improve signal-to-noise performance, provided adequate depth resolution is maintained.

Angular Response Characteristics

The response of a cosine collector to a collimated light source incident at an angle ( ) from the normal must be such that:

1) for E_u measurements, the integrated response to a radiance distribution of the form L( ) $\propto$ 1+4 sin should vary as cos accurate to within 2%; and

2) for E_d measurement, the response to a collimated source should vary as cos accurate to less than 2% for angles $0^o<$ 65° and 10% for angles $65^o<$ 85°.

Departures from cos will translate directly to approximately equal errors in E_d in the case of direct sunlight. The in-water FOV for upwelled radiance bands should be approximately 10° (half-angle). The resulting solid angle FOV (approximately 0.1 sr) is large enough to provide reasonable levels of flux, using silicon detectors, yet small enough to resolve the slowly varying (with for $<30^o$) field of upwelled radiance. Smaller FOV sensors are appropriate, of course, if all of the other performance specifications are satisfied.

Operating Depth

The instruments shall be capable of operating to depths of 200m. Depths should be measured with an uncertainty of 0.5m and a repeatability of 0.2m for radiometric profiles at visible wavelengths.

Instrument Attitude

The orientations of the instrument with respect to the vertical shall be within $\pm 10^o$, and the attitude shall be measured with orthogonally oriented sensors from 0-30° with an uncertainty of $\pm 1^o$ in a static mode; it is not intended that this uncertainty be maintained while an instrument is subject to large accelerations induced by surface waves. These data shall be recorded with the radiometric data stream for use as a data quality flag.

Red and Near-Infrared Wavelengths

The fact that red and near-IR channels---e.g. SeaWiFS bands 6, 7, and 8 at wavelengths of 665, 780, and 865nm, respectively---have such short attenuation lengths in water requires that special attention must be paid to these measurements. Problems due to instrument self-shading (Gordon and Ding 1992) and very rapid attenuation of L_u (z,) must be considered at these wavelengths. Large diameter instruments, and radiometers mounted on large instrument packages, are not adaptable to these measurements.

Suggested procedures for making the measurements are to use either fiber optic probes carrying light back to a remote instrument, or very small single-wavelength discrete instruments. Each of these concepts is adaptable to deployment from a small floating platform. Care must be taken to avoid direct shading by the supporting platform, but at these wavelengths, the large attenuation coefficients of water makes shadowing by objects more than a few meters away irrelevant.

The minimum measurement scheme would be two discrete (10 nm FWHM) channels at 780 and 875 nm. Additional channels at 750 and 850 nm, or more elaborately, high resolution spectroradiometry, would be useful in determining the spectral distribution of the upwelling light field in these bands.

These measurements should be performed as part of the standard validation data acquisition, because of their importance in the atmospheric correction algorithms. It is anticipated that in the majority of cases, and particularly in most Case-1 waters, these measurements will show negligible

upwelling light. In Case-2 waters, cases of extremely high productivity, or in coccolithophore blooms, at these wavelengths may be significant, and these measurements will become very important. When in-water measurements are performed at these wavelengths, the deck cell channels should be expanded to include bands at 750 and 875 nm (Table 4-1).

4.3 SURFACE IRRADIANCE

The spectral irradiance at the ocean surface shall be measured at wavelengths that correspond to the SeaWiFS spectral bands (Table 4-1), but with 10 nm FWHM bandwidth. A total radiation pyranometer may provide helpful ancillary information, but this is not a required instrument.

Instruments mounted aboard ships must be positioned to view the sky with minimum obstruction or reflections from the ship's superstructure, antennas, etc. Particular care must be taken to prevent sun shadows from antennas falling on the irradiance-collecting surface. Gimbal mounting of the deck sensor may be helpful to keep the surface of the sensor horizontal. Improperly designed gimbal systems, however, can accentuate fluctuations caused by ship motion, and if there is obvious oscillation in the measured irradiance, the gimballing should be improved to eliminate the problem.

An intuitively attractive technique, which was suggested in previous versions of the optics protocols (Mueller and Austin 1992, 1995), is to measure irradiance with a sensor floated a fraction of a meter below the sea surface, far enough away from the ship to avoid ship shadows. The flotation assembly should be designed to avoid shadowing the radiometric FOV and to damp wave-induced motions. This type of arrangement has an additional potential for supporting a small sensor to also measure upwelling radiance, L_u ( ), just below the surface. Over the past several years, the ocean color community has gained experience with this approach, and has encountered consistent and significant difficulties due to wave-induced fluctuations in near-surface E_d. This method is no longer recommended for determining either $E_d(0^-$,) or $E_S($). An acceptable variant of the approach is to use a similar flotation assembly, tethered to allow the instrument to drift away from the ship, but with the irradiance collector raised 50 to 100 cm above the sea surface to measure $E_S($) in air.

Surface Radiometer Characteristics

The specified number of channels and spectral characteristics of deck cells are the same as those for subsurface irradiance measurements as shown in Table 4-1, augmented as necessary for validation of satellite sensors other than SeaWiFS (Appendix A). Saturation irradiances are the same as for E_d ( ) (Table 4-3). The dynamic operating range for these sensors needs to only be 25db, with a SNR of 100:1 but must include the nominal calibration irradiance (Table 4-3). Linearity must be within ± 0.5 %. Sampling frequency should match the frequency of the underwater radiometer, which should be 1 Hz or faster, and all wavelengths should be sampled within an interval less than or equal to 10^{-2} s. Cosine response characteristics should give relative responsivity to a collimated source (in air) which matches cos θ accurate within 2% for $0^o ≤ θ <65^o$, and within 10% for $65^o ≤ θ <90^o$. If a floating above-water surface radiometer is used, its cosine response must meet the same specifications as those for profiling irradiance meters.

For some oceanographic process studies, it may be acceptable to use a radiometer system measuring E_s ( ) at only a single wavelength. If only a single channel deck radiometer is available, its spectral characteristic should closely match one of channels 2--5 with a 10 nm FWHM bandwidth. A broad-band, or photosynthetically available radiation (PAR), radiometer should never be used for this purpose.

4.4 ABOVE-WATER RADIOMETRY

The performance characteristics to be specified for an above-water ocean color radiometer will vary, depending on how a particular instrument is to be employed in SeaWiFS validation experiments. For radiometric comparisons with SeaWiFS and in-water measurements, the fundamental criterion to be met is that estimates of spectral normalized water-leaving radiance derived from shipboard or airborne measurements must have the same uncertainty specified for those derived from in-water measurements of L_u (z,) (Table 4-3). A less accurate radiometer may be used to semi-quantitatively characterize spatial variability near ship stations.

In general, the spectral characteristics of above-water radiometers should match those specified for $L_u($) in Table 4-1. In some cases, however, it may be acceptable for a radiometer to match the SeaWiFS – or other sensor -

specifications, which specify center wavelength within 2 nm and 20 nm FWHM bandwidth. Recalling the sensitivity of solar radiometry to the exact center wavelength and detailed spectral response function (Sections 4.1.1 and 5.1.2), any use of airborne radiometers must quantitatively account for the different spectral responsivity functions between measurements of radiance by, e.g., SeaWiFS, in-water radiometers, and above-water radiometers at each channel's nominal center wavelength.

A high-altitude imaging radiometer must have a radiometric uncertainty and SNR in all channels equal to those of the satellite ocean color instrument if its imagery is to be used for direct radiometric verification of the satellite sensor's radiometric performance. In some cases, the requisite SNR may be realized through pixel averaging to a 1km spatial resolution commensurate with that of, e.g., SeaWiFS. Direct radiometric comparisons between aircraft and SeaWiFS radiances, however, also require that the different atmospheric path effects be carefully modeled, and that the uncertainty in those modeled adjustments be independently estimated. This can be done most effectively when the aircraft measurements are combined with the full suite of shipboard in-water, atmospheric, and ancillary measurements (Table 2-1). In this case, direct comparisons between aircraft and ship radiometry may require that both the SNR *and* the uncertainties realized in combined analyses of the two data sets will represent a smaller spatial resolution than the nominal 1 km instantaneous field-of-view (IFOV) for SeaWiFS. Finally, the viewing zenith and azimuth angles at the matched pixel must also be nearly the same for both sensors, if uncertainties associated with modeled corrections for the ocean's surface and internal bi-directional reflectance distribution function (BRDF) are to be avoided.

Performance characteristic specifications are similar for ocean color radiometers used to measure water-leaving radiance from either the deck of a ship or an aircraft flown at low altitude, i.e., 200m altitude or lower. Radiometric characteristics should match the criterion set forth for in-water L_u ( ) radiometers in Sections 4.1.1--4.1.4 and Tables 4-1 through 4-3. The instrument FOV should be between 5^0 and 10^0 (full angle), and all wavelengths must be coregistered within 10% of the IFOV. All channels must be scanned simultaneously, or within less than 10^{-2} s (depending on the digitizing design), to avoid aliasing due to varying wave reflectance in shipboard measurements, and to avoid time-space aliasing in airborne measurements. This constraint precludes use of

filter wheel radiometers and others which scan channels sequentially over a time interval greater than 10^{-2} s. Sampling over longer periods of time may be done by either electronic integration of all channels simultaneously, or by averaging multiple scans.

A radiometer's sensitivity to the polarization of aperture radiance is critical for ocean color remote sensing applications. Polarization sensitivity is likely to be present in any radiometer having mirrors, prisms or gratings in its optical path. To measure accurate water-leaving radiances using instruments of these types, it is necessary to depolarize aperture radiance using either fiber-optics or a *pseudo-depolarizer*. Shipboard and airborne ocean color radiometers must have a polarization sensitivity of less than 2% in all channels. The sole exception to this rule will occur in the case of instruments designed to actually measure the polarization components of aperture radiance, e.g., the polarization channels of the French Polarization and Directionality of the Earth's Reflectances (POLDER) instrument and of the hand-held SIMBAD radiometers.

Each application of a particular above-water radiometer system, if it is proposed for satellite ocean color sensor validation, must be evaluated on its own merits. The instrument's responsivity, uncertainty, stability, FOV, and spectral characteristics must be evaluated in the context of the models to be used to compare its radiance measurements to in-water, or SeaWiFS, radiance measurements. The suitability of spatial averaging to improve SNRs must be evaluated in terms of the spatial variability prevailing in the experiment site, particularly when in-water and aircraft radiances are to be directly compared. Finer resolution aircraft imagery, or low-altitude trackline data, will often be essential for determining the validity of attempts to directly compare in-water and, e.g., SeaWiFS radiances measured at a particular site.

In summary, airborne and shipboard above-water radiometry can obviously contribute extremely valuable data for validating the radiometric performance of satellite ocean color instruments and the algorithms employed with their data. There is, however, a wide possible range of radiometer characteristics that can be applied to this program, and detailed specification of required characteristics can only be done in the context of each particular experiment's design. Only the guiding principals and desired end-to-end performance are specified here.

4.5 INHERENT OPTICAL PROPERTY INSTRUMENTS

The primary Inherent Optical Properties (IOP) are:

1. the beam attenuation coefficient, $c(z, \lambda)$, in units of m^{-1};
2. the absorption coefficient, $a(z, \lambda)$, in units of m^{-1}; and
3. the volume scattering function, $\beta(z, \lambda, \theta_o, \phi_o, \theta, \phi)$, in units of $m^{-1} sr^{-1}$, describing the distribution of photons scattered into direction (θ, ϕ) from an incident (path) direction (θ_o, ϕ_o).

The integral of the volume scattering function over 4π steradians is the total scattering coefficient, $b(z, \lambda)$, with units of m^{-1}. The integral of the volume scattering function over the back hemisphere is the backscattering coefficient, $b_b(z, \lambda)$, with units of m^{-1}.

It is possible to measure vertical profiles of $a(z, \lambda)$ and $c(z, \lambda)$ *in situ*. Instruments for making these measurements should, at a minimum, have the characteristics given in Table 4-4. In the case of beam attenuation coefficients, the requirements for uncertainty and precision correspond to changes in $c(\lambda)$ resulting from changes in concentration of approximately 5 and 2 $\mu g\ l^{-1}$ of suspended mass, respectively. Stability should be tested with instruments connected to the data acquisition system. Stability with time should be better than $0.005\ m^{-1}$ between calibrations.

Dual path (reflective tube and open path) instruments for measuring $a(z, \lambda)$ and $c(z, \lambda)$ *in situ* are commercially available, meet the specifications of Table 4-4 for SeaWiFS wavelengths, and have found widespread use in the ocean optics and color communities. In some cases, two such instruments are mounted together, one having a 0.2 μm filter attached to the water inlet port. The filtered input instrument measures absorption and beam attenuation by dissolved substances, which allows the total absorption and attenuation measured by the unfiltered instrument to be partitioned into dissolved and particulate components. Hyperspectral resolution (10 nm) instruments of this type are also commercially available, but the community has not yet established that the performance characteristics of these more sophisticated underwater spectrophotometers reliably meet the specifications of Table 4-4.

Table 4-4. Minimum instrument characteristics for the measurement of the spectral absorption and attenuation coefficients.

Instrument Characteristics	
Spectral Resolution:	410, 443, 490, 510 555, and 670 nm
Bandwidth:	10 nm
Uncertainty:	0.005 m–1
Precision for $\lambda < 650$ nm:	0.002 m–1
Precision for $\lambda \geq 650$ nm:	0.005 m–1
Stability with Temperature:	0.005 m–1 over 0–25° C
Sampling Interval:	4 samples m–1
Source Collimation Angle:	5 mrad
Detector Acceptance Angle:	20 mrad
Depth Capability:	200 m

The spectral total scattering coefficient cannot be measured directly. It can be obtained from $b(\lambda) = c(\lambda) - a(\lambda)$, with an uncertainty equal to the quadrature sum of the uncertainties in those measurements.

Using commercially available instruments, it is also possible to measure photons scattered at a fixed angle in the backward direction, and to estimate from this measurement $b_b(\lambda)$ *in situ*. The spectral backscattering coefficient, $b_b(\lambda)$ has the same requirements for spectral resolution, bandwidth, and linearity as $a(\lambda)$ and $c(\lambda)$ (Table 4-4). Since $b_b(\lambda)$ is not a transmission-like measurement, however, the uncertainty of its determination will be approximately 10%.

Despite the many recent advances in our ability to measure IOP's, the shape of the volume scattering function, $\beta(z, \lambda, \theta_o, \phi_o, \theta, \phi)$, has still been determined *in situ* only crudely with devices like the ALPHA and Scattering Meter (ALSCAT) and the General Angle Scattering Meter (GASM), which were built more than two decades ago at the Visibility Laboratory of the Scripps Institution of Oceanography. These are single angle measurement devices, which must be scanned as a function of angle and wavelength. Because measuring scattering with these old instruments is a slow process, they do not lend themselves readily to incorporation into other instrument platforms. Since it is possible to independently determine $b(\lambda)$ and $b_b(\lambda)$, the shape of the volume scattering coefficient could possibly be determined with acceptable uncertainty by also measuring a few moments of the scattering function. Efforts to develop new instruments, either following this approach, or attempting to measure the full scattering function directly, remain in an embryonic stage.

4.6 ATMOSPHERIC AEROSOLS

Sun photometers should be used to measure atmospheric aerosol optical thickness. These sun photometers should have specifications in agreement with (or exceeding) the World Meteorological Organization (WMO) sun photometer specifications (Frohlich 1979). Specifically, the instruments should have a 2° FOV, temperature stabilization, and a precision of $\pm$ 0.01%. The specific wavelengths of channels should correspond to the recommended WMO wavelengths of 380, 500, 675, 778, and 862nm. Additional wavelengths corresponding to the SeaWiFS (Table 4-1), or other satellite ocean color sensor (Appendix A), channel combinations may be desireable in some applications, but they are not required for the SIMBIOS validation database. More detailed specifications associated with specific photometers are given in Chapters 6 & 15.

4.7 SPECTRAL SKY RADIANCE

Measurements of spectral sky radiance distribution should be made using a photoelectric all-sky camera. Spectral characteristics of the sky radiance camera channels are those specified for E_s ( ) (Table 4-1). Data should be in a format such that absolute radiance values can be obtained with an uncertainty of 5% and sky irradiance can be determined from integrals of the data to within 10%. If the dynamic range of the camera is insufficient to capture both the sun and sky distribution, neutral density filters (or some other method) should be used so that radiance from both the sun and sky can be measured.

Alternatively, sky radiance distributions are made using radiometers that are mechanically scanned through the solar principal plane. More detailed specifications for these instruments are described in Chapters 6 & 15.

4.8 PHYTOPLANKTON PIGMENTS & CTD PROFILES

HPLC equipment and associated standards must conform to protocols specified in Chapter 20. *In situ* chlorophyll fluorometers should have a resolution of at least 0.001 mg of chlorophyll a per m^3. A calibrated CTD system should be used to make profiles to maximum depths between 200 and 500 m. The instrument should meet the minimum specifications given in Table 4-5.

Table 4-5. The minimum instrument characteristics for the measurement of hydrographic profiles are listed.

Parameter	Range	Uncertainty	Resolution
Pressure [dbars]	0–500	0.3%	0.005%
Temperature [°C]	–2– 35	0.015° C	0.001° C
Salinity [PSU]	1– 45	0.03 PSU	0.001 PSU

REFERENCES

Frohlich, C., 1979: WMO/PMOD Sun photometer: instructions for manufacture. *World Meteor. Org.,* Geneva, Switzerland, 3 pp., (plus tables and drawings).

Gordon, H.R., and K. Ding, 1992: Self shading of in-water optical instruments. *Limnol. Oceanogr.,* **37**, 491--500.

Morel, A., *et al*., 1998. *Minimum Requirements for an Operational Ocean-Colour Sensor for the Open Ocean*. IOCCG Report Number **1**, 46pp.

Morel, A. and B. Gentili, 1996. Diffuse reflectance of oceanic waters. III. Implication of bidirectionality for the remote-sensing problem.

Mueller, J.L., and R.W. Austin, 1992: Ocean Optics Protocols for SeaWiFS Validation. *NASA Tech. Memo. 104566, Vol. 5,* S.B. Hooker and E.R. Firestone, Eds., NASA Goddard Space Flight Center, Greenbelt, Maryland, 43 pp.

Mueller, J.L., and R.W. Austin, 1995: Ocean Optics Protocols for SeaWiFS Validation, Revision 1. *NASA Tech. Memo. 104566, Vol. 25,* S.B. Hooker and E.R. Firestone, Eds., NASA Goddard Space Flight Center, Greenbelt, Maryland, 66 pp.

Chapter 5

Characterization of Oceanographic and Atmospheric Radiometers

James L. Mueller and Roswell Austin

Center for Hydro-Optics and Remote Sensing, San Diego State University, California

5.1 INTRODUCTION

Presented in this chapter are procedures for characterizing environmental radiometers, including special characteristics of underwater radiometers, to verify compliance with the specifications of Chapter 4. The characterization of any radiometer used to acquire field data for SIMBIOS validation and algorithm development shall include the determination of those instrument characteristics that affect its calibration as used in the field environment. These characteristics include a sensor's:

1. spectral irradiance, or radiance, responsivity calibration, traceable to NIST standards;
2. spectral sensitivities of the various measurement channels;
3. effects on responsivity caused by water immersion;
4. angular response sensitivities in the medium, i.e., air or water, in which it is to be used;
5. the temporal response of the system; and
6. the effects of temperature and pressure on the above characteristics.

The elements of radiometer characterization and calibration are outlined schematically in Figure 5.1. For any instrument to provide suitable data for SIMBIOS and SeaWiFS use, the investigator must be certain that the instrument characterization has not changed beyond accepted limits and that the

Title:
(chart1.eps)
Creator:
Adobe Illustrator(R) 8.0
Preview:
This EPS picture was not saved
with a preview included in it.
Comment:
This EPS picture will print to a
PostScript printer, but not to
other types of printers.

Figure 5.1.Elements of radiometer characterization and calibration.

time history of the calibration is traceable. Certain attributes, such as a sensor's angular response characteristics, are sufficiently constant that they only need to be determined once, unless the instrument is modified. The exact nature of instrument modifications during maintenance will determine which characterization procedures must be repeated. When practical, on the other hand, radiometric calibrations and the assessment of system spectral characteristics of filter radiometers should be repeated before and after each major field deployment.

5.2 RADIOMETRIC RESPONSIVITY CALIBRATION

Determination of the absolute radiometric responses of the irradiance and radiance sensors requires the availability of a properly manned and equipped radiometric calibration facility. Such a facility must be equipped with suitable stable sources and radiometric scale transfer sensors, e.g., lamp standards of spectral irradiance and NIST calibrated transfer radiometers, respectively. The sources and transfer sensors must have defined spectral radiometric characteristics that are traceable to NIST. The calibration facility must also have a variety of specialized radiometric and electronic equipment, including: reflectance plaques, spectral filters, integrating spheres, and highly regulated power supplies for the operation of the lamps. Precision electronic measurement capabilities are also required, both for setting and monitoring lamp current and voltage and for measuring the output of the radiometer.

It is not expected that every investigator will be able to independently perform radiometric calibrations. Instrument manufacturers and a few university laboratories are equipped and staffed to perform these calibrations for the ocean color research community. The facilities will perform frequent intercomparisons to assure the

maintenance of the radiometric traceability to the NIST standard of spectral irradiance. The goal shall be to provide reproducible calibrations from 400-850 nm to within better than ± 1 %; the minimum requirement for radiometric data to be used in SeaWiFS validation is for repeatable calibrations within less than 5%.

This section describes sources and methods by which the NIST scale of spectral irradiance is transferred to calibrate irradiance and radiance sensors. The principal working standards used for spectral irradiance responsivity calibration are FEL lamp working standards. The spectral irradiance scales of the FEL lamps are in turn transferred to spectral radiance scales using plaques of known bidirectional reflectance, or integrating spheres, or both. An ongoing series of SeaWiFS Intercalibration Round-Robin Experiments (SIRREXs) has been initiated by the SPO to assure internal consistency between the laboratories which calibrate radiometers for SeaWiFS validation (Mueller 1993 and Mueller et al. 1994). In SIRREX-3 (Mueller *et al*. 1996) and –4 (Johnson *et al*. 1996), it was demonstrated that with properly maintained FEL standards, throrough training of laboratory personnel in calibration procedures, and careful attention to measurement setups, it was possible to maintain an uncertainty level of < 2% for spectral irradiance and < 3% for spectral radiance calibrations.

The variety of instruments available for validation measurements makes it imperative that some common calibration traceability exists. Recognizing that it would be impractical to characterize and calibrate all oceanographic and airborne radiometers at GSFC, several remote calibration facilities should be identified (instrument manufacturers and a few laboratories at academic and government institutions), and working standards and protocols used at these facilities should all be traced directly to the NIST scale (Johnson et al. 1996). This organizational structure is shown schematically in Figure 5.2 Methods of standards intercomparison may include use of NIST calibrated filter radiometers to track and document the operation of each facility (radiometer wavelengths for this intercomparison will be determined). Round-robin calibration comparisons of a *standard* instrument were also implemented to benchmark the internal consistency of calibrations performed at the various facilities involved with calibrations throughout the ocean color community; the first of these determined that the level of relative uncertainty between these laboratorie is approximately 2% (Riley and Bailey, 1998).

Spectral Irradiance Calibrations

Radiometric calibrations of irradiance sensors will be performed after it has been ascertained that: the conformity of the sensor angular response to the required cosine function is satisfactory, the sensor linearity is satisfactory, and the spectral sensitivity, including out-of-band blocking, is known and satisfactory.

The options available for radiometric calibration standards are limited to standard sources or standard detectors. Lamp standards of spectral irradiance are provided by NIST, and NIST traceable secondary standards are available from various commercial standardizing laboratories and manufacturers. The uncertainty cited by NIST for these standards is, at best, 1% in the visible and 2% is a more realistic estimate of absolute uncertainty attainable using lamp standards alone. Over the calibration range from 250--2,500 nm, the uncertainty is approximately 6% at the endpoints.
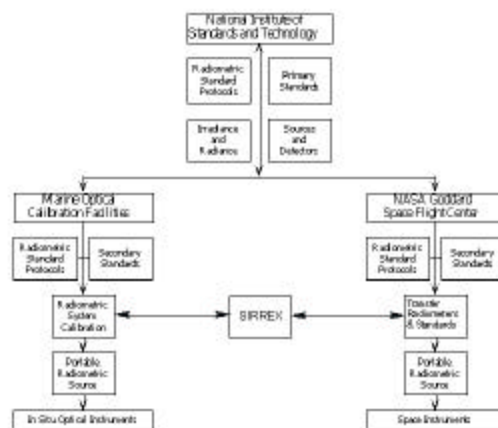
Figure 5.2. Organizational structure for optical instrumentation characterization and calibration.

The lamp standard of spectral irradiance is traditionally used for radiometric calibration, mainly because of its ease of use compared to the spectral radiance lamp. NIST publishes guidelines for the setup, alignment, and use of these standards. The vendors that manufacture and calibrate these lamps also issue guidelines for their use.

Radiometers shall be calibrated using a 1,000 W FEL standard of spectral irradiance, with calibration traceable to NIST and lamp operation in accordance with Walker et al. (1987). The irradiance collector is placed normal to, and at the prescribed distance from, a working standard lamp

of spectral irradiance. The lamp should be of appropriate size to provide an irradiance at the sensor that will be at least 30%, and preferably above 50%, of full-scale for the sensor channel being calibrated, although this is not always achievable in practice (Table 5.4). The lamp-sensor space shall be appropriately baffled and draped so that occulting the direct path between lamp and sensor will result in a response of less then 0.1% of the response to the lamp flux.

For multispectral instruments, all channels may be calibrated simultaneously if sufficient flux is available at all wavelengths. The instrument response is recorded for all channels together with associated dark responses. Ambient and photosensor temperatures are recorded, where available. For characterization, the radiometric calibration should be performed at temperature extremes of -2^0 C and 40^0 C for in-water sensors, and at -10^0 C and $45\ ^0$C for irradiance sensors used above the surface. If responses differ significantly at temperature extremes, responses should also be determined at intermediate temperatures.

Spectral Radiance Calibrations

Radiance calibration activities require a uniform source of known radiance that will fill the angular field of view of the radiance sensor. The two procedures that may be used are given below.

Calibration Methods

1. A working lamp standard of spectral irradiance is placed at the prescribed distance from a plaque of known Lambertian reflectance. The plaque is normal to, and centered on, the lamp calibration axis. The radiance sensor is positioned to view the plaque at an angle of 45^0 from the plaque normal (any other angle at which the diffuse reflectance of the plaque is known is acceptable also). It must be established that the plaque fills the sensor's FOV and that the presence of the sensor case has not perturbed the irradiance on the plaque. The instrument response and dark signal is recorded. It must be verified that the plaque fills the FOV with uniform radiance for each channel of a multichannel radiance sensor. Separate calibration setups may be required for different channels and the lamps may have to be moved as much as 3 m away from the plaque to assure uniform illumination. This procedure is difficult to apply to sensors with a large FOV.

2. An integrating sphere with an exit port of sufficient size to fill the FOV of the radiance sensor may be used if the radiance of the exit port, at the channel wavelengths, can be determined with sufficient uncertainty.

Spectral radiance may be obtained by using an irradiance standard lamp and a Lambertian reflecting plaque. The standard lamp is positioned on axis and normal to the center of the plaque at the calibrated distance. The instrument or detector package to be calibrated is nominally positioned to view the plaque at 45^0 measured from the axis. The radiance, then, is given by

$$L(\lambda) = \frac{1}{\rho}\, \rho\left(\lambda, 0^o, 45^o\right) E(\lambda), \qquad (5.1)$$

where ρ ($\lambda, 0^o, 45^o$) is the bidirectional reflectance of the plaque for 0^0 incidence and 45^0 viewing, $E(\lambda)$ is the known spectral irradiance from the lamp during calibration and the total FOV of the instrument being calibrated is filled by the illuminated plaque.

The known radiance of the plaque provides an uncertainty comparable with that of the irradiance standard lamp, i.e., less than or equal to 3%, for calibrating a radiance detector with a very narrow FOV ($\approx 1^0$). Large plaques, e.g., 40 cm^2, have been successfully used to calibrate radiance sensors having up to 25^0 full-angle FOVs. Intercomparisons of calibrations on underwater radiance sensors (possessing in-air full-angle FOVs ranging from 20--24^0, made using this technique at different laboratories, have generally agreed within approximately 5%.

A better approach to calibrating multispectral radiance sensors is to view an integrating sphere that is uniformly illuminated by stable, appropriately baffled lamps, and that also has an exit port large enough to completely fill the sensor's FOV. The sphere and exit port must be large enough to place the radiance sensor far enough away to prevent significant secondary illumination of the sphere walls due to retro-reflection off the sensor's entrance optics; if the sensor is too close, the retro-reflected light will both increase and distort the uniformity of the radiance distribution within the sphere. Traditionally, the calibration of an integrating sphere radiance source has been accomplished by appropriately transferring the known output from a standard lamp irradiance source.

The approach used at NASA/GSFC is to view the irradiance output of the lamp, initially, and then the sphere, with a spectroradiometer equipped with

integrating input optics (McLean and Guenther 1989 and Walker et al. 1991). The spectral irradiance responsivity of the radiometer is calibrated using the lamp data, and the (assumed) Lambertian radiance of the sphere is determined by dividing the measured spectral irradiance output of the sphere by π. Johnson et al. (1996) made several recommendations for improving the quality of the *co-axial sphere* method of transferring a scale of spectral radiance to an integrating sphere from a NIST traceable FEL scale of spectral irradiance.

5.3 PORTABLE STANDARDS

The portable irradiance and radiance reference standard to be used to trace instrument stability during field deployments (Chapter 7) should be placed in position on the sensor immediately following the calibration to establish the instrument response to this reference unit.

Between radiometric calibration activities, stable lamp sources in rugged, fixed geometric configurations should be used to track instrument performance. Irradiance channels can be monitored with irradiance sources at fixed distances from the collectors, while radiance sources can be monitored by filling the FOV with diffuser plates placed in front of the irradiance sources, or by using integrating cavity sources. In each case, careful attention must be given to fixing specific geometries of source and detector in each use. The stability of the lamp output and the repeatability of measurement must be sufficient to detect 2% variations in an instrument's performance. An instrument should be connected to the portable standard and its response recorded daily, keeping a record of instrument responsivity throughout an experiment. Furthermore, these sources would provide an essential warning of problems if they appear. The portable field reference source must be available when the complete radiometric calibrations are performed so that a baseline may be established and maintained for each sensor channel (Section 4.1.1). These sources are not a substitute for complete calibrations. The temporal record they provide will, however, be invaluable in cases where the pre- and post-cruise calibrations disagree or if the instrument is disturbed, e.g., opened between calibrations or if the data quality are otherwise suspect. These portable standards are an important part of the recommended instrument package.

Although several manufacturers offer somewhat portable irradiance and radiance sources, there has been very little previous work to validate and use portable radiometric standards to test oceanographic radiometers in the field. Therefore,

detailed hardware specifications and procedural protocols must be developed through a series of laboratory and field tests using candidate equipment and standards.

5.4 SPECTRAL BANDPASS CHARACTERIZATION

These instruments should be characterized to define the nominal wavelengths and bandwidths, defined as the full width of the passband as measured to the FWHM intensity points. The nominal, or center wavelength, will usually be defined as the wavelength halfway between wavelengths at which the normalized response is 0.5, and the channel is characterized by this wavelength and the FWHM bandwidth. The determination of the spectral response function, i.e., the passband, will be made for each channel with a scanning monochromatic source, with a bandwidth less than 0.2 nm; the source output must be normalized to a detector of known spectral sensitivity. The response function thus measured is then normalized to the maximum (peak).

Although the results of this characterization are usually represented by only the nominal wavelength and FWHM bandpass, the full normalized response function should be recorded for use in detailed wavelength adjustments and comparisons with the SeaWiFS and other sensor channel response functions, which will not be known until shortly before launch. It is further recommended that the internal instrument temperature be monitored during these tests, and that the test be repeated at two temperatures at least 15^0 C apart, e.g., 10^0 and 25^0 C. If a significant shift, greater than 1.0 nm, with temperature of either the center wavelength or bandwidth is detected, then additional temperature calibration points are recommended. Dark offsets must be recorded during each test.

For spectral characterizations of irradiance diffusers, the entire surface of the diffuser should be illuminated by the monochromator's output. In the case of radiance detectors, a diffuser should be used to diffuse the monochromator slit image and uniformly fill the instrument's FOV.

The wavelength response of a monochromator-based radiometer is calibrated by scanning over line sources, with sharp peaks at well known wavelengths. Suitable spectral calibration sources, such as, mercury, cadmium, and neon lamps, are provided by several vendors, together with tabulations of the wavelengths of the emission lines generated by each source.

The width of the slit function of a monochromator may be estimated by scanning over a laser line, e.g., helium-neon, at a very small wavelength interval. The instrument FOV must be filled during the test.

It is anticipated that the monochromator-based spectral characterization will not be able to adequately measure leakage of broadly distributed out-of-band radiation; therefore, blocking of blue light in channels longer than 540 nm must be routinely tested. Where continuous wave (CW) argon lasers are available, out-of-band response should be measured at 488 nm. One recommended test that can be performed during the absolute calibrations at 640 nm is the sequenced measurement of three Schott BG-18 filters, each 1 mm thick, using an FEL-type light source. The procedure is to measure the channel signal using each filter separately, then in combination, and comparing the computed and measured transmissions. If a significantly higher combined transmission of the three filters, when they are used in combination, is measured relative to the calculated transmittance, then spectral leakage is present. At wavelengths greater than 640 nm, other filters that attenuate the wavelength of interest, with a transmission value of less than or equal to 0.1 and which pass shorter wavelength light with significantly greater transmission, should be substituted for the BG-18.

Consideration must also be given to unblocked fluorescence by the filters, or other optical elements, as a possible source of light leaks. Methods to test for fluorescence contamination specifically, are not well established at this time.

While leakage of blue light into red channels is the most significant oceanographic optical problem, the leakage of red and IR light into blue channels can cause significant errors when the instrument is calibrated using a red-rich source. A convenient way to measure this leakage is to place a long wavelength-pass, sharp-cut, absorbing glass filter that does not exhibit fluorescence between a broad band (e.g., incandescent) source and the sensor. A non-zero response indicates unwanted out-of-band red response and the need for improved red blocking.

5.5 IMMERSION FACTORS

Irradiance Sensor Immersion Factors

When a plastic, opal-glass, or Teflon diffuser is immersed in water, its light transmissivity is less than it was in air. Since an instrument's irradiance responsivity is calibrated in air, a correction for this change in collector transmissivity must be applied to obtain irradiance responsivity coefficients for underwater measurements.

The change in a collector's immersed transmissivity is the net effect of two separate processes: a change in the reflection of light at the upper surface of the collector, and internal scattering and reflections from the collector's lower surface. A small part of the light flux falling on the collector is reflected at the air-plastic, or water-plastic, interface, and the majority of the flux passes into the collector body. The relative size of this reflectance, called *Fresnel reflectance*, depends on the relative difference in refractive indices between the diffuser material and the surrounding medium.

The refractive index of the collector material is always larger than that of either water or air, and because the refractive index of water is larger than that of air, Fresnel reflectance is smaller at a diffuser-water interface than at a diffuser-air interface. Thus, the initial transmission of light through the upper surface of an irradiance collector is larger in water than in air. The immersed upper surface is, on the other hand, also less effective at reflecting the upward flux of light backscattered within the diffuser body and light reflected at the lower diffuser-air interface in the instrument's interior, processes that are not affected by immersion. Therefore, a larger fraction of the internally scattered and upwardly reflected light passes back into the water column than would be lost into air. Because the increased upward loss of internally reflected flux exceeds the gain in downward flux through the diffuser-water interface, the net effect of these competing processes is a decrease in the collector's immersed transmissivity.

Experience has shown that the immersion factors for an irradiance collector must be experimentally characterized in the laboratory. Some manufacturers perform this characterization procedure only for a prototype of a particular collector design and material specification. They sometimes then provide only these nominal immersion factors for all production radiometers using that collector design. Mueller (1995) applied the characterization procedure described below to determine irradiance immersion factors for 11 radiometers having cosine collectors of the same design and material. The measurements were replicated 2 to 4 times for each radiometer, using independent setups on different days and varying the lamp-to-collector distance between replications, to determine that Type A uncertainty associated with the experimental procedure is less than 1%.

On the other hand, root-mean-square differences between immersion factors in this group of irradiance sensors ranged from 3% to 5%, at different wavelengths, and differences between individual collectors were as large as 10% at some wavelengths.

To measure this effect, a suggested and acceptable procedure (Petzold and Austin 1988) is as follows: The instrument is placed in a tank of water with the irradiance collector level and facing upward. A tungsten-halogen lamp with a small filament, powered by a stable power supply, is placed at a carefully measured distance above the surface of the irradiance collector. An initial reading is taken in air, before the water level in the tank is raised above the dry collector. The water is raised initially to a carefully measured depth z above the collector surface and readings are recorded for all wavelengths. The water level is then increased stepwise in, e.g., 5 cm increments, and the instrument responses are measured and recorded for each depth z. A maximum water depth of 40 to 50 cm is normally adequate to obtain data covering a sufficient range of responses. The water level is then lowered, and data recorded, over a similar series of incremental depths. A final reading is taken with the water level below the collector, after drying the collector. It is recommended to then change and remeasure the lamp-to-collector distance d, and repeat the entire procedure to verify that a Type A experimental uncertainy less than 1% has been achieved.

A minimum water depth of 5 cm is recommended to avoid artifacts due to multiple reflections between the collector and water surfaces. These reflections would otherwise artificially increase the transmitted flux, and therefore, decrease the apparent immersion effect. The magnitude of this artifact will increase with decreased depth z below some critical limit, which is the order of the diameter of the collector. With very small diameter collectors, it may be possible to acquire good immersion effect data at values of z < 5 cm, but the absence of this artifact should be demonstrated experimentally if this is done.

The amount of energy arriving at the collector varies with the water depth and is a function of several factors:

1. the attenuation at the air-water interface, which varies with wavelength;
2. the attenuation over the water pathlength, which is a function of depth and wavelength; and
3. the change in solid angle of the light leaving the source and arriving at the collector, caused

by the light rays changing direction at the air-water interface, which varies with wavelength and water depth.

Using Fresnel reflectance equations, the transmittance through the surface is

$$T_s(\lambda) = \frac{4n_w(\lambda)}{\left[1+n_w(\lambda)\right]^2}, \qquad (5.2)$$

where $n_w(\lambda)$ is the index of refraction of the water at wavelength λ. The transmittance through the water path is given by

$$T_w(\lambda) = e^{-K(\lambda)z}, \qquad (5.3)$$

where $K(\lambda)$ is the attenuation coefficient of the water and z is the path length in corresponding units.

The change with water depth z of the refracted solid angle subtended by the collector, as viewed from the lamp filament, is given by the factor

$$G(z,\lambda) = \left[1-\frac{z}{d}\left(1-\frac{1}{n_w(\lambda)}\right)\right]^{-2}, \qquad (5.4)$$

where d is the distance of the lamp source from the collector surface.

The immersion correction factor $F_i(\lambda)$ for irradiance is then calculated for each depth z as

$$F_i(\lambda) = \frac{E_a(\lambda)}{E_w(z,\lambda)}T_s(\lambda)T_w(\lambda)G(z,\lambda), \qquad (5.5)$$

where $E_a(\lambda)$ and $E_w(\lambda,z)$ are the irradiance in air and the irradiance underwater at depth z, respectively.

There are two unknowns in (5.2)-(5.5): the attenuation coefficient of the water $K(\lambda)$ and the immersion factor $F_i(\lambda)$. A minimum of three measurements must be made to solve for $F_i(\lambda)$ and $K(\lambda)$: one in air to get $E_a(\lambda)$ and two at different water depths for $E_w(\lambda,z)$. The recommended method is to take readings of $E_w(\lambda,z)$ at many depths. If (5.2) is substituted into (5.5), and the result is log transformed and rearranged, each measurement $E_w(\lambda,z)$ and depth z may be expressed as

$$\ln\left[\frac{E_a(\lambda)}{E_w(z,\lambda)}T_s(\lambda)G(z,\lambda)\right] = \ln\left[F_i(\lambda)\right]+K(\lambda)z. \quad (5.6)$$

The unknown slope $K(\lambda)$ and intercept $\ln[F_i(\lambda)]$ are then determined by a linear least-squares regression analysis. The complete derivation of (5.2)--(5.6) is given in Petzold and Austin (1988).

Radiance Immersion Factors

The absolute calibration for the spectral radiance channels is found by viewing a surface of known radiance in air in the laboratory. When the instrument is submerged in water, a change in responsivity occurs and a correction must be applied. This change in responsivity is caused by the change in the indices of refraction of the different media in which the instrument is immersed--in this case air and water. Two optical changes occur, both of which are caused by the change in refractive index. The two effects to be corrected are:

1. the change in transmission through the interface between the air and the window during calibration, and the same effect through the water-window interface during data measurement, and
2. the change in the solid angle included in the underwater FOV relative to that in air.

Since the refractive index of seawater, $n_w(\lambda)$ is a function of wavelength (λ) the correction factor $F_i(\lambda)$ will also be a function of wavelength .If the refractive index of air is assumed to be 1.000 at all wavelengths, and if $n_g(\lambda)$ is the index of refraction for the (glass) window and $n_w(\lambda)$ is the index of refraction for water, then, as shown in Austin (1976), the correction for the change in transmission through the window is

$$T_g(\boldsymbol{\lambda}) = \frac{\left[n_w(\boldsymbol{\lambda}) + n_g(\boldsymbol{\lambda})\right]^2}{n_w(\boldsymbol{\lambda})\left[1 + n_g(\boldsymbol{\lambda})\right]^2}, \qquad (5.7)$$

and the correction for the change in the FOV is

$$F_v(\boldsymbol{\lambda}) = \left[n_w(\boldsymbol{\lambda})\right]^2. \qquad (5.8)$$

The index of refraction of a Plexiglas^{TM} window, n_g (λ) may be computed using an empirical fit to the Hartmann formula, that is,

$$n_g(\boldsymbol{\lambda}) = 1.47384 + \frac{7.5}{\boldsymbol{\lambda} - 174.71}, \qquad (5.9)$$

where λ is the wavelength in nanometers (Austin 1976). The refractive indices of other materials must be obtained from the manufacturer.

The index of refraction for seawater $n_w(\lambda)$ may be similarly computed using an empirical fit of the data from Austin and Halikas (1976),

$$n_w(\boldsymbol{\lambda}) = 1.325147 + \frac{6.6096}{\boldsymbol{\lambda} - 137.1924}. \qquad (5.10)$$

The immersion factor $F_i(\lambda)$ is then obtained as

$$F_i(\boldsymbol{\lambda}) = T_g(\boldsymbol{\lambda}) F_v(\boldsymbol{\lambda}), \qquad (5.11)$$

or by subsitution from (5.7) and (5.8) as

$$F_i(\boldsymbol{\lambda}) = \frac{n_w(\boldsymbol{\lambda})\left[n_w(\boldsymbol{\lambda}) + n_g(\boldsymbol{\lambda})\right]^2}{\left[1 + n_g(\boldsymbol{\lambda})\right]^2}. \qquad (5.12)$$

5.5 RADIANCE FIELD-OF-VIEW

It is required that the radiance FOV of the instrument be known. The FOV should not normally enter into the absolute calibration, however, if the FOV is fully filled by a calibration source of uniform radiance. In this test, the instrument is placed on a rotational stage with the entrance aperture of the radiometer over the rotation axis. A stable light source with a small filament is placed several meters in front of the instrument, which is then scanned from -30^0 to $+30^0$ in 2^0 increments. The angle positioning should be within $\pm$ 0.1^0. The on axis, 0^0, mechanical alignment is made using the window surface as reference, by adjusting to get the reflection of the lamp filament to return on axis. The error in this alignment is approximately $\pm$ 0.1^0. The in-air measurement angles, θ_a are converted to corresponding angles in seawater , θ_w, using the relation $\theta_w = \theta_{a}/n_w$ where n_w is the index of refraction of seawater at the particular wavelength of each channel.

5.6 COLLECTOR COSINE RESPONSE

The directional response of cosine collectors must be characterized. The directional response of the deck cell is determined in air, and those of the in-water instruments are measured immersed in water. Full spectral determinations are required. For

instruments measuring upwelling irradiance E_u (z, λ) it is recommended that the cosine response of each instrument be measured individually. For downwelling irradiance E_d (z, λ) instruments, checking a production run may be satisfactory if the vendor's material and design are demonstrated to be uniform throughout the duration of the run. Given the variations observed in immersion factors of collectors of the same design and materials (Mueller 1995), however, this possibility should be accepted only with caution. Whenever possible, it is strongly recommended that the cosine response of irradiance collectors be characterized individually.

Absolute responsivity calibration of an irradiance meter is done in air, using light incident normal to the collector. To properly measure irradiance incident on the plane at all angles θ (relative to the normal), the instrument's response should follow a cosine function. In other words, for an instrument response V(0) to a given collimated irradiance incident at θ =0, if the instrument is rotated to the angle θ away from the original normal axis, the response should be V(θ) =V(0)cos θ. If this requirement is met, then the on-axis calibration is sufficient and the device will correctly measure irradiance arriving at the plane of the collector, regardless of the directional distribution at which the light arrives.

The preferred irradiance collector design has an improved cosine response over that of a simple flat plate diffuse collector (Boyd 1955 and Tyler and Smith 1979). This improvement is mostly for near-grazing angles (θ approaching 90^0 to the normal) and is particularly important when measurements of the upwelling underwater irradiance are made, i.e., with the collector facing downward. In that case, most of the light is from the sides, in the region of these near-grazing angles.

Since E_d (z, λ) measurements are to be made underwater, the testing to determine the fidelity of the instrument to the cosine function must be made with the instrument submerged. A description of the suitable experimental procedure follows Petzold and Austin (1988).

The instrument is suspended in a tank of water while supported by a fixture designed to allow rotation about an axis through the surface and center of the collector. A tungsten-halogen lamp with a small filament is enclosed in a housing with a small exit aperture and placed approximately 1 m from a large window in the tank. The collector is placed approximately 25 cm behind this window; an equivalent lamp distance of 1.25 m or more is required. A circular baffle should be placed immediately in front of the window to reduce stray light. The water should be highly filtered to the extent that the effects of scattered light are indiscernible.

The equivalent air path lamp distance should be approximately 1.25 m or greater. At this distance, the fall-off at the outer edge of a 6 cm diameter diffuse collector would be 0.9994, or -0.06 %, when the diffuser is at θ = 0^0 with the normal. The net effect over the entire area of the diffuser would be 0.9997 or -0.03 %. When θ = 90^0, with the diffuser edge-on to the lamp, the distance to the lamp varies for different points on the surface. The net error over the entire surface for this condition is 0.99997 or -0.003 %. All other angles fall between these limiting cases.

The signals from the instrument are recorded for θ = 0^0 and at 5^0 intervals to θ = ± 75^0 and 2.5^0 intervals over 75^0<θ<90^0. The readings at θ = 0^0 are recorded at the beginning, the middle, and the end of each run and examined as a measure of lamp and instrument stability over the time involved. At least two runs should be made about different axes through the surface of the diffuser. All readings are normalized to 1.000 at θ = 0^0 and then compared with the value of the cosine of each angle. If V(θ) is the normalized measured value, relative local error at angle θ is given as V(θ)/cos θ - 1.

Assuming the average response to the four measurements made at each θ (four separate azimuth angles φ adequately represent the overall mean cosine response of the collector, then the error, ε in measuring irradiance over the interval $θ_n$ <θ< $θ_N$ for a uniform radiance distribution is approximately

$$e = \frac{\sum_{i=n}^{N} \overline{V}(\theta_i)\sin\theta_i\Delta\theta}{\sum_{i=n}^{N} \cos\theta_i \sin\theta_i\Delta\theta} -1, \qquad (5.13)$$

using a simple trapezoidal quadrature. Similarly, for a radiance distribution of the form 1+ 4sin θ, to simulate upwelled irradiance

$$e = \frac{\sum_{i=n}^{N} \overline{V}(\theta_i)(1+4\sin\theta_i)\sin\theta_i\Delta\theta}{\sum_{i=n}^{N} \cos\theta_i (1+4\sin\theta_i)\sin\theta_i\Delta\theta} -1, \quad (5.14)$$

where $\theta_0 = 0$, $\theta_N = \dfrac{\pi}{2}$ and $\Delta\theta = \dfrac{\pi}{2N}$.

The asymmetry of the cosine response, δ is equivalent to an effective tilt of an ideal cosine collector with respect to the instrument's mechanical axis, which can be quantified as

$$\boldsymbol{d} = \frac{\int_{\boldsymbol{q}_1}^{\boldsymbol{q}_2} \cos(\boldsymbol{q}+\boldsymbol{q}_i)\sin\boldsymbol{q}\,d\boldsymbol{q}}{\int_{\boldsymbol{q}_1}^{\boldsymbol{q}_2} \cos(\boldsymbol{q}-\boldsymbol{q}_i)\sin\boldsymbol{q}\,d\boldsymbol{q}}, \qquad (5.15)$$

where θ_t is the tilt angle.

The measured asymmetry is computed as the ratio of sums of measurements at opposite $\boldsymbol{f}(\boldsymbol{q} \geq 0)$ and $-\boldsymbol{p}(\boldsymbol{q} < 0)$ in the same plane, that is,

$$\boldsymbol{d} = \frac{\sum_{i=0}^{q_N \frac{\boldsymbol{p}}{2}} \overline{V}(\boldsymbol{q},0)\sin\boldsymbol{q}\Delta\boldsymbol{q}}{\sum_{i=0}^{q_N = -\frac{\boldsymbol{p}}{2}} \overline{V}(\boldsymbol{q})\sin\boldsymbol{q}\Delta\boldsymbol{q}} - 1, \qquad (5.16)$$

for $\Delta\boldsymbol{q} = \pm\dfrac{\boldsymbol{p}}{2N}$.

Variations in asymmetry from channel to channel may be due to the placement of the individual detectors behind the diffuser. Any offset of the average asymmetry with the mechanical axis could be due to any one of a variety of causes:

1. the alignment on the rotating test fixture not being correct,
2. tilt of the diffuser,
3. the detector array not being centered,
4. nonuniformity of the reflectance of the internal surfaces of the instrument between the diffuser and the sensor array, or
5. nonuniformity of the diffuser.

5.7 LINEARITY AND ELECTRONIC UNCERTAINTY

The linearity of the radiometric channels must be determined over their expected range of use. The above-surface (deck cell) and underwater irradiance sensors intended for the measurement of downwelling irradiance have full-scale (saturation) values that are not readily obtained with the usual incandescent blackbody sources, such as 1,000 W 3,200 K tungsten-halogen projection lamps. The linearity at the high end of the calibrated range may be determined by using 900--2,000 W high pressure xenon arc lamps, which provide a small, stable source of high intensity (approximately 6,000 K)

radiation. With such lamps, irradiance levels approximating full sunlight can be attained. Using such sources for the high end, and the more easily managed tungsten-halogen lamps over the range below 20-30% of full scale, the linearity of the response characteristic of the radiometric channels can be assessed. The flux should be changed in 5 db (0.5 log), or less, steps using a proven and accepted procedure for controlling irradiance such as inverse square law, or calibrated apertures. These suggested procedures for testing linearity at the higher levels are not well established in practice, and research is needed to determine the precision which can be attained.

If departures from linearity are found, they must be incorporated into the calibration function for the instrument and be properly applied to the raw data to obtain calibrated irradiance and radiance data.

It is recommended that all instruments utilizing inputs from ancillary sensors, e.g., transmissometers, be characterized for the linearity and uncertainty of the voltage measurement covering the full output range of the ancillary sensor. For instruments with range dependent gain changing, either manual or automatic, the scale offset and linearity for each range should, at a minimum, be tested annually. Uncertainties exceeding 0.1% of any reading within the normal working range must be investigated and corrected.

Other characteristics of electronic sensor systems may adversely affect measurement uncertainty. During the design and engineering prototype development of a radiometer, the design and implementation must be analyzed to characterize, and correct as needed, possible effects of hysteresis, overload, recovery times, cross talk between either optical transducers or electronic channels, and sensitivity to orientation in the Earth's magnetic field, which is particularly likely with photomultiplier tubes.

5.8 TEMPORAL RESPONSE

The temporal response of a spectrometer may be examined by introducing a step function of near full-scale flux to the system using an electrically operated shutter and measuring the system's transient response at 0.1 s, or shorter, intervals. The response should be stable within one digitizing step, or 0.1%, whichever is greater, of the steady state value in one second or less.

5.9 TEMPERATURE CHARACTERIZATION

Two major types of temperature-induced variation may be seen in an optical radiometric instrument: 1) offset or *dark* changes, and 2) scale *responsivity* changes. Each underwater instrument must be individually characterized over the range of -2--40^0 C. In the case of deck cells, the temperature range for testing should be extended to 10—45^0 C. Sensors exhibiting temperature coefficients greater than 0.01% per ^{0}C over this temperature range, should be fully characterized over their respective ranges to establish the means and precision with which post-acquisition processing can be used to correct for temperature dependency. Although knowledge of the zero, or dark current, drift is essential for working at the lowest radiances or irradiances, it should be emphasized that more significant near-surface errors may be induced by temperature variations in responsivity.

These possible responsivity changes must be individually determined across the spectrum. In the above discussion, the temperatures cited are *environmental* temperatures, but it should be emphasized that any correction must use the temperature of the affected element, which is normally in the interior of the instrument. This is best accomplished by routinely using temperature sensors placed at critical locations within the instrument. For highest precision, dynamic temperature testing involving temporal transients, as well as possible temperature gradients within an instrument, may be appropriate.

5.10 PRESSURE EFFECTS

Pressure can cause radiometric measurement errors by deforming irradiance collectors. Pressure coefficients associated with polytetrafluoroethylene (PTFE) based irradiance diffusers are known to exist, but they are not uniform and there may be hysteresis effects. It is recommended that each type of irradiance detector be examined for variations in responsivity with pressure. If a significant effect is observed, then pressure-dependent responsivity coefficients should be determined separately for each instrument and collector. The pressure characterization should also test for, and quantify, hysteresis and temporal transients in responsivity under a time varying pressure load. The characterization of pressure effects has not previously been common practice, and the requisite procedures are therefore poorly defined; new protocols must be developed.

5.11 PRESSURE TRANSDUCER CALIBRATION

The radiometer's pressure transducer, which is used to measure instrument depth during profiles, should be tested and calibrated before and after each major cruise.

5.12 POLARIZATION SENSITIVITY

Polarization sensitivity is more critical in above-water radiometry than underwater radiometry. If a radiometer measures polarization components of radiance, then its responsivity and rejection of cross-polarization radiance must be characterized for each component channel. For above-water scalar radiance instruments, as with the SeaWiFS and other ocean color radiometers, sensitivity to linear polarization must be less than 2%, and the actual degree of polarization sensitivity must be characterized for each channel.

A generalized protocol for characterizing the polarization sensitivity of a radiometer is given here. The instrument should view a source of linearly polarized radiance, and its apparent radiance response L_1 (λ) should be recorded. The instrument should then be rotated 90^0 about its FOV axis, still viewing the linearly polarized radiance source, and the apparent radiance response L_2 (λ) should be recorded. The polarization sensitivity of the instrument will be calculated as

$$P(\lambda) = \left| \frac{2\left[L_1(\lambda) - L_2(\lambda)\right]}{L_1(\lambda) + L_2(\lambda)} \right|. \tag{5.17}$$

As required for SeaWiFS and other satellite ocean color radiometers, airborne and shipboard radiometers must satisfy P (λ)<0.02.

A very simple, semi-quantitative test of a radiometer's polarization sensitivity can be performed outdoors on a cloud- and haze-free day. The instrument should be pointed at the sky in the zenith-sun plane at an angle of approximately 90^0 from the sun, and its response L_1 (λ) recorded. Since singly-scattered Rayleigh radiance is 100% polarized at a scattering angle of 90^0, if aerosol scattering is small, the sky radiance viewed at this angle will be strongly polarized. If the instrument is

then rotated 90^0 about its FOV axis to measure L_2 (λ), an approximate estimate of $P(\lambda)$ may be computed, as above.

Specification of detailed protocols for laboratory characterization of a radiometer's polarization sensitivity will require more attention than is available here. In particular, protocols should be developed which describe in detail:

1. laboratory setups for producing a stable, uniform, extended source of linearly polarized radiance; and
2. laboratory procedures for measuring the actual degree of polarization of the polarized radiance source and for determining the uncertainty of the polarization sensitivity estimate achieved using a particular experimental setup.

Temperature dependence of an airborne radiometer's polarization sensitivity should initially be characterized at 5^0 and 30^0C. If significant differences in $P(\lambda)$ exist at these extremes of instrument operating temperatures, then polarization sensitivity measurements should be made at several additional temperatures in that range.

REFERENCES

Austin and Halikas 1976: The index of refraction of seawater. *SIO Ref. 76-1*, Vis. Lab., Scripps Inst. Of oceanography, La Jolla, California, 64pp.

Johnson, B.C., S.S. Bruce, E.A. Early, J.M. Houston, T.R. O'Brian, A. Thompson, S.B. Hooker and J.L. Mueller, 1996: The Forth SeaWiFS Intercalibration Round-Robin Experiment (SIRREX-4), May 1995. *NASA Tech. Memo. 104566, Vol. 37,* S.B. Hooker, E.R. Firestone and J.G. Acker, Eds., NASA GSFC, Greenbelt, Maryland, 65 pp.

McLean, J.T., and B.W. Guenther, 1989: Radiance calibration of spherical integrators. Optical Radiation Measurements II**,** *SPIE*, 1,**109**,114--121.

Mueller, J.L., 1993: The First SeaWiFS Intercalibration Round-robin Experiment SIRREX-1, July 1992. NASA Tech. Memo. 104566, Vol. 14, S.B. Hooker and E.R. Firestone, Eds., NASA Goddard Space Flight Center, Greenbelt, Maryland, 60 pp.

Mueller, J.L., 1995: Comparison of irradiance immersion coefficients for several marine environmental radiometers (MERs), In: Mueller, J.L. and others, Case Studies for SeaWiFS Calibration and Validation, Part 3. *NASA TM 104566*, Vol. **27**: 3-15*,* Hooker, S.B., E.R. Firestone and J.G. Acker, Eds.

Mueller, J.L.,B.C Johnson, C.L. Cromer, J.W. Cooper et al. 1994: The Second SeaWiFS Intercalibration Round-robin Experiment SIRREX-2, June 1993. NASA Tech. Memo. 104566, Vol. 16, S.B. Hooker and E.R. Firestone, Eds., NASA Goddard Space Flight Center, Greenbelt, Maryland, 121 pp.

Mueller, J.L., and R.W. Austin, 1995: Ocean Optics Protocols for SeaWiFS Validation, Revision 1. *NASA Tech. Memo. 104566, Vol. 25,* S.B. Hooker and E.R. Firestone, Eds., NASA Goddard Space Flight Center, Greenbelt, Maryland, 66 pp.

Petzold T.J. & R.W. Austin 1988: Characterization of MER-1032. *Tech.Memo.*EV-001-88t, Vis.Lab.,Scripps Institution of Oceanography, La Jolla, Califoirnia,56 pp.

Riley, T. and S. Bailey, 1998: The Sixth SeaWiFS Intercalibration Round-Robin Experiment (SIRREX-6) August—December 1997. *NASA/TM-1998-206878*. NASA, Goddard Space Flight Center, Greenbelt, MD. 26pp.

Walker, J.H., R.D. Saunders, J.K. Jackson, and D.A. McSparron, 1987: Spectral Irradiance Calibrations. NBS Special Publication 250--20, U.S. Dept. of Commerce, National Bureau of Standards, Washington, DC, 37 pp. plus appendices.

Walker, J.H., C.L. Cromer, and J.T.McLean, 1991: Technique for improving the calibration of large-area sphere sources. *Ocean.Optics*, B.W.Guenther, Ed., SPIE, **1,493**, 224-230.

Chapter 6

Calibration of Sun Photometers and Sky Radiance Sensors

Christophe Pietras[1], Mark Miller[2], Ewa Ainsworth[1], Robert Frouin[3], Brent Holben[4] and Ken Voss[5]

[1]*SAIC Genaral Sciences Corporation, Beltsville, Maryland*
[2]*Department of Applied Science, Brookhaven National Laboratory, Upton, New York*
[3]*Scripps Institution of Oceanography, University of California, San Diego, California*
[4]*Biospheric Sciences Branch, NASA Goddard Space Flight Center, Greenbelt, Maryland*
[5]*Physics Department, University of Miami, Florida*

6.1 INTRODUCTION

Atmospheric sensors are designed to measure direct solar signals and sky radiances in order to retrieve the radiative properties of the atmosphere. There are two major types of instruments which perform these measurements: sun photometers and sky radiance scanning systems including fast rotating shadow-band radiometers.

Sun photometers capture photometric intensity of the direct solar beam. Their fields of view are typically small, between 1° and 3°, in order to minimize contamination of the transmitted solar signal by scattered skylight. Some photometers are manually aimed at the sun using sun targeting mechanisms. MicroTops II (Morys et al., 1998, Porter et al, 1999) and SIMBAD (Deschamps et al., 2000, Fougnie et al., 1999a, 1999b) are two examples of hand-held sun photometers. Other are fixed and equipped with automated sun tracking mechanisms. Such instruments include CIMEL (Holben et al., 1998) and PREDE (Nakajima et al., 1996). The sun tracking mechanism is dependent on its implementation on a moving platform (e.g., PREDE POM-01 Mark II) or on a stable station (e.g., CIMEL, PREDE POM-01L). The field of view of hand-held sun photometers is generally larger than the automatic sun photometers within 2 and 3°. A higher field of view allows aiming at the sun on board a moving ship. The wider field of view of SIMBAD is intended to measure the solar signal as well as marine reflectance. Sky radiance scanning systems measure the solar aureole and sky radiance distributions.

CIMEL and PREDE instruments perform both sun photometric and sky radiance measurements.

They are dedicated to measure sky radiances 3° away from the sun in the aureole. The field of view of CIMEL and PREDE is as lower ($<1.5^o$) and the instruments are equipped with collimators for stray light rejection (O'Neill et al., 1984, Holben et al., 1998, Nakajima et al., 1996). Fast rotating shadow-band radiometers measure solar intensity values indirectly from diffuse and global upper hemispheric irradiance. They have a 2π field of view and are equipped with a solar occulting apparatus. Finally, electronic camera systems have "fisheye" lenses to obtain the full sky radiance distributions (Voss et al, 1989).

Sun photometers and sky radiometers commonly have several channels from $0.3\mu m$ to $1.02\mu m$ and narrow bandwidths ($0.01\mu m$). Their characteristics are summarized in Table 6.1. This chapter will describe calibration techniques, and limitations and accuracies of the sun photometers and sky radiometers. Measurement and data analysi protocols and procedures are discussed in Chapter 15.

Table 6.1   Characteristics of sun photometers

Channels nm	Micro Tops	SIMBAD	CIMEL	PREDE
315				✓
340			✓	
380			✓	
400				✓
440	✓	✓	✓	
490		✓		
500	✓		✓	✓
560		✓		
675	✓	✓	✓	✓
870	✓	✓	✓	✓
940	✓		✓	✓
1020			✓	✓
FOV	2.5	3	1.2	1.5

6.2 CALIBRATION TECHNIQUES FOR SUN PHOTOMETERS

In order to calibrate sun photometers, it is necessary to take into account degradation of detectors, and interference filters. The absolute calibration using lamp standards is generally not recommended for the retrieval of aerosol optical thickness (AOT). However, in case of a strong loss of sensitivity over time, Schmid et al., 1998, advised combing lamp calibration with solar calibration. Schmid et al., 1998, discussed the applicability and accuracy of the method. The following sections will present techniques commonly used with sun photometers and their validities.

Langley – Bouguer Technique

The signal measured by a sun photometer can be expressed by equation 6.1, assuming that the instrument is aimed directly into the sun and its spectral channels are not affected by gaseous absorption.

$$V(\lambda) = V_0(\lambda) * \left(\frac{d_0}{d}\right)^2 * \exp(-M(q_o) t_R(\lambda))$$
$$* \exp(-M(q_o) t_o(\lambda)) * \exp(-M(q_o) t_a(\lambda)) \quad (6.1)$$

where, $V_0(\lambda)$ is the signal representing the instrument response to solar flux at the top of the atmosphere (TOA), as derived from the Langley-Bouguer calibration procedure, $\left(\frac{d_0}{d}\right)^2$ is the earth-sun distance correction obtained according to Iqbal, 1983, q_o is the solar zenith angle, M is a function of the solar zenith angle computed according to Kasten and Young, 1989, $t_R(\lambda)$ is the Rayleigh optical thickness calculated according to Penndorf, 1957, $t_o(\lambda)$ is the ozone optical thickness acquired from the ozone amount retrieved from a satellite ozone sensor, such as Total Ozone Mapping Spectrometer (TOMS) and $t_a(\lambda)$ is the aerosol optical thickness.

The purpose of the Langley-Bouguer technique is to obtain the unknown instrument response to the solar flux at the top of the atmosphere, $V_0(\lambda)$. It is achieved by plotting the logarithm of the signal $V(\lambda)$ against the airmass M and extrapolating the signal to $M=0$. The slope of the logarithmic signal is the total optical depth (Rayleigh, ozone and aerosol). The protocol is detailed below:

1. When the air mass values vary from 1 to 6, take five successive measurements each time the airmass changes by 0.25.
2. Measure the dark current in order to avoid temperature effects.
3. Record the sky condition in case of clouds or thin cirrus occurrences (includes cloud coverage and cloud positions in the sky).
4. Stop when M reaches 7 or the sky condition changes.

The main constraint in the Langley-Bouguer technique is the stability of the atmospheric optical extinction. Hence, the accuracy greatly depends on the geographical location of the calibration experiment. The calibration is generally performed in conditions where the stability of the atmosphere and a low aerosol contribution enable high accuracy of the method (Holben et al. 1998, Schmid et al. 1998). The site of Mauna Loa Observatory (MLO), Hawaii, is particularly well suited for calibrating optical instruments. The facilities and research activities at the observatory are reported on its web site http://mloserv.mlo.hawaii.gov/. The altitude of the Mauna Loa site (3397m) reduces the uncertainties due to variabilities in aerosols and water vapor which commonly affect measurements in the lower atmospheric layers.

Variations in the atmosphere dramatically affect $V_0(\lambda)$ retrievals. Several improvements to the Langley-Bouguer technique have been proposed, such as using a calibrated reference channel (Soufflet et al., 1992) and the circumsolar radiation (Tanaka et al., 1986). A review of different methods and their accuracies are discussed in Forgan, 1994.

Accuracy and Limitations of the Langley – Bouguer Technique

The Langley-Bouguer technique has been commonly used, although it is not an absolute calibration method and has large uncertainties. Combining several Langley-Bouguer sessions in high altitude conditions minimizes of the uncertainties. AERONET reference instruments are typically recalibrated at MLO every 2-3 months using the Langley-Bouguer technique. According to Holben et al., 1998, the uncertainties in TOA voltages are estimated to be as low as 0.2 to 0.5% for the MLO calibrated instruments. Therefore, the uncertainty in AOT due to the ambiguities in TOA voltages for the reference instruments is better than 0.002 to 0.005 in absolute values.

Figure 6.1 presents typical Langley-Bouguer plot for CIMEL #101 at MLO (circles) and at

GSFC (squares). The total optical thickness at MLO is nearly half that of GSFC. The maximal difference in AOTs derived from GSFC and MLO sites is 0.05 for the air mass of 1. Therefore, MLO is an attractive calibration site for this technique.
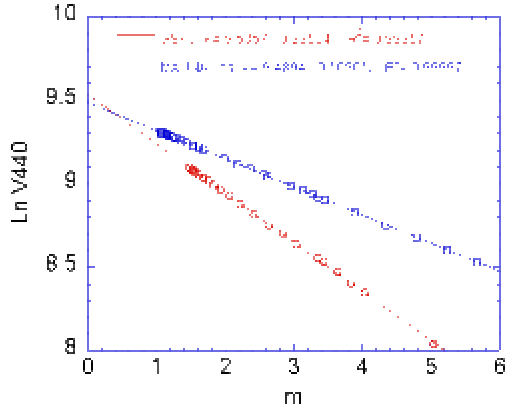

Figure 6.1   The Langley-Bouguer technique applied to CIMEL # 10 sun photometer measurements at 440nm. (o) - Mauna Loa Observatory, September 11, 1999, and (ÿ) - GSFC, October 15, 1999.

In addition to the retrieval of $V_0(\lambda)$ variable, there are other biases which influence the accuracy of the Langley-Bouguer technique, such as computations of the solar zenith angle, air mass, earth-sun distance and Rayleigh and ozone corrections. These issues are described below.

1.   Solar zenith angle computation

The solar position is retrieved using a simple algorithm based on codes from Michalsky, 1988 and Spencer, 1989, and *The Astronomical Almanac*. The uncertainty of the solar position calculated using this algorithm is 0.01^0 until the year 2050.

2.   Earth-sun distance correction

The earth-sun distance correction, $\left(\dfrac{d_0}{d}\right)^2$, is dependent on the ratio of the average to the actual earth-sun distance. It can be computed according to Platridge, 1977 (Chapter 15, Equation 15.2), or Iqbal, 1983 (Equation 6.2). Differences between the two algorithms vary between 0 and 3%.

$$\left(\frac{d_0}{d}\right)^2 = 1 + \left(0.034\cos\left(\frac{2\pi J}{365}\right)\right) \qquad (6.2)$$

3.   Air mass computation

The precise Langley-Bouguer technique requires taking into account the structure of atmospheric attenuators (Schotland et al., 1986 and Forgan, 1988). The air mass, *M*, can be computed according to Kasten, 1966, or Kasten and Young, 1989. For the solar zenith angle, θ, lower than 75° the differences between these two formulations are lower than 0.1%. For larger zenith angles, the air mass changes differently for different atmospheric attenuators. This problem is avoided by limiting the range of θ in the Langley-Bouguer technique. Various authors use different computations of the air mass for the ozone attenuator. Holben et al., 1988, uses the ozone air mass calculation proposed by Komhyr et al., 1989, and Schmid et al., 1998, uses the formulation introduced by Stähelin et al., 1995.

4.   Ozone and Rayleigh correction

The ozone optical depth is determined from TOMS measurements of ozone amounts in dobson units and ozone absorption coefficients derived from Nicolet et al., 1981.

The Rayleigh optical depth is computed using Penndorf, 1957, and additionally corrected for the elevation. Another formulation is used by Deschamps et al., 1983. Differences between the results are not more than 2.5% in the spectral range from 0.3 to 1.02µm.

The uncertainties in the retrieval of the Rayleigh optical thickness come from atmospheric pressure variabilities. Eck et al., 1989, computed the combination of calibration uncertainties and the uncertainty in ozone and Rayleigh optical thickness. The total uncertainty was estimated from 0.010 to 0.021 in terms of AOT for field instruments, and approximately from 0.002 to 0.009 for the reference instruments calibrated using the Langley-Bouguer technique.

Cross Calibration Technique

The cross calibration technique enables a cost-effective and efficient calibration of sun photometers relative to the instruments which are already calibrated using the demanding Langley-Bouguer methodology.   The cross calibration technique is based on simultaneous measurements taken from both calibrated and non-calibrated sun photometers. Observations with the lowest time difference between measurements and an air mass less than 3 are required. TOA voltages are computed according to equation 6.3:

$$V_0(\lambda_i) = V_0^{ref}(\lambda_i) * \frac{V(\lambda_i)}{V^{ref}(\lambda_i)} \qquad (6.3)$$

where, $V_0^{ref}(\lambda_i)$ is the TOA signal of a reference CIMEL sun photometer calibrated at Mauna Loa by the Langley-Bouguer technique and $V(\lambda_i)$ and $V^{ref}(\lambda_i)$ are the signals measured by the non-calibrated and reference sun photometers, respectively, for the same channel λ_i.

Some sun photometers have channels λ_i which are slightly different from any of the channels of the reference sun photometer. Therefore, the closest channel λ_j of the reference sun photometer is used. TOA voltages are then obtained using equation 6.4:

$$
\begin{aligned}
V_0(\lambda_i) = V_0^{ref}(\lambda_j) * \frac{V(\lambda_i)}{V^{ref}(\lambda_j)} * & \\
\exp\left[M(\theta_0) * (t_R(\lambda_i) - t_R(\lambda_j)) \right] * & \\
\exp\left[m(\theta_0) * (t_o(\lambda_i) - t_o(\lambda_j)) \right] * & \\
\exp\left[m(\theta_0) * t_a(1\mu m)(\lambda_i^{-a} - \lambda_j^{-a}) \right]. &
\end{aligned}
\qquad (6.4)
$$

where, the first exponential term is the differential Rayleigh effect between λ_i and λ_j, the second term corresponds to the differential ozone effect, and the third term incorporates the differential aerosol effect. The variables a and $t_a(1\mu m)$ are, respectively, the Angström coefficient and the aerosol optical thickness at $1\mu m$ determined from CIMEL reference measurements using the Angström law:

$$t_a(\lambda) = t_a(1\mu m) * \lambda^{-a} \qquad (6.5)$$

The reference sun photometer is a CIMEL reference sun photometers managed by the AERONET group and calibrated at MLO every three months using the Langley-Bouguer technique. According to Table 6.2, most of the sun photometers have common channels with the CIMEL reference sun photometer, allowing for the application of the cross calibration technique. The stability of the aerosol extinction is not very critical with this method. However, standard deviations of TOA voltages over time still need to be determined. The protocol is summarized below:

1. Set the GMT time on both calibrated and non-calibrated sun photometers.
2. Initiate measurements as soon as the calibrated sun photometer starts working.
3. Take measurements concurrently with the calibrated sun photometer.
4. Take all the measurements between 10 a.m. and 3 p.m. local time to have suitable air mass.
5. Measure the dark current in order to avoid temperature effects.
6. Record the sky condition in case of clouds or thin cirrus occurrences (cloud coverage and cloud positions in the sky).
7. Stop when M reaches 3 or the sky condition changes.

Accuracy and Limitations of the Cross Calibration Technique

SIMBIOS sun photometers are routinely cross calibrated at least every three months or before each campaign. Calibrations are performed during days with clear and stable atmospheric conditions (AOT at $0.44\mu m$ typically lower than 0.15). The uncertainties of the cross calibration are composed of uncertainties in the calibrated reference sun photometer and non-calibrated sun photometer. The calibration of the reference sun photometers is performed by the AERONET group. The calibration transfer from the MLO reference sun photometers to non-calibrated instruments using at least doubles the $V_0(\lambda)$ uncertainty for instruments of the same design. According to Holben et al., 1998, the uncertainties in AOTs obtained for cross-calibrated CIMEL instruments are estimated to be 0.01-0.02. The uncertainties are higher when the cross-calibrated sun photometer is not of the same design as the reference sun photometer.

Cross-calibrated MicroTops, SIMBAD and PREDE sun photometers determine TOA voltages with uncertainties lower than 1% (i.e. 0.02 in terms of AOT). Figure 6.2 shows the ratio of TOA voltages to the TOA voltage obtained on the first day during the cross calibration at the GSFC site on August 21, 1998, for SIMBAD and MicroTops and October 16, 1998, for PREDE. The ratios are shown for channels 440 and 870nm. The reference CIMELs were S/N 94, 37, 27 and 101 calibrated at MLO. Long-term variations in the TOA voltages between 1998 and 1999, reported in Table 6.2, are within 3% in all bands for SIMBAD and MicroTops. The variations are higher for PREDE because after October 1998 the sun sensor had problems and required repairs.
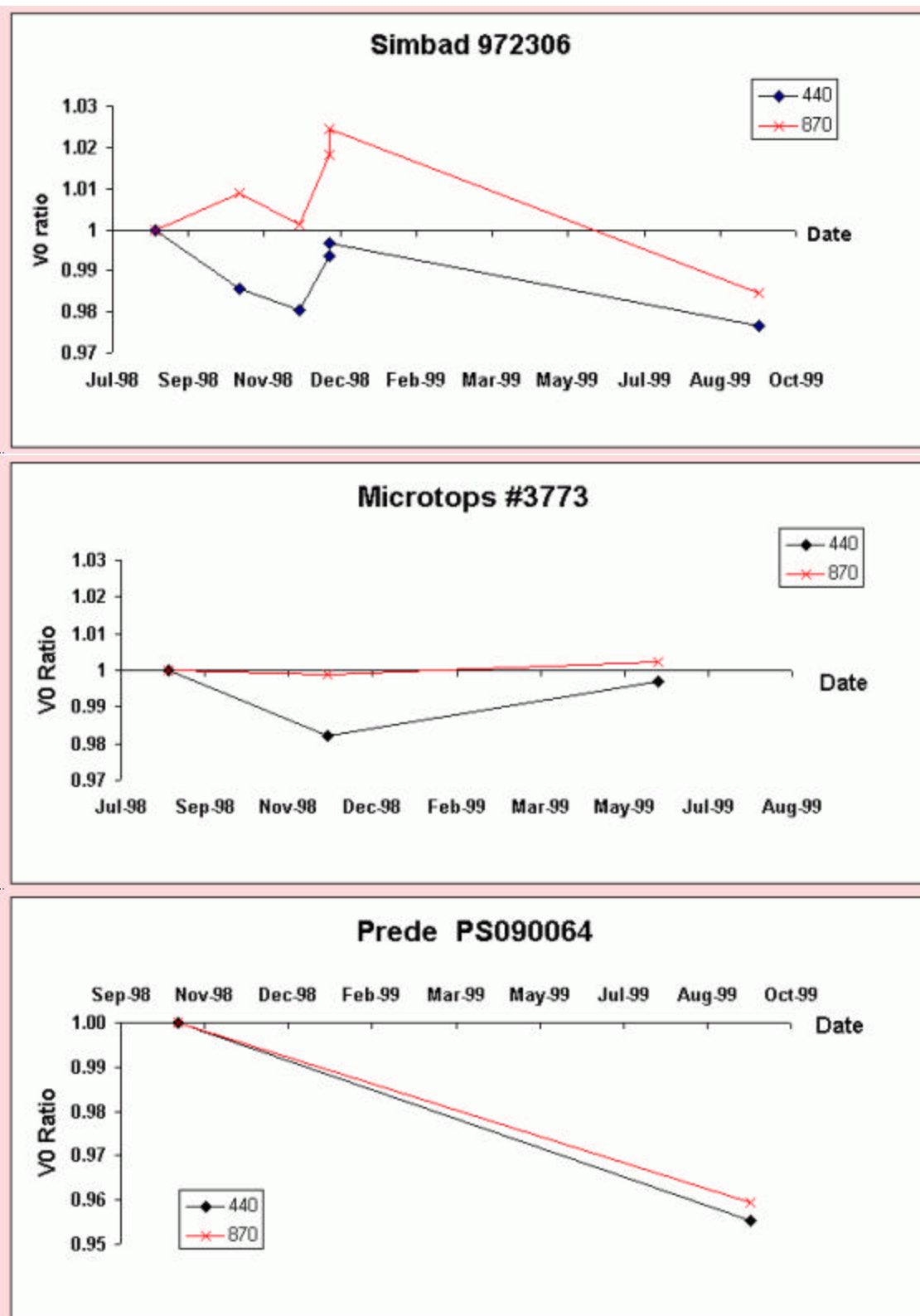
Figure 6.2 Ratios of TOA voltages to the TOA voltage obtained on the first day during the cross calibration with the reference CIMEL sun photometer at the GSFC site. Chanels 440 and 870nm are presented. August 21, 1998, is the first day for the top and middle figures. October 16, 1998, is the first day for the bottom figure.
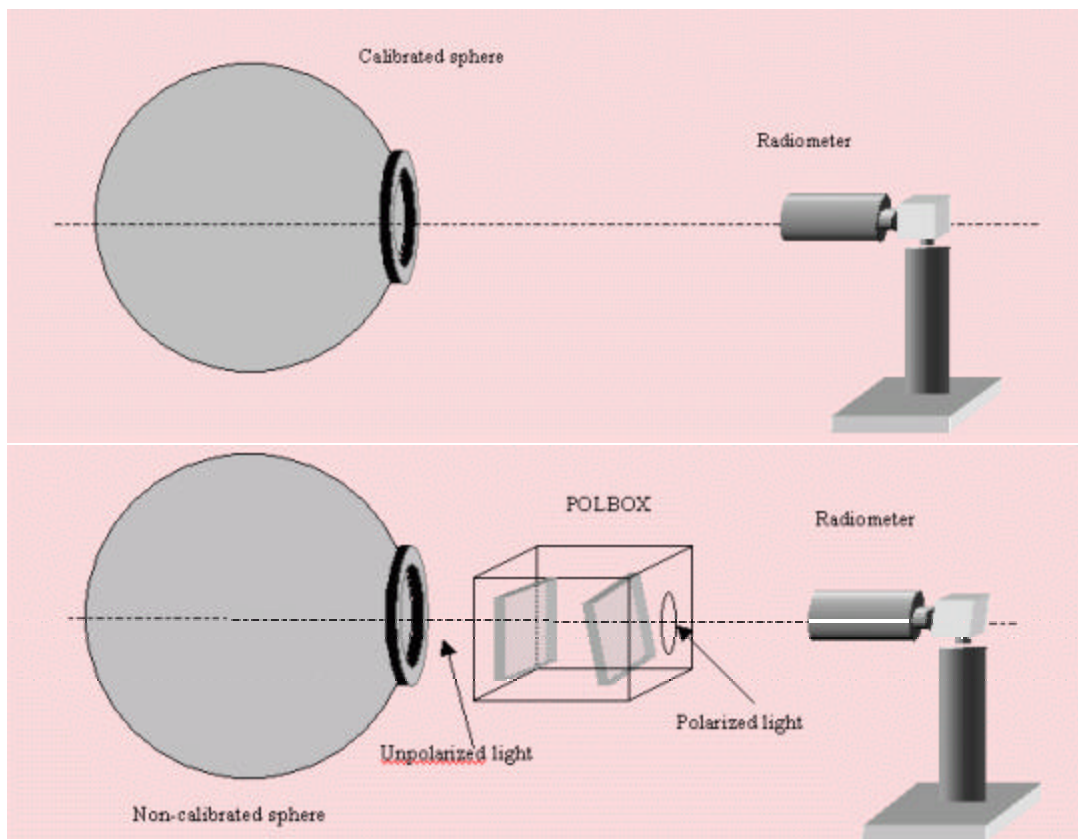
Figure 6.3   Absolute calibration of the CIMEL sun photometer (top); and calibration of the polarized channels of the CIMEL sun photometer (bottom).
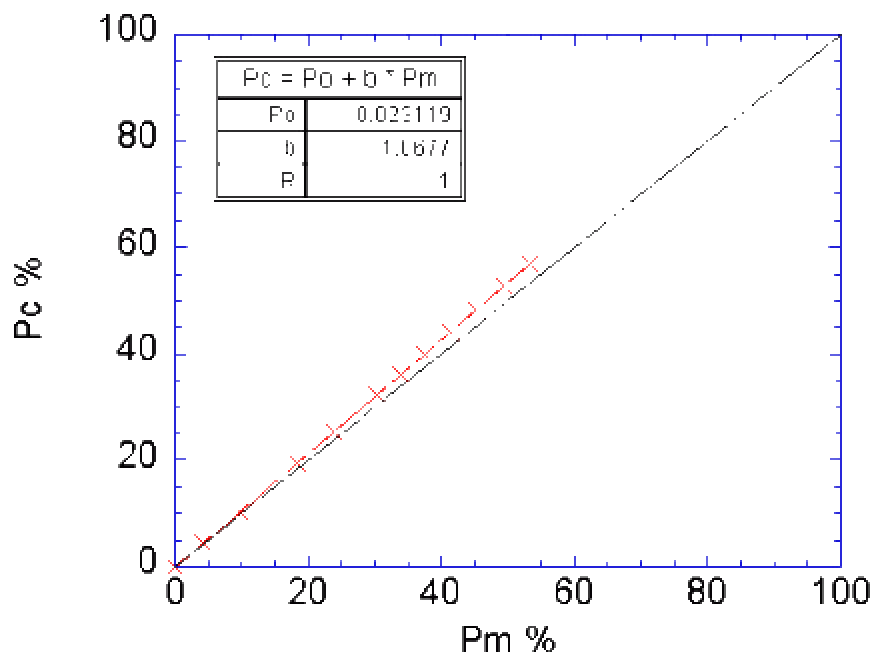
Figure 6.4   Degree of computed polarization versus measured polarization by the CIMEL #191 in May 1999 at GSFC Calibration Facilities.

Table 6-2. Top-of-atmosphere (TOA) voltages and variations since 1998 for three sun photometers cross-calibrated with respect to reference CIMELs.

MicroTops 03773		440 nm	500 nm	675nm	870nm	940nm	
CIMEL 37 8/21/98	Vo	1244	988	1218	824	1421	
CIMEL 27 11/24/98	Ä Vo	-1.77%	-1.21%	-2.13%	-0.12%	-0.70%	
CIMEL 101 6/9/ 99	Ä Vo	-032%	0.00%	-1.31%	-0.24%	-1.06%	
SIMBAD 932706		440 nm	490 nm	560nm	675nm	870nm	
CIMEL 37 8/21/98	Vo	388591	479111	407006	421086	304820	
CIMEL 27 11/24/98	Ä Vo	-1.45%	-1.61%	-3.13%	-2.63%	0.88%	
CIMEL 27 11/24/98	Ä Vo	-1.95%	-1.67%	-1.37%	-1.58%	0.12%	
CIMEL 101 6/9/99	Ä Vo	-0.65%	-1.65%	-3.42%	-2.73%	1.83%	
CIMEL 94 12/14/98	Ä Vo	-0.34%	-1.06%	-2.76%	-2.05%	2.45%	
CIMEL 94 9/23/99	Ä Vo	-2.34%	-2.49%	-3.44%	-1.27%	-1.56%	
Land Prede PS090064		440 nm	500 nm	675nm	870nm	940nm	1020nm
CIMEL 37 10/16/98	Io	1.3630E-04	2.7940E-04	3.5220E-04	2.7790E-04	2.6090E-04	1.5570E-04
CIMEL 37 9/23/ 99	Ä Vo	-4.48%	-2.61%	-3.55%	-4.07%	2.41%	-4.17%

The main source of error in retrieving AOT using sun photometry is the TOA voltages. Since Voltz, 1959, several papers have discussed different methods to improve the solar calibration. Schmid et al., 1998, used lamp and solar calibrations in conjunction with each other. O'Neill et al., 1984, combined solar aureole and solar beam extinction. Soufflet et al., 1992, and Holben et al., 1998, used a well-calibrated sun photometer as a reference.

The degradation of interference filters is the most important source of the long-term variability in the cross calibration. Although major improvements have been made on the filter design (interference filters, ion-assisted deposition), the filters remain the main factor limiting performance of sun photometers. Degradation of filters necessitates frequent calibration of sun photometers, and measurements of the filter transmission or the relative system response (Schmid et al., 1998). The degradation of the filters mounted on the CIMEL sun photometers has been monitored since 1993. Degradation reported by Holben et al., 1998, within the first 2 years of CIMEL operation is between 1 and 5%.

6.3 CALIBRATION TECHNIQUES FOR SKY RADIOMETERS

Sky radiance scanning systems are automated instruments dedicated to measure sky radiances in the aureole and in the principle plane of the sun. Radiative properties of aerosols are retrieved using an inversion algorithm of the sky radiances (Dubovik et al., 2000; Nakajima et al., 1996) and of the polarized component of the sky radiances (Vermeulen et al., 2000). This section is dedicated to the description of calibration techniques for accurate retrievals of sky radiances.

Calibration of Unpolarized Sky Radiometers

Unpolarized radiometers, such as CIMEL and PREDE, are calibrated using an integrating sphere. The radiometer is aligned in front of the sphere (Figure 6.3, top) and 10 measurements are taken for each channel. Radiances of the integrating sphere are then integrated through the domains of each channel of the radiometer. As a result, ratios of raw radiometer voltages to the integrated sphere radiances are obtained. These ratios constitute radiometer calibration parameters C_i:

$$C_i = \frac{V_i}{\int L(\lambda) \cdot R_i(\lambda) \cdot d\lambda} \qquad (6.6)$$

where V_i are the voltages measured in the considered channel i, $R_i(\lambda)$ is the response of the radiometer and $L(\lambda)$ is the radiance of the integrating sphere.

Accuracy and Limitations of the Calibration of Unpolarized Sky Radiometers

The accuracy of the radiometer calibration is dependent on the calibration of the integrating sphere, sphere's size, clarity of the calibration protocols and precision of the calibration process. A two-meter integrating sphere is available and managed by NASA GSFC Calibration Facility (http://spectral.gsfc.nasa.gov/). The uncertainty of the radiances provided by this integrating sphere is estimated to be less than 5%.

Calibration of Polarized Sky Radiometers

The technology to calibrate polarized sun photometers is now available to the SIMBIOS Project. The method was initially designed by the Laboratoire d'Optique Atmosphérique (LOA), Lille, France, for the calibration of POLDER sensor (POLarization and Directionality of the Earth's Reflectances), its airborne (Deuze et al., 1992) and space version (Bret-Dibat T. et al., 1995, Hagolle et al., 1999).

The polarization box named "POLBOX" is a passive system including neither optical source nor electrical power supply. POLBOX transforms natural light to polarized light. The user's guide for the device (Balois, 1999) is available at LOA and GSFC. A Lambertian source is necessary to provide the input light to the box, therefore, an integrating sphere is usually used. POLBOX is composed of two adjustable glass blades which have a high refractive index. The blades are placed in a black anodized aluminum alloy box. The box can turn around the optical axis. The degree of polarization and the direction of the linear polarization plane are tunable by the user by adjusting the position of the box and the blades. The alignment of the blades, relative to the optical axis, is performed by auto-collimation using a basic laser and a mirror. Alignment is required each time the blades are cleaned and replaced in the POLBOX. The required equipment consists of:

1. Polarization device POLBOX.
2. Calibrated light source (integrating sphere).
3. Lambertian light source (integrating sphere or lamp with scattering opaline diffuser).
4. Sun photometer.

The calibration process for polarized radiometers is composed of the following steps:

1. Perform the absolute calibration using the calibrated sphere (Figure 6.3, top) for all radiometer channels including the polarized ones.
2. Place POLBOX between an integrating sphere and the sun photometer (Figure 6.3, bottom). The integrating sphere is highly recommended for the stability, but its calibration is not essential for determining the relative polarized responses of the instrument.
3. Perform one measurement for each tilt of both blades in POLBOX. A combined tilt is defined and measured by the rotating unit. The tilt of each blade is identical in absolute degrees but shifted in opposite directions.

4. The polarization of the light is given by:

$$P_c(i) = \frac{A(n)\cos^2(2i) + B(n)\cos(2i) + C(n)}{D(n)\cos^2(2i) + E(n)\cos(2i) + F(n)} \quad (6.7)$$

where A, B, C, D, E, and F are functions of the refractive index *n* of the blades and *i* is the tilt angle of the blades (the same but opposite).

5. Plot the computed degree of polarization against the measured polarization and obtain the intercept of 0^0 polarization and the slope.

Due to the mechanical limitations of the POLBOX system the maximum degree of polarization which can be reached is 60%. A 100% polarization can be obtained using an analyzing polarizing sheet. If needed, the orientation of the polarization can also be determined using POLBOX. Indeed, the orientation of the polarized light is marked on the POLBOX device and a rotating system allows turning POLBOX around the optical axis in order to change the orientation.

The polarized version of CIMEL sun photometers has three polarized channels centered at 870nm with identical spectral characteristics and positioned exactly 120^0 apart. The rotating filter wheel of the CIMEL photometer has 9 filter positions, including one opaque filter to measure the dark current. Polarizing covers attached to the filter wheel allow measurement of the three components of the polarized light.

The CIMEL calibration process measures non-polarized signals from the calibrated integrating sphere. The signals are noted Vs_0, Vs_{-60}, and Vs_{+60}. The use of an unpolarized source implies that each polarized channel measures the same signal. A normalization of the measured signals is then required in order to define the coefficients K_1 and K_2:

$$K_1 = Vs_0/Vs_{-60}, \quad (6.8)$$
$$K_2 = Vs_0/Vs_{+60}.$$

Next, the sun photometer is placed in front of the POLBOX device and an integrating sphere is used as a light source (Figure 6.3, bottom). Polarized signals are measured in the three polarized channels and noted V_0, V_{-60}, V_{+60}. The degree of polarization of the light is consequently derived as follows:

$$P_m = \frac{2*\sqrt{K_1^2 V_{-60}^2 + V_0^2 + K_2^2 V_{+60}^2 - K_1 V_{-60} V_0 - K_2 V_{+60} V_0 - K_1 K_2 V_{-60} V_{+60}}}{K_1 V_{-60} + V_0 + K_2 V_{+60}}$$

$$(6.9)$$

The calibration is accomplished by plotting the computed degree of polarization against the measured polarization to obtain the 0^0 of polarization, P_0, and the slope b. Figure 6.4 presents the calibration of the CIMEL #191 performed at GSFC in May 1999. The angle of the polarized light (Ψ) may also be retrieved:

$$\tan(2\Psi) = \frac{\sqrt{3} * (V_{+60} - V_{-60})}{2 * V_0 - V_{+60} - V_{-60}} \qquad (6.10)$$

Accuracy and Limitations of the Calibration of Polarized Sky Radiometers

Accuracy of the calibration of polarized radiometers depends on the Lambertian light source and the polarization device which should be kept in good condition. Dirty glass blades may introduce a polarization by the device itself. Greasy prints on blade surfaces need to be avoided when manipulating the device during cleaning and maintenance.

The degree of polarization obtained at the output of the device is 60% at maximum due to the mechanical design of POLBOX. 100% of degree of polarization can be obtained using polarizing sheets placed in front of the radiometer. However, it is highly recommended to use the same polarizing sheets as those mounted on the radiometer. Then, adjustment of the polarizing sheets to obtain the extinction of the signal can be performed accurately.

Calibration and Characterization of Sky Radiance Distribution Cameras

Camera systems for sky radiance distribution measurements, and their uses, are described in Chapter 11 of these protocols. Absolute and spectral calibrations should be performed on the radiance distribution camera before and after each cruise. A full characterization of the instrument should be performed initially, including camera lens roll-off characteristics for each camera (Voss and Zibordi 1989). If attenuation devices are used to prevent solar saturation, these should be calibrated frequently to track drift. Linearity calibrations should also be performed with the same frequency as the absolute and spectral calibration. Procedures for characterizing this class of instruments are essentially the same as for other radiance detector systems. Each individual detector element in the detector array is essentially regarded as an independent radiometer.

6.4 CALIBRATION OF SHADOW-BAND IRRADIANCE RADIOMETER

Calibration is the most essential element of the shadow-band radiation measurement program. A thorough and on-going calibration process is required before the fast rotating shadow-band radiometer (FRSR) can make accurate radiometric measurements at sea. To insure accurate measurements, there are two important elements for FRSR measurement protocol: calibration of the instrument circuitry which includes temperature stabilization of the detector during measurements, and determination of the extra-terrestrial constants. The following two subsections discuss these elements and establish protocols.

Calibration of Instrument Circuitry and Temperature Stabilization of the Detector

Laboratory calibration is done in two parts: the optical detector and the electronics attached to the detector. The electronic gains are combined with the direct-normal detector irradiance gains coefficients to make a single calibration equation relating direct-normal irradiance to the electronic measurement in millivolts.

Initial values for the detector calibration, band-pass response, and zenith angle correction are supplied by the vendor. In addition, the instrument should be periodically recalibrated using the protocols of Chapter 5. Each of the narrow-band filters has a bandwidth of approximately 10nm and the vendor calibration provides gains at 1nm spacing. The zenith angle correction is measured on two planes, one on a south-to-north plane and one on a west-to-east plane. The zenith angle corrections are determined by holding the head in a tilting fixture under a collimated beam and tilting the head through 180° in one-degree steps from horizon to horizon in each plane.

The end-to-end electronic gains are calibrated using the data collection software and a precision reference voltage source in place of each radiometer channel. One-minute averages and standard deviations of voltages for each channel are logged for a full range of input voltages. Electronic calibrations are repeated at regular intervals and for a variety of ambient temperatures. Calibration of the electronics is performed before and after each deployment.

A silicone cell photodiode has a small leakage current which is called a ``dark current.'' After amplification in the electronics a ``dark voltage''

results, and if the dark voltage is not negligible, it must be measured and removed. In some instruments, such as the MICROTOPS II hand-held sun photometer, the operator covers the detector before taking a solar measurement. For an autonomous instrument an electronic design eliminates the dark voltage. For the FRSR, the largest deviation from a straight-line fit is less than 0.1% of full scale and no "dark voltage" adjustment is required.

Calibration drift in the multi-frequency head has caused a great deal of concern in the sun photometer community. Calibration shift is detectable as a permanent change in apparent extraterrestial irradiance E_0 as computed by the Langley-Bouguer technique. Calibration shift is erratic and quite variable; it can occur suddenly, over a few weeks, or can degrade slowly over months. The 610 nm and 660 nm channels are most prone to drift though all narrow-band channels are suspect due to gain drift shifting band-pass response. In earlier heads, the filter material, a stack of laminated films, apparently became delaminated as a result of temperature cycling and humidity. A different filter material became available after approximately December 1998 and many researchers are in the process of retrofitting their heads with the new material.

Determination of the Extra-terrestrial Constants

The Langley-Bouguer technique works whenever the skies are perfectly clear, no cirrus or other layers are present, and if t is constant over the time duration of the observations. In practice, a Langley-Bouguer calibration can be produced from about one hour of clear sky in the early morning just after sunrise or late evening just before sunset when $2 < M < 6$ ($60° < θ_r < 80°$). All measurements of E_N, the normal-beam solar irradiance (see section 11.4), are plotted on a log-linear plot and a best estimate straight line is fitted to the data. For sites other than ideal calibration locations, such as the MLO described below, a median-fitting algorithm provides the best objective fit to the data. Over the ocean, there are almost always clouds on the horizon. In the tropics these are usually high cumulus clouds or cirrus. As a result, Langley-Bouguer from ships are rare gems that must be collected whenever they occur.

As a protocol, E_0's used in final data products should be computed using the Langley-Bouguer technique at Mauna Loa. The Langley-Bouguer technique should also be used at sea as often as possible as a quality assurance tool because it provides an excellent means of detecting calibration

changes. The top-of-the-atmosphere irradiance, $F_0(λ)$, depends on the Sun-Earth separation, but its mean value, should not change significantly over time. The absolute calibration of the instrument can be compared to the mean reference solar irradiance at the top of the atmosphere, $\overline{F}_0(λ)$ (Neckel and Labs, 1984) by integrating the reference solar spectrum over the bandpass of the to obtain

$$\overline{F}_0 = \frac{\int_0^\infty w(λ)\,\overline{F}_0(λ)\,dλ}{\int_0^\infty w(λ)\,dλ} \qquad (6.11)$$

In a well-calibrated absolute instrument, $E_0 \cong \overline{F}_0$. However, as long as the calibration constant, E_0, is constant, as determined from multiple applications of the Langley-Bouguer technique, accurate AOT estimates are possible. While many investigators use raw voltages to calibrate their instruments, the extra step of computing E_0 is important since it defines the radiative impact of the aerosol at the surface.

Accuracy and Limitations of the Calibration of Shadow-Band Irradiance Radiometers

The filter material in shadow-band radiometers is sensitive to temperature. If the head temperature varies from 20 to 30°C, the 500nm filter will drift by less than 1nm (Mark Beaubean, Yankee Environmental Systems, personal communication, 1999). Keeping the temperature of the optical detector relatively stable over the range of conditions encountered on a ship can be a challenge. The internal heater in the optical detector is occasionally insufficient for the observed conditions. Providing adequate insulation is the best deterrent, although this issue remains problematic in some conditions and is the subject of current engineering efforts.

The calibration of the shadow-band radiometer is realized using the Langley-Bouguer technique. The technique is subject to the same accuracy constraints and limitations as the Langley-Bouguer calibrated sun photometers described earlier in the chapter.

REFERENCES

Balois J.Y., 1998: Polarizing box POLBOX User's Guide, *Tech. Report*, Laboratoire d'Optique Atmosphérique, Lille, France, 12pp.

Bret-Dibat T., Y. Andre' and J.M. Laherrere, 1995: Pre-flight calibration of the POLDER instrument, in *SPIE Proc.* Infrared spaceborne remote sensing III, **2553,** 218-231.

Deschamps P. Y., B. Fougnie, R. Frouin, P. Lecomte and C. Verwaerde, 2000: SIMBAD: an advanced field radiometer to measure aerosol optical thickness and marine reflectance, *Applied Optics* (submitted).

Deschamps P. Y., M. Herman M. and D. Tanre, 1983: Model calculation of the reflected solar radiation by the atmosphere and the earth between 0.35 and 4 μm., *ESA Report,* **4393/80/F/DD,** 156pp.

Deuze J.L., F.M. Breon, P.Y. Deschamps, P. Goloub and M. Herman, 1992: Polarization measurements with the airborne version of the POLDER instrument, in *SPIE* Proc. Polarization and Remote Sensing, **1747**, 178-187.

Dubovik O., and M.D. King, 2000: A flexible inversion algorithm for retrieval of aerosol optical properties from Sun and sky radiance measurements, *J. Geophys. Res.* (submitted).

Eck, T.F, B.N. Holben, J.S. Reid, O. Dubovik, A. Smirnov, N.T. O'Neill, I. Slutsker and S. Kinne, 1999: The wavelength dependence of the optical depth of biomass burning urban and desert dust aerosols, *J. Geophys. Res.*, **104**, 31, 333-31,350.

Forgan B. W., 1988: Bias in a solar constant determination by the Langley method due to Structured atmospheric aerosol: comment, *App. Opt.*, **27**, **12**, 2546-2548.

Forgan B. W., 1994: General method for calibrating Sun photometers, *App. Opt.*, **33**, **21**, 4841-4850.

Fougnie B., R. Frouin, P. Lecompte and P.Y. Deschamps, 1999a: Reduction of skylight reflection effects in the above-water measurements of diffuse marine reflectance, *Appl. Opt.,* **38**, **18**, 3,844-3,856.

Fougnie B., P.Y. Deschamps, R. Frouin, 1999b: Vicarious Calibration of the POLDER ocean color spectral bands using in situ measurements, *IEEE Trans. Geosc. & Remote Sensing*, ADEOS special issue, **37**, **3**, 1,567-1,574.

Goloub P., J.L. Deuze, M. Herman and Y. Fouquart, 1994: Analysis of the POLDER polarization measurements performed over cloud covers, *IEEE Tran.s Geosc. & Remote Sensing.,* **32**, **1**, 78-88.

Hagolle O., P. Goloub, P.Y. Deschamps, H. Cosnefroy, X. Briottet, T. Bailleul, J.M. Nicolas, F. Parol, B. Lafrance and M. Herman, 1999: Results of POLDER in-flight calibration, *IEEE Trans. Geosc. & Remote Sensing*, **37**, **3**, 1550-1566.

Holben B.N., T.F. Eck, I. Slutsker, D. Tanre, J.P. Buis, A. Setzer, E. Vermote, J.A. Reagan, Y.L. Kaufman, T. Nakajima, F. Lavenu, I. Jankowiak, A. Smirnov, 1998: A federated instrument network and data archive for aerosol characterization, *Remote Sens. Environ.*, **66**, 1-16.

Iqbal M., 1983: An introduction to Solar Radiation, Academic, San Diego, CA, 390pp.

Kasten F. and A.T. Young, 1989: Revised optical air mass tables and approximation formula, *Appl. Opt.*, **28**, **22**, 4735-4738.

Kasten F., 1965: A new table and approximation formula for relative optical airmass, *Arch. Meteorol. Geophys. Bioklimatol. Ser.*, **B14**, 206-223.

Komhyr W. D., R.D. Grass, and R.K. Leonard, 1989: Dobson Spectrophotometer 83: a standard for total ozone measurements, 1962-1987, *J. Geophys. Res.*, **94**, 9847-9861.

Morys, M., F.M. Mims, S.E. Anderson, 1998: Design calibration and performance of MICROTOPS II hand-held ozonemeter, http://www.solar.com/ftp/papers/mtops.pdf, 12pp.

Nakajima T., G. Tonna, R. Rao, P. Boi, Y.L. Kaufman, B. Holben, 1996: Use of Sky brightness measurements from ground for remote sensing of particulate polydispersions, *Appl. Opt.*, **35**, **15**, 2672-2686.

Neckel, H. and D. Labs, 1984: The solar radiation between 3,300 and 12,500 AA. *Solar Phys.,* **90**, 205-258.

Nicolet M., 1981: The solar spectral irradiance and its action in the atmospheric photodissociation processes, *Planet. Space Sci*., **29**, 951-974.

O'Neill N.T., and J.R. Miller, 1984: Combined solar aureole and solar beam extinction measurement, 1: Calibration considerations, *Appl. Opt*., **23**, 3691-3696.

Penndorf R., 1957: Tables of the refractive index for standard air and the Rayleigh scattering coefficient for the spectral region between 0.2 and 20.0 microns and their application to atmospheric optics, *J. Opt. Soc. Am.*, **47**, 176-182.

Porter, J.N., M. Miller, C.Pietras, C. Motell, 1999: Ship Based Sun Photometer Measurements Using Microtops Sunphotometers, *J. Atmos. Ocean. Technol* .(submitted), 21pp.

Schmid B. and C. Wehrly, 1995: Comparaison of Sun photometer calibration by Langley technique and standard lamp, *Appl. Opt*., **34**, 4500-4512.

Schmid B., P.R. Spyak, S.F. Biggar, C. Wehrli, J. Sekler, T. Ingold, C. Mätzler, and N. Kämplr, 1998: Evaluation of the applicability of solar and lamp radiometric calibrations of a precision Sun photometer operating between 300 and 1025 nm, *App. Opt*., **37**, **18**, 3923-3941.

Schotland R. M. and T.K. Lea, 1986: Bias in a solar Constant Determination by the Langley Method due to Structured Atmospheric Aerosol, App. Opt., **25**, 2486-2491.

Soufflet V., C. Devaux, D. Tanre, 1992: A modified Langley Plot method for measuring the spectral aerosol optical thickness and its daily variations, *Appl. Opt*., **31**, 2154-2162.

Stahelin J., H. Schill, B. Högger, P. Viatte, G. Levrat, and A. Gamma, 1995: Total ozone observation by Sun photometry at Arosa, Switzerland, *Opt Eng*., **34**, 1977-1986.

Tanaka M., T. Nakajima, M. Shiobara, 1986: Calibration of a sunphotometer by simultaneous measurements of direct-solar and circumsolar radiations, *App.Opt*., **25**, **7**, 1170-1176.

Vermeulen A., C. Devaux., and M. Herman, 2000: Retrieval of the scattering and microphysical properties of aerosols from ground-based optical measurements including polarization, *Appl.Opt*. (submitted).

Volz F., 1959: Photometer mit selen-photoelement zur spectralen messung der sonnenstrahlung und zur bestimmung der wellenlangenabhangigkeit der dunsttrubung, *Arch. Meteor. Geophys. Bioklimatol*. Ser., **B10**, 100-131.

Voss, K.J., and G. Zibordi, 1989: Radiometric and geometric calibration of a spectral electro-optic ``fisheye'' camera radiance distribution system. *J. Atmos. Ocean. Technol*., **6**, 652-662.

Chapter 7

Stability Monitoring of Field Radiometers Using Portable Sources

Stanford B. Hooker

NASA Goddard Space Flight Center, Greenbelt, Maryland

7.1 INTRODUCTION

Mueller and Austin (1995) included a discussion on tracking instrument performance in between calibration activities with stable lamp sources in rugged, fixed geometric configurations. The recommended specifications of the device included the stability of the lamp output and the repeatability of measurement must be sufficient to detect 2 % variations in an instrument's performance. In terms of the protocols for using the source, it was recommended that an instrument should be connected to the portable standard and its response recorded daily, keeping a record of instrument responsivity throughout an experiment. Furthermore, these sources would provide an essential warning of problems if they appear.

One of the more important requirements in the use of the portable source was it must be available when the complete radiometric calibrations are performed, so a baseline may be established and maintained for each sensor channel, but recognizing that the source cannot be a substitute for complete calibrations. The temporal record they provide will, however, be invaluable in cases where the pre-and post-cruise calibrations disagree or if the instrument is disturbed, e.g., opened between calibrations, subjected to harsh treatment during deployment or transport, or if the data quality are otherwise suspect. These portable standards are an important part of the recommended instrument package.

7.2 The SQM

Although Mueller and Austin (1995) specified the need for, and described some of the requirements of, a portable source, no such device was then commercially available. In response to the need for a portable source, NASA and NIST developed the SQM. The engineering design and characteristics of the SQM are described by Johnson et al. (1998), so only a brief description is given here. A separate rack of electronic equipment, composed principally of two computer-controlled power supplies and a multiplexed, digital voltmeter (DVM), are an essential part of producing the stable light field. All of the external components are controlled by a computer program over a general purpose interface bus (GPIB).

The SQM has two sets of halogen lamps with eight lamps in each set; both lamp sets are arranged symmetrically on a ring and operate in series, so if one lamp fails, the entire set goes off. The lamps in one set are rated for 1.05 A (4.2 V) and are operated at 0.95 A, and the lamps in the other set are rated for 3.45 A (5.0 V) and are operated at 3.1 A; the lamp sets are hereafter referred to as the 1 A and 3 A lamps, respectively. The lamps are operated at approximately 95 % of their full amperage rating to maximize the lifetime of the lamps.

A low, medium, and high intensity flux level is provided when the 1A, 3A, and both lamp sets are used, respectively. Each lamp set was *aged* for approximately 50 hours before deploying the SQM to the field. The interior light chamber has bead-blasted aluminum walls, so the diffuse component of the reflectance is significant. The lamps illuminate a circular plastic diffuser protected by safety glass and sealed from the environment by o-rings. The diffuser is resilient to ultraviolet yellowing, but can age nonetheless. The exit aperture is 20 cm in diameter and has a spatial uniformity of 98 % or more over the interior 15 cm circle. The SQM does not have, nor does it require, an absolute calibration, but it has design objectives of better than 2 % stability during field deployments.

A faceplate or *shadow collar* provides a mounting assembly, so the device under test (DUT), usually a radiance or irradiance sensor, can be positioned in the shadow collar. The DUT has a D-shaped collar fitted to it at a set distance, 3.81 cm (1.5 inch), from the front of the DUT. This distance was chosen based on the most restrictive clearance requirement of the radiometers used in the different

deployment rigs. The D-shaped collar ensures the DUT can be mounted to the SQM at a reproducible location and orientation with respect to the exit aperture each time the DUT is used. The former minimizes uncertainties (principally with irradiance sensors) due to distance differences between measurement sessions, while the latter minimizes uncertainties (principally with radiance sensors) due to inhomegeneities in the exit aperture light field. In either case, the D-shaped collar keeps these sources of uncertainties below the 1 % level. A schematic of the original SQM is given in Fig.7-1. The SQM faceplate can be changed to accept a variety of instruments from different manufacturers. Radiometers above a certain size, approximately 15 cm, would be difficult to accomodate, but the entire mounting assembly can be changed to allow for reasonable viewing by seemingly difficult to handle radiometers. To date, three radiometer designs have been used with the SQM, and there were no problems in producing the needed faceplates, D-shaped collars, or support hardware to accomodate these units.

The SQM light field can change because of a variety of effects; for example, the presence of the DUT, the aging of the lamps, a deterioration in the plastic diffuser, a change in the transmittance of the glass cover, a drift in the control electronics, a repositioning of a mechanical alignment, etc. To account for these changes, three photodiodes, whose temperatures are kept constant with a precision thermoelectric cooler ($\pm$ 0.01 K), measure the exit aperture light level: the first has a
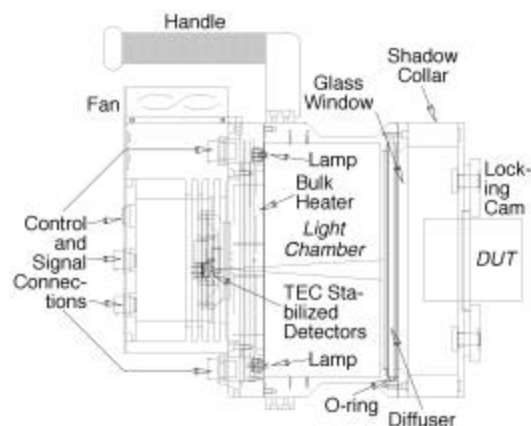

Figure 7.1. A schematic of the SQM showing a DUT kinematically mounted to the shadow collar.

responsivity in the blue part of the spectrum, the second in the red part of the spectrum, and the third has a broad-band or *white* response. All three

internal monitors view the center portion of the exit aperture. The back of the SQM is cooled by a fan to prevent a build up in temperature beyond what the thermoelectric cooler can accomodate. The SQM has an internal heater to help maintain temperature stability in colder climates and to shorten the time needed for warming up the SQM.

Another SQM quality control procedure is provided by three special DUTs called *fiducials*: a white one, a black one, and a black one with a glass face (the glass is the same as that used with the field radiometers). A fiducial has the same size and shape of a radiometer, but is non operational. The reflective surface of a fiducial is carefully maintained, both during its use and when it is not being used. Consequently, the reflective surface degrades very slowly, so over the time period of a field expedition, it remains basically constant. A field radiometer, by comparison, has a reflective surface that is changing episodically from the wear and tear of daily use. This change in reflectivity alters the loading of the radiometer on the SQM and is a source of variance for the monitors inside the SQM that are viewing the exit aperture, or the radiometer itself when it is viewing the exit aperture. The time series of a fiducial, as measured by the internal monitors, gives an independent measure of the temporal stability of the light field. The SQM has been used to track changes in instruments between calibrations and on multiple cruises lasting approximately 5--6 weeks each (Hooker and Maritorena 2000). Although there was some controversy at the design stage about operating the lamps below their rated current (approximately 95 % of rating), there has been no observable degradation in the performance of the lamps as a result of this--indeed, they have survived long shipment routes (US to UK to Falkland Islands and back) on repeated occasions, as well as, the high vibration environment of a ship. The SQM is clearly a robust instrument well suited to the task of calibration monitoring in the field at the 1\% level (Hooker and Aiken 1998). There are two commercialized versions of the SQM: the OCS-5002 built by Yankee Environmental Systems (YES), Inc. (Turners Falls, Massachusetts), and the SQM-II built by Satlantic, Inc. (Halifax, Canada). Altough both companies based their designs on the SQM, the OCS-5002 is most like the original.

7.3 OCS-5002

The OCS-5002 is composed of the lamp housing, with shadow collar and kinematic mounting system, plus a power supply, both of

which are operated and monitored via a serial port interface to a computer. All system operations, including powering on and off the lamps, controlling the cooling fan and preheater, as well as monitoring system performance during warm up and operation are controlled by the external software. The power supply and control system were specially designed to enhance performance and are enclosed in a waterproof enclosure. A picture of the lamp housing with shadow collar attached is shown in Fig. 7-2.

Figure 7.2.   A picture of the OCS-5002 without a DUT mounted to the shadow collar

An internal thermally stabilized current regulation circuit ensures precise current regulation to the two independent lamp sets (with low- and high-power lamps). The lamps in the original design were potted into aluminum mounts which held the bulbs in their correct orientations. The mounts were soldered to a circular circuit board and were difficult to replace. In the OCS-5002, porcelain sockets are used for each lamp, which are held in place with epoxy in aluminum mounting rings. This design allows for rapid individual bulb replacement.

Shunt temperatures as well as the lamp housing temperatures are monitored during operation. A two-channel filter-detector and a third unfiltered detector are positioned within the lamp housing to permit direct optical monitoring of the lamp rings and the integrating cavity itself. These three detectors are thermally stabilized via a thermoelectrically cooled housing to approximately 35^0C, and their outputs are continuously monitored during system operation.

7.4 SQM-II

The main difference between the SQM-II (Fig. 7-3) and the original unit is the high degree of integration in the former. The entire system consists of two components, a deck box that provides DC power to the SQM-II, and the SQM-II itself (McLean et al. 1998). The latter contains the lamp rings (which use the same lamps as the original SQM), heating and cooling subsystems, control circuitry, the system computer, plus display and data storage. The SQM-II system is designed to be self contained and does not require a computer to operate. Only two cables are required to complete system assembly (an AC power cord for the deck box and a DC power cord to link the deck box to the SQM-II). Although this integration reduces system complexity, it comes with increased vulnerability: a failure in any one of the subsystems can render the entire system inoperable with no opportunity for simply swapping in a new (external) subassembly, like a power supply or DVM. As was done with the original SQM, Satlantic recommends running the SQM-II on an uninterruptable power supply (UPS).

User input to start and monitor the system is via a simple 4-button keypad and a 4 x 20 fluorescent display at the rear of the device. Commands can be entered using the menus on the display or remotely from a computer. A computer can also be connected to the system to log data during a measurement session, or the data can be stored internally in a flash card and downloaded later.
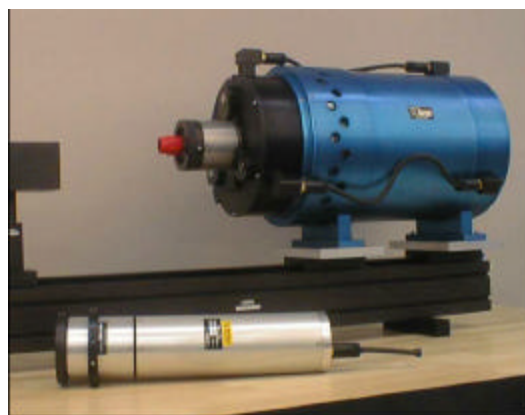

Figure 7.3.   A picture of the SQM-II with a DUT mounted to the shadow collar.

The differences between the two SQM units are not restricted to their control architecture. The SQM-II has many improvements that use of the

original unit has shown to be desirable under different circumstances:

1. The bulbs are mounted at the front, facing away from the exit aperture, which increases the average path length of the light emitted by each bulb, and it makes it easier to service the lamps (individually and as a subassembly);
2. The light chamber is lined with Spectralon, so the emitted flux is higher, and the aperture uniformity is greater; and
3. At 490 nm, the SQM-II is about seven times more intense than the SQM (the apparent blackbody temperature of the SQM-II is 3,100 K, whereas, the SQM is about 2,400 K);

Although the greater flux of the SQM-II is a desireable attribute for the blue part of the spectrum, the high output in the red saturates many in-water field radiometers. This was subsequently corrected by adding a blue filter to the exit aperture.

7.5 METHODOLOGY

To check the stability of radiometers in the field, and to monitor the performance of the SQM, a calibration evaluation and radiometric testing (CERT) session and a data acquisition sequence (DAS) needs to be defined. In its simplest form, a CERT session is a sequence of DAS events which are executed following a prescribed methodology. Each DAS represents enough data to statistically establish the characteristics of the instrument involved within a reasonable amount of time. In most cases, 3 minutes is sufficient. A typical sequence of procedures for each CERT session is as follows:

1. The electronics equipment (the lamp power supplies and the digital multimeter, the SQM fan and internal heater power supplies, the lamp timers, etc.) are turned on 1-2 hours before the CERT session begins. The total number of hours on each lamp set are tracked by recording the starting and ending number of hours on each lamp set.
2. The SQM is preheated using the internal electrical heater for 30--60 minutes, depending on the environmental conditions at the time. This is done to achieve a time efficient thermal equilibrium of the instrument from the power dissipation of the lamps.
3. If the mixture of radiometers used in the CERT sessions change over time, at least one radiometer (preferably two of different types,

i.e., radiance and irradiance) should be recurringly used in all sessions. The first data collected during the CERT session should be the dark voltages for this radiometer (usually achieved by putting an opaque cap on the radiometer) and the SQM internal dark voltages (usually acquired by blocking the SQM exit aperture with a fiducial).

4. Once the SQM is powered up at the selected lamp level, it should be allowed to warm up for at least 1 hour (and frequently for as long as 2 hours in highly variable environments). The warm-up period can be considered completed when the internal SQM monitor data are constant to within 0.1 %. The radiometric stability usually coincides with a thermal equilibrium as denoted by the internal thermistors.
5. Upon the completion of the warm-up period, the individual radiometers are tested sequentially. First, the previous DUT is removed and replaced with a fiducial. Second, dark voltages for the radiometer to be tested and SQM monitor data for glass fiducial are simultaneously collected. Third, the fiducial is removed from the SQM and replaced with the radiometer. Finally, data from the SQM and the radiometer are recorded. Each time a DUT is mounted to the SQM, the lamp voltages and internal temperatures of the SQM are recorded.
6. If multiple flux levels are to be measured, and the current lamp set is not to be used, it is powered down. The needed lamp set is powered on and allowed to warm up for 1-2 hours. The individual radiometers are tested sequentially with fiducial measurements taken during dark voltage measurements (step 5).
7. Before the SQM is finally shut down, any remaining fiducials are measured. These measurements, plus the fiducial data acquired in between the radiometer dark and light (SQM) measurements, are the primary sources for tracking the stability of the SQM flux. After the lamps are powered down, the ending number of hours on each lamp set is recorded.

It is important to note the warm-up process only involves the SQM and it is done only once before the individual DUTs are measured; the DUTs are not warmed up per se, although, they are usually kept in the same room as the SQM, so they are at room temperature.

The point for radiometric stability of the internal SQM monitors (0.1 %) is usually achieved within 30-90 minutes of powering up the lamps, depending on the amount of preheating. In general,

the warm-up period is extended another 30 minutes past this point to ensure that stability can be maintained. The radiometric stability of the SQM immediately after powering on the lamps (i.e., within 1 minute) is usually less than 0.2% with preheating, and as much as 2% without preheating depending on the environmental conditions. If a radiometer is subjected to some kind of trauma and needs to be checked as quickly as possible for an impending deployment, it is usually possible to check it to within reasonable limits using a rapid start of the SQM, particularly if the SQM is kept in the preheated mode.

If CERT sessions are conducted outside, the SQM should be shaded from direct sunlight and ambient wind conditions to prevent rapid changes in heating and cooling. A major source of noise in the stability of the lamps is vibration, particularly if the SQM is used at sea. Vibrational damping is recommended under such conditions and 0.5 in. high density felt has been demonstrated to be a good damping material.

7.6 DATA ANALYSIS

The approach for presenting the data analysis procedures is assumed to involve more than one radiometer, since most deployment systems involve a solar reference and one or more above- or in-water instruments. In the most general terms, the quantity of interest is a voltage or digital count level associated with a radiometer (or DUT), $V^C(\lambda_i, t_j)$, where V is the voltage of the radiometer under illumination at the time of the measurement, C is the instrument code of the DUT, λ_i is an individual wavelength or channel of the instrument, and t_j is a particular time for the data record. The instrument code is just a simple mnemonic for keeping track of which DUT was measured when. A suitable coding scheme is to assign a letter for a particular type of radiometer (e.g., R for radiance, I for irradiance, etc.) and then to add on the serial number).

An SQM has two lamp sets, so multiple flux levels are possible. Under most circumstances the lamp sets are different, so three basic voltage levels for the SQM monitors and for the radiometers while they are mounted to the SQM are possible: L, M, and H, which correspond to low, medium, and high lamp levels, respectively. (In situations where the two lamp sets are identical, it is customary to denote the two levels as L and M.) In addition, dark voltages are measured for the radiometers (D^C) and the SQM internal monitors (D_S). For the latter, the S code denotes the internal monitor channel (B for blue, R for red, and W for white or broadband.) Note the SQM-II has a single internal monitor in

the blue part of the spectrum. All of the data for a particular CERT session are acquired at a single lamp level.

The process of determining a parameter for monitoring the radiometric stability of a radiometer during a field deployment begins by first defining the average signal level acquired with the radiometer during a DAS:

$$\overline{V}^c\left(\boldsymbol{I}_i,\overline{t}_k\right) = \frac{1}{n}\sum_{j=1}^{n} V^c\left(\boldsymbol{I}_i,t_j\right) \qquad (7.1)$$

where (¯) denotes a time average of the total number of samples, n, collected during a DAS, and t_k is the average time over DAS time period k. Following (7-1), the average dark voltage for a DAS is defined as

$$\overline{D}^c\left(\boldsymbol{I}_i,\overline{t}_k\right) = \frac{1}{n}\sum_{j=1}^{n} D^c\left(\boldsymbol{I}_i,t_j\right) \qquad (7.2)$$

In (7.2), the temporal assignment for the average dark voltage is associated with the average signal level even though the dark values are taken a few minutes before the signal data (this is a simplification in the process that is purely cosmetic).

The average internal monitor signal level acquired during a DAS while the DUT was mounted to the SQM is:

$$\overline{V}_s^c\left(\overline{t}_k\right) = \frac{1}{n}\sum_{j=1}^{n} V^c\left(\boldsymbol{I}_i,t_j\right) \qquad (7.3)$$

where, again, S is used to denote the internal SQM monitor used for normalization: B, R, or W. The average dark voltage for an internal monitor is defined as

$$\overline{D}_s\left(\boldsymbol{I}_i\right) = \frac{1}{n}\sum_{j=1}^{n} D_s\left(t_j\right) \qquad (7.4)$$

The internal monitor dark data is collected before the lamps are warmed up, so the temporal information is not important and has been omitted. While the dark readings for a radiometer were being collected, a fiducial was placed inside the SQM and the signals from the internal SQM monitors were recorded. The voltages from the monitors are denoted by X_s^c where X can be either L , M, or H depending on the selected SQM lamp level, C is the instrument code for the DUT in the SQM, and S indicates the internal monitor under

consideration: B for the blue monitor, R for the red monitor, and W for the broad-band or white monitor.

Changes in a radiometric signal can arise from changes in the light source, the digitization electronics, or the detector electronics. Tracking the performance of a radiometer over extended time periods must take into account these three influences on the signal. The basic parameter for tracking the radiometers is constructed by taking the average voltage from the radiometer when it was mounted to the SQM, subtracting the average dark voltage, and then normalizing the difference by one of the average internal SQM monitor voltages:

$$\tilde{V}_s^c\left(\boldsymbol{I}_i,\overline{t_k}\right)=\frac{\overline{V}^c\left(\boldsymbol{I}_i,\overline{t_k}\right)-\overline{D}^c\left(\boldsymbol{I}_i,\overline{t_k}\right)}{\overline{V}_s^c\left(\overline{t_k}\right)-\overline{D}_s} \qquad (7.5)$$

where ($\sim$) denotes a normalized result for a DAS. Within the uncertainties of the measurements, $\tilde{V}_s^c\left(\boldsymbol{I}_i\right)$ should be a constant from one CERT session to the next, since an increase (decrease) in SQM intensity should coincide with an increase (decrease) in the radiometer signal.

If N is the total number of CERT sessions at a particular lamp level, the average normalized signal for a particular radiometer at that lamp level is given by:

$$\hat{V}_s^c\left(t_k\right)=\frac{1}{n}\sum_{j=1}^{n}\tilde{V}_s^c\left(\boldsymbol{I}_i,\overline{t_j}\right) \qquad (7.6)$$

where ($\wedge$) denotes the average of the normalized signals.

The temporal performance of a radiometer is determined by calculating the percent deviation of the radiometer (during a particular DAS time, t_k) from the average of all of the normalized signals (7-4):

$$\breve{V}_s^c\left(\boldsymbol{I}_i,\overline{t_k}\right)=100\left[\frac{\tilde{V}_s^c\left(\boldsymbol{I}_i,\overline{t_k}\right)}{\hat{V}_s^c\left(\boldsymbol{I}_k\right)}-1\right] \qquad (7.7)$$

where ($\cup$) denotes the percent deviation of the normalized signals with respect to the average for a particular lamp level, the average being determined from the time series of data collected during a field deployment. Thus, $\breve{M}_W^{R21}\left(421\right)$ is the percent deviation of the radiances for the 412 nm channel of radiometer OCR-200 serial number 21 (instrument code R21) at the medium lamp level normalized with the white SQM internal monitor.

The time series of corresponding fiducial measurements are formed in a similar fashion. The only data available for a fiducial is the internal SQM monitor data, so the equivalent of (7.5) for a fiducial is simply the average signal level for the monitor minus the average dark dark level:

$$\tilde{V}_s^{\%c}\left(\boldsymbol{I}_i\right)=\overline{V}_s^c\left(\overline{t_k}\right)-\overline{D}_s \qquad (7.8)$$

where C is the DUT code for a glass, black, or white fiducial (usually G, B, and W, respectively, although when many fiducials are available, the serial numbers of the fiducials are included in the coding scheme). The average signal over all CERT sessions is calculated using (7.6) and the individual percent deviations using (7.7).

The time series of fiducial measurements within a CERT gives the performance of the SQM during the CERT, and the time series of all fiducial measurements across the CERT sessions gives the long-term performance of the SQM. Because one fiducial is being used repeatedly, and two others are being used only once per CERT session, the ability to discern short- and long-term changes in the SQM is available, with the longer-term changes being measured by more than one fiducial.

7.7 FUTURE APPLICATIONS

Figure 7.4 presents a summary of SQM performance during three at-sea deployments. The data is from Atlantic Meridional Transect (AMT) cruises (Aiken et al. 2000) AMT-5 through AMT-7 plus laboratory experiments, and covers a time period of approximately 460 days. It shows the internal blue monitor signal as measured with the glass fiducial as a function of time, but presented as the percent difference with respect to the mean value for the entire time period (i.e., across all CERT sessions). A confirmation of the signal is given by the R035 radiometer for the 443 nm channel (which is very similar to the blue internal monitor for the SQM), and it very nearly mirrors the internal monitor signal. The two detectors yield similar decay rates of approximately 0.007% per day, or approximately 0.25% for a 35-day cruise.

This is an underestimate, however, because the degradation is due mostly to lamp usage, and this is obviously most significant during use, and not during shipping and storage. This is best seen by looking at the individual cruises, and comparing them to the postcruise laboratory work after AMT-7.

The stability and behavior of the SQM during AMT-5 was very similar to its performance on AMT-3 when it was first commissioned for field use (Hooker and Aiken 1998): the data indicate a

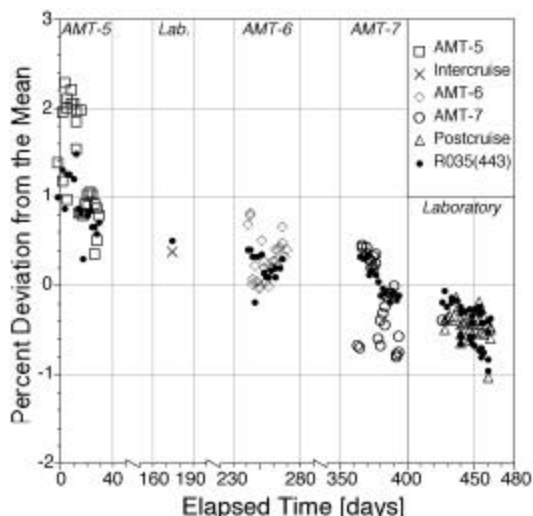stepwise change in the SQM flux level halfway through the cruise.

Figure 7.4. The long-term stability of the original SQM as measured, using its internal blue monitor and one radiometer (R035) at 433 nm, on a series of AMT cruises and laboratory exercises.

All three detectors show the change, and if the three detector signals are averaged together, the emitted flux of the SQM decreased by approximately 0.87 %. The change in flux was due to a partial short in one of the bulbs which resulted in a 1.2 % decrease in the operating voltage of the lamp. The stability of the SQM during the periods before and after the change in light output, as estimated by one standard deviation (1σ) in the average of the three internal monitor signals, was to within 0.60 % and 0.53 %, respectively.

During AMT-6, the 1σ values of the red, blue, and white detectors while measuring the glass fiducial were 0.36, 0.46, 0.39 %, respectively. The performance of the SQM during AMT-6 was the best out of all the cruises; no lamp anomalies were experienced and the standard deviation in the emitted flux was the lowest ever recorded in the field. The AMT-7 data show a stepwise change halfway through the cruise, as was seen during AMT-3 and AMT-5. Although the stability for the entire cruise was very good, to within ± 0.43 % as measured by the blue detector, the stability improves to ± 0.38 % and ± 0.28 % if the cruise is split into a first and second half, respectively.

Lamp performance after AMT-7 in the laboratory was very similar to that seen during AMT-6: the range of changes are all within 1 %. The long- and short-term stability of the SQM raises the possibility that this device can be used for

absolute calibrations in the laboratory and in the field. Although a definitive analysis of using the SQM in this fashion has not been completed, one of the objectives of SIRREX-7 was to evaluate several SQMs for this purpose (Hooker et al. 2000). The preliminary results indicate this may be possible, but a well-prescribed protocol is contingent upon completion of the SIRREX-7 data analysis and on acceptance through a rigorous independent review.

REFERENCES

Aiken, J., D.G. Cummings, S.W. Gibb, N.W. Rees, R. Woodd-Walker, E.M.S. Woodward, J. Woolfenden, S.B. Hooker, J-F. Berthon, C.D. Dempsey, D.J. Suggett, P. Wood, C. Donlon, N. González-Benítez, I. Huskin, M. Quevedo, R. Barciela-Fernandez, C.de Vargas, and C. McKee, 1999: AMT-5 Cruise Report. *NASA Tech. Memo. 1998--206892, Vol. 2*, S.B. Hooker and E.R. Firestone, Eds., NASA Goddard Space Flight Center, Greenbelt, Maryland, 113 pp.

Aiken, J., N. Rees, S. Hooker, P. Holligan, A. Bale, D. Robins, G. Moore, R. Harris, and D. Pilgrim, 2000: The Atlantic Meridional Transect; overview and synthesis of data. *Prog. Oceanogr.,*(in press).

Hooker, S.B., and J. Aiken, 1998: Calibration evaluation and radiometric Testing of field radiometers with the SeaWiFS Quality Monitor (SQM). *J. Atmos. Oceanic Tech.* ,**15**, 995-1,007.

Hooker, S.B. and S. Maritorena, 2000: An evaluation of oceanographic radiometers and deployment methodologies. *J Atmos. Oceanic Technol.*, 17,811-830.

Hooker, S.B., S. McLean, J. Sherman, M. Small, G. Zibordi, and J. Brown, 2000: The seventh SeaWiFS Intercalibration Round-Robin Experiment (SIRREX-7), March 1999. *NASA Tech. Memo. 2000--206892, Vol. 13*, S.B. Hooker and E.R. Firestone, Eds., NASA Goddard Space Flight Center, (in prep.)

Johnson, B.C., P-S. Shaw, S.B. Hooker, and D. Lynch, 1998: Radiometric and engineering performance of the SeaWiFS Quality Monitor (SQM): A portable light source for field radiometers. *J. Atmos. Oceanic Tech.*, **15**, 1,008-1,022.

McLean, S., S. Feener, J. Scrutton, M. Small, S. Hooker, and M. Lewis,1998: SQM-II: A commercial portable light source for field radiometer quality assurance. *Proc. SPIE Ocean Optics XIV*, (in press).

Mueller, J.L. and R. W. Austin, 1995: Ocean Optics Protocols for SeaWiFS Validation, Rev 1. *NASA Tech. Memo. 1995--104566, Vol. 25*, S.B. Hooker, E.R. Firestone and J.G. Aker, Eds., NASA Goddard Space Flight Center, Greenbelt, Maryland, 67 pp.

Chapter 8

Overview of Measurement and Data Analysis Protocols

James L. Mueller

Center for Hydro-Optics and Remote Sensing, San Diego State University, California

8.1 INTRODUCTION

Variables to be measured at each validation station are summarized in Table 2.1 (Chapter 2). This present chapter covers, in varying detail, the methods of measurement and data analysis associated with each of the variables listed in Table 2.1. The level of detail presented for each topic area falls into one of three categories:

- complete protocol descriptions that are not covered elsewhere in individual chapters;
- brief abstracts of protocols covered in other chapters of this document; and
- abstracted reviews of validation measurement and analysis methods for which comprehensive, up-to-date protocol descriptions have not been developed in time for publication of this document.

Clearly, the Category 3 topics are prime candidates for workshops, and supporting research, to develop protocols for a future revision to the Ocean Optics Protocols. The following outline is presented as a guide to the contents of this chapter. "Category 1" entries (material covered only here) are highlighted in bold text, "Category 2" entries (material covered in other chapters) are listed in normal text, and "Category 3" entries (material covered only here, but indadequately) are underlined.

8.2 VALIDATION SAMPLING STRATEGIES
Initialization and Validation
Case-1 Water: Sampling Strategies
Case 2 Waters: Sampling Strategies

8.3 RADIOMETRIC MEASUREMENTS AND ANALYSIS PROTOCOLS
In-Water Radiometric Profiles (Chapter 9)
Above-Water Remote-Sensing Reflectance (Chapter 10)
Normalized Water-Leaving Radiance and Remote-Sensing Reflectance: Bidirectional Reflectance and Other Factors
Sun and Sky Radiance Measurements (Chapter 11)

8.4 INHERENT OPTICAL PROPERTY MEASUREMENTS AND ANALYSIS PROTOCOLS

In Situ Reflective-Tube Absorption and Beam Attenuation Meters
Absorption Using Gershun's Equation
Absorption Spectrophotometry of Filtered Particles and Dissolved Materials (Chapter 12)
Comparative Analyses of Absorption Coefficients
Single-Wavelength Transmissometers
Volume Scattering Function and Backscattering Meters
Laboratory Measurements of Scattering in Water Samples

8.5 BIOGEOCHEMICAL AND BIO-OPTICAL PROTOCOLS
High Performance Liquid Chromatography (HPLC) Measurements and Analysis (Chapter 13)
Fluorometric Measurement of Chlorophyll a Concentration (Chapter 14)
Phycoerythrin and other Phycobiliproteins
Suspended Particulate Matter
Particle Size Distributions

8.6 ANCILLARY MEASUREMENTS AND METADATA
Logbooks
Wind Speed and Direction
Barometric Pressure
Cloud Conditions
Wave Height
Secchi Depth
Conductivity, Temperature and Depth (CTD) Profiles
Metadata

8.7 RADIOMETRIC AND OPTICAL MEASUREMENTS FROM MOORED AND DRIFTING BUOYS.

8.8 AIRBORNE MEASUREMENTS

8.2 VALIDATION SAMPLING STRATEGIES

The following discussion of bio-optical sampling protocols is organized into three subtopics: sampling for the initial and ongoing validation of a satellite radiometric system's performance, algorithm development and validation in Case-1 waters, and algorithm development and validation in Case-2 waters. The distinction between the first subtopic and the second two is clear-cut, but what precisely is meant by *Case-1* and *Case-2* water masses ?

In its literature and reports, the ocean color research community has formally adopted

definitions originally due to Morel and Prieur (1977), who stated:

``Case-1 is that of a concentration of phytoplankton [which is] high compared to that of other particles. The pigments (chlorophyll, [and] carotenoids) play a major role in actual absorption. In contrast, the inorganic particles are dominant in Case-2, and pigment absorption is of comparatively minor importance. In both cases, [the] dissolved yellow substance is present in variable amounts and also contributes to total absorption."

In practice, however, only those water masses where the CZCS-type blue-green ratio algorithms for phytoplankton pigment concentration (plus pheopigment *a*) work reasonably well have been treated as *Case-1*. All other water masses have often been loosely lumped into the *Case-2* definition, albeit with considerable confusion over how to categorize coccolithophorid blooms, and similar phenomona normally classified as *Case-1* waters, in which strong concentrations of Gelbstoff vary independently from pigment concentration.

In the present discussion of sampling protocols, Case-1 will be considered to refer to what might be called *ordinary open ocean Case-1* waters, wherein scattering and absorption are dominated by phytoplankton, pigments, and Gelbstoff concentrations, and where *global* blue-green color ratio algorithms for chlorophyll a concentration and K(490) work well. Most areas in the deep ocean belong to this case. Water masses that do not satisfy these criteria will be grouped under the heading Case-2. Within Case-2, by this definition, water masses with a wide diversity of bio-optical characteristics will be found. Prominent subcategories include:

1. coccolithophorid blooms, wherein the detached coccoliths dominate light scattering and remote sensing reflectance independently from pigment concentration;
2. coastal areas, wherein DOM of terrestrial origin contributes a strong absorption component which does not co-vary with pigment concentration;
3. phytoplankton blooms with unusual accessory pigment concentrations, e.g., *red tides*, which require the use of special regional or local ocean color algorithms; and
4. classical extreme Morel and Prieur (1977) Case-2 waters where optical properties are dominated by inorganic particles, with many possible variations in chemical and geometric characteristics.

It is important to recognize that some aspects of the water mass distinctions given above are dependent on the spectral regions in which measurements are to be made. Strong absorption at UV, red, and near-IR wavelengths requires the use of radiometric techniques similar to those required for Case-2 waters.

In addition to determining the bio-optical category and characteristics of a particular water mass, the validation sampling strategy must be concerned with spatial and temporal variability. Spatial and temporal variability in bio-optical properties will profoundly affect the validity of comparisons between satellite and in-water optical measurements. A single SeaWiFS instantaneous FOV measurement, for example, will integrate $L_W(\lambda)$ over approximately a square kilometer, or a larger area at viewing angles away from nadir. Furthermore, the location uncertainty for a single pixel may be several kilometers, except in near-shore areas where image navigation can be improved by using land-navigated anchor points.

Bio-optical profiles measured at a single station are representative of a spatial scale that is only a small fraction of a kilometer. Data from a grid of several station locations may be required to estimate the spatial averages of optical properties represented by a satellite pixel, or a block of pixels. Because the ship measurements over the grid are not instantaneous, temporal variability in bio-optical properties can add additional uncertainty to the comparisons. Aircraft radiometric observations can, conceptually, be used both to locate comparison sites away from areas of strong spatial variability and to document changes in the pattern of spatial variability over the period required for a ship to occupy all stations in a comparison grid.

Vertical stratification of water temperature, salinity, and density often affect the vertical structure of variability in bio-optical properties. This variability, in turn, affects the remote sensing reflectance. Vertical stratification of the water column becomes especially important in many Case-2 waters, where the top attenuation depth may be as shallow as 1—2 m and the entire euphotic zone may be confined to less than 10 m depth. It is important, therefore, to minimize ship-induced disruption of vertical stratification in the water column. Whenever possible, the ship should be maneuvered as little as possible while on station with its propellers and bow thruster, and the practice of backing down hard to stop quickly when on station should be strongly discouraged. If wind and sea conditions permit, the preferred method of approaching a station is to take enough speed off the ship to coast to a stop over approximately the

last 0.5 km of approach to the station. The approach should be planned to allow the ship to be turned, preferably using only the rudder, to place the sun abaft the beam or off the stern, depending on where the radiometers will be deployed. It must be realized, however, that depending on wind and sea conditions, and a particular ship's hull and superstructure configuration, it may not be possible to maintain an acceptable orientation, with respect to the sun, while the ship is adrift. In these situations, some use of the engines to maintain an acceptable ship's heading may be unavoidable.

The chief scientist should also consult with the ship's captain and chief engineer to avoid, or at least minimize, overboard discharges while the ship is on station. Material from a ship's bilge or sewage treatment system can significantly change near-surface chemical and optical properties if discharged near the immediate site of a bio-optical profile or water sample.

In some coastal areas, where a relatively transparent water mass overlies a highly reflective bottom, $L_W(\lambda)$ includes light reflected from the sea floor. These cases require special treatment of bottom reflectance effects whether the local water mass regime is Case-1, Case-2, or a combination of both. Methods of measurement, experiment design, and sampling strategies to study bottom reflectance effects are beyond the scope of this revision to the ocean optics protocols. There is a significant current research effort focused in this area (Carder et al. 1993, Hamilton et al. 1992, and Lee et al. 1998, 1999), and new protocols in this topic area may be included in a future revision of this document.

The bottom reflection of areas with a water depth exceeding 30 m normally does not contribute to the water leaving radiance, $L_W(\lambda)$. Areas with a depth shallower than 30 m are flagged in the SeaWiFS level two data product. Pixels covering very turbid waters may, however, even be usable even in shallower areas. As a general rule, the water depth should be deeper than 2.5 attenuation lengths, $1/K(490)$, at all ocean color algorithm development and validation stations. The prime exception to this rule is in developing local ocean color algorithms where bottom reflectance contributions must be taken into account (Lee et al. 1998, 1999).

Initialization and Validation

Data intended for direct comparisons between normalized water-leaving radiance $L_{WN}(\lambda)$ measured *in situ* and $L_{WN}(\lambda)$ determined from satellite data should usually be acquired in areas where bio-optical variability is known to be very small. This will ordinarily dictate that such data be acquired from optically clear and persistently oligotrophic Case-1 water masses. Potentially suitable sites include the northeastern Pacific central gyre off Baja, California (to the southwest), and the central Sargasso Sea. When planning validation cruise locations and timing, seasonal and regional cloud cover statistics should also be considered in order to maximize the likelihood of simultaneous satellite and shipboard observations. A Moored Optical BuoY (MOBY) is maintained and operated in a semi-oligotrophic site in the Northeast Pacific, near Hawaii, to provide continuous time-series radiometric comparisons with SeaWiFS, MODIS and other satellite $L_{WN}(\lambda)$ estimates (Clark et al. 1997).

A series of radiometric comparison stations should be made over a wide range of latitude in both the Northern and Southern Hemispheres, to look for evidence of cyclic thermal sensitivity affecting a satellite ocean color sensor. The spacecraft and instrument will be heated by sunlight throughout the descending (daylight) data acquisition segment of each orbit and will be cooled by thermal radiation while in the Earth's shadow throughout the remainder of the orbit. This cycling is likely to induce transient thermal gradients in the instrument, as well as a time varying cycle in the temperatures of its detectors and other components; these thermal variations could affect the spectral bandpass or responsivity of one or more of its channels. Unfortunately, a set of stations covering the full range of latitudes cannot all be sited in regions where mesoscale variability in ocean optical properties can be neglected.

As when acquiring data for developing and validating Case-1 bio-optical algorithms (see below), a significant effort must be exerted to quantify spatial variability in normalized water-leaving radiance. When possible, airborne radiometer data, in combination with careful characterization of atmospheric aerosol and cloud conditions, should be employed to augment shipboard radiometry at the stations selected for this aspect of the validation. If aircraft support is not available, semi-synoptic shipboard transects covering a 20 x 20 km^2 grid should be used to characterize spatial bio-optical variability near a sampling station (Clark et al. 1997).

The minimum set of variables to be measured for "match-up" validation analyses are those identified as "Required" in Table 2.1. Measurements used to calculate normalized water-leaving radiance for direct comparison to SeaWiFS radiances must be made under cloud-free

conditions and within five minutes of the satellite overpass.

Case-1 Water: Sampling Strategies

In open-ocean oligotrophic water, it is usually practical to assume that a station is in a Case-1 water mass, although some caution must be taken to detect coccolithophorid blooms and suspended coccoliths. In more turbid coastal transition regimes, however, the classification of the local water mass as Case-1 or Case-2 may be less obvious. In this environment, moreover, Case-1 and Case-2 water masses may both be present in the domain sampled by a ship. One example of this situation would be Case-1 water within an eddy-like intrusion from offshore into coastal areas normally occupied by Case-2 water masses. Another would be Case-2 waters in a major river plume intruding into an ambient Case-1 water mass regime. In general, a water mass may be categorized as Case-1 if:

1. Gelbstoff [Colored Dissolved Organic Matter (CDOM)] absorption at 380 nm, $a_g(380)$, is less than 0.1 m^{-1};
2. total Suspended Particulate Matter (SPM) concentration is less than 0.5 mg l^{-1} (dry weight);
3. measured $L_{WN}(\lambda)$ values, used in the ocean color Case-1 algorithm, predict measured fluorometric chlorophyll a concentration within 35%; and
4. measured $L_{WN}(\lambda)$, used in the ocean color algorithm, predicts measured remote sensing K(490) within 20%.

The determination of criterion 2 above (Doerffer pers. comm.) will ordinarily require retrospective analysis. On the other hand, *in situ* $a_g(z,380)$ profiles (e.g. using an AC9 – see below), radiometric profiles, and fluorometric pigment samples can ordinarily be analyzed on board to allow determination of criteria 1, 3 and 4 shortly after the samples are acquired.

Ocean color Case-1 algorithm development and validation requires measurements from Case-1 water masses spanning a wide range of optical properties and phytoplankton pigment concentrations. In optically transparent low-chlorophyll oligotrophic water masses, spatial variability is usually small and a station location and sampling strategy like that discussed *Initialization and Validation* is appropriate.

In high-chlorophyll mesotrophic Case-1 water masses with increased turbidity, mesoscale and smaller scale variability is often significant. In very productive Case-1 water masses, station placement and many other aspects of sampling schemes are similar to those discussed below under *Case-2 Waters: Sampling Strategy*. At algorithm development stations, where measurements need neither be coincident with, nor matched to, satellite observations, it will be necessary to characterize spatial and temporal variability only over the relatively short scales distinguishing the separate in-water radiometric, optical, and pigment measurements. Airborne ocean color, or lidar characterizations, of spatial variability in the vicinity of these stations will not usually be essential, although such additional information may be very helpful.

At stations where data are acquired for algorithm validation, and where a match to concurrent satellite ocean color measurements is required, it will be necessary to determine the patterns of spatial variability over a domain extending approximately 20 x 20 km^2 centered at the station, and to place the ship in a 2 x 2 km^2 domain over which K(490) and chlorophyll concentrations vary less than 35% about the mean. Within a few hours before and after a satellite overpass, in-water measurements should be made at several random locations to characterize variability within the 2 x 2 km^2 validation comparison site. In some cases, it may be possible to determine spatial variability adequately from ship station data and alongtrack measurements alone. One approach is to measure the alongtrack profile of *in situ* chlorophyll a fluorescence at a depth of approximately 3 m, calibrated by filtered samples to determine chlorophyll a concentration at 15-minute intervals (Section 8.5 and Chapter 14). The model of Gordon et al. (1988) may then be used to estimate $L_{WN}(\lambda)$ from the alongtrack chlorophyll profile (Clark et al. 1997). In regions of strong mesoscale variability, concurrent aircraft ocean color or lidar measurements are also valuable as a guide for selecting the ship's location, and as a basis for spatially extrapolating the in-water measurements to match the much coarser resolution of the satellite ocean color measurements.

Case 2 Waters: Sampling Strategies

Although coastal and continental shelf areas comprise only 10% of the total ocean area, they provide roughly half of the oceanic new production and most of the sequesterable DOC (Walsh et al. 1981). These areas are typically higher in phytoplankton pigment concentration, and may include colored terrigenous constituents such as

CDOM and suspended sediments. In these *Case-2* waters, the global color ratio algorithms break down because two or more substances with different optical properties are present which do not co-vary with chlorophyll a concentration. These might be waters with exceptional plankton blooms (such as red tides), areas discolored by dust transported by the wind from deserts into the sea, or coastal areas influenced by river discharge of mineral and organic suspended materials, and CDOM, i.e. *gelbstoffe*, such as humic acids.

It is not always easy to decide to which case a water mass belongs. As a starting point, the water belongs to Case-2 if any of the four Case-1 criteria, set forth above, are not satisfied. For Case-2 waters defined by any one of these criteria, it remains a further problem to determine the specific bio-optical characteristics that distinguish it from Case-1. Case-2 sampling must usually include both the "Required" and "Highly Desired" variables, as identified in Table 2.1, plus SPM. For example, it may be necessary to determine complete pigment composition and other optically important characteristics of exceptional phytoplankton blooms for such planktonic groups as *Coccolithophorids*, *Trichodesmium*, diatoms, cyanobacteria, or microflagellates.

To achieve valid comparisons between the ship and satellite data, sharp horizontal gradients and sub-pixel patchiness must be avoided, and accurate image navigation requires land anchor points near the study site. Suitable landmarks are usually available in near-shore coastal waters. The other conditions are difficult to meet in Case-2 water masses, where mesoscale and sub-mesoscale variability is typically very strong. Sub-pixel variations of no more than $\pm\,35\%$ of the mean pixel chlorophyll will be tolerated, but variability must be measured and taken into account statistically in the analysis (see below).

From the above generalities, it is clear that significant problems are encountered in near-shore coastal waters characterized by small-scale patchiness and dynamic variability due to tidal currents. A particular problem occurs in the shallow areas that are influenced by strong tidal currents -- areas that are normally well mixed during part of the tidal cycle. In the slack water tidal phase, however, a vertical gradient of the suspended matter concentration may form, which may cause problems in relating water-leaving radiance to the concentration of suspended matter. During calm periods with strong insolation, even water that is normally well mixed can become stratified. In these cases, the formation of very dense phytoplankton blooms, such as red tides, can be observed. Such

blooms will occur in coastal seas when nutrient concentrations are elevated by the influx of river water. In these circumstances, it is especially critical to avoid disturbing the vertical stratification of the water column with the ship's propellers.

One approach to sampling in this environment has been suggested by R. Doerffer (pers. comm.). In order to get a good statistical base, water samples are first taken in a random order within the area under research. The concentrations derived from the satellite image data are then compared with the ground truth data by statistical parameters, such as the mean, median, standard deviation, and the shapes of histograms (frequency distribution). For this type of statistical comparison, only sections of satellite images that match the area covered by the ship should be analyzed. Water samples and satellite data should also be temporally concurrent within the same tidal phase in order to avoid biases due to temporal variability. In these regimes, analyses to validate algorithms cannot be based on satellite ocean color data directly, but must instead be based on water-leaving radiance spectra measured *in situ* (Chapter 9) or from a ship (Chapter 10). This approach has the advantage that water samples and radiance spectra are taken nearly simultaneously.

Using either flow-through pumping systems or systems towed outside the ship's wake, fluorometry can be used to assess chlorophyll patchiness if frequent, i.e., every 10-15 minutes, chlorophyll fluorescence-yield calibration measurements are performed. Towed absorption, scattering, reflectance, and beam transmission meters can also be used to characterize spatial variability. Within a few hours of the overpass, the ship should occupy several stations at random locations within a 2 x 2 km^2 area central to the area selected for comparison with satellite data. Sampling stations placed across a tidal front during a satellite overpass may help to identify two different water masses even when the front has moved. Comparisons between *in situ* and satellite data in patchy coastal areas may be enhanced by using horizontal radiance profiles measured from an aircraft flying at low altitude (Section 8.9). Subsets of such airborne profiles allow direct comparisons with shipboard data. A corresponding profile may then be extracted from the satellite image data for a direct comparison to the aircraft trackline profiles. In Case-2 situations, such direct radiometric comparisons are valuable for validating and tuning local algorithms, but are not appropriate for satellite ocean color sensor system validation *per se*.

To validate ocean color atmospheric corrections, water-leaving radiances measured *in*

situ from the ship should be compared with those derived from the satellite data. Sample matching problems aside, Case-2 waters are often characterized by strongly varying patchiness in optical properties, pigment concentrations, and remote sensing reflectance at spatial scales smaller than a single pixel resolution of any of the current generation of ocean color sensors. Because of the nonlinear relationship between absorption by pigments, through $b_b(\lambda)/a(\lambda)$, and normalized remote-sensing reflectance $R_{RSN}(\lambda)$, the pigment concentration derived from spatially averaged satellite radiance data will systematically underestimate the true spatial average concentration by as much as a factor of 2 when sub-pixel variability is significant. It is, therefore, essential to describe sub-pixel scale variability in Case-2 waters both statistically and in terms of organized structure. Such a description may be accomplished through rapid sampling at closely spaced ship stations in combination with airborne ocean color or LIDAR measurements -- for this purpose, trackline data from low altitudes and high-resolution imagery from high altitudes are both acceptable (Section 8.9).

Absorption coefficients are large enough in all Case-2 waters to require instrument self-shading corrections to $L_u(0^-, \lambda)$, even though the correction model (Gordon and Ding 1992) has been experimentally verified only for the case where $a(\lambda)r$ is less than 0.1 (Section 9.4). In extreme Case-2 waters, large values of spectral absorption may confine the first optical attenuation depth to the top 1—2 m, where it is difficult to measure remote sensing reflectance *in situ*. Such short absorption scale lengths lead to instrument self-shading effects in $L_u(0^-,\lambda)$ which are correctable within ~5% only for instruments with diameters no larger than approximately 1 cm (Gordon and Ding 1992). Radiometers with such a small shadow cross section are conceptually feasible, and a few prototype instruments exist which may be suitable, but they are not commercially available, and self-shading sensitivities have not yet been experimentally verified for these extreme conditions. In these extreme cases, direct *in situ* measurements of $a(\lambda)$, $c(\lambda)$ and $b_b(\lambda)$ (Sections 3.7 and 8.4), together with $L_{WN}(\lambda)$, or $R_{RSN}(\lambda)$, determined from above-water radiometric measurements (Chapter 10), may provide the only practical means of developing and validating semi-analytic Case-2 algorithms. This topic remains an important area for near-term research and development.

8.3 RADIOMETRIC MEASUREMENTS AND ANALYSIS PROTOCOLS

In-Water Radiometric Profiles (Chapter 9)

Methods for measuring radiometric profiles of spectral upwelled radiance $L_u(z,\lambda)$, downward irradiance $E_d(z,\lambda)$, upward irradiance $E_u(z,\lambda)$ and surface incident irradiance $E_s[t(z),\lambda]$ (above-water) are presented in Chapter 9. The notation t(z) indicates that $E_s[t(z),\lambda]$ is measured simultaneously with the underwater measurements at depth z. The content of this chapter is largely derived from Mueller and Austin (1995), but the presentation has been reorganized to treat the topic in a more unified way. The measurement methods protocols address ship shadow avoidance, depth resolution in profiles, acquisition of instrument dark readings, and instrument attitude alignment. The protocols identify ancillary measurement and metadata to be acquired and recorded in a log during each radiometric profile measurement. Data analysis recommendations include methods for determining of the respective diffuse attenuation coefficients $K_L(z,\lambda)$, $K_d(z,\lambda)$ and $K_u(z,\lambda)$ profiles, extrapolating $L_u(z,\lambda)$ to the surface to determine $L_u(0^-,\lambda)$ and its transmission through the interface to estimate water-leaving radiance $L_W(\lambda)$ and remote sensing reflectance $R_{RS}(\lambda)$. The omission of directional notation in these quantities (cf. below) indicates they are oriented normal to the sea surface, e.g. $L_W(\lambda)$ is emitted from the surface in the zenith direction $\theta = 0$. The analysis protocols also address application of instrument calibration factors, dark corrections and depth offsets, as well as a recommended method for instrument self-shading of $L_u(0^-,\lambda)$. The effects which finite bandwidths and Raman scattering have on the radiometric quantities are briefly reviewed, but the present version of the protocols does not include a recommended method for corrections related to either phenomenon.

Above-Water Remote-Sensing Reflectance

Proposed protocols are reviewed in Chapter 10 for deriving water-leaving radiance $L_w\left(\lambda,\theta,\phi \in \Omega_{FOV};\theta_o\right)$ and remote-sensing reflectance $R_{RS}\left(\lambda,\theta,\phi \in \Omega_{FOV};\theta_o\right)$ from above-water measurements of radiance emitted from the sea surface and sky at zenith and azimuth angles (θ,ϕ)

and (θ^*,ϕ^*), respectively, with the sun at zenith angle θ_o. In the convention adopted for these protocols, azimuth angles ϕ are measured relative to the sun's azimuth. The explicit directional notation used in this context arises, because of the directional nature of skylight reflection (Chapter 10) and the bi-directional nature of ocean's remote sensing reflectance (discussed below in the next subsection). Both $L_w\left(\mathbf{1},\mathbf{q},\mathbf{f}\in\Omega_{FOV};\mathbf{q}_o\right)$ and $R_{RS}\left(\mathbf{1},\mathbf{q},\mathbf{f}\in\Omega_{FOV};\mathbf{q}_o\right)$ are AOP, which for any combination of IOP in a water mass, are dependent on the incident radiance distribution at the sea surface. For clear sky conditions, variations in surface radiance distribution are governed primarily by variations in solar zenith angle θ_o and aerosol types and amounts. For a given radiance distribution, the radiance measurements are sensitive to the observation angles (θ,ϕ) relative to the sun's principal plane and the unit vector normal to the sea surface, and to a lesser extent, to the magnitude of the radiometer's solid angle field of view Ω_{FOV} [in sr].

Chapter 10 is organized around 3 alternative proposed $R_{RS}\left(\mathbf{1},\mathbf{q},\mathbf{f}\in\Omega_{FOV};\mathbf{q}_o\right)$ measurement concepts: 1) calibrated radiance and irradiance measurements; 2) uncalibrated radiance and reflectance plaque measurements; and 3) calibrated polarized surface radiance measurements with modeled irradiance and sky radiance. The discussion of provisional protocols for measurement and analysis methods distinguish between special considerations applicable to methods 1, 2 and 3. Required ancillary measurements include sun photometer measurements of aerosol optical depth, wind speed and direction, and cloud conditions – variables of special significance for removing reflected sky radiance from the measured surface radiance. The sky radiance reflectance of the sea surface, its sensitivity to (θ,ϕ) and θ_o, and proposed methods for estimating it under clear and cloudy sky conditions, are reviewed in Section 10.4.

The Mueller and Austin (1995) provisional protocols for above-water radiometric measurements are seriously flawed and should not be used under any circumstances. Currently, there is no firm basis for recommending any of the three proposed measurement concepts, and the protocols remain provisional in many respects. For any of the three methods, recommended viewing angles are $(\theta,\phi) = (40^o,135^o)$. Specific recommendations are also made regarding preferred methods for estimating skylight reflectance under clear and overcast sky conditions; corrections for skylight reflectance under partially cloudy skies are problematic.

Normalized Water-Leaving Radiance and Remote-Sensing Reflectance: Bidirectional Reflectance and Other Factors

The water-leaving radiances and remote-sensing reflectances defined in Chapters 9 and 10 are apparent optical properties which vary as functions of the solar zenith angle θ_o, the radiance viewing azimuth and zenith angles (θ, ϕ), the earth-sun distance d on a particular day of the year, the transmission of the sun through the earth's atmosphere, and the ocean's Bidirectional Reflectance Distribution Function (BRDF) (Morel and Gentili 1990, 1993, 1996; Morel et al. 1995). In the present context, azimuth angles ϕ are measured counterclockwise from the sun's azimuth ϕ_o, i.e. $\phi_o = 0$ by convention. The ocean's BRDF is a function of the sea state and seawater IOP: $a(\lambda)$, $b(\lambda)$, $b_b(\lambda)$ and scattering phase function $\beta(\lambda,\theta,\phi,\theta",\phi")/b(\lambda)$.

Gordon and Clark (1981) were the first to point out that a more robust measure of radiance was needed to develop consistent ocean color algorithms. They therefore defined *Normalized Water-Leaving Radiance* to be water-leaving radiance emitted normal to the surface (zenith direction), with the sun at zenith and at the mean Earth-sun distance d_o, and with the effects of the atmosphere removed. Mueller and Austin (1992, 1995) followed this definition, and noted that the corrections for variations Earth-sun distance and atmospheric diffuse transmission effects $t(\theta_o)$ (including scattered skylight and reflections from clouds) may be computed as

$$\frac{E_s\left(\mathbf{1}\right)}{\overline{F}_o\left(\mathbf{1}\right)} = \left(\frac{d}{d_o}\right)^2 t\left(\mathbf{q}_o\right)\cos\mathbf{q}_o, \qquad (8.1)$$

within measurement uncertainty. $E_s(\lambda)$ is incident irradiance measured just above the sea surface, and $\overline{F}_o\left(\mathbf{1}\right)$ is mean extraterrestial solar irradiance (Neckle and Labs 1984). In the Gordon and Clark (1981) definition, the *in situ* measurement of water-leaving radiance could be simply "normalized" by the multiplicative scaling factor $\dfrac{\overline{F}_o\left(\mathbf{1}\right)}{E_s\left(\mathbf{1}\right)}$.

Morel and Gentili (1990, 1993, 1996) explored the effects of the ocean's BRDF, using radiative transfer models and realistic assumptions regarding

phase functions and other IOP. Their modeled approximations of the solar zenith angle θ_O and BRDF effects on Normalized Water-Leaving Radiance were experimentally confirmed with *in situ* measurements of the underwater radiance distribution (Morel et al. 1995). The Gordon and Clark (1981) definition of Normalized Water-Leaving Radiance, and the resulting Mueller and Austin (1992, 1995) protocols for computing it from *in situ* measurements, were thus shown to be inadequate.

The effects, on incident irradiance and water-leaving radiance, of refraction and reflection at the sea surface are combined into the reflectance term $\Re(\boldsymbol{q})$, which varies strongly with viewing zenith angle θ and wind speed, but negligibly with solar zenith angle θ_O. Using the assumptions of Morel and Gentili (1996), this term may be expressed within approximately 3.5% as

$$\Re(\boldsymbol{q}) = 0.540\left[1 - \boldsymbol{r}(\boldsymbol{q}',\boldsymbol{q})\right], \qquad (8.2)$$

where $\boldsymbol{r}(\boldsymbol{q}',\boldsymbol{q})$ is Fresnel reflectance for upwelled radiance incident on the sea surface from below at angle θ' and refracted into radiance at the observing zenith angle θ above the sea surface, i.e. $\boldsymbol{q}' = \sin^{-1}\left(\dfrac{\sin\boldsymbol{q}}{n_w}\right)$, where the refractive index of water relative to air is $n_w \cong 1.34$. Because of surface wave slopes, $\boldsymbol{r}(\boldsymbol{q}',\boldsymbol{q})$ increases with increasing wind speed in the manner shown by Austin (1974), who published tables of $\boldsymbol{r}(\boldsymbol{q}',\boldsymbol{q})$ for wind speeds of 0, 4, 10 and 16 m s^{-1}. Using (8.2), water-leaving radiance emerging normal to the surface can be estimated by multiplying observations made at zenith angle θ by the ratio $\dfrac{\Re_o}{\Re(\boldsymbol{q})}$, defining the symbol $\Re_o \equiv \Re(\boldsymbol{q} = 0^o) \approx 0.529$. $\Re_o$ is not significantly dependent on wind speed or sea state (Austin 1974; Morel and Gentili 1996).

To emphasize its observation angles, solar-zenith angle and BRDF dependencies, the notation used here and in Chapter 10 to denote water-leaving radiance is $L_w(\boldsymbol{l},\boldsymbol{q},\boldsymbol{f} \in \Omega_{FOV};\boldsymbol{q}_o)$. Water-leaving radiance at $\theta = 0^O$, as derived from in-water profiles of $L_u(z,\lambda)$ (Chapter 9), is denoted $L_w(\lambda;\theta_O)$ (see above). Morel and Prieur (1977) related irradiance reflectance to IOP as

$$\frac{E_u\left(0^-,\boldsymbol{l}\right)}{E_d\left(0^-,\boldsymbol{l}\right)} = f\,\frac{b_b(\boldsymbol{l})}{a(\boldsymbol{l})}, \qquad (8.3)$$

and defined the factor $Q \equiv \dfrac{E_u\left(0^-,\boldsymbol{l}\right)}{L_u\left(0^-,\boldsymbol{l}\right)}$ to model water-leaving radiance for $\theta = \theta_O = 0$ as

$$L_w(\boldsymbol{l};\boldsymbol{q}_o) = \Re_o\,\frac{f}{Q}\,\frac{b_b(\boldsymbol{l})}{a(\boldsymbol{l})}\,E_s(\boldsymbol{l};\boldsymbol{q}_o). \qquad (8.4)$$

Gordon et al. (1975) derived a similar model that is closely related to (8.4). The assumption that f and Q were constants made (8.4) an extremely useful approximation underlying early ocean color remote sensing algorithms for the Nimbus-7 Coastal Zone Color Scanner (CZCS). It was nevertheless understood conceptually that f and Q both varied as functions of IOP, sea state, solar zenith angle, and observation zenith and azimuth angles.

Morel and Gentili (1991, 1993, 1996) carried out an extensive series of numerical experiments, using a radiative transfer model to explore the BRDF aspects of water-leaving radiance. Their results document the functional dependencies of $f\left[\boldsymbol{q}_o,\boldsymbol{t}(\boldsymbol{l}),W,\boldsymbol{w}_o(\boldsymbol{l}),\boldsymbol{h}_b(\boldsymbol{l})\right]$ and $Q\left[\boldsymbol{q}',\boldsymbol{q},\boldsymbol{f},\boldsymbol{t}(\boldsymbol{l}),W,\boldsymbol{w}_o(\boldsymbol{l}),\boldsymbol{h}_b(\boldsymbol{l})\right]$ on observation angles, the incident radiance distribution (calculated from θ_0 and $\tau(\lambda)$ for clear sky cases only), wind speed W, the single scattering albedo $\boldsymbol{w}_o(\boldsymbol{l}) = \dfrac{b_b(\boldsymbol{l})}{c(\boldsymbol{l})}$, and the ratio of molecular to total backscattering coefficients $\boldsymbol{h}_b(\boldsymbol{l}) = \dfrac{b_{bw}(\boldsymbol{l})}{b_b(\boldsymbol{l})}$.

Petzold's (1976) San Diego Bay scattering phase function Bay was assumed for particles, and held fixed for all of the numerical experiments; the molecular volume scattering function for pure water was that of Morel (1974).

Morel and Gentili (1996) redefined *Normalized Water-Leaving Radiance*, including BRDF dependencies as

$$L_{WN}(\boldsymbol{l}) \equiv \frac{\Re_o f_o\left[W,\boldsymbol{w}_o(\boldsymbol{l}),\boldsymbol{h}_b(\boldsymbol{l})\right]}{Q_o\left[W,\boldsymbol{w}_o(\boldsymbol{l}),\boldsymbol{h}_b(\boldsymbol{l})\right]}\,\frac{b_b(\boldsymbol{l})}{a(\boldsymbol{l})}\,\overline{F}_o(\boldsymbol{l}), \quad (8.5)$$

where f_O and Q_O denote f and Q when $\theta' = \theta_O = \phi = 0$ and $\tau(\lambda) = 0$. Combining (8.1) with the definition (8.5), it can be readily shown that $L_{WN}(\lambda)$ may be computed from incident irradiance and water-

leaving radiance measured at any angles (θ,ϕ) and solar zenith θ_o as

$$L_{WN}(\boldsymbol{l}) = \frac{\Re_o}{\Re(\boldsymbol{q})} \frac{f_o(\boldsymbol{l})}{Q_o(\boldsymbol{l})} \frac{Q\left[\boldsymbol{q}',\boldsymbol{q}_o,\boldsymbol{f},\boldsymbol{t}(\boldsymbol{l}),W,\boldsymbol{w}_o(\boldsymbol{l}),\boldsymbol{h}_b(\boldsymbol{l})\right]}{f\left[\boldsymbol{q}_o,\boldsymbol{t}(\boldsymbol{l}),W,\boldsymbol{w}_o(\boldsymbol{l}),\boldsymbol{h}_b(\boldsymbol{l})\right]}$$
$$\frac{\overline{F}_o(\boldsymbol{l})}{E_s(\boldsymbol{l};\boldsymbol{q}_o)} L_w(\boldsymbol{l},\boldsymbol{q},\boldsymbol{f}\in\Omega_{FOV};\boldsymbol{q}_o). \tag{8.6}$$

where the IOP, wind speed and atmospheric optical depth dependencies of the functions f_o and Q_o have been suppressed for the sake of brevity. For the case of water-leaving radiance $L_{WN}(\lambda;\theta_o)$ at $\theta = \theta'$ = 0 with ϕ = 0 (actually it is undefined), as derived from in-water radiance profiles (Chapter 9), equation (8.6) simplifies to

$$L_{WN}(\boldsymbol{l}) = \frac{f_o(\boldsymbol{l})}{Q_o(\boldsymbol{l})} \frac{Q\left[0,\boldsymbol{q}_o,0,\boldsymbol{t}(\boldsymbol{l}),W,\boldsymbol{w}_o(\boldsymbol{l}),\boldsymbol{h}_b(\boldsymbol{l})\right]}{f\left[\boldsymbol{q}_o,\boldsymbol{t}(\boldsymbol{l}),W,\boldsymbol{w}_o(\boldsymbol{l}),\boldsymbol{h}_b(\boldsymbol{l})\right]}$$
$$\frac{\overline{F}_o(\boldsymbol{l})}{E_s(\boldsymbol{l};\boldsymbol{q}_o)} L_w(\boldsymbol{l};\boldsymbol{q}_o). \tag{8.7}$$

For this surface-normal radiance case, the function $Q\left[0,\boldsymbol{q}_o,0,\boldsymbol{t}(\boldsymbol{l}),W,\boldsymbol{w}_o(\boldsymbol{l}),\boldsymbol{h}_b(\boldsymbol{l})\right]$ is denoted by the symbol $Q_n[\lambda,\theta_o]$ in Morel and Gentili (1996). The corresponding variable *Normalized Remote-Sensing Reflectance*

$$R_{RSN}(\boldsymbol{l}) \equiv \frac{L_{WN}(\boldsymbol{l})}{\overline{F}_o(\boldsymbol{l})}, \tag{8.8}$$

may also be calculated from measured radiance and irradiance by substituting (8.6), or (8.7), for $L_{WN}(\lambda)$.

To apply equations (8.6) through (8.8) requires that one know the values of the ratios f/Q for the observation and solar angles and water mass IOP. Morel and Gentili (1996) calculated look-up tables of this ratio for a range of IOP, atmospheric optical depths, and geometric angles. They also recognized that, while aerosol optical depths could be estimated from remotely sensed ocean color data, the IOP's needed to determine f/Q could not be derived directly, nor would they always be independently measured during *in situ* experiments. Therefore, they fit to their computed data a polynomial expression giving a chlorophyll concentration estimate *Chl* [mg m^{-3}] in terms of a blue-green reflectance ratio as

$$\ln[Chl] = \sum_{n=0}^{5} A_n \left\{ \ln\left[\frac{a(443)b_b(555)}{a(555)b_b(443)}\right] \right\}^n . \tag{8.9}$$

Coefficients A_n are listed in Morel and Gentili (1996) for the 443 and 555 nm wavelength combination, and similar sets of coefficients for other wavelength combinations are available on request. In the present context, *Chl* is used solely as a bio-optical water mass index and proxy variable for the IOP. The computed values of *Chl* were matched against their results to produce lookup tables giving values of the ratio $f(\lambda,\theta_o,Chl)/Q(\lambda,\theta',\theta_o,\phi,Chl)$. The tabulated f/Q values apply only to *Case-1* water masses and values of *Chl* less than 3 mg m^{-3}. These tables may be obtained from the authors via anonymous ftp at ccrv.obs-vlfr.fr, or from the SIMBIOS Project Office.

To apply the Morel and Gentili (1996) algorithm to radiances measured *in situ*, a first estimate of *Chl* is obtained by substituting the measured, non-normalized radiance ratio $\dfrac{L_W(555,\boldsymbol{q},\boldsymbol{f}\in\Omega_{FOV};\boldsymbol{q}_o)}{L_W(443,\boldsymbol{q},\boldsymbol{f}\in\Omega_{FOV};\boldsymbol{q}_o)} \dfrac{E_s(443)}{E_s(555)}$ for $\dfrac{a(443)b_b(555)}{a(555)b_b(443)}$ in (8.9). The estimated Chl is used to enter the $f(\lambda,\theta_o,Chl)/Q(\lambda,\theta',\theta_o,\phi,Chl)$ lookup table, and the results are applied in (8.6) to determine an initial estimate of $\dfrac{L_{WN}(555,\boldsymbol{q},\boldsymbol{f}\in\Omega_{FOV};\boldsymbol{q}_o)}{L_{WN}(443,\boldsymbol{q},\boldsymbol{f}\in\Omega_{FOV};\boldsymbol{q}_o)} \dfrac{\overline{F}_o(443)}{\overline{F}_o(555)}$, which is used in turn to update the Chl estimate, and the process is iterated until convergence is obtained.

Sun and Sky Radiance Measurements

Protocols for atmospheric radiometric measurements were addressed only superficially in Mueller and Austin (1995). The new Chapter 11, by Frouin et al., provides detailed protocols for two types of radiometric measurements essential to verify atmospheric correction algorithms and to calibrate vicariously satellite ocean color sensors. The first type is a photometric measurement of the direct solar beam to determine the optical thickness of the atmosphere. The intensity of the solar beam can be measured directly, or obtained indirectly from shadow-band radiometer measurements of diffuse global upper hemispheric irradiance. The second type is a measurement of the solar aureole and sky radiance distribution using a radiance

distribution camera, or a scanning radiometer viewing in and perpendicular to the solar principal plane. From the two types of measurements, the optical properties and concentration of aerosols can be derived.

Chapter 11 presents measurement protocols for radiometers commonly used to measure direct atmospheric transmittance and sky radiance, namely standard sun photometers, fast-rotating shadow-band radiometers, automating sky scanning systems, and CCD cameras. Methods and procedures to analyze and quality control the data are discussed, as well as proper measurement strategies for evaluation of atmospheric correction algorithms and satellite-derived ocean color.

8.4 INHERENT OPTICAL PROPERTY MEASUREMENTS AND ANALYSIS PROTOCOLS

The present version of the protocols does not include a comprehensive, up-to-date set of protocols for measuring inherent optical properties (IOP). Refer to the brief discussion in Section 3.7 for more background on this topic. It is planned to remedy this situation and add IOP protocol chapters to the next revision of Ocean Optics Protocols (in 2001), but for the present IOP protocols are presented here only as brief abstracts of the current state-of-the-art. The main exception to this situation is that newly expanded protocols for spectrophotometric measurements of absorption by particles on filters, and by CDOM in filtrate, are presented in Chapter 12, which is contributed by Mitchell et al.

In Situ Reflective-Tube Absorption and Beam Attenuation Meters

For the development of bio-optical algorithms describing the inherent and apparent optical properties of the water, and for algorithms estimating primary productivity, more stringent requirements are recommended for transmissometer calibration and characteristics. Spectral measurements of beam transmittance should be made with absolute uncertainties of 0.1% transmittance per meter, or 0.001 m^{-1} beam attenuation coefficient c(λ).

It is always best to determine optical properties *in situ*, if possible. Sampling variability, changes of light intensities, filtration procedures, and sample degradation over time all affect the particulate matter and distort its true optical properties as they existed in the ocean, and as they determine the remote sensing reflectance viewed by SeaWiFS. The reflecting tube method has been used to measure spectral absorption in the laboratory for many decades (James and Birge 1938). In recent years, this method has been adapted for use in the ocean (Zaneveld et al. 1992). Suitable instruments are now commercially available and are coming into general use within the oceanographic community. Detailed protocols for using these instruments are not included in this revision of the Ocean Optics Protocols. This is also the situation regarding their calibration (Section 3.7). As with calibrations, protocols for using the instruments and analyzing the measurements are provided by the instrument manufacturer. The best known example of this type of instrument is, perhaps the AC9 manufactured by WETLABS Inc.; protocols and for using this instrument and analysing its measurements are available at (www.wetlabs.com). As with the AC9 calibration protocols (Section 3.7), extensions to the manufacturer's measurement and analysis protocols are described by Twardowski et al. (1999) and on the web site maintained by the Oregon State University Optical Oceanography Group at (http://photon.oce.orst.edu) (S. Pegau, Pers. Comm.). Perhaps the most critical of the protocols and protocol extensions is the absolute necessity of calibrating the instrument daily with optically pure water if high quality measurements are to be made at sea (Twardowski et al.1999; Pegau, Pers. Comm.).

The reflecting tube does not perfectly gather all scattered light and transmit it to the detector, and as a result, there is a scattering error on the order of 13% of the scattering coefficient. This error can be largely corrected if the beam attenuation coefficient is measured simultaneously. In that case, the scattering coefficient is obtained as b(λ) = c(λ)-a(λ). By assuming that the measured absorption is due to water and scattering error at a wavelength in the infrared, and by subsequent correction at other wavelengths using a provisional b(λ), it is possible to correct the spectral absorption to within a few percent of the scattering coefficient. Only in waters with very high scattering and very low absorption would this error pose a serious absorption error (Zaneveld et al. 1994).

Corrections for ambient temperature and salinity (Pegau and Zaneveld 1993; Pegau et al. 1995) require that a CTD profile (Section 8.6) be acquired in conjunction with a profile made using an AC9 or similar instrument. It is strongly recommended that a CTD and the absorption and attenuation meter be attached together on the same profiling package. This correction is in addition to

the correction for the instrument's internal temperature, as determined by the manufacturer's calibration (Section 3.7).

If the intake port of an AC9, or similar *in situ* reflecting tube meter, is fitted with a large area 0.2 m filter, the spectral absorption of the dissolved component can be measured (Twardowski et al. 1999). A pair of reflecting tube absorption meters can thus be used to determine the separate constituents of absorption due to particulate and dissolved substances--a distinction of fundamental importance in relating absorption to remote sensing reflectance. More traditionally, the filtration and spectrophotometry techniques developed over the last decade also lend themselves well to this task. Using the methods described in Chapter 12, the spectral absorption coefficient is partitioned into components associated with Gelbstoff, pigments, and non-pigmented particles (the latter sometimes referred to misleadingly as *detritus*).

Absorption Using Gershun's Equation

In situ spectral absorption coefficient profiles can also be measured with spectral radiometers conforming to the performance specifications listed in Chapter 4, if the radiometric package is extended to measure $E_d(z,\lambda)$ and $E_u(z,\lambda)$, as well as scalar irradiances $E_{0d}(\lambda)$ and $E_{0u}(\lambda)$. This combination may be approached either using hemispherical collectors to measure upwelling and downwelling hemispherical irradiances (Hojerslev 1975), or by using cosine collectors on one radiometer in tandem with spherical collectors on another radiometer. Given these irradiance components, spectral absorption is then computed using Gershun's equation (Gershun 1939) as

$$a(z,\lambda) = K(z,\lambda)\frac{E(z,\lambda)}{E_o(z,\lambda)}, \qquad (8.10)$$

where $E(z,\lambda) = E_d(\lambda) - E_u(\lambda)$ is vector irradiance, $K(\lambda)$ is the vertical attenuation coefficient for vector irradiance, and scalar irradiance $E_0(\lambda) = E_{0d}(\lambda) + E_{0u}(\lambda)$.

Comparisons between absorption profiles measured using Gershun's equation with $E(\lambda)$ and $E_0(\lambda)$ (scalar irradiance) data, and absorption profiles measured with a reflecting tube instrument, agreed within 8% (Pegau et al. 1994). This level of agreement is well within the calibration uncertainties of the particular prototype instruments used for that experiment, which were approximately 10% uncertainties in both the scalar

irradiance radiometer and in the reflecting tube instrument. Less than 5% uncertainty in absorption is expected in future experiments. In very clear oligotrophic water, however, uncertainty in water absorption values may make it impossible to realize this level of relative agreement. Radiometers equipped with hemispherical irradiance collectors, a prerequisite to application of this method, have only recently become commercially available (HOBILABS Inc; www.hobilabs.com). To date, there is insufficient community experience, in the form of published results based on measurements with this instrument, to include more detailed protocols and uncertainty estimates for this approach. Expanded protocols for Gershun measurements of absorption may appear in a future revision to this document.

Absorption Spectrophotometry of Filtered Particles and Dissolved Materials

Protocols in Chapter 12, by Mitchell et al., describe methods for filtering seawater to capture suspended particles on GF/F filters, and for measuring the absorption spectra of the particle-laden filters with a laboratory spectrophotometer. Methods are also described for extracting phytoplankton pigments from the filters, and measuring the residual spectrum of particulate materials other than phytoplankton. Finally, laboratory methods are also described for measuring the absorption spectrum of CDOM in filtered seawater samples. The new material in this chapter derives from the results of recent experimental intercomparison workshops in which the authors participated.

Comparative Analyses of Absorption Coefficients

Data from a reflective tube absorption and beam attenuation meter may be analyzed to obtain vertical profiles of $a(z, \lambda)$, $a_g(z, \lambda)$, and $c(z, \lambda)$, and by difference $b(z, \lambda) = c(z, \lambda) - a(z, \lambda)$ and $a_p(z, \lambda) = a(z, \lambda) - a_g(z, t)$. Optical density spectra for filtrate and filtered water samples (Chapter 12) may be analyzed to obtain independent measures of $a_g(z, \lambda)$, $a_p(z, \lambda)$, and $a(\lambda, t)$, and by difference $a_\phi(z, \lambda) = a_p(z, \lambda) - a(z, \lambda)$. Methods for merging and comparing the two independent types of absorption measurements, and for interpreting the results in terms of remote sensing reflectance, are the subject of currently active research by several investigators. The next revision to this document may be expected to contain extensive modifications and extensions of these protocols.

Single-Wavelength Transmissometers

Single wavelength transmissometers based on Light Emitting Diode (LED) sources have been in widespread use for nearly 20 years. The initial LED transmissometers all measured beam transmission in the red, at wavelengths near 660 nm. Based on recent improvements LED technology, transmissometers of this type are now also available at blue and green wavelengths. The discussion in Section 3.7 related to the calibration of this type of transmissometer is also relevant to the present subsection.

The windows on the beam transmissometer must be cleaned with lens cleaner or a mild detergent solution and a soft cloth or tissue, rinsed with distilled water, then rinsed with isopropyl alcohol and wiped dry. An approximate *air calibration* reading should be made before every cast to verify that the windows are clean. A transmissometer *dark voltage* should also be measured at this time. These on-deck air calibrations should be logged and compared to the more careful air calibrations done under dry laboratory conditions before and after each cruise (Section 3.7). If pre- and post-cruise air calibrations are significantly different, the time history should indicate whether the change occurred suddenly (e.g. a scratch in the window), or as a drift over time.

Raw beam transmissometer voltage profiles, $V'(z)$, are first corrected for any range-dependent bias of the A/D data acquisition system (Equation 3.1). The corrected voltages, $\hat{V}(z)$, are then further adjusted for instrument drift (occurring subsequent to the factory calibration) with the equation

$$V\left((z)\right)=\left[\hat{V}\left(z\right)-V_{dark}\right]\frac{V'_{air}}{V_{air}}, \qquad (8.11)$$

where V_{dark} is the instrument's current dark response with the light path blocked, and V'_{air} and V_{air} are, respectively, the current air calibration voltage (Section 3.7) and the air calibration voltage recorded when the instrument was calibrated at the factory. $V(z)$ is then converted to transmittance, $T(z,\lambda)$ over the transmissometer's path length, r, following the manufacturer's instructions for the particular instrument. The beam attenuation coefficient $c(z,\lambda)$ is then computed as

$$c\left(z,\lambda\right)=-\frac{1}{r}\ln\left[T\left(z,\lambda\right)\right], \qquad (8.12)$$

which has units of m^{-1}. The apparent values of $c(z,\lambda)$ should be further corrected, again following the manufacturer's instructions, for the finite acceptance angle of the instrument's receiver; this is usually a small, but significant, correction. Finally, the beam attenuation coefficient due to particles is computed as

$$c_p\left(z,\lambda\right)=c\left(z,\lambda\right)-c_w\left(\lambda\right), \qquad (8.13)$$

where $c_w(\lambda)$ is the beam attenuation coefficient, i.e., $c_w(\lambda) = a_w(\lambda) + b_w(\lambda)$ for pure water. The recommended values of $a_w(\lambda)$ are Pope and Fry (1997), and of $b_w(\lambda)$ are Morel (1974) over the spectral range of interest here (Section 3.7).

Scattering Coefficient Determinations

Given measurements of absorption and beam attenuation coefficients, corrected as outlined above, the volume scattering coefficient may computed simply as

$$b\left(z,\lambda\right)=c\left(z,\lambda\right)-a\left(z,\lambda\right), \text{ all in } m^{-1}. \qquad (8.14)$$

Volume Scattering Function and Backscattering Meters

The relationships between the volume scattering function $\beta(\theta,\lambda)$, the integral moment measurements $\overline{b}\left(\overline{q},\overline{l};c\right)$ made by scattering sensors, and the backscattering coefficient $b_b(\lambda)$ are explained in Section 3.7. That information will not be repeated here. Maffione and Dana (1996) describe the methods for estimating $b_b(\lambda)$ from scattering measurements at a single angle in the backward direction, e.g. using a HOBILABS HydroScat instrument and following protocols provided by the manufacturer (www.hobilabs.com). WETLABS provides protocols for estimating $b_b(\lambda)$ from scattering measurements at 3 angles using their ECO-VSF instrument (www.wetlabs.com).

Stramska et al. (2000) combined measured IOP and AOP in a radiative transfer model, and calculated backscattering coefficients agreeing with measurements using a HydroScat sensor within reasonable uncertainty. As emphasized in the discussion of the methods for calibrating scattering sensors (Section 3.7), however, additional research and evaluation are needed to address several key questions before the community will converge on a consensus supporting detailed protocols for backscattering measurements. It is anticipated that

considerable progress will be made towards those protocols as part of the next revision (Revision 3, scheduled for 2001)

Laboratory Measurements of Scattering in Water Samples

Tassan and Ferrari (1995) proposed a method for measuring backscattering and total scattering using a standard dual-beam spectrophotometer and integrating sphere. Balch et al. (1999) describe methods for estimating backscattering coefficients using a commercial benchtop laser device. A comprehensive review and development of protocols for methods of this type are deferred to a later revision to this document.

8.5 BIOGEOCHEMICAL AND BIO-OPTICAL PROTOCOLS

High Performance Liquid Chromatography (HPLC) Measurements and Analysis

Mueller and Austin (1995) simply adopted the JGOFS HPLC protocols for measuring phytoplankton pigment concentrations by reference (UNESCO 1994), and supplemented them with some brief instructions on sampling and sample handling procedures. Although this approach embraced protocol documentation describing a complete methodology, and represented a community consensus, the lack of a comprehensive end-to-end protocol statement has proved to be a source of confusion and debate within the ocean color community. Furthermore, the JGOFS protocols (UNESCO 1994) specified that pigment concentrations should be reported in units of pigment mass per mass of seawater (ng Kg^{-1}), rather than in units of pigment mass per volume of seawater (either μg L^{-1}, or mg m^{-3}). The use of volumetric concentrations is critical because radiative transfer in the ocean, and absorption by pigments, are volumetric processes. One could use the mass concentration values preferred by JGOFS, but it would be essential to supplement them with densities computed from CTD data, and make the conversion to volumetric concentrations. Therefore, a complete set of protocols for HPLC measurement of phytoplankton pigment concentrations has been written by Bidigare and Trees and added as Chapter 13 of the present revision (2.0) to the Ocean Optics Protocols. Chapter 13 provides complete protocols for obtaining water samples, filtering them, freezing the filtered samples in liquid nitrogen, sample handling and storage, extraction, HPLC calibrations and measurements, data analysis and quality control.

Fluorometric Measurement of Chlorophyll a Concentration

For reasons similar to those described above for HPLC pigment measurements, it was decided that the protocols for fluorometric measurement of chlorophyll a and phaeopigments were too briefly abstract in Mueller and Austin (1995). Therefore, the present document covers this topic in a new Chapter 14, by Trees et al., which provides complete protocols for obtaining water samples, filtering them, freezing the filtered samples in liquid nitrogen, sample handling and storage, extraction, fluorometer calibrations and measurements, data analysis and quality control.

In addition, Chapter 14 discusses geographic and temporal variabilities in the relationship between fluorometric chlorophyll concentrations and combined concentrations of total chlorophyll pigments determined by the HPLC methods (Chapter 13). It is both easier and less expensive to measure chlorophyll a and pheopigment concentrations using the fluorometric method, which has the added advantage of allowing shipboard analyses at sea during lengthy cruises. When these data are used for remote sensing algorithm development or validation, however, regional and temporal (i.e. cruise-to-cruise) dispersions and/or biases may be introduced unless the fluorometric data are first statistically adjusted (on a local basis) to agree with HPLC determinations of the concentration of total chlorophylls. A cost-effective strategy is to acquire, on each cruise, a majority of filtered pigment samples for fluorometric chlorophyll a and pheopigment analysis, supplemented by a smaller number of replicate samples for HPLC pigment analysis. The HPLC replicates should provide a representative distribution over geographic location, depth and time during a cruise, and will be used to determine a local regression relationship between the two measurements. This approach is now required for pigment data submitted for SeaBASS archival and SIMBIOS validation analysis.

Finally, Chapter 14 includes protocols for measuring and analysing profiles of *in situ* fluorescence by chlorophyll *a*, F(z) (Table 2.1). Together with c(z,660) profiles (Section 8.4), the structure of F(z) provides valuable guidance for selecting depths of water samples, analyses of

structure in $K(z,\lambda)$ derived from radiometric profiles, and various aspects of quality control analysis. It is often useful to also digitally record one-minute averages of F(z, lat, lon) in water pumped from a near-surface depth (z ~ 3 m) to measure horizontal variability while underway steaming between stations, especially in water masses where mesoscale and sub-mesoscale variability is strong (Section 8.2). If supplemented by frequent fluorometric chlorophyll *a* samples filtered from the flow-through system, the alongtrack profile of F(z ~ 3m, lat, lon) can be "calibrated" in units of chlorophyll a concentration (mg m^{-3}).

Phycoerythrin and other Phycobiliproteins

$R_{RS}(\lambda)$ may be enhanced by fluorescence by phycoerythrin (PE) in a band near 565 nm (e.g. Hoge et al. 1998; Wood et al. 1999). The detection from aircraft of laser-induced phycoerythrin fluorescence is already well established (Hoge et al. 1998). It is more difficult to detect and quantify solar induced phycoerythrin fluorescence, but some work has been done in that area as well (Morel et al. 1993; Morel 1997; Hoge et al. 1999; Subramaniam et al. 1999).

Various phycoerythrins differ from one another in chromophore composition. All phycoerythrins contain phycoerythrobilin chromophores [PEB; maximum $a(\lambda)$ near λ ~550 nm]; many others also contain phycourobilin chromophores [PUB; maximum $a(\lambda)$ near λ ~500 nm] which extends the range of wavelengths absorbed by the pigment molecule into the blue regions of the spectrum. The ratio of PUB:PEB chromophores in the PE pigments synthesized by different *Synechococcus* strains greatly affects the absorption spectrum of the whole cells (Wood *et al*. 1985). Clearly, the dependence of $a(\lambda)$ on the PUB:PEB ratio of phycoerythrin will affect also $R_{RS}(\lambda)$ in water masses dominated by cyanobacteria. The PUB:PEB ratio for the PE in a given water mass may be characterized using scanning fluorescence spectroscopy (Wood et al., 1999; Wyman, 1992).

The measurement of phycoerythrin is not yet as routine or as accurate as the measurement of chlorophylls or carotenoids. The techniques introduced by Stewart and Farmer (1984) work well for measuring biliproteins in freshwater and estuarine species but are less successful for natural populations of marine species. Wyman (1992) reported a linear relationship between the *in vivo* fluorescence emission intensity of PE measured in the presence of glycerol and the PE content of

Synechococcus strain WH7803. Scanning spectral fluorescence measurements have been used to estimate PE concentration of extracted bulk samples (Vernet *et al*., 1990). Nevertheless, there are few direct measurements of separated PE proteins from natural samples. High Performance Capillary Electrophoresis (HPCE) is a powerful analytical tool currently used in clinical, biochemical, pharmaceutical, forensic, and environmental research. In HPCE, high voltages (typically 10-30 kV) are used to separate molecules rapidly in narrow-bore (25-100 µm), fused-silica capillaries based on differences in the charge-to-mass ratio of the analytes. HPCE is an automated analytical separation system with reduced analysis times and on-line quantification of compounds, ideally suited to the separation and quantification of water-soluble proteins (like phycobilins) from seawater. HPCE methods for separation analyses of phycoerythrin from cyanobacterial cultures and natural samples are currently under development and may be included in a future revision to the ocean optics protocols (C. Kinkade, Pers. Comm.).

Suspended Particulate Matter

All suspended particulate material (SPM) dry weight (mg L^{-1}) will be determined gravimetrically as outlined in Strickland and Parsons (1972) and as specified in JGOFS protocols (UNESCO 1994). In general, samples are filtered through 0.4 m preweighed polycarbonate filters. The filters are washed with three 2.5--5.0 ml aliquots of DIW and immediately dried, either in an oven at 75^0 C, or in a dessicator. The filters are then reweighed in a laboratory back on shore using an electrobalance with at least seven digits of precision.

Particle Size Distributions

Particle size distributions can potentially provide important information about the shape of the volume scattering function, which strongly influences the bi-directional aspects of remote-sensing reflectance (e.g. Morel and Gentili 1996). Particle size distributions have been measured for many years using Coulter Counters and related to IOP, including $c(\lambda)$ (e.g. Kitchen et al. 1982). More recently, particle size distributions have also been measured by several investigators using the Spectrix Particle Size Analyzer. Again, specific manufacturers and equipment items are mentioned here as examples only and no recommendations are to be implied. Protocols for measurements and analyses of particle size distributions are not included in this version of the ocean optics

protocols, but protocols should be written and added to the next revision.

8.6 ANCILLARY MEASUREMENTS AND METADATA

The "Required" and "Highly Desired" ancillary measurements and metadata are listed in Table 2.1. Ancillary observations are often of key importance in flagging and interpreting apparently aberrant data. In addtion, some of ancillary measurements are essential for corrections to optical measurements, for example the Temperature and Salinity dependence of spectral absorption by pure water must be used in the processing and analysis of AC9 data (Pegau and Zaneveld 1993; Pegau et al. 1997). Metadata peculiar to a particular type of measurement, such as instrument calibration information, serial numbers, etc., are specificied in the protocols for making those measurements. The present section identifies recommended methods for acquiring and recording the information and data of more general applicability.

Logbooks

The person, or group, making a particular set of measurements normally maintains a separate logbook to record complete metadata unique to a particular instrument, including names of measurement and dark reference data files. It is the chief scientist's responsibility to also maintain a master logbook in which essential metadata (event, time, location) and general environmental conditions are recorded to link all measurements and samples acquired at each station. At the end of each cruise, the chief scientist should also obtain a photocopy of the ship's bridge log from the vessel's master.

Wind Speed and Direction

If possible, anemometer measurements of wind speed and direction should be recorded continuously throughout each station, and underway between stations if alongtrack data are recorded. As a precaution, the wind speed and direction should be read and recorded manually in the master and individual instrument log entries for each measurement made during a station. If the only available anemometer is not digitally recorded, these manual log entries will obviously be the only record available.

Barometric Pressure

Surface barometric pressure should be read from both the ship's barometer, and from any barometer that is part of an automatically recorded meteorological system, and recorded in the chief scientist's master logbook. This information should be manually logged at the beginning, end, and hourly during sampling at each station. If possible, it is also desireable to digitally record barometric pressure, along with wind speed and direction, throughout each station, and while steaming between stations also if other alongtrack meteorological data are recorded.

Cloud Conditions

The percent of the sky covered by clouds should be logged at the time of each measurement event. Identification of cloud types, including such comments as "thin cirrus", is "Highly Desired", but not "Required" (Table 2.1). It is also very useful, for broken and partial overcast conditions, to comment on the relationship between locations of clouds and the zenith and azimuth angles of the sun and satellite, and whether the sun is occluded. For validation cruises, predictions of approximate satellite and solar zenith and azimuth angles for given locations and days are available on request from the SIMBIOS Project Office.

All-sky photographs, using a digital camera equipped with a fisheye lens are useful documentation of sky conditions. Digital photographs of segments of the sky, using a camera with a smaller field-of-view lens, are also useful if annotated with zenith and azimuth pointing angles.

Wave Height

The overall wave height, peak to trough in m, estimated visually by a trained and experienced observer is adequate for purposes of these protocols. As is explained in any introductory textbook on general oceanography, this type of height estimate closely corresponds to *Significant Wave Height*, defined as the average of the highest one-third waves in a 20-minute record of measured wave amplitudes. More sophisticated measurements of ocean surface wave characteristics are beyond the scope of these protocols. Where the protocols for a particular measurement require it, e.g. above-water remote-sensing reflectance protocols (Chapter 10), the wave slope spectrum is calculated from wind speed. Estimates of the percent of the surface covered by whitecaps are also useful as comments, but this may usually be

adequately estimated from wind speed as well. Digital photographs of the sea surface conditions are useful documentation of sea state and whitecap conditions at the time of radiometric measurements.

Secchi Depth

A *Secchi Disk* is a white circular disk, approximately 25 cm in diameter, attached to a line marked with a stripe at 25 cm intervals and a broader stripe (or double stripe) at each full meter. A lead weight (~5 Kg) is attached to the bottom of the rig to maintain the disk in a horizontal orientation as it is lowered and raised through the water. The disk should be lowered through the ship's shadow on the side away from the sun to reduce surface glint. The observer pays out the line, lowering the disk until it just disappears from his view and then raises it until just the depth where it again becomes discernable. The depth indicated by the line markings at the water surface when the disk disappears from the observer's view is recorded as Secchi depth in m.

At depths shallower than Secchi depth, the high reflectance of the white disk (~90%) produces a target with strong visual contrast to the lower reflectance (~2%) of the ambient water column. As the disk is lowered deeper in the water, irradiance illuminating the disk is reduced and the light reflected from it is also attenuated during its transmittance to the sea surface surface. The apparent contrast between the target and surrounding water is therefore reduced with increasing depth, until at Secchi depth, the contrast disappears between the target and water column. The reader interested in a more quantitative analysis and interpretation of Secchi depth should begin with the treatment by Preisendorfer (1986).

Secchi depth should be taken at least once at each station and recorded in the chief scientist's master log and in the separate logbooks maintained for radiometric, IOP and CTD-Rosette profiles. It is the author's experience that in optically deep water masses, Secchi depths, in m, display a strong linear correlation with $K(490)^{-1}$, also in m. $K(490)$ is the diffuse attenuation coefficient $K_d(z,490)$ averaged over the top diffuse attenuation length, and its inverse corresponds to the depth at which measured $E_d(z,490)$ is 37% of $E_d(0^-,490)$. A useful quality control procedure is to plot Secchi depth against $K(490)$ for every station on a cruise. Departures from a strong linear trend between these variables are indicative of either suspect data, or of anomalous conditions. For instance, if bottom reflectance is significant at a station, then the

Secchi depth from that station will be significantly less than that predicted by its deep water correlation with $K(490)^{-1}$. This occurs because the ambient background brightness is enhanced by light reflected by the bottom, and the disk's contrast disappears at a shallower depth that would have occurred in deeper water with the same K(490).

Conductivity, Temperature and Depth (CTD) Profiles

Although Temperature T(z) and Salinity S(z) profiles measured with a CTD are listed as only "Highly Desired" in Table 2.1, the availability of a combined CTD and Rosette-sampling system strongly affects the quality of discrete water samples acquired to measure phytoplankton pigment concentrations, which are important "Required" measurements. This is particularly true if the CTD+Rosette system is also equipped with a single-wavelength beam transmissometer to measure, e.g., c(z,660) (Section 8.4), and a fluorometer to measure *in situ* chlorophyll *a* fluorescence intensity F(z) (Section 8.5). The recommended sampling protocol is to measure, and display in real time on a computer monitor during the downcast, profiles of T(z), S(z), the sea water density anomaly $\sigma_t(z)$, c(z,600), and F(z). The profile of $\sigma_t(z)$ provides the best indicator of the depth of the mixed layer and strength of the underlying pycnocline. Structure in the T(z) and S(z) profiles may be used to indicate the presence of interleaving water masses with possibly different bio-optical origins and characteristics. The F(z) profiles will identify depths of subsurface maxima and strong gradient features in the chlorophyll profile. The $c_p(z,660) = c(z,660) - c_w(660)$ will reveal depths of gradients, maxima and minima in the concentration of suspended particulates. This graphical information can be used to quickly select appropriate depths at which water samples should be taken to best represent the bio-optical structure of the water column. Finally, during the upcast, the CTD+Rosette package is stopped at each selected depth, a selected bottle is closed, and its identification number and digitally displayed depth from the CTD unit are recorded in the water sample log.

The combined CTD, transmissometer and fluorescence profiles should be measured in conjunction with, preferably immediately before and after, the irradiance and radiance profile measurements. This is feasible, because more than one cast is typically required to obtain enough water samples for all measurements on each station.

The $c_p(z,660)$ and $F(z)$ profiles are very useful as guides for, and constraints on, the determinations of attenuation coefficients $K(z,\lambda)$ from the radiometric profiles (Chapter 10). These data are also useful information for analyses to develop and validate pigment and primary productivity algorithms.

Vertical profiles of CTD should be measured to at least the depth of the deepest bio-optical profile. If the station schedule will permit it, sections of CTD casts extending to 500 m, or deeper, will be useful for computing relative quasi-geostrophic currents and shear, which may affect the advection and mixing of bio-optical properties during a cruise.

If possible, a few deep (1,500 m depth or greater) CTD and bottle sample profiles should be made during each cruise to obtain data for calibrating the CTD's conductivity probe. During these *CTD calibration casts*, water samples should be taken at depths where the vertical gradient of salinity is very small. This practice will minimize errors in the conductivity calibration resulting from the spatial separation of the water bottle and CTD profile. The bottled salinity samples may be stored for post-cruise analyses ashore at a laboratory equipped with an accurate salinometer and IAPSO Standard Seawater, if suitable equipment and standard water are not available aboard the ship (Section 3.9).

Each CTD profile should be prefiltered to remove any depth reversal segments resulting from violent ship or hydrowire motions. This will remove many instances of salinity spiking, an artifact which occurs when water temperature changes at a rate faster than the conductivity probe can follow. The CTD data should then be processed to profiles of potential temperature (^{o}C), salinity (Practical Salinity Units [PSU] based on the Practical Salinity Scale of 1978, PSS78), and density (kg m^3) using the algorithms which have been endorsed by the United Nations Educational, Scientific, and Cultural Organization (UNESCO)/SCOR/International Council of Exploration of the Seas (ICES)/IAPSO Joint Panel on Oceanographic Tables and Standards, and also by SCOR Working Group 51 (Fofonoff and Millard 1983).

At this stage, each set of CTD profiles should be carefully examined to detect any significant static instability artifacts resulting from salinity spiking. After any such major artifacts are removed by editing, the data should be further smoothed by averaging temperature and conductivity data into 2 m depth bins, and the final profiles of salinity,

density, and other derived parameters should be recomputed using the smoothed CTD profile.

For any hydrographic station, descriptive hydrographic analyses should include T-S profile characterizations of water masses. Features in the density profile which appear to be related to physical mixing and stability should be compared with features in the corresponding bio-optical profiles. CTD profiles from horizontal transects (i.e., two-dimensional grids) should be used in the computation of two-dimensional sections, or three-dimensional gridded arrays, for such variables as geostrophic currents, temperature, salinity, and the density anomaly σ_t These analysis products, together with corresponding two- or three-dimensional representations of bio-optical variability, can be used to estimate the relative importance of advection and isopycnal mixing in redistributing or modifying upper ocean optical properties during a cruise.

Metadata

For each water sample and measured variable (of all categories) listed in Table 2.1, it is critical to record the date, time (UTC), and geographic position (latitude and longitude in decimal degrees to the nearest 0.001) of its acquisition or measurement. Position and time metadata should be obtained using a Global Positioning System receiver, if possible.

Depths of measurements made with profiling instruments are usually recorded electronically in the profile data records and files. If measurements are made at depths determined by means other than a pressure transducer integrated with the data acquisition system, then the source of that information must be logged (e.g. reference to another file containing time synchronized depth records from an independent instrument on the same package). In the case of a visually read depth scale (e.g. line markings, or a rigid scale attached above an instrument), as is sometimes done to obtain depths with uncertainty < 1 cm in very turbid Case-2 waters under calm conditions, each individual depth must be identified with the measurement and entered in a logbook.

The depth from which each water sample is acquired must be recorded in a log, together with all other information required for each measurement to be made from that sample, including pigments (Chapter 13 and 14) and spectrophotometric absorption measurements (Chapter 12). This depth is ordinarily read from the CTD system attached to a rosette sampler. If a CTD, or other instrument equipped with a pressure

transducer, and rosette sampler are not used (e.g. as with bottles hung directly on the hydro-wire), then the method used to determine bottle depth on closing must be fully described, together with an estimate of the uncertainty in each depth, in comments accompanying the data.

Wire angles should be logged at different depths during each instrument and bottle sampling cast. These entries are critically important for radiometric casts, and for bottle casts when a CTD+Rosette system is not used.

The depth of the water column should be read from the vessel's fathometer and recorded in the log. If the water depth exceeds the range of the fathometer, the recorded depth should be taken from a navigation chart. The distance off the ship of a profiling radiometer, and its direction, and that of the sun, relative to the ship's heading provides an important indication of the likelihood that ship shadow effects may be present in the data. Similarly, the ship's heading relative to the sun may help identify possible shading (or reflection) artifacts in $E_s(\lambda)$ if the shipboard reference radiometer cannot be mounted higher than all masts, antennas, and superstructure elements. It is usually adequate to simply enter a sketch in the log showing the sun and package positions relative to the ship. Of course if the ship's compass heading (in degrees – Magnetic or True) are recorded, the solar azimuth and zenith may be easily computed from the time and position metadata.

8.7 RADIOMETRIC AND OPTICAL MEASUREMENTS FROM MOORED AND DRIFTING BUOYS

Radiometric and bio-optical measurements from buoys are becoming increasingly common within the ocean color and bio-optical research community. The Moored Optical Buoy (MOBY), a highly sophisticated radiometric array sited in the lee of Lanai, Hawaii, has proved a key source of water-leaving radiance data for radiometric validation and vicarious calibration of OCTS, SeaWiFS and MODIS ocean color systems (Clark et al. 1997; Fargion et al. 1999). Other examples of long-term moored arrays incorporating commercially available radiometers of the same type used for underwater profiles (Chapters 4, 5 and 9) include the bio-optical sensors on the Tropical Atmosphere Ocean mooring array (Chavez et al. 1998), the Bermuda Test-bed Mooring (Dickey 1995) and a mooring in Bedford Basin (Cullen et

al. 1997). Examples of radiometers mounted on drifting buoys, and applications to ocean color science, are described in Abbott et al. (1995) and Cullen et al. (1997).

The applications of moored radiometric arrays within a satellite ocean color validation sampling strategy are briefly described in Section 8.3. The MOBY example stands out prominently in this regard (Clark et al. 1997; Fargion et al. 1999). There is also a powerful potential for combining satellite ocean color imagery with data from moored and drifting radiometers and bio-optical sensors for cost-effective long term monitoring of the ocean. A prime example of this potential was the description of the biological and chemical response of the Equatorial Pacific Ocean to the 1997-98 El Nino observed by combining time series of SeaWiFS and AVHRR imagery with bio-optical and chemical data from the TAO array (Chavez et al. 1999). Cullen et al. (1997) and Schofield et al. (1999) discuss the combined roles of optical buoys and satellite ocean color image data in proposed systems for monitoring harmful algal blooms. Although the present scope of the Ocean Optics Protocols does not embrace a monitoring sampling strategy, it may be approproriate and beneficial to do so in a future revision.

Within the short time constraints imposed for publication of this document, it proved impossible to develop and include protocols for the specialized aspects of radiometric, IOP and fluorometric measurements from buoys. These special considerations include the need to extrapolate radiometric measurements made at fixed near-surface depths to the surface, and bio-fouling of windows and other optical surfaces during extended, unattended deployments.

8.9 AIRBORNE MEASUREMENTS

Many references are made in the protocols, for example in Section 8.2, to potential applications of airborne measurements in validation of satellite ocean color systems and data products. Unfortunately, protocols comparable to those Chapters 4, 5, 10 and 11 describing accepted instruments and methods for in situ ocean radiometry have not yet been distilled and articulated for airborne remote sensing. An effort will be made to enlist the input of such protocols from key members of the aircraft ocean remote sensing community as an addition to the next

protocol revision. For the present, some of the discussion of this topic in Mueller and Austin (1995) is abstracted below.

Airborne measurements of fluorescence by chlorophyll, CDOM, and phycoerythrin, both by laser and solar excitation, are useful to evaluate spatial and temporal variability near ship and mooring stations and to provide independent assessments of bio-optical algorithms (e.g. Hoge et al. 1998, 1999).

Airborne ocean color data may also be used to determine spatial variability in ocean optical properties during shipboard algorithm development and validation experiments. Ocean color may be measured from aircraft using either imaging radiometers (usually flown at high altitude), or single FOV spectral radiometers (usually flown at low altitude to measure profiles of ocean color beneath an aircraft's trackline). Aircraft measurements observe the horizontal variability in ocean color radiance spectra on spatial scales that are much smaller than individual pixels in satellite ocean color images; therefore, these data are more comparable to shipboard measurements. At a qualitative level, this information can indicate how well shipboard radiometric and bio-optical measurements can be compared to satellite ocean color data at typically 1 km pixel resolution. In this context, airborne ocean color measurements will be especially valuable in productive Case-1 and Case-2 waters, where variability in ocean optical properties can be large over mesoscale and smaller distances. Synoptic maps of ocean color distributions can be advantageously utilized to guide sampling by ships. It can also be used to place in-water data from an individual station in context with respect to nearby variability, and thus provide a basis for spatial interpolation and averaging when comparing in-water bio-optical measurements with SeaWiFS image data. This application can be accomplished using aircraft radiometers meeting somewhat less stringent performance specifications than is demanded for direct validation comparison between satellite and aircraft radiance measurements.

For more quantitative work, an airborne radiometer's characteristics must be comparable to radiometric specifications of Chapter 4. Moreover, accurate corrections are applied for atmospheric and surface reflection (sun and sky glitter) effects. Methods for atmospheric correction and estimation of normalized water-leaving radiances from high altitude airborne ocean color imagery are nearly identical to, and as challenging as, those methods which must be applied to SeaWiFS data itself (Carder et al. 1993 and Hamilton et al. 1992).

These problems and their solutions lie beyond the scope of the ocean optical protocols per se, at least in this revision.

REFERENCES

Abbott, M.R., K.H. Brink, C.R. Booth, D. Blasco, M.S. Swenson, C.O. Davis and L.A. Codispoti, 1995: Scales of variability of bio-optical properties as observed from near-surface drifters. J. Geophys. Res., 100:13333-13344.

Austin, R.W., 1974: The remote sensing of spectral radiance from below the ocean surface. In: *Optical Aspects of Oceanography*, N.G. Jerlov and E.S. Nielson, Eds., pp 317-344..

Balch, W.M., D.T. Drapeau, T.L. Cucci, R.D. Vaillancourt, K.A. Kilpatrick and J.J. Fritz, 1999: Optical backscattering by calcifying algae – separating the contribution by particulate inorganic and organic carbon fractions. *J. Geophys. Res.* **104**: 1541-1558.

Beardsley, G.F. and J.R.V. Zaneveld, 1969: Theorectical dependence of the near-asymptotic apparaent optical properties on the inherent optical properties of sea water. *J. Optical Soc. Amer.* **59**: 373-377.

Carder, K.L., P. Reinersman, R. Chen, F. Muller-Karger, and C.O. Davis, 1993: AVIRIS calibration and application in coastal oceanic environments. *Remote Sens. Environ.,* **44**: 205--216.

Chavez, F.P., P.G. Strutton, G.E. Friederich, R.A. Feeley, G.C. Feldman, D.G. Foley and M.J. McPhaden, 1999: Biological and chemical response of the Equatorial Pacific Ocean to the 1997-98 El Nino. Science 286:2126-2131.

Chavez, F.P., P.G. Strutton and M.J. McPhaden, 1998. Biological-physical coupling in the central Pacific during the onset of the 1997-1998 El Nino, Geophys. Res. Lett. 25: 3543.

Clark, D.K., H.R. Gordon, K.J. Voss, Y. Ge, W. Broenkow, an C.C. Trees, 1997: Validation of atmospheric correction over oceans. J. Geophys. Res., 102: 17,209-17217.

Cullen, J.J., A.M. Ciotti, R.F. Davis and M.R. Lewis, 1997: Optical detection and assessment

of algal blooms. Limnol. Oceangr., 42(5, Part 2): 1223-1239.

Dickey, T. 1995: Bermuda testbed mooring program. Bull. Amer. Meteor. Soc. 76: 584.

Fargion G.S., C.R. McClain, H. Fukushima, J.M. Nicolas and R.A. Barnes, 1999: Ocean color instrument intercomparisons and cross-calibrations by the SIMBIOS Project. SPIE Vol. 3870,397-403.

Fofonoff, N.P., and R.C. Millard, Jr., 1983: Algorithms for computation of fundamental properties of seawater. *UNESCO Tech. Papers in Marine Science*, **44**, UNESCO, 53 pp.

Gershun, A., 1939: The light field. *J. Math. Phys*. **18**: 51-151.

Gordon, H.R., and D.K. Clark, 1981: Clear water radiances for atmospheric correction of Coastal Zone Color Scanner imagery. *Appl. Opt*., **20**: 4,175--4,180.

Gordon, H.R., and K. Ding, 1992: Self shading of in-water optical instruments.*Limnol. Oceanogr.,* **37**: 491--500.

Gordon, H.R., O.B. Brown, R.H. Evans, J.W. Brown, R.C. Smith, K.S. Baker, and D.K. Clark, 1988: A semi-analytic radiance model of ocean color. *J. Geophy. Res.* **93**(D9): 10,909-10,924.

Gordon, H.R., O.B. Brown and M.M. Jacobs, 1975: Computed relationships between the inherent and apparent optical properties of a flat homogeneous ocean. *Appl. Opt.* **14**(2): 417-427.

Hamilton, M.K., C.O. Davis, W.J. Rhea, S.H. Pilorz, and K.L. Carder, 1993: Estimating chlorophyll content and bathymetry of Lake Tahoe using AVIRIS data. *Remote Sens. Environ.*, **44**: 217--230.

Hoge, F.E., C.W.Wright, T.M. Kana, R.N. Swift and J.K. Yungel. 1998: Spatial variability of oceanic phycoerythrin spectral types derived from airborne laser-induced fluorescence emissions. *Appl. Opt*., **37**(21): 4744-4749.

Hoge, F. E., C. W. Wright, P. E. Lyon, R. N. Swift, and J. Yungel. 1999: Satellite retrieval of the absorption coefficient of phytoplankton phycoerythrin pigment: Theory and feasibility status. MODIS ATBD document 27.

Hojerslev, N.K., 1975: A spectral light absorption meter for measurements in the sea. *Limnol. Oceanogr.*, **20**: 1024-1034.

James, H.R., and E.A. Birge, 1938: A laboratory study of the absorption of light by lake waters. *Trans. Wis. Acad. Sci*., **31**: 1--154.

Kitchen, J.C., J.R.V. Zaneveld and H. Pak, 1982: Effect of particle size distribution and chloropyll content on beam attenuation spectra. Applied Optics. **21**: 3913-3918.

Lee, Z.P., K.L. Carder, C.D. Mobley, R.G. Steward and J.S. Patch, 1998: Hyperspectral remote sensing for shallow waters: 1. A semianalytical model. *Appl. Opt*., **37**(27): 6329-6338.

Lee, Z.P., K.L. Carder, C.D. Mobley, R.G. Steward and J.S. Patch, 1999: Hyperspectral remote sensing for shallow waters: 2. Deriving bottom depths and water properties by optimization. *Appl. Opt.*, **38**(18): 3831-3843.

Maffione, R.A. and D.R. Dana, 1996: Instruments and methods for measuring the backward-scattering coefficient of ocean waters. *Appl. Opt*. **36**: 6057-6067.

Morel, A., 1974: Optical properties of pure water and pure sea water. In: *Optical Aspects of Oceanography*, N.G. Jerlov and E.S. Nielson, Eds., pp1-23.

Morel, A. 1997: Consequences of a Synechococcus bloom upon the optical properties of oceanic (case 1) waters. *Limnol. Oceanogr.*, **42**: 1746-1754.

Morel, A., Y.H. Ahn, F. Partensky, D. Vaulot, and H. Claustre. 1993: *Prochlorococcus* and *Synechococcus*: A comparative study of their optical properties in relation to their size and pigmentation. *J. Mar. Res*., **51**: 617-647.

Morel, A. and B. Gentili, 1991: Diffuse reflectance of oceanic waters: its dependence on sun angle as influenced by the molecular scattering contribution. *Applied Optics*. 30(30): 4427-4438.

Morel, A. and B. Gentili, 1993: Diffuse reflectance of oceanic waters. II. Bidirectional aspects. *Appl. Opt*. **32**(33): 6864-6879

Morel, A. and B. Gentilli, 1996: Diffuse reflectance of oceanic waters. III. Implication of bidirectionality for the remote-sensing problem. *Appl. Opt*., **35**(24): 4850-4862.

Morel, A., and L. Prieur, 1977: Analysis of variations in ocean color. *Limnol. Oceanogr.,* **22**: 709--722.

Morel, A., K.J. Voss, and B. Gentili, 1995: Bidirectional reflectance of oceanic waters: a comparison of modeled and measured upward radiance fields. *J. Geophys. Res*. **100**: 13,143-13,151.

Mueller, J.L., and R.W. Austin, 1995: Ocean Optics Protocols for SeaWiFS Validation, Revision 1. *NASA Tech. Memo. 104566, Vol. 25,* S.B. Hooker, E.R. Firestone and J.G. Acker, Eds., NASA Goddard Space Flight Center, Greenbelt, Maryland, 67 pp.

Neckel, H., and D. Labs, 1984: The solar radiation between 3,300 and 12,500 AA. *Solar Phys*., **90**: 205--258.

Pegau, W.S. and J.R.V. Zaneveld, 1993: Temperature dependent absorption of water in the red and near infrared portions of the spectrum. *Limnol. Oceanogr*., **38**(1): 188-192.

Pegau, W.S., J.S. Cleveland, W. Doss, C.D. Kennedy, R.A. Maffione, J.L. Mueller, R. Stone, C.C. Trees, A.D. Weidemann, W.H. Wells, and J.R.V. Zaneveld, 1995: A comparison of methods for the measurement of the absorption coefficient in natural waters. *J. Geophys. Res.*, **100**(C7): 13,201-13,220.

Pegau, W.S., D. Gray and J.R.V. Zaneveld, 1997: Absorption and attenuation of visible and near-infrared light in water: dependence on temperature and salinity. Appl. Opt., **36**(24): 6035-6046.

Pope, R.M. and E.S. Fry. 1997: Absorption spectrum (380-700 nm) of pure water. II. Integrating cavity measurements. *Appl. Opt*. **36**: 8710-8723.

Preisendorfer, R. W., 1986: Secchi disk, science: Visual optics of natural waters. *Limnol. Oceanogr.,* **31**(5): 909-926.

Stewart, D.E. and F.H. Farmer. 1984: Extraction, identification, and quantification of phycobiliprotein pigments from phototrophic plankton. *Limnol. Oceanogr.,* **29**: 392-397.

Schofield, O., J. Grzymski, W.P. Bissett, G.J. Kirkpatrick, D.F. Millie, M. Moline and C.S. Roesler, 1999: Optical monitoring and forecasting systems for harmful algal blooms: Possibility or pipe dream?, J. Phycol. 35: 1477-1496.

Stramska, M., D. Stramski, B.G. Mitchell and C.D. Mobley. 2000: Estimation of the absorption and backscattering coefficients from in-water radiometric measurements. *Limnol. Oceanogr*., **45**: 628-641.

Strickland, J.D.H., and T.R. Parsons, 1972: *A Practical Handbook of Sea Water Analysis,* Fisheries Research Board of Canada, 310 pp.

Subramaniam, A., E. J. Carpenter, and P. G. Falkowski, 1999: Bio-optical properties of the marine diazotrophic cyanobacteria Trichodesmium spp. II. A reflectance model for remote sensing. *Limnol. Oceanogr*., 44: 618-627.

Tassan, S. and G.M. Ferrari, 1995: Proposal for the measurement of backward and total scattering by mineral particles suspended in water. *Appl. Opt*. **34**: 8345-8353.

Twardowski, M.S., J.M. Sullivan, P.L. Donaghay and J.R.V. Zaneveld. 1999: Microscale quantification of the absorption by dissolved and particulate material in coastal waters with an ac-9. *J. Atmos. Oceanic Tech*. **16**: 691-707.

UNESCO, 1994: Protocols for the Joint Global Ocean Flux Study (JGOFS) Core Measurements, Manuals and Guides **29**: 170pp

Vernet, M., B.G. Mitchell, and O. Holm-Hansen. 1990: Adaptation of *Synechococcus* in situ determined by variability in intracellular phycoerythrin-543 at a coastal station off the Southern California coast, USA. *Mar. Ecol. Prog. Ser*., **63**: 9-16.

Walsh, J.J., G.T. Rowe, R.L. Iverson, and C.P. McRoy, 1981: Biological export of shelf carbon is a sink of the global CO_2 cycle. *Nature,* **291**: 196--201.

Wood, A.M., P.K. Horan, K. Muirhead, D. Phinney, C.M. Yentsch, and J.M. Waterbury, 1985: Discrimination between types of pigments in marine Synechococcus by scanning spectroscopy, epifluorescence microscopy, and flow cytometry. *Limnology and Oceanography*, **30**: 1303-1315.

Wood, A.M., M. Lipsen and P. Coble, 1999: Fluorescence based characterization of phycoerythrin-containing cyanobacterial communities in the Arabian Sea during the Notheast and early Southwest Monsoon (1994-1995). *Deep-Sea Res. II*, **46**: 1769-1790.

Wyman, M. 1992: An in vivo method for the estimation of phycoerythrin concentrations in marine cyanobacteria (*Synechococcus* spp.). *Limnol. Oceangr.*, **37**: 1300-1306.

Zaneveld, J.R.V., J.C. Kitchen, A. Bricaud, and C. Moore, 1992: Analysis of *in situ* spectral absorption meter data. *Ocean Optics XI,* G.D. Gilbert, Ed., SPIE, 1750, 187--200.

Zaneveld, J.R.V., J.C. Kitchen, and C. Moore, 1994: The scattering error correction of reflecting-tube absorption meters. *Ocean Optics XII, Proc. SPIE*, **2258**: 44-55.

Chapter 9

In-Water Radiometric Profile Measurements and Data Analysis Protocols.

James L. Mueller

Center for Hydro-Optics and Remote Sensing, San Diego State University, California

9.1 INTRODUCTION

Determinations of in-water spectral downwelling irradiance $E_d(z,\lambda)$, upwelling irradiance $E_u(z,\lambda)$ and upwelling irradiance $L_u(z,\lambda)$, both near the surface and as vertical profiles, are required for calibration and validation of the water-leaving radiance as retrieved from the SeaWiFS and other satellite ocean color sensors. Near-surface measurements should profile through at least the top three optical depths to reliably extrapolate to z = 0; it is essential to obtain a profile through at least the top optical depth. To better characterize the water column for remote sensing applications, e.g., primary productivity estimation, deeper vertical profiles should be made to 200 m, or seven diffuse attenuation depths whenever possible. Sea bed reflection influences on $L_u(z,\lambda)$ and $E_u(z,\lambda)$ should be avoided for SeaWiFS validation and algorithm development by collecting data only from water deeper than six diffuse attenuation depths for E_d (490); remote sensing applications for optically shallow situations where bottom reflectance is present are not within the scope of these protocols.

At the present state of the art, the most reliable *in situ* method of determining water leaving radiance $L_W(\lambda)$ is to extrapolate an in-water profile measurement of $L_u(z,\lambda)$ to the sea surface to estimate $L_u(0^-,\lambda)$. Then, $L_W(\lambda) = t\, L_u(0^-,\lambda)n^{-2}$, where t is the Fresnel transmittance of the air-sea interface (~0.98) and n is the refractive index of seawater. It is also necessary to measure incident spectral irradiance $E_s(\lambda)$ above the sea surface to determine remote sensing reflectance $R_{RS}(\lambda) = L_W(\lambda)/E_s(\lambda)$. Recent intercomparisons have demonstrated the uncertainty in $L_W(\lambda)$ and $R_{RS}(\lambda)$ determined by this approach to be < 5% under varied cloud and sea state conditions and for Case 1 waters, at least in the sense of internal consistency of the measurements (Hooker and Maritorena 2000). To date, the best demonstrated uncertainties are >10% in $R_{RS}(\lambda)$ determined from above-water measurements of water and sky radiances and $E_s(\lambda)$ (see Chapter 10), due primarily to difficulty in accurately removing the contribution of skylight reflected from a wave-roughened sea surface (e.g. Toole et al. 2000).

9.2 MEASUREMENT METHODS

There are three primary sources of uncertainty in the determination of $E_d(z,\lambda)$, $E_u(z,\lambda)$, and $L_u(z,\lambda)$ and their respective attenuation coefficients $K_d(z,\lambda)$, $K_u(z,\lambda)$, and $K_L(z,\lambda)$: the perturbation of the in-water radiant energy field by the ship (Gordon 1985, Smith and Baker 1986, Voss et al. 1986, and Helliwell et al. 1990), shading of the measured water volume by the $E_u(z,\lambda)$, or $L_u(z,\lambda)$, sensor itself (Gordon and Ding 1992), and atmospherically induced variability in radiant energy incident on the sea surface during in-water measurements (Smith and Baker 1984). The influence of ship shadow on the vertical profiles of $E_d(z,\lambda)$, $E_u(z,\lambda)$, and $L_u(z,\lambda)$ is dependent upon the following variables: solar zenith angle, the spectral attenuation properties of the water column, cloud cover, ship size (length, beam, draft, and freeboard) and color, and the geometry of instrument deployment. Self-shading is dependent on solar zenith angle, the fractional contributions of direct sunlight and diffuse skylight to total incident irradiance, and the diameter of the instrument relative to the absorption scale length $a(\lambda)^{-1}$ of the water in which the measurement is made. Atmospheric variability is primarily dependent upon sun elevation and variations in cloud cover. The near surface in-water data also show variability caused by wave focusing, which can be minimized at a fixed depth by averaging over several wave periods, but which can pose severe problems in vertical profiles during which the instrument descends at speeds of $0.5-1\ \mathrm{ms}^{-1}$. Raman scattering and fluorescence result in second-order errors near 490 nm (CDOM fluorescence), and at

longer wavelengths, contributions from phycoerythrin and fluorescence and water Raman scattering are significant. Based on recent experimental measurements of the Raman scattering cross section and its wavelength dependence (Bartlett et al. 1998, and references cited therein), Gordon (1999) recently determined that Raman contributions to remote sensing reflectance are 50% to 100% larger than had been previously estimated and is significant at all wavelengths of interest to ocean color remote sensing.

Ship Shadow Avoidance

The complete avoidance of ship shadow, or reflectance, perturbations is a mandatory requirement for all radiometric measurements to be incorporated into the SIMBIOS validation and algorithm database. The influence of ship shadow is best characterized in terms of attenuation length $1/K_d(\lambda)$ (Gordon 1985). Because $L_W(\lambda)$ is required with an uncertainty of 5% or better, the protocol requires that vertical profiles be measured outside the effects of ship perturbation to the radiant energy field. To accomplish this, the instrument must be deployed from the stern, with the sun's relative bearing aft of the beam. Yet a better approach is to deploy a free falling, profiling radiometer well away from the ship on an umbilical tether.

Estimates of the minimum distance away from the ship, under conditions of clear sunny skies, are given below. The distances are expressed in attenuation lengths to minimize error. For $E_d(z,\lambda)$ measurements, the general equation for distance away, ξ in meters is given as

$$\boldsymbol{x} = \frac{\sin\left(48.4^o\right)}{K_d\left(\boldsymbol{I}\right)}. \tag{9.1}$$

The distance from the ship is required to be $3/K_u(\lambda)$ m for $E_u(z,\lambda)$ and $1.5/K_L(\lambda)$ m for $L_u(z,\lambda)$ measurements. These distances should be increased if the instrument is deployed off the beam of a large vessel. A variety of methods have been used to deploy optical instruments beyond the influence of the ship. During CZCS algorithm development, floating plastic frames were equipped with small winches and instruments to obtain near surface optical profiles at some distance away from the ship. An umbilical cable provided power and data transfer. These platforms, while being somewhat difficult to deploy, worked well at avoiding ship shadow. Alternatively, extended booms can be used to deploy the instrument away from the ship and have the advantages of allowing relatively rapid

deployment and simultaneous rosette bottle sampling. As a point of caution, however, very long booms may accentuate unwanted vertical motions due to ship pitch and roll.

Waters et al. (1990) used an optical free-fall instrument (OFFI) that allows optical data to be obtained outside the influence of ship perturbation. In addition, the OFFI approach allows optical data to be obtained independently from violent ship motion, which may be transmitted to the instrument via the hydrowire, especially on a long boom. Over the past few years, OFFI-like radiometer systems have become commercially available from several manufacturers and have found widespread use in the ocean color community. In comparisons between several deployment configurations (Hooker and Maritorena 2000), free-fall radiometer systems, in combination with shipboard surface irradiance sensors, yielded water-leaving radiances with the lowest uncertainties. Yet another method for the deployment of optical sensors is via an ROV. Some groups, e.g., Smith (pers. comm.), have deployed a spectrometer on an ROV and obtained data completely free of ship influences.

The above criteria for ship shadow avoidance are admittedly very conservative. Unfortunately, the above cited models and observations provide only approximate guidance on minimum distances at which ship reflectance and shadow effects become insignificant under all circumstances. Therefore, the SIMBIOS ocean optics protocols embrace relatively extreme distance criteria, recognizing that in many specific combinations of lighting conditions, ships and optical properties, ship shadow, and reflection effects may become unimportant much closer to the ship. The essential requirement is that each investigator establishes that any measurements of $E_d(z,\lambda)$, $E_u(z,\lambda)$, and $L_u(z,\lambda)$ submitted for SIMBIOS validation and algorithm development are free from ship-induced errors. The simplest way to do this is to adhere to the above distance criterion, which is not difficult when using either a tethered free-fall system or instruments mounted on an ROV. In other cases, it is incumbent on the investigator to otherwise demonstrate the absence of ship effects, e.g., through analysis of a series of profiles at increasing distance.

Depth Resolution in Profiles

The instrument sampling rate and the speed at which the instrument is lowered or raised through the water column should yield at least two, and preferably six to eight, samples per meter.

Instrument Dark Readings

The dark current of optical sensors is frequently temperature dependent. As a consequence, accurate radiometric measurements require that careful attention be given to dark current variability. It is recommended that each optical measurement be accompanied by a measurement of the instrument dark current. When there is a large temperature difference between the instrument on the deck and the water temperature, the instrument should be allowed to equilibrate with ambient water temperature at the beginning of each cast.

Deep casts, e.g., 500 m, may permit the determination of the dark current in each optical channel at the bottom of each cast. Many instruments are not designed to be safely lowered to 500 m, however, and this approach is usually not feasible. Furthermore, there is some intrinsic uncertainty over possible contamination by bioluminescence when dark readings are obtained in this way. If the instrument is equipped with a shutter, dark currents can be measured at any depth in the cast. If the dark current is not determined during the cast, it should be determined as soon as possible after the instrument is returned to the deck.

Temperature effects on sensor responsivity can be significant and should not be ignored. Therefore, sensors should be equipped with thermistors on detector mounting surfaces to monitor temperatures for data correction. Otherwise, deck storage should be under thermally protected conditions prior to deployment and on-deck determination of dark voltages.

Surface Incident Irradiance

Atmospheric variability, especially under cloud cover, leads directly to variability of the in-water light field and must be corrected to obtain accurate estimations of optical properties from irradiance or radiance profiles. First order corrections for this variability can be made using above water (on deck) measurements of downwelling spectral irradiance, $E_s(\lambda) = E_d(0^+,\lambda)$. Smith and Baker (1984) and Baker and Smith (1990) theoretically computed the irradiance just below the air-water interface, $E_d(0^-,\lambda)$, from deck measurements to correct in-water profile data.

The deck sensor must be properly gimbaled to avoid large errors in $E_s(\lambda)$ due to ship motion in a seaway. Improper gimballing can actually accentuate sensor motion under some circumstances, however, and this aspect of a shipboard radiometer system must be engineered with some care.

In previous versions of the ocean optics protocols (Mueller and Austin 1992, 1995), it was suggested that an improved, more direct determination of $E_d(0^-,\lambda)$ might be obtained by deploying a floating instrument to obtain continuous downwelling irradiance data just below the air-water interface (Waters et al. 1990). Over the past several years, instruments implementing this concept have become commercially available and the ocean color community has used them extensively. Unfortunately, experience has demonstrated that downwelling irradiance fluctuations associated with focusing and defocusing of sunlight by surface waves renders such measurements far noisier than measurements of $E_s(\lambda)$ made above the sea surface. A variant on this approach, wherein the sensor is floated away from the ship but is elevated a meter or so above the water surface, has proved to be a viable alternative, especially in circumstances when it is impossible to install and/or gimbal a deck cell properly.

Instrument Attitude

An instrument's attitude with respect to the vertical is a critical factor in measurements of $E_d(z,\lambda)$ and $E_u(z,\lambda)$, and is only slightly less critical for $L_u(z,\lambda)$. Roll and pitch sensors must, therefore, be installed in the underwater radiometers used for acquiring SIMBIOS validation data. The data from these attitude sensors are to be recorded concurrently with the data from the radiometric channels and are to be used as a data quality indicator. It is not deemed necessary to determine or control attitude determination errors resulting from surface wave-induced accelerations at very shallow depths.

9.3 ANCILLARY MEASUREMENTS AND LOGS

The following ancillary data and information must be recorded in header files and/or logs for each radiometric profile cast:

1. date and time (UTC) of the station and cast;
2. geographic location (latitude and longitude in decimal degrees to the nearest 0.001);
3. the distance between the profiling sensor and the ship, and its direction relative to the ship's heading;

4. the direction of the sun relative to the ship's heading;
5. Secchi depth;
6. cloud cover and sky conditions;
7. wind speed and direction;
8. barometric pressure;
9. dark (zero-offset) data file, to be recorded at the time of the cast and the dark filename logged with the profile entry;
10. times, locations and file identification of associated CTD, in situ fluorescence, and inherent optical property profiles, if any;
11. and times of associa depths ted water samples, if any;
12. names of files with data from comparisons with a portable irradiance and radiance reference standard made in the field and used to track the instrument's stability during a deployment (Chapter 7);
13. instrument identification;
14. calibration date and file identification (constant throughout a cruise, usually); and
15. depth offsets (to nearest cm) between the pressure transducer and all sensor probes, including $L_u(z,\lambda)$ window, $E_d(z,\lambda)$ and $E_d(z,\lambda)$ collectors, and all ancillary probes on a package.

9.4 DATA ANALYSIS METHODS

This section provides descriptions and discussion of the methods and procedures required to process profile measurements of $E_d(z,\lambda)$, $E_u(z,\lambda)$, and $L_u(z,\lambda)$ from raw counts to radiometric units and attenuation coefficient profiles $K_d(z,\lambda)$, $K_u(z,\lambda)$, and $K_L(z,\lambda)$, and for extrapolating the data to the sea surface to determine $E_d(0^-,\lambda)$, $E_u(0^-,\lambda)$, and $L_u(0^-,\lambda)$. Water-leaving radiance is then determined as

$$L_w(\boldsymbol{1}) = \Re_o L_u(0^-, \boldsymbol{1}), \qquad (9.2)$$

where $\Re_o \cong 0.529$ is the upward radiance transmittance of the sea surface for normal incidence from below (Austin 1974; see also Section 8.3). Remote sensing reflectance is then calculated as

$$R_{RS}(\boldsymbol{1}) = \frac{L_w(\boldsymbol{1})}{E_s(\boldsymbol{1})}, \qquad (9.3)$$

where $E_s(\lambda)$ is downwelling incident irradiance measured above the sea surface, and is equivalent to $E_d(0^+,\lambda)$. It is not recommended to estimate $E_d(0^+,\lambda)$ from in-water determinations of $E_d(0^-,\lambda)$, because wave-focusing effects yield uncertainties approaching 10% under even ideal circumstances (Siegel et al. 1995). The lack of directional notation in (11.2) and (11.3) signifies that the quantities represent nadir values of $L_w(\lambda)$ and $R_{RS}(\lambda)$. Directional (off-nadir at a given azimuth angle from the sun) above-water measurements of surface radiance and remote-sensing reflectance are discussed in Chapter 12.

Methods for estimating normalized water-leaving radiance LwN( ) and normalized remote-sensing reflectance RRSN( ), including corrections for solar zenith angle and the ocean's Bidirectional Reflectance Distribution Function (Morel and Gentili 1996), are discussed in Section 8.3.

Dark Corrections

The instrument's dark responses in each channel, which should recorded either during or immediately after each profile, must be subtracted from the raw data prior to further processing.

Instrument Calibration Analysis

Instrument data from pre- and post-deployment calibrations should be compared with: (1) each other; (2) the long-term history of an instrument's calibrations; and (3) the record of comparisons with a portable field irradiance and radiance standard, to be made frequently during a cruise (Chapter 7).

Based on this analysis of the instrument's history, a calibration file will be generated and applied to transform the dark-corrected data from raw counts to radiance and irradiance units. This analysis, and the rationale for adopting a particular set of calibration coefficients, both for responsivity and wavelength, should be fully described in the documentation accompanying the data set, preferably in an ASCII file to be retained on line with each data set.

Depth Offset Adjustments

The distance of each irradiance collector and radiance window above, or below, the instrument's pressure transducer port must be subtracted, or added, to the nominal recorded depth so that $E_d(z,\lambda)$, $E_u(z,\lambda)$, and $L_u(z,\lambda)$ are associated with the depths where they were actually measured. These

depth adjustments may be applied either before, or during, attenuation profile analysis, but in either case must be applied before extrapolating values to the sea surface.

Profile Normalization by Surface Irradiance

The dominant errors in measured $K(z,\lambda)$ profiles result from changes in cloud cover during a cast. Cloud cover variability causes strong variations in incident surface irradiance, $E_s(t(z),\lambda)$ measured at time t(z), during the time required to complete a radiometric cast. In present usage, $E_s(t(z),\lambda)$ refers to incident spectral irradiance measured with a deck cell aboard a ship. It is strongly recommended that all incident irradiance measurements be made above the sea surface. Smith and Baker (1984 and 1986) discuss a method for propagating $E_s(\lambda)$ through the sea surface to estimate $E_d(0^-,\lambda)$, and they also present a model for adjusting $E_d(0^-,\lambda)$ to compensate for solar zenith angle. An alternative scheme for estimating $E_d(0^-,\lambda)$ by measuring $E_d(z_r,\lambda)$ with a radiometer floated away from the ship and held at a shallow depth z_r during a cast (Waters et al. 1990) was also recommended in Mueller and Austin (1995). However, community experience has since demonstrated in-water estimates of $E_d(0^-,\lambda)$ to be far noiser than those based on measurements of $E_s(t(z),\lambda)$ made above the sea surface (e.g. Siegel et al. 1995; Hooker and Maritorena 2000).

The record of $E_s(t(z),\lambda)$ is recorded simultaneously and together with profiles of $E_d(z,\lambda)$, $E_u(z,\lambda)$, and $L_u(z,\lambda)$. Assuming that transmission of $E_s(t(z),\lambda)$ through the surface does not vary with time, then a simple and effective normalization of the profiles is obtained as

$$E'_d(z,\boldsymbol{\lambda}) = \frac{E_d(z,\boldsymbol{\lambda})E_s(t(0^-),\boldsymbol{\lambda})}{E_s(t(z),\boldsymbol{\lambda})}, \qquad (9.4)$$

where $E_s(t(z),\lambda)$ is the deck cell irradiance measured at the time t(z) when the radiometer was at depth z and $E_s(t(0^-),\lambda)$ is the measurement at time $t(0^-)$ when the radiometer was at the surface.

Some investigators have used $E_s(t(z),\lambda)$ at a single reference wavelength, e.g., 550 nm, to normalize profiles, and have thus ignored the usually small spectral variations in incident irradiance. For SIMBIOS validation and algorithm development, however, the recommended protocol

is to use multispectral $E_s(t(z),\lambda)$ measurements. Under no circumstances should a PAR, or other broad-band (e.g. photopic response), sensor ever be used for this purpose.

Because of spatial separation between the surface and underwater radiometers, cloud shadow variations are neither measured identically, nor in phase, by the two instruments. The $E_s(t(z),\lambda)$ profiles should, therefore, be smoothed to remove high frequency fluctuations while retaining variations with periods of 15 seconds or greater. The smoothed $E_s(t(0^-),\lambda)/E_s(t(z),\lambda)$ profiles should then be applied as a normalizing function to adjust the measured irradiance and radiance profiles to correct for variations in incident irradiance during a cast.

Some investigators (e.g. Sorensen et al. 1995), who are faced with the need to process hundreds of radiometric profiles, have implemented automated, semi-autonomous processing and analysis systems which do not include a profile normalization like that embodied in (11.4). In this approach, radiometric profiles are simply rejected and not analyzed if overall variability in $E_s(t(z),\lambda)$ exceeds a minimum acceptance threshold. For all accepted profiles, it is implicitly assumed that $E_s(t(0^-),\lambda)/E_s(t(z),\lambda)=1.0$ and is constant throughout the measurement. The only drawback to this approach is that many otherwise usable profiles are not analysed.

K-Analysis

Normalized profiles of $E_d(z,\lambda)$, $E_u(z,\lambda)$, and $L_u(z,\lambda)$ (with z corrected for pressure transducer depth offset relative to each sensor) should be fit to the equations

$$E_d(z,\boldsymbol{\lambda}) = E_d(0^-,\boldsymbol{\lambda})e^{-\int_o^z K_d(z',\boldsymbol{\lambda})dz'}, \qquad (9.5)$$

$$E_u(z,\boldsymbol{\lambda}) = E_u(0^-,\boldsymbol{\lambda})e^{-\int_o^z K_u(z',\boldsymbol{\lambda})dz'}, \qquad (9.6)$$

and

$$L_u(z,\boldsymbol{\lambda}) = L_u(0^-,\boldsymbol{\lambda})e^{-\int_o^z K_L(z',\boldsymbol{\lambda})dz'}, \qquad (9.7)$$

respectively. The vertical profiles of attenuation coefficients $K_d(z,\lambda)$, $K_u(z,\lambda)$, and $K_L(z,\lambda)$, together with the respective values of $E_d(0^-,\lambda)$, $E_u(0^-,\lambda)$, and $L_u(0^-,\lambda)$ at the surface, provide the needed specifications for the smoothed irradiance and radiance profiles.

If the natural logarithm of (9.5), (9.6), or (9.7) is taken, an equation of the following form is obtained:

$$-\int_0^z K(z')dz' = \ln\left[E(z)\right] - \ln\left[E(0^-)\right], \quad (9.8)$$

so that

$$K(z) = -\frac{d\ln\left[E(z)\right]}{dz}\bigg|_z. \quad (9.9)$$

The traditional method of K-analysis, e.g., Smith and Baker (1984 and 1986), is to estimate K(z) as the local slope of ln[E(z)] measured within a depth interval spanning a few meters, and centered at depth z_m. It is assumed that K(z) is constant over the depth interval centered at z_m, so that

$$\ln\left[E(z)\right] \cong \ln\left[\hat{E}(z_m)\right] - (z - z_m)K(z_m). \quad (9.10)$$

The unknowns $\ln\left[\hat{E}(z_m)\right]$ and K(z_m) are determined as the intercept and (negative) slope of a least-squares regression fit to measured ln[E(z)] data within the depth interval $z_m - \Delta z \le z < z_m + \Delta z$. The half-interval Δz is somewhat arbitrary. Smith and Baker (1984 and 1986) suggest a Δz of approximately 4 m, but for noisy profiles, a Δz as large as 10 m may be needed to smooth over incident irradiance fluctuations left as residuals by the deck cell normalization.

When this method is used, the shallowest possible values in the smoothed $\ln\left[\hat{E}(z_m)\right]$ and K(z_m) profiles are at depth Δz m and the deepest values are Δz m above the deepest measurements in the profile. If obvious ship shadow effects are present in the data, the shallowest valid smoothed data point will be at depth $z_s + \Delta z$ where z_s is the depth to which the data are regarded as contaminated and are excluded from the analysis. It is often convenient, although not necessary, to pre-average radiometric data into, e.g., 1 m, bins prior to performing the least-squares analysis. If this is done, the data should be pre-filtered to remove any noise spikes and then averaged before it is log-transformed.

Each step in the analysis yields increasingly refined information, which requires various amounts of intervention from the analyst. After appropriate editing to remove artifacts, such as the effects of ship shadow, vertical profiles of $K(z,\lambda)$ are computed from the logarithmic decrement with depth of the radiometric profiles. Direct derivative

method calculations of $K(z,\lambda)$ profiles using computer techniques (see above) may require the use of a depth interval as large as 20 m, with the result that information about the slope, and hence, about $K(z,\lambda)$ near the top and bottom of the profile, is lost. Averaging over such a large interval also causes the slopes in sharply defined layers, e.g., regions of high gradients, to be poorly represented. Attempts to reduce these effects by using a significantly smaller depth interval often results in unacceptably noisy $K(z,\lambda)$ profiles.

An alternative method of determining K-profiles (Mueller 1995) is to keep (9.8) in integral form, expressed in terms of diffuse attenuation depth (optical depth) $\tau(z,\lambda)$ as

$$\boldsymbol{t}(z,\boldsymbol{l}) = -\int_0^z K(z',\boldsymbol{l})dz' = \ln\left[\frac{E(0^-)}{E(z)}\right]. \quad (9.11)$$

The K-profile is represented analytically by Hermitian cubic polynomials with unknown coefficients, consisting of K(z_n) and its derivative dK(z_n)/dz, at each of several discrete depths dividing the profile into finite depth elements. [Hermitian cubic polynomials are defined in any text on finite element modeling, e.g., Pinder and Gray (1977).] The measured set of equations (9.11), corresponding to each measured value E(z) in the profile and depth z in the profile, are assembled into matrix form and the unknown set of coefficients K(z_n) and dK(z_n)/dz are determined using classical least-squares minimization. E(0$^-$) must be specified externally, and in the current implementation is estimated from the profile itself and adjusted iteratively to yield a minimum least-squares solution to the overall profile. The complete formulation of the method is given in Mueller (1995). Compared to results of the derivative solution, the integral method yields significantly more detailed representation of very sharp layers in bio-optical profiles (when compared to concurrent beam attenuation and chlorophyll fluorescence profiles). The integral solution is more robust in handling data gaps, e.g. due to extreme cloud shadows which are not corrected by deck-cell normalization. And the integral solution automatically extrapolates the profile to E(0$^-$) based on a best fit to the entire profile, and not simply to the noisy near-surface layer. On the other hand, the integral method of solution is considerably more difficult to implement than the derivative approach. Moreover, the approach requires an interactive analysis of each profile, and is more time consuming than an automated analysis using the derivative method. For these reasons, the integral

solution is not widely used within the ocean color community.

Extrapolation to the Sea Surface

Because of surface waves, it is rarely possible to measure $E_d(z,\lambda)$, $E_u(z,\lambda)$, and $L_u(z,\lambda)$ at depths that closely approximate $z \cong 0^-$. The shallowest reliable readings typically occur at depths ranging from 0.5—2 m. The data from this zone usually exhibit strong fluctuations associated with surface waves, and thus require some form of smoothing or averaging. It is almost always necessary to apply some means of extrapolating the data upward to the sea surface. Whatever method is used should reconcile extrapolated $E_d(0^-,\lambda)$ with deck measurements of $E_s(\lambda)$.

If K(z) profiles are determined using the derivative method, the shallowest smoothed estimates will occur at depth $z_o = \Delta z$, if there are no ship shadow effects. The usual procedure is to extrapolate values to z=0⁻ as

$$E_d\left(0^-,\boldsymbol{\lambda}\right)= E_d\left(z_o,\boldsymbol{\lambda}\right)e^{K_d\left(z_o,\lambda\right)z_o}, \qquad (9.12)$$

$$E_u\left(0^-,\boldsymbol{\lambda}\right)= E_u\left(z_o,\boldsymbol{\lambda}\right)e^{K_u\left(z_o,\lambda\right)z_o}, \qquad (9.13)$$

and

$$L_u\left(0^-,\boldsymbol{\lambda}\right)= L_u\left(z_o,\boldsymbol{\lambda}\right)e^{K_L\left(z_o,\lambda\right)z_o}. \qquad (9.14)$$

If ship shadow is present, z_o may be 20 m or more, and the extrapolation becomes somewhat tenuous.

If K(z) profiles are determined by means of the integral method, then $E_d(0^-,\lambda)$, $E_u(0^-,\lambda)$, and $L_u(0^-,\lambda)$ are automatically determined as part of the fitting procedure. The surface values thus obtained are not necessarily superior to those obtained by extrapolating the derivative method solutions, but they do have the advantage of representing an internally consistent least-squares fit to the entire profile beneath the surface boundary layer.

By either method, extrapolation of measured $E_d(z,\lambda)$, $E_u(z,\lambda)$, and $L_u(z,\lambda)$ to z=0⁻ becomes very difficult at $\boldsymbol{\lambda} \geq 650$ nm. At these wavelengths, the rapid decrease in daylight over an extremely shallow first attenuation length may compete with an increase in flux with depth due to inelastic scattering. Indeed, it is not unusual to find negative values of $K_d(z,\lambda)$ and $K_L(z,\lambda)$ in strong chlorophyll maxima. Additional research is needed to address measurement and estimation of $E_d(0^-,\lambda)$, $E_u(0^-,\lambda)$,

and $L_u(0^-,\lambda)$ at these wavelengths, especially in chlorophyll-rich Case-2 waters.

Instrument Self-Shading

Gordon and Ding (1992) modeled the errors introduced by an instrument's own shadow in direct measurements used to determine $E_u(0^-,\lambda)$ and $L_u(0^-,\lambda)$. For this source of error to be less than 5%, without modeled corrections, the instrument radius r must satisfy $r \leq \left[40a\left(\boldsymbol{\lambda}\right)\right]^{-1}$ for $E_u(0^-,\lambda)$ and $r \leq \left[100a\left(\boldsymbol{\lambda}\right)\right]^{-1}$ for $L_u(0^-,\lambda)$. They calculate for λ = 865 nm in pure water, as an example, that the instrument radius must be approximately 0.3 cm to measure $E_u(0^-,865)$ with a maximum of 5% error; the instrument radius must be significantly smaller for direct measurement error in $L_u(0^-,\lambda)$ to be 5% or less.

Gordon and Ding (1992) also propose a simple model for correcting $E_u(0^-,\lambda)$ and $L_u(0^-,\lambda)$ for the self-shadowing effect. They write

$$\hat{L}_u\left(\boldsymbol{\lambda}\right)=\frac{L_u^o\left(\boldsymbol{\lambda}\right)}{1-\boldsymbol{e}\left(\boldsymbol{\lambda}\right)} \qquad (9.15)$$

and

$$\boldsymbol{e}\left(\boldsymbol{\lambda}\right)= 1- e^{-\kappa'a\left(\lambda\right)r}, \qquad (9.16)$$

where $\hat{L}_u\left(\boldsymbol{\lambda}\right)$ is the true value, $L_u^o\left(\boldsymbol{\lambda}\right)$ is the measured value, κ'=y/tan θ_{ow}, θ_{ow} is the refracted solar zenith angle and y is an empirical factor for which they give values determined by fitting their model results ($y \approx 2$). A similar correction, with a different table of values for y applies to $E_u(0^-,\lambda)$.

When the above geometric corrections are applied, Gordon and Ding (1992) estimate that errors less than or equal to 5% in $L_u(0^-,\lambda)$ could be determined from measurements with instruments having maximum diameters of 24 cm for $\boldsymbol{\lambda} \leq 650$ nm, and with instruments of maximum diameter 10 cm for $650 < \boldsymbol{\lambda} \leq 700$ nm at solar zenith angles $\boldsymbol{\theta}_o \geq 20°$, and maximum chlorophyll concentrations of 10 mg m^{-3}. To measure $L_u(0^-,\lambda)$ correctable to less than 5% error at $\boldsymbol{\theta}_o = 10°$ (with chlorophyll concentrations less than or equal to 10 mg m^{-3}), maximum instrument diameters are 12 cm for $\boldsymbol{\lambda} \leq 650$ nm and 5 cm for $650 < \boldsymbol{\lambda} \leq 700$ nm. Even with these corrections, however, instrument diameters of 1 cm or less must be used to assure

self-shading $L_u(0^-,\lambda)$ errors are 5% or less at 780 and 875 nm.

The Gordon and Ding (1992) model predictions were compared to experimental measurements of $L_u(0^-,\lambda)$ just beneath the sea surface, using a fiber-optic radiometric probe (Zibordi and Ferrari 1995). The experiment was performed in a lake, with solar zenith angles ranging between 25° and 50°, on several days with cloud-free skies. Spectrophotometric methods (similar to those in Chapter 18) were used to measure absorption by particles and Gelbstoff. At wavelengths of 500, 600, and 640 nm, a series of discs was employed to vary instrument self-shading geometry in several steps over the range $0.001 < a(1)r \leq 0.1$. The Gordon and Ding (1992) model predicted self-shading radiance and irradiance effects that may be applied as corrections, and which agreed with measured values within 5% and 3% respectively. The model corrections were all biased high relative to the measured values. Zibordi and Ferrari (1995) chose to compare their measurements to the Gordon and Ding (1992) *point-sensor* model, and use of their *finite-sensor* model results may have further improved the comparisons.

This initial confirmation of the Gordon and Ding (1992) instrument self-shading model is confined to clear-sky conditions, solar zenith angles greater than 25°, near-surface $L_u(0^-,\lambda)$ and $E_u(0^-,\lambda)$, and $a(1)r \leq 0.1$. Additional theoretical and experimental research will be necessary to generalize this correction for cloudy sky conditions and for variations with depth in $L_u(z,\lambda)$ and $E_u(z,\lambda)$ profiles. The above restrictions notwithstanding, the excellent agreement shown so far covers a very important range of conditions for SeaWiFS and SIMBIOS algorithm development and validation.

A provisional protocol is given here for radiometer self-shading corrections to $L_u(0^-,\lambda)$ and $E_u(0^-,\lambda)$ derived from in-water radiometric measurements. The protocol is based on the model of Gordon and Ding (1992) and the limited experimental confirmation by Zibordi and Ferrari (1995). Although additional research is necessary to extend and verify these correction algorithms, the results published to date show clearly that even a provisional correction will significantly improve $L_u(0^-,\lambda)$ and $E_u(0^-,\lambda)$ estimated from underwater measurements.

It is first necessary to measure or estimate the spectral absorption coefficient $a(\lambda)$, preferably using measurements following the protocols of Chapter 17, or if necessary those of Chapter 18. It is also possible to estimate $a(\lambda)$ using other approximations suggested by Gordon and Ding (1992), based either on measurements of phytoplankton pigment concentrations or of irradiance attenuation coefficients.

It will also be necessary to measure, or estimate, the direct solar, $E_{sun}(\lambda)$ and skylight, $E_{sky}(\lambda)$ components of incident spectral irradiance, $E_s(\lambda)$, where $E_{sun}(\lambda) + E_{sky}(\lambda) = E_s(\lambda)$. The preferred method is to measure these components following the protocols of Chapter 15. Zibordi and Ferrari (1995) also describe a method of estimating the ratio $E_{sky}(\lambda)/E_{sun}(\lambda)$, and Gordon and Ding (1992) suggest yet other alternatives.

Following Zibordi and Ferrari (1995), the coefficients, κ', given in Table 2 of Gordon and Ding (1992), are fit to linear regression models as functions of the solar zenith angle θ_0 in the range $30° \leq q_o \leq 70°$. The results given for $L_u(0^-,\lambda)$, with sun only, for a point sensor may be computed as

$$k'_{suno} \tan q_{ow} = 2.07 + 5.6 \times 10^{-3} q_o, \qquad (9.17)$$

and for a finite sensor occupying the full diameter of the instrument,

$$k'_{sunl} \tan q_{ow} = 1.59 + 6.3 \times 10^{-3} q_o, \qquad (9.18)$$

where θ_0 and θ_{ow} are the solar zenith angles in air and water, respectively, measured in degrees. In practice, the diameter of the radiance sensor aperture is usually a small fraction of the instrument diameter. In the results reported by Zibordi and Ferrari (1995), the point sensor model always overestimated ε and use of the finite sensor model (11.18) will always yield a lower estimate of ε. Pending new insights from future theoretical and experimental work, it is suggested to estimate

$$k'_{sun} \tan q_{ow} = (1-f) k'_{suno} \tan q_o + f k'_{sunl} \tan q_o, \qquad (9.19)$$

where f is the ratio of sensor-to-instrument diameters. The coefficient, k'_{sky} for the self-shading effect on $L_u(0^-,\lambda)$ caused by incident diffuse skylight is similarly estimated as

$$k'_{sky} = 4.61 - 0.87 f, \qquad (9.20)$$

where the coefficients are derived from values given in Table 3 of Gordon and Ding (1992). Self-shading errors $\varepsilon_{sun}(\lambda)$ and $\varepsilon_{sky}(\lambda)$ for $E_{sun}(\lambda)$ and

94

$E_{sky}(\lambda)$ components, respectively, are then computed as

$$\boldsymbol{e}_{sun}(\boldsymbol{l}) = 1 - e^{-k'_{sun}a(\boldsymbol{l})r}, \qquad (9.21)$$

and

$$\boldsymbol{e}_{sky}(\boldsymbol{l}) = 1 - e^{-k'_{sky}a(\boldsymbol{l})r}, \qquad (9.22)$$

where r is the instrument radius in meters, and the absorption coefficient $a(\lambda)$ is in units of m^{-1}.

The self-shading error in $L_u(0^-,\lambda)$ is then calculated as

$$\boldsymbol{e}(\boldsymbol{l}) = \frac{\boldsymbol{e}_{sun}(\boldsymbol{l}) + \boldsymbol{e}_{sky}(\boldsymbol{l})}{1 + h}, \qquad (9.23)$$

where

$$h = \frac{E_{sky}(\boldsymbol{l})}{E_{sun}(\boldsymbol{l})}. \qquad (9.24)$$

Finally, the corrected radiance $L_u(0^-,\lambda)$ is estimated as

$$L_u(0^-,\boldsymbol{l}) = \frac{L'_u(0^-,\boldsymbol{l})}{1 - \boldsymbol{e}(\boldsymbol{l})}, \qquad (9.25)$$

where $L'_u(0^-,\boldsymbol{l})$ is determined by analysis of the measured upwelled radiance profiles.

Similarly, for $E_u(0^-,\lambda)$, the values given in Tables 2 and 3 of Gordon and Ding (1992) determine that for a point irradiance sensor,

$$\boldsymbol{k}'_{sun,o} = 3.41 - 1.55 \times 10^{-2} \boldsymbol{q}_o. \qquad (9.26)$$

For an irradiance collector with a diameter equal to that of the instrument,

$$\boldsymbol{k}'_{sun,l} = 2.76 - 1.21 \times 10^{-2} \boldsymbol{q}_o, \qquad (9.27)$$

so that

$$\boldsymbol{k}'_{sun} = (1-f)\boldsymbol{k}'_{sun,o} + f\boldsymbol{k}'_{sun,l}, \qquad (9.28)$$

where f is the ratio of the diameter of the irradiance collector to that of the instrument. For the sky component, $\boldsymbol{k}'_{sky}$ is defined as

$$\boldsymbol{k}'_{sky} = 2.70 - 0.48f. \qquad (9.29)$$

Values of $\boldsymbol{k}'_{sun}$ and $\boldsymbol{k}'_{sky}$ from (9.28) and (9.29) are then substituted in equations (9.21) and (9.22) to obtain $\varepsilon_{sun}(\lambda)$ and $\varepsilon_{sky}(\lambda)$ that are then used in (9.23) to solve for $\varepsilon(\lambda)$. Finally, corrected upwelled spectral irradiance $E_u(0^-,\lambda)$ is estimated as

$$E_u(0^-,\boldsymbol{l}) = \frac{E'_u(0^-,\boldsymbol{l})}{1 - \boldsymbol{e}(\boldsymbol{l})}, \qquad (9.30)$$

where $E'_u(0^-,\boldsymbol{l})$ is determined from the upwelled spectral irradiance profile. It is recommended that this correction algorithm be applied to all $L_u(0^-,\lambda)$ and $E_u(0^-,\lambda)$ measurements used for SeaWiFS and SIMBIOS validation and algorithm development. Recognizing the provisional nature of the correction, however, the uncorrected measured values must also be reported. Moreover, the method and data used to estimate $a(\lambda)$, $E_{sun}(\lambda)$ and $E_{sky}(\lambda)$ must be documented and reported with all data sets corrected using this protocol.

Finite Bandwidth Correction

In wavelength regions where the absorption coefficient of water varies rapidly (e.g. near 565 nm), sensors having FWHM bandwidths exceeding 5 nm interact with water attenuation spectrum to shift the effective wavelength of attenuation coefficients computed from the data. A protocol is not currently provided for correcting this effect.

Siegel et al. (1986) and Marshall and Smith (1990) discuss the effects of finite spectral FWHM bandwidth, and the normalized response function, on determination of the attenuation coefficient, $K(\lambda)$, for a vertically homogeneous water column. Given a channel's nominal wavelength, $\boldsymbol{l}'$ and normalized response function, $h(\lambda)$, the apparent attenuation coefficient measured in a homogeneous water column is approximately

$$K_s(z,\boldsymbol{l}') = \frac{\int_0^\infty K(\boldsymbol{l})h(\boldsymbol{l})e^{-K(\boldsymbol{l})z}d\boldsymbol{l}}{\int_0^\infty h(\boldsymbol{l})e^{-K(\boldsymbol{l})z}d\boldsymbol{l}}. \qquad (9.31)$$

Marshall and Smith (1990) applied a correction for this effect to clear-water profiles of $E_d(z,589)$. In general, correction of $K_s(z,\boldsymbol{l}')$ for finite bandwidth effects associated with K for pure water is straightforward. Additional research will be needed to model, from the spectral irradiance data itself, additional bandwidth effects associated with attenuation by phytoplankton and other particles, and to correct $K_s(z,\boldsymbol{l}')$ accordingly.

Raman Corrections

Marshall and Smith (1990), and the references cited therein, show transpectral Raman scattering contributes significantly to measured irradiance between 500 and 700 nm. At a particular wavelength, the Raman contribution is excited by ambient irradiance at a wavenumber shift of $3,400, cm^{-1}$. For example, Raman scattering at a wavelength of 500 nm ($20,000\ cm^{-1}$) is excited by light at wavelength 427 nm ($23,400\ cm^{-1}$), and at 700 nm ($14,286\ cm^{-1}$) by light at 565 nm ($17,686, cm^{-1}$). Marshall and Smith (1990) give a transverse Raman scattering cross section (at 90°) of $8.2 \times 10^{-30}\ cm^{-2} molecule^{-1} sr^{-1}$, a value within the range of other published observations. By integration, they derive a total Raman scattering coefficient of:

$$b_r\left(488\right) = 2.6 \times 10^{-4} m^{-1}, \qquad (9.32)$$

a result recently confirmed by Bartlett et al. (1998), as well as by the in situ measurements of Hu and Voss (1997a, 1997b).

The wavelength dependence of the Raman scattering cross section is theoretically about the same as that for Rayleigh scattering

$$b_r\left(\pmb{1}\right): b_r\left(488\right)\left(\frac{\pmb{1}}{488}\right)^{-4}. \qquad (9.33)$$

Bartlett et al (1998) recently measured the wavelength dependence of Raman Scatter, however, and found that for excitation wavelengths λ_e

$$b_r\left(\pmb{1}\right) = b_r\left(488\right)\left(\frac{\pmb{1}}{488}\right)^{-5.5 \pm 0.4}, \qquad (9.34)$$

for radiance expressed in energy units, i.e. $mW\ cm^{-2} \mu m^{-1} sr^{-1}$.

A method for applying Raman corrections to measured profiles of irradiance and radiance is suggested and applied to homogeneous clear-water profiles by Marshall and Smith (1990). Additional work is needed to develop a robust Raman scattering correction model for general application in more turbid and vertically stratified water masses. The relative magnitude, and thus importance, of the Raman signal at each wavelength in the upper three attenuation lengths should also be investigated more thoroughly than has been done to date. Gordon (1999) applied the recent results of Bartlett et al. (1998), i.e the

confimation of (9.32) and wavelength dependence of (9.34), together with recently improved absorption coefficients for pure water (Sogandares and Fry 1997; Pope and Fry 1997), to model the relative contributions of Raman scattering to water-leaving radiance at wavelengths of interest for ocean color remote sensing. He found that Raman contributions ranged between 20% and 30% in clear, oligotrophic waters, and was ~8% near chlorophyll concentrations of 1 mg m^{-3}. It seems likely that a Raman scattering correction algorithm for water leaving radiance could be developed following Gordon's (1999) modeling approach, and an appropriate protocol may emerge in the near future.

REFERENCES

Austin, R.W., 1974. The remote sensing of spectral radiance from below the ocean surface. In: Optical Aspects of Oceanography, N.G. Jerlov and E.S. Nielson, Eds., pp 317-344.

Baker, K.S., and R.C. Smith, 1990: Irradiance transmittance through the air/water interface. *Ocean Optics X*, R.W. Spinrad, Ed., *SPIE*, **1**,302, 556-565.

Bartlett, J.S., K.J. Voss, S. Sathyendranath, and A. Vodacek, 1998: Raman scattering by pure water and seawater. *Appl. Opt.*, **37**, 3324-3332.

Gordon, H.R., 1985: Ship perturbations of irradiance measurements at sea, 1: Monte Carlo simulations. *Appl. Opt.*, **24**, 4,172--4,182.

Gordon, H.R., 1999: Contribution of Raman Scattering to water-leaving radiance: a reexamination. *Appl. Opt.*, **38**: 3166-3174.

Gordon, H.R., and K. Ding, 1992: Self shading of in-water optical instruments.*Limnol. Oceanogr.,* **37**, 491--500.

Helliwell, W.S., G.N. Sullivan, B. Macdonald, and K.J. Voss, 1990: Ship shadowing: model and data comparison. *Ocean Optics X*, R.W. Spinrad, Ed., *SPIE*, **1,** 302, 55--71.

Hooker, S.B. and S. Maritorena, 2000: An evaluation of oceanographic radiometers and deployment methodologies. *J. Atmos. Oceanic Technol.*, (in press).

Hu, C. and K.J. Voss, 1997a: Solar stimulated inelastic light scattering in clear sea water, In: Ackleson , S.G. and R. Frouin, Eds: *Ocean Optics XIII.* Proc. *SPIE*, **2963**, 266-271.

Hu, C. and K.J. Voss, 1997b: In situ measurements of Raman scattering in clear ocean water, *Appl. Opt.* **36**,2686-2688.

Marshall, B.R., and R.C. Smith, 1990: Raman scattering and in-water optical properties. *Appl. Opt.,* **29**, 71--84.

Morel, A., and B. Gentili, 1996: Diffuse reflectance of oceanic waters. III. Implication of bidirectionality for the remote-sensing problem. *Applied Optics*, **35**, 4850-4862.

Mueller, J.L., 1995: Integral method for analyzing irradiance and radiance attenuation profiles. Ch. 3 In: Siegel, D.A., et al. 1995: Results of the SeaWiFS Data Analysis Round Robin, July 1994 (DARR-94). *NASA Tech. Memo. 104566, Vol. 26,* S.B. Hooker and E.R. Firestone, Eds., NASA Goddard Space Flight Center, Greenbelt, Maryland, pp 44-48.

Mueller, J.L., and R.W. Austin, 1992: Ocean Optics Protocols for SeaWiFS Validation. *NASA Tech. Memo. 104566, Vol. 5,* S.B. Hooker and E.R. Firestone, Eds., NASA Goddard Space Flight Center, Greenbelt, Maryland, 43 pp.

Mueller, J.L., and R.W. Austin, 1995: Ocean Optics Protocols for SeaWiFS Validation, Revision 1. *NASA Tech. Memo. 104566, Vol. 25,* S.B. Hooker, E.R. Firestone and J.G. Acker, Eds., NASA Goddard Space Flight Center, Greenbelt, Maryland, 67 pp.

Pinder, G.F., and W.G. Gray, 1977: *Finite Element Simulation in Surface and Subsurface Hydrology*, Academic Press, 29 pp.

Siegel, D.A., C.R. Booth, and T.D. Dickey, 1986: Effects of sensor characteristics on the inferred vertical structure of the diffuse attentuation coefficient spectrum. *Ocean Optics VIII*, M.A. Blizard, Ed., *SPIE*, 637, 115--124.

Siegel, D.A., M.C. O'Brien, J.C. Sorenson, D.A. Konnoff, E.A. Brody, J.L. Mueller, C.O. Davis, W.J. Rhea, and S.B. Hooker, 1995: Results of the SeaWiFS Data Analysis Round Robin, July 1994 (DARR-94). *NASA Tech. Memo. 104566, Vol. 26,* S.B. Hooker and E.R. Firestone, Eds., NASA Goddard Space Flight Center, Greenbelt, Maryland, pp 44-48.

Smith, R.C., and K.S. Baker, 1984: Analysis of ocean optical data, *Ocean Optics VII*, M. Blizard, Ed., *SPIE*, 478, 119--126.

Smith, R.C., and K.S. Baker, 1986: Analysis of ocean optical data. *Ocean Optics VIII,* P.N. Slater, Ed., *SPIE*, 637, 95--107.

Sorensen, J.C., M.C. O'Brien, D.A. Konnoff, and D.A. Siegel, 1995: The BBOP data processing system. Ch. 2 In: Siegel, D.A., et al. 1995: Results of the SeaWiFS Data Analysis Round Robin, July 1994 (DARR-94). *NASA Tech. Memo. 104566, Vol. 26,* S.B. Hooker and E.R. Firestone, Eds., NASA Goddard Space Flight Center, Greenbelt, Maryland, pp 37-43.

Toole, D.A., D.A. Siegel, D.W. Menzies, M.J. Neumann and R.C. Smith, 2000: Remote-sensing reflectance determinations in the coastal ocean environment: impact of instrumental characteristics and environmental variability. *Appl. Opt.*, **39**: 456-469.

Voss, K.J., J.W. Nolten, and G.D. Edwards, 1986: Ship shadow effects on apparent optical properties. *Ocean Optics VIII,* M. Blizard, Ed., *SPIE*, 637, 186--190.

Waters, K.J., R.C. Smith, and M.R. Lewis, 1990: Avoiding ship induced light field perturbation in the determination of oceanic optical properties. *Oceanogr.,* **3**, 18--21.

Zibordi, G., and G.M. Ferrari, 1995: Instrument self-shading in underwater optical measurements: experimental data. *Appl. Opt.* **34**,2750--2754.

Chapter 10

Above-Water Radiance and Remote Sensing Reflectance Measurement and Analysis Protocols

James L. Mueller[1], Curtiss Davis[2], Robert Arnone[3], Robert Frouin[4], Kendall Carder[5], Z.P. Lee[5], R.G. Steward[5], Stanford Hooker[6], Curtis D. Mobley[7] and Scott McLean[8]

[1]*Center for Hydro-Optics and Remote Sensing, San Diego State University, California*
[2]*Naval Research Laboratory, Washington, District of Columbia*
[3]*Naval Research Laboratory, Stennis Space Center, Mississippi*
[4]*Scripps Institution of Oceanography, University of California, San Diego, California*
[5]*University of South Florida, St. Petersburg, Florida*
[6]*NASA, Goddard Space Flight Center, Greenbelt, Maryland*
[7]*Sequoia Scientific Inc., Redmond, Washington*
[8]*Satlantic Inc., Halifax, Nova Scotia, Canada*

10.1 INTRODUCTION

As an alternative to the in-water methods of Chapter 11, water-leaving radiance can be measured from the deck of a ship. A shipboard radiometer is used to measure radiance $L_{sfc}(\lambda,\theta,\phi \in \Omega_{FOV};\theta_o)$ emanating from the sea surface at zenith angle θ (usually chosen between 30° and 50°) and azimuth angle ϕ (usually chosen between 90° and 180° away the sun's azimuth ϕ_o). In the convention used here, azimuth angles ϕ are measured relative to the sun's azimuth, i.e. $\phi_o = 0$.

The surface radiance measured with a radiometer having a solid-angle field of view (FOV) of Ω_{FOV} sr may be expressed, following Mobley (1999), as

$$L_{sfc}(\lambda,\theta,\phi \in \Omega_{FOV};\theta_o) = L_w(\lambda,\theta,\phi \in \Omega_{FOV};\theta_o) + \rho L_{sky}(\lambda,\theta',\phi' \in \Omega'_{FOV};\theta_o). \quad (10.1)$$

$L_w(\lambda,\theta,\phi \in \Omega_{FOV};\theta_o)$ is water-leaving radiance centered at angles (θ, ϕ) and averaged over Ω_{FOV} [as weighted by the radiometer's directional response function (see Chapter 5)]. $L_{sky}(\lambda,\theta',\phi' \in \Omega'_{FOV};\theta_o)$ is sky radiance measured with the radiometer looking upward at angles (θ', ϕ'). In practice, θ and θ' are numerically equal angles in the nadir and zenith directions, respectively, and the sea and sky viewing azimuths $\phi = \phi'$. The reflectance factor ρ is operationally defined as the total skylight actually reflected from

the wave-roughened sea surface into direction (θ,ϕ) divided by sky radiance measured with the radiometer from direction θ',ϕ'), both quantities being averaged over Ω_{FOV} (Mobley 1999). Remote sensing reflectance is then determined, using water-leaving radiance calculated from (10.1), as

$$R_{RS}(\lambda,\theta,\phi \in \Omega_{FOV};\theta_o) = \frac{L_w(\lambda,\theta,\phi \in \Omega_{FOV};\theta_o)}{E_s(\lambda;\theta_o)}, \quad (10.2)$$

where $E_s(\lambda;\theta_O)$ is incident spectral irradiance measured above the sea surface. All of the above variables vary with solar zenith angle θ_O.

A simplified notation is used in Chapter 9 (and elsewhere in the protocols) when discussing water leaving radiance $L_W(\lambda)$ and remote sensing reflectance $R_{RS}(\lambda)$ derived from in-water profile measurements of $L_u(z,\lambda)$. Because $L_u(z,\lambda)$ is measured viewing the nadir direction, $L_W(\lambda)$ represents radiance leaving the surface in the zenith direction $(\theta, \phi) = (0^o, 0^o)$. Therefore, $L_W(\lambda)$ in Chapter 11 corresponds to $L_w(\lambda,0,0 \in \Omega_{FOV};\theta_o)$, and $R_{RS}(\lambda)$ to $R_{RS}(\lambda,0,0 \in \Omega_{FOV};\theta_o)$, in the present notation

10.2 PROPOSED MEASUREMENT CONCEPTS

Proposed protocols for measuring remote sensing reflectance group essentially into three basic categories of measurement concepts, each of which is described briefly in this section. Remote

sensing reflectance determination by some, but not all three, of the proposed above-water methods have been compared to each other (Hooker et al. 1999, 2000). Comparisons have also been made between each method and $R_{RS}(\lambda)$ determined from in-water $L_u(z,\lambda)$ and above-water $E_s(\lambda;\theta_o)$ measurements (e.g. Rhea and Davis, 1997; Mueller *et al.* 1997; Fougnie *et al.* 1999; Hooker *et al.* 1999), finding root-mean-square differences generally larger than 20% for any sample spanning a reasonably large range of environmental conditions. Some of these investigators have normalized the measurements, using the method of Morel and Gentili (1996) to account for variations in viewing and solar zenith angles and in the ocean Bidirectional Reflectance Distribution Function (BRDF), prior to making the comparisons (e.g. Mueller *et al.* 1997; Toole *et al.* 2000), and some have not (e.g. Rhea and Davis 1997; Fougnie et al. 1999).

Method 1: Calibrated radiance and irradiance measurements.

Radiometers which have been fully characterized and calibrated, following the methods of Chapter 5, are used to measure $L_{sfc}(l,q,f\in\Omega_{FOV};q_o)$, $L_{sky}(l,q',f'\in\Omega'_{FOV};q_o)$ and $E_s(\lambda;\theta_o)$. Assumptions are chosen to estimate surface reflectance ρ, and $L_w(l,q,f\in\Omega_{FOV};q_o)$ and $R_{RS}(l,q,f\in\Omega_{FOV};q_o)$ are calculated using equations (12.1) and (12.2). Example implementations of this straightforward instrumental approach, and comparisons with remote sensing reflectance determined from in-water measurements, are described in Rhea and Davis (1997), Mueller et al. (1997), Hooker et al. (1998), Hooker and Lazin (2000), and Toole et al. (2000).

Method 2: Uncalibrated radiance and reflectance plaque measurements

In this approach, a radiance sensor that has not been calibrated is used to measure signals proportional to $L_{sfc}(l,q,f\in\Omega_{FOV};q_o)$, $L_{sky}(l,q',f'\in\Omega'_{FOV};q_o)$ and radiance reflected from a horizontal plaque, or "grey-card", having a known bi-directional reflectance (often assumed to be near-Lambertian) for the solar and viewing directions. The raw uncalibrated radiance signals are substituted in (10.1) to express $L_w(l,q,f\in\Omega_{FOV};q_o)$ as

$$L_w(l,q,f\in\Omega_{FOV};q_o)=F_L(l)\begin{bmatrix}S_{sfc}(l,q,f\in\Omega_{FOV};q_o)-\\rS_{sky}(l,q',f'\in\Omega'_{FOV};q_o)\end{bmatrix},$$
(10.3)

where $F_L(\lambda)$ is the instrument's unknown radiance response calibration factor, and $S_{sfc}(l,q,f\in\Omega_{FOV};q_o)$ and $S_{sky}(l,q',f'\in\Omega'_{FOV};q_o)$ are the radiometer's measured responses. The radiance reflected from the plaque is scaled to estimate $E_s(\lambda;\theta_o)$ as

$$E_s(l;q_o)=\frac{p}{R_g(l,q',f''\in\Omega_{FOV};q_o,f_o)}\times$$
$$F_L(l)S_g(l,q',f''\in\Omega_{FOV};q_o,f_o),$$
(10.4)

where $S_g(l,q'',f''\in\Omega_{FOV};q_o,f_o)$ is the sensor response signal when the plaque (grey-card) is viewed at angles (q'',f'') with the sun at (q_o,f_o), and $R_g(l,q'',f''\in\Omega_{FOV};q_o,f_o)$ is the plaque's bi-directional reflectance function (BRDF) for that sun and viewing geometry [including whatever is assumed regarding the contribution of sky irradiance to $E_s(\lambda;\theta_o)$]. The most straightforward BRDF geometry is for the sensor to view the center of the plaque normal to its surface (i.e. $q''=0$), allowing the BRDF to be determined for illumination angles between normal and 90° at, e.g. 5° increments. When expressions (10.3) and (10.4) are substituted into (10.2) to calculate $R_{RS}(l,q,f\in\Omega_{FOV};q_o)$, the unknown radiance response calibration factor $F_L(\lambda)$ cancels. As with the other methods, the reflectance of the sea surface ρ is estimated using one of several possible sets of assumptions and approximations.

For quantitative determinations of $E_s(\lambda;\theta_o)$ and $L_w(l,q,f\in\Omega_{FOV};q_o)$ by this method, the radiometer must be calibrated to determine the coefficients $F_L(\lambda)$.

This method was adapted for ocean color applications, initially by Carder and Steward (1985), from an approach used widely in the LANDSAT remote sensing community to measure reflectance spectra of terrestial surfaces. Carder et al. (1993) used the method with a vertical polarizer to minimize reflected skylight, and Lee et al. (1997b) compared measurements with and without the polarizer (and found little difference – a result subsequently explained by Fougnie et al. 1999). Other aspects and applications of this approach are described in Lee *et al.* (1997a). In particular, they spectrally deconvolve the Rayleigh from aerosol

skylight reflected from the sea surface using a Fresnel value for the Rayleigh, and a variable reflectance value for wave-modulated aerosol radiance. When sunglint is not an issue, the $(\theta, \phi) = (30^o, 90^o)$ angle provides less uncertainty due to wave modulation in the Fresnel reflectance using the Lee et al. (1997a) method. Rhea and Davis (1997), Toole et al. (2000), and Hooker et al. (1999) compared reflectances determinations by this method with determinations from in-water measurements.

Method 3: Calibrated surface polarized radiance measurements with modeled irradiance and sky radiance

A radiance sensor is fitted with a polarizing filter set to pass only vertically polarized component of viewed radiance. The polarizer minimizes the skylight reflectance term in (10.1) when the surface is viewed near the Brewster angle. The instrument is calibrated using the methods of Chapter 5, and is used to measure only $L_{sfc}(\lambda, \theta, \phi \in \Omega_{FOV}; \theta_o)$. A sun photometer is used to determine aerosol optical thicknesses at each wavelength (Chapter 9). A radiative transfer model is then used to calculate $E_s(\lambda; \theta_o)$ and $L_{sky}(\lambda, \theta', \phi' \in \Omega'_{FOV}; \theta_o)$ so that (10.1) and (10.2) may be solved for $R_{RS}(\lambda, \theta, \phi \in \Omega_{FOV})$. The details of this method, which is the protocol recommended for use with the SIMBAD radiometer (see also Chapters 6 and 11), are described by Fournie *et al.* (1999).

10.3 RADIOMETRIC MEASUREMENT METHODS

Field of View Considerations

In the protocols for determining $L_W(\lambda)$ from in-water measurements of radiance profiles (Chapter 11), the radiance sensor's angular FOV is not critical, because the upwelling radiance distribution varies relatively little over zenith angles up to 30°. When measuring $L_{sfc}(\lambda, \theta, \phi \in \Omega_{FOV}; \theta_o)$, however, the size of an instrument's solid angle FOV Ω_{FOV} affects its sensitivity to variability in the skylight reflection term of (10.1) (Lee *et al.* 1997a; Fournie et al. 1999; Mobley 1999). This situation arises because the slope of the wind roughened sea surface varies spatially and temporally on scales small compared to the typical area subtended by Ω_{FOV} and sensor integration time, respectively. The

surface slope distribution varies strongly as a function of, and may be estimated from, local wind speed (Cox and Munk 1954). For a small area of sea surface at a fixed location, wind gustiness may cause variations in the slope distribution (visible as "cat's paws") on time scales from seconds to minutes. The surface slope distribution is also systematically varied on time scales of order 10 sec by gravity waves, primarily through interactions with capillary waves through periodic modulations of surface tension, and secondarily by very small direct variations in surface slope (gravity waves break before slopes reach 6°). [In SIMBAD measurements of polarized surface radiance, for example, the oscillations associated with the primary swell appear clearly in the data. The minimum values are selected in the data processing. (R. Frouin, Pers. Comm.)]

The average surface slope variability, in combination with angular variability in $L_{sky}(\lambda, \theta', \phi' \in \Omega'_{FOV}; \theta_o)$, introduces strong variability in the skylight reflectance term of (10.1), which increases remarkably with a large Ω_{FOV} (Mobley 1999; Fournie *et al.* 1999; Toole *et al.* 2000). With a very small Ω_{FOV}, on the other hand, measurements made from close above the surface view an extremely small area that is subject to large temporal variations in slope, and thus also in the directions in which the sky is viewed through surface reflection. The ideal, which can only be effectively realized from satellite orbital elevations above the earth's surface, is a very small Ω_{FOV} (to minimize viewing angle variation across the FOV) combined with a subtended surface area (pixel) large enough to average surface slope variations associated with wind gusts, capillary waves and gravity waves.

Large FOV measurements also integrate over a significant range of variability in the ocean's BRDF, and it may prove difficult to determine normalized remote sensing reflectance $R_{RSN}(\lambda)$ from these data (Section 8.3; Morel and Gentili 1996).

Full-angle FOV's used, or assumed in model computations, by various investigators have ranged from approximately 2° (e.g. Fournie *et al.* 1999) up to 18° (e.g. Gould *et al.* 2000).

Radiance Measurements

The surface and sky radiance measurements should be made from a location that minimizes both shading and reflections from superstructure. A good position for measuring the water-leaving radiance may often be found near the bow of the ship.

Especially while steaming, ocean color radiance measurements should usually be made from the bow, because from this location it is practical to view a spot where the water is undisturbed by the ship's wake or associated foam. It must also be easy, in the selected position, to point in a direction away from the sun to reduce specular reflection of sunlight.

To measure $L_{sfc}(\boldsymbol{1}, \boldsymbol{q}, \boldsymbol{f} \in \Omega_{FOV}; \boldsymbol{q}_o)$ the radiometer should be pointed toward the sea surface at viewing angles, measured at the pixel, $\theta, \phi) = (40\text{-}45^o, 135^o)$, if possible (Mobley 1999; Fougnie et al. 1999), and in all circumstances the viewing azimuth must be in the range $90^o < \phi < 180^o$ relative to the sun's azimuth. For polarized measurements a viewing angle of $\theta = 45^o$ is strongly recommended (Fougnie et al. 1999). A viewing angle that is 180° away from the sun's azimuth should be avoided. The measurements at this angle may be contaminated by the *glory* phenomenon, and ship shadow might also be a problem in this configuration. Measurements should also not be made when the sun is close overhead ($\theta_O < 20^o$), for reasons discussed in Section 10.4 (Mobley et al. 1999). In addition, whitecaps, foam and floating material should be avoided during measurements, but at wind speeds exceeding 10 m s^{-1} extensive whitecap coverage may unavoidably contaminate the data record to some extent.

Because of temporal variability in surface reflectance, due to wind gusts and waves, it is important to record a number of spectra within a period of several seconds, or minutes if necessary. With filter radiometers (Mueller 1997; Fougnie et al. 1999; Hooker et al. 1999, 2000), it is feasible to sample individual spectra at rates of several Hz, and the electronic gain changes account for the different magnitudes of the water and sky signals.

If miniature, fiber-optic spectroradiometers are used, on the other hand, the detector integration time is varied to provide the necessary dynamic range. Sky radiances may be integrated over a few hundred msec, while the ocean surface radiance may be integrated over 1 to 2 sec. A separate dark reading must be obtained each time the integration time is changed. A typical measurement sequence with this type of spectroradiometer is to measure plaque-reflected, sea and sky and radiances (each preceded by a dark offset reading), in that order, and repeat the sequence 5 or more times.

Data records of longer duration may be advisable to improve averaging over modulation of capillary waves by wind variability and gravity waves, but there has been little research on that aspect of the problem. Before calculating final mean and standard deviation spectra, positive outliers due to briefly viewed foam patches, whitecaps and strong glint should be removed by inspection of the data record.

When using *Method 3*, described above, only $L_{sfc}(\boldsymbol{1}, \boldsymbol{q}, \boldsymbol{f} \in \Omega_{FOV}; \boldsymbol{q}_o)$ need be measured, together with a sun photometer measurement, and $L_{sky}(\boldsymbol{1}, \boldsymbol{q}', \boldsymbol{f}' \in \Omega'_{FOV}; \boldsymbol{q}_o)$ and $E_s(\lambda; \theta_O)$ are modeled. This can only be done accurately when clouds do not obscure the solar disk and fractional cloud cover is less than 20%. These are the necessary conditions for the measurement.

To measure $L_{sky}(\boldsymbol{1}, \boldsymbol{q}', \boldsymbol{f}' \in \Omega'_{FOV}; \boldsymbol{q}_o)$ (*Methods 1 and 2*), the radiometer is pointed upward to view the sky at angles $(\theta', \phi') = (\theta, \phi)$, e.g. $(40^o, 135^o)$. When pointing the radiometer, θ' is measured from the zenith, and θ from the nadir, direction as seen from the ship. In radiative transfer calculations, the origin is taken to be located at the pixel and both angles are zenith angles (following the usual convention used in, e.g., ocean color atmospheric correction algorithms). When measurements are made in partly cloudy sky conditions, viewing angles should be selected to cover a clear segment of the sky, if possible. Corrections for reflected sky radiance are problematic unless the cloud fraction is very small in the hemisphere centered on the selected viewing azimuth (Mobley 1999).

Ideally, it can be argued that sky radiance should be measured simultaneously with $L_{sfc}(\boldsymbol{1}, \boldsymbol{q}, \boldsymbol{f} \in \Omega_{FOV}; \boldsymbol{q}_o)$ and $E_s(\lambda; \theta_O)$, using separate radiometers (e.g. Hooker et al. 1999). For reasons of economy, however, most investigators will use the same radiometer for both radiance measurements, which therefore, must be measured sequentially (e.g. Carder and Steward 1985; Lee et al. 1997; Mueller 1997). If separate radiometers are used, they must be calibrated and fully characterized (Chapters 4 and 5), following the approach described above as *Method 1* (although one could use two calibrated radiance sensors, and still use a reflectance plaque to estimate $E_s(\lambda; \theta_O)$ as in *Method 2*).

Incident Irradiance Measurements

Measurements of $E_s(\lambda; \theta_O)$ with a calibrated irradiance sensor are an essential component of *Method 1* (above). The radiometer should be mounted in a location that is free of both shadows and reflections of light from any part of the ship's

superstructure ships (see also Section 9.2). This can usually be accomplished by mounting the radiometer high on a mast, albeit in some combinations of location and ship's heading, intermittent shadowing by antennas, stays and other parts of the ship's rigging may contaminate the $E_s(\lambda;\theta_o)$ measurements. The data must also be edited to remove measurements when the irradiance collector's orientation is more than 5° away from horizontal. When a hand-held irradiance sensor is used to measure $E_s(\lambda;\theta_o)$ at the same location where $L_{sfc}(1,q,f \in \Omega_{FOV};q_o)$ and $L_{sky}(1,q',f' \in \Omega'_{FOV};q_o)$ are measured, it may be more difficult to find an ideal location on some.

Time series of $E_s(\lambda;\theta_o)$ should be recorded synchronously with measurements of both $L_{sfc}(1,q,f \in \Omega_{FOV};q_o)$ and $L_{sky}(1,q',f' \in \Omega'_{FOV};q_o)$. If the average incident irradiances associated with the surface and sky radiance measurements agree within a few percent, their ratio should be used to scale one, or the other, radiance to adjust for the apparent change in atmospheric radiometric conditions during the time interval between the two measurements. If the average $E_s(\lambda;\theta_o)$ values differ significantly, the entire measurement sequence is suspect and the data should be flagged as suspect, and probably discarded. In this quality control context, time series measurements of $E_s(\lambda;\theta_o)$ with a deck cell may also be useful when either *Method 2* or *3* is used to determine $R_{RS}(1,q,f \in \Omega_{FOV};q_o)$.

Reflectance Plaque Measurements

When following *Method 2* (above), a Spectralon (or alternative material) reflectance plaque having a known BRDF is used to normalize the uncalibrated radiance measurements for $E_s(\lambda;\theta_o)$. In this approach, an accurately characterized BRDF for the plaque is as critical as are the accuracies of radiometric calibrations in *Methods 1 and 3*. Traditionally, gray reflectance plaques with approximately 10% nominal reflectance have been used for this measurement (Carder and Steward 1985; Rhea and Davis 1997; Hooker et al. 1999), but white Spectralon plaques with 99% reflectance offer better homogeneity in BRDF (over the plaques surface area) and have been used by some investigators (e.g. Hooker et al. 1999; Toole et al. 2000).

The plaque must be held horizontally, and exposed to the sun and sky in a position free from both shading by, and reflections from, any part of the ship's superstructure, observer, or radiometer.

It may be difficult, on some ships, to find a location that meets this requirement and also affords an unobstructed view of the sea surface at an acceptable (θ, ϕ) relative to the sun. In such situations, the alternative approaches should be considered. With the horizontal plaque thus located, it is viewed by the radiance sensor at the angles consistent with the solar direction and the plaque's BRDF characterization. The simplest approach is to determine the BRDF for the sensor view normal to the plaque center and use that viewing geometry in the field. Finally, the radiance reflected from the plaque is recorded.

Sun Photometer Measurements

It is strongly recommended that sun photometer measurements be made to determine aerosol optical thicknesses, following the protocols of Chapter 11, coincident with every set of above-water remote-sensing reflectance measurements. Note that this measurement is an important element of *Method 3* (above), where it is needed to correctly model $L_{sky}(1,q',f' \in \Omega'_{FOV};q_o)$ and $E_s(\lambda;\theta_o)$ (Fougnie *et al.* 1999).

Ancillary Measurements and Records

The following ancillary data and information must be recorded in header files and/or logs for each radiometric measurement:

1. date and time (UTC) of the station and cast;
2. geographic location (latitude and longitude in decimal degrees to the nearest 0.001);
3. the viewing zenith and azimuth angles of surface and sky radiance, and the solar azimuth relative to the ship's heading;
4. the direction of the sun relative to the ship's heading;
5. cloud cover and sky conditions;
6. wind speed and direction;
7. sea state, as significant wave height, whitecap fraction, and the direction, height and period of the dominant swell. period);
8. barometric pressure;
9. Secchi depth;
10. dark (zero-offset) data file, to be recorded, and the dark filename logged, at the time of the measurements;
11. times, locations and file identification of associated CTD, in situ fluorescence, in-water radiometry and inherent optical property profiles, if any;

12. geographic locations, times and depths of associated water samples, if any;

13. names of files with data from comparisons with a portable irradiance and radiance reference standard made in the field and used to track the instrument's stability during a deployment (Chapter 7);

14. instrument identification; and

15. calibration date and file identification (constant throughout a cruise, usually).

Protocols describing measurement and analysis methods for the standard ancillary variables (Table 2.1) are presented in Section 8.6.

Wind speed and direction, sea state, and sky conditions are essential information for accurate corrections for reflected sky radiance (see below). Photographs of sky and sea surface conditions are highly desirable. Viewing and solar geometry are fundamental to this type of measurement.

It is desirable to also measure in-water radiometric and IOP profiles at stations where above-water measurements of remote-sensing reflectance are made.

10.4 SKY RADIANCE REFLECTANCE OF THE SEA SURFACE

For a flat sea surface and a uniform sky radiance distribution, ρ reduces to the Fresnel reflectance of the sea surface averaged over Ω_{FOV}. In this limit, $r \approx 0.02$ for $q \leq 30°$ and increases slowly to $r \approx 0.03$ at $q \cong 40°$ (Austin 1974). The sea surface is usually wave-roughened and clear sky radiance distributions are not uniform, however, with the result that ρ can be much significantly larger than these simple values and is furthermore very difficult to determine for most wind and sea state conditions (Mobley, 1999; Fougnie *et al.* 1999; Lee *et al.* 1997; Mueller *et al.* 1997; Toole *et al.* 2000).

Clear Skies

In general, the sky radiance reflectance of the sea surface is an apparent optical property that has a functional dependence on many variables, $\rho = \rho(\theta', \phi', \theta, \phi, \Omega_{FOV},$ wind speed, sea state, sky radiance distribution), the complexities of which have been rigorously explored using radiative transfer computations by Mobley (1999) for unpolarized radiance. Assuming $(\theta, \phi) = (40°,$

135°) and a clear-sky radiance distribution for a solar zenith angle $\theta_o = 30°$, Mobley's results show that ρ increases from 0.026 with wind speed U = 0 m s^{-1} to approximately 0.043 when U = 15 m s^{-1}. As solar zenith angles increase, the upper limit of ρ at U = 15 m s^{-1} decreases monotonically to a value $r \approx 0.036$ at $\theta_o = 80°$. For viewing angles $(\theta, \phi) = (30°, 90°)$, the clear-sky ρ at U = 15 m s^{-1} is ~0.08 when $\theta_o = 30°$ and is comparable to $(\theta, \phi) = (40°, 135°)$ for $\theta_o > 40°$. For solar zenith angles $\theta_o > 30°$, Mobley found that the clear-sky ρ for $(\theta, \phi) = (40°, 135°)$ was independent of wavelength at all wind speeds. For viewing angles $(\theta, \phi) = (30°, 90°)$, however, he found that clear-sky ρ at U = 15 m s^{-1} varied by factor of 2 over wavelength due to the spectral differences between reflected skylight and sun glint. For both sets of viewing angles, the reflectance factor ρ increases much more rapidly with wind speed for $\theta_o < 30°$, due to increased sun glint, and this type of measurement would not seem to be practical at solar zenith angles $\theta_o < 20°$. It is perhaps noteworthy that, at least with present atmospheric correction algorithms, sun glint also renders satellite ocean color measurements unusable when the sun is less than 20° from zenith.

Fougnie et al. (1999) made similar model calculations, and experimentally verified them, for vertical and horizontally polarized components of reflected skylight. Their model calculations showed that for a rough water surface, the zenith angle where vertically polarized reflectance is a minimum shifts from the Brewster angle, approximately $\theta = 52°$, to approximately $\theta = 45°$. They also found that the minimum reflected skylight effect was obtained at viewing angles $(\theta, \phi) = (45°, 135°)$. For the more widely used viewing angles $\theta, \phi = (30°, 90°)$ (Carder and Steward 1985; Lee et al. 1997; Mueller et al. 1997), vertically and horizontally polarized reflectances are both larger and nearly equal, which explains why no significant differences were found between total and vertically polarized measurements at these angles by Lee *et al.* (1997), or Mueller *et al.* (1997).

Scattered and Broken Clouds

Radiance scattered from clouds is typically greater than, and spectrally different from, clear-sky radiance. Therefore, the presence of randomly distributed clouds within 90° of the viewing azimuth ϕ may significantly increase the magnitude

of reflected skylight and alter its wavelength dependence, a phenomenon noted by many investigators (e.g. Mobley 1999; Toole et al. 2000; Fougnie et al. 1999). Moreover, the temporal variability and uncertainty of both attributes of reflected skylight will increase. Obviously, effects related to mixed cloudy and cloud-free segments of the sky become progressively more pronounced as wind speed increases, and the effectiveness of correction algorithms becomes problematic in these circumstances (Mobley 1999).

Overcast Skies

When skies are totally overcast, the sky radiance distribution becomes more uniform and its wavelength dependence becomes gray (Mobley 1999; Toole et al. 2000). There is some evidence that $R_{RS}(l,q,f \in \Omega_{FOV};q_o)$ determined from above-water measurements under overcast skies may have significantly lower uncertainty than can be realized in either clear skies or partially cloudy skies (Toole 2000). Measurements under cloudy skies are of little interest in the context of SIMBIOS and SeaWiFS validation studies. On the other hand, measurements under overcast conditions provide insight into phytoplankton dynamics under conditions that cannot be observed from space.

Residual Reflectance Corrections

If the ocean is assumed to be totally absorbing ("black") at 750 nm (and longer wavelengths), then we should find $R_{RS}(750,q,f \in \Omega_{FOV};q_o) = 0$ if the reflected skylight term is properly estimated in equation (12.1). Following the "quick and easy" algorithm of Carder and Steward (1985), if it is further assumed that any error in skylight reflection term is white (not wavelength dependent), one may apply a calculated value of $R'_{RS}(750,q,f \in \Omega_{FOV}) \neq 0$ as a simple offset correction at other wavelengths, i.e.

$$R_{RS}(l,q,f \in \Omega_{FOV};q_o) = R'_{RS}(l,q,f \in \Omega_{FOV};q_o) + \\ - R'_{RS}(750,q,f \in \Omega_{FOV};q_o).$$

This adjustment was previously recommended as part of the provisional protocol for determining above-water remote sensing reflectance (Mueller and Austin 1995). Other suggested wavelengths that have been suggested for determining such a "black-ocean" residual offset include 670, 765, 865 and 1012 nm (Hooker et al. 1999).

In turbid coastal waters, where the above-water technique would be most useful, it is clearly not

appropriate to assume that

$$R_{RS}(750,q,f \in \Omega_{FOV};q_o) = 0$$

(Sydor and Arnone 1997; Sydor et al. 1998; Lee et al. 1997; Gould et al. 2000). Moreover, skylight reflection variability, and uncertainty in its estimation, is largely associated with sun glint and radiance from clouds, neither of which produces a strictly white offset (Lee et al. 1997; Mobley 1999).

Lee et al. (1997) proposed an alternative algorithm which partitions the skylight reflectance term of (12.1) into Rayleigh (λ^{-4} dependence) and aerosol (λ^{-n} dependence, n to be determined on a case-by-case basis) scattering terms, using a non-linear optimization analysis to minimize residuals from expected spectral variations in remote-sensing reflectance at a selected set of wavelengths.

Gould et al. (2000) proposed an algorithm to partition the surface radiance at 720 nm into remote-sensing reflectance and sky reflectance components estimated from the difference between apparent reflectances measured at 715 and 735 nm. Following Lee *et al.* (1997), they assumed a coefficient for exponential wavelength dependence and extrapolated the skylight reflectance to lower wavelengths. When *in situ* IOP are also measured at a station, they derived an improved wavelength dependence model for the sky reflectance correction based on remote-sensing reflectance at 400 nm calculated from a(400) and b(400).

Sydor *et al.* (1998) proposed combining polarized and unpolarized measurements to derive an estimate of the wavelength dependence of reflected skylight. These wavelength-dependency approaches show initial promise, and with further development and experimental validation, some variant on these methods may yet lead to a robust algorithm for correcting above-water determinations of remote-sensing reflectance.

So far, evaluations of the uncertainty associated with the simple white-offset adjustment have not supported its general use, on either experimental (Lee et al. 1997; Hooker et al. 1999; Toole et al. 2000) or theoretical (Mobley 1999) grounds. Its use is not recommended in the present version of the protocols, even though the results of Toole et al. (2000) suggest it may be appropriate under totally overcast skies.

10.5 DISCUSSION AND RECOMMENDATIONS

The protocols recommended, provisionally, in Mueller and Austin (1995) for above-water

measurements of $R_{RS}(\lambda,\theta,\phi \in \Omega_{FOV};\theta_o)$ were seriously flawed. The viewing zenith angles (20°) recommended there were too small to avoid serious sun glint contamination. The recommendation that one might measure sky radiance using a first surface mirror would, if followed, introduce significant repolarization of the measured radiance and yield a serious radiometric artifact. And finally, two key equations of that protocol contained serious typographical errors. The Mueller and Austin (1995) protocols related to above-water measurements of water-leaving radiance and remote-sensing reflectance should not be followed under any circumstances.

The above-water methods for determining normalized remote-sensing reflectance (NRSR), as described above, and their associated uncertainty budgets, have been discussed at length in several meetings and workshops over the last few years, as well as in the literature cited here. In particular, a SIMBIOS sponsored NRSR Workshop was held at Old Dominion University (Norfolk, VA) in December 1997. At that workshop, the participants agreed that the uncertainty budgets associated with the above-water methods proposed for determining NRSR are poorly known, and that a unified data set was needed as a basis for correcting that deficiency. It was also the workshop consensus that additional research and analyses should be pursued to:

1. Determine uncertainties in and between $E_S(\lambda;\theta_o)$ determined by a) direct measurement with a calibrated radiometer (*Method 1*), b) estimation based on measurement of radiance reflected from a gray target have a known BRDF (*Method 2*), and radiative transfer models for clear sky conditions (*Method 3*), with and without independent measurements of aerosol and ozone optical thicknesses;
2. Determine uncertainties between the different *Methods 1, 2 and 3* for measuring $R_{RS}(\lambda,\theta,\phi \in \Omega_{FOV};\theta_o)$;
3. Determine uncertainties between NRSR values determined from above- and in-water radiance measurements; and
4. Evaluate uncertainties between NRSR measured, either above- or in-water, NRSR modeled from measured inherent optical properties (IOP), and NRSR modeled based on IOP estimated from phytoplankton pigments (e.g. chlorophyll a) and other optically important constituents of the water column.

The workshop participants recommended the following priorities, guidelines and constraints for this research:

1. Preceding any intercomparisons of measured $R_{RS}(\lambda,\theta,\phi \in \Omega_{FOV};\theta_o)$, all measurements must be *normalized* to account for the influence of the solar zenith angle and the ocean's BRDF, following the methods of Morel and Gentili (1996). This applies both to in-water and above-water methods (Section 8.3).
2. Initial intercomparisons should be limited to wavelengths $\lambda < 600$ nm, relatively clear waters where $K_d(490) < 0.1$ m^{-1}, cloud cover $< 20\%$, wind speeds U < 10 m s^{-1}, and solar zenith angles in the range $30^o < \phi_o < 60^o$. In these limited circumstances, an uncertainty of approximately 5% may be assumed for NRSR determined from in-water profile measurements of upwelled radiance, an estimate based on results of profile analyses (Siegel et al. 1995) and radiometric calibration uncertainties (Mueller et al. 1996; Johnson et al. 1996).

Finally, the workshop participants agreed that a viewing zenith angle of $\theta = 40^o$, rather than the then more widely used $\theta = 30^o$, should be routinely used for above-water measurements of $R_{RS}(\lambda,\theta,\phi \in \Omega_{FOV})$ without a polarizer.

Hooker et al. (1999) and Hooker and Lazin (2000) report experimental intercomparisons, and results of preliminary analyses, which closely follow the above guidelines. The measurement intercomparisons reported by Toole et al (2000) and Fougnie et al. (1999) were made in turbid, to very turbid, coastal water masses, which contributes to the large uncertainties (10%-15% for in-water and 20%-40% for above-water remote sensing reflectances) they reported. Neither of the latter comparisons was made using normalized reflectances, and the polarized reflectances measured by Fougnie et al. (1999) are not directly comparable to reflectances determined from unpolarized in-water radiance measurements.

There is currently insufficient information on which to conclusively recommend any preference between *Methods 1, 2 or 3* for making above-water measurements of $R_{RS}(\lambda,\theta,\phi \in \Omega_{FOV};\theta_o)$.

For *Method 3*, or any polarized version of either of the other 2 methods, research is needed to establish and validate a robust relationship between vertically polarized normalized

$R_{RSNv}(\lambda, 0, 0 \in \Omega_{FOV}; q_o)$ determined from the above-water measurements and total $R_{RSN}(\lambda)$ determined from total radiance measurements. Since the water body polarizes incident sunlight, polarized measurements of water-leaving radiance must be corrected to estimate total radiance. For 150-160^0, the effect is small (typically 10%), and can be corrected to within a few percent (Fougne et al., 1999). Indeed, a method must be developed to determine a polarized equivalent to $R_{RSN}(\lambda)$.

Again, normalization consists of adjustments from the measured viewing and solar geometry to radiance emitted in the zenith direction with the sun at zenith and adjusted to remove atmospheric effects (Morel and Gentili 1996). Methods for calculating $R_{RSN}(\lambda)$ from measurements of total $R_{RS}(\lambda, q, f \in \Omega_{FOV}; q_o)$ are given in Section 8.3. The present version of the Ocean Optics Protocols do not provide methods for determining $R_{RSN}(\lambda)$ from polarized radiance measurements.

It is further recommended that total surface and sky radiances should be measured at $(\theta, \phi) = (\theta', \phi') = (40^o, 135^o)$ (Fougnie et al. 1999; Mobley 1999). Unpolarized surface reflectance for skylight (i.e., polarized plus unpolarized components) ρ should be estimated as a function of wind-speed following the method of Mobley (1999: Fig. 9), and for completely overcast skies use $r \approx 0.028$.

REFERENCES

Austin, R.W., 1974: Inherent spectral radiance signatures of the ocean surface. In: S.Q. Duntley, R.W. Austin, W.H. Wilson, C.F. Edgerton, and S.W. Moran, *Ocean Color Analysis*, SIO Ref. 74-10, Scripps Institution of Oceanography, La Jolla, CA.

Carder, K.L. and R.G. Steward, 1985: A remote-sensing reflectance model of a red tide dinoflagellate off West Florida. *Limnol. Oceanogr.* **30**: 286-298.

Carder, K.L., P. Reinersman, R.F. Chen, F. Muller-Karger, C.O. Davis and M. Hamilton, 1993: AVIRIS calibration and application in coastal oceanic environments. *Remote Sens. Environ.* **44**: 205-216.

Cox, C. and W. Munk, 1954: Measurement of the roughness of the sea surface from photographs of the sun's glitter. *J. Opt. Soc. Am*. **44**: 11838-11850.

Fougnie, B., R. Frouin, P. Lecomte and Pierre-Yves Deschamps, 1999: Reduction of skylight reflection effects in the above-water measurement of diffuse marine reflectance. *Appl. Opt.* **38**: 3844-3856.

Gould, R.A., R.A. Arnone and M. Sydor, 2000: Improved techniques for determining remote sensing reflectance in coastal waters, *Appl. Opt.* (In press).

Hooker, S.B. and G.Lazin, 2000: *The SeaBOARR-99 Field Campaign*. NASA Tech. Memo. 206892, Vol. **8**, S.B. Hooker and E.R. Firestone, eds., NASA Goddard Space Flight Center, Greenbelt, MD. 46pp.

Hooker, S.B., G. Zibordi, G.Lazin, and S. McLean, 1999: *The SeaBOARR-98 Field Campaign*. NASA Tech. Memo. 206892, Vol. **3**, S.B. Hooker and E.R. Firestone, eds., NASA Goddard Space Flight Center, Greenbelt, MD. 40pp.

Johnson, B.C., S.S. Bruce, E.A. Early, J.M. Houston, T.R. O'Brian, A. Thompson, S.B. Hooker and J.L. Mueller, 1996: The Fourth SeaWiFS Intercalibration Round-Robin Experiment (SIRREX-4), May 1995. *NASA Tech. Memo. 104566, Vol. 37,* S.B. Hooker, E.R. Firestone and J.G. Acker, Eds., NASA Goddard Space Flight Center, Greenbelt, Maryland, 65 pp.

Lee, Z.P., K.L. Carder, T.G. Peacock, C.O. Davis and J.L. Mueller, 1997a: Remote-sensing reflectance and inherent optical properties of oceanic waters derived from above-water measurements. In: *Ocean Optics XIII*, S.G. Ackleson, ed., Proc. SPIE **2693**: 160-166.

Lee, Z.P., K.L. Carder, T.G. Peacock, and R.G. Steward, 1997b: Remote sensing reflectance measured with and without a vertical polarizer. In: *Ocean Optics XIII*, S.G. Ackleson, ed., Proc. SPIE **2693**: 483-488.

Mobley, C.D., 1999: Estimation of the remote-sensing reflectance from above-surface measurements. *Appl. Opt.* **38**: 7442-7455.

Morel, A., and B. Gentili, 1996: Diffuse reflectance of oceanic waters. III. Implication of

bidirectionality for the remote-sensing problem. *Appl. Opt.* **35**: 4850-4862.

Mueller, J.L., B.C. Johnson, C.L. Cromer, S.B. Hooker, J.T. McLean and S.F. Biggar, 1996: The Third SeaWiFS Intercalibration Round-Robin Experiment (SIRREX-3), 19-30 September 1994: *NASA Tech. Memo. 104566, Vol. 34,* S.B. Hooker, E.R. Firestone and J.G. Acker, Eds., NASA Goddard Space Flight Center, Greenbelt, Maryland, 78 pp.

Mueller, J.L., and R.W. Austin, 1995: Ocean Optics Protocols for SeaWiFS Validation, Revision 1. *NASA Tech. Memo. 104566, Vol. 25,* S.B. Hooker, E.R. Firestone and J.G. Acker, Eds., NASA Goddard Space Flight Center, Greenbelt, Maryland, 67 pp.

Mueller, J.L., J.R.V. Zaneveld, S. Pegau, E. Valdez, H. Maske, S. Alvararez-Borrego and R. Lara-Lara, 1997: Remote sensing reflectance: preliminary comparisons between in-water and above-water measurements, and estimates modeled from measured inherent optical properties, In: *Ocean Optics XIII*, S.G. Ackleson, ed., Proc. SPIE **2693**: 502-507.

Rhea, W.J. and C.O. Davis, 1997: A comparison of the SeaWiFS chlorophyll and CZCS pigment algorithms using optical data from the 1992 JGOFS Equatorial Pacific Time Series. *Deep Sea Res. II* **44**: 1907-1925.

Siegel, D.A., M.C. O'Brien, J.C. Sorenson, D.A. Konnoff, E.A. Brody, J.L. Mueller, C.O. Davis, W.J. Rhea, and S.B. Hooker, 1995: Results of the SeaWiFS Data Analysis Round Robin, July 1994 (DARR-94): *NASA Tech. Memo. 104566, Vol. 26,* S.B. Hooker and E.R. Firestone, Eds., NASA Goddard Space Flight Center, Greenbelt, Maryland, pp 44-48.

Sydor, M. and R.A. Arnone, 1997: Effect of suspended and dissolved organic matter on remote-sensing of coastal and riverine waters. *Appl. Opt.* **36**: 6905-6912.

Sydor, M., R.A. Arnone, R.W. Gould, Jr., G.E. Terrie, S.D. Ladner and C.G. Wood, 1998: Remote-sensing technique for determination of the volume absorption coefficient of turbid water. *Appl. Opt.* **37**: 4944-4950.

Toole, D.A., D.A. Siegel, D.W. Menzies, M.J. Neumann and R.C. Smith, 2000: Remote-sensing reflectance determinations in the coastal ocean environment: impact of instrumental characteristics and environmental variability. *Appl. Opt.* **39**: 456-468.

Chapter 11

Sun and Sky Radiance Measurements and Data Analysis Protocols

Robert Frouin[1], Brent Holben[2], Mark Miller[3], Christophe Pietras[4], Ewa Ainsworth[4], John Porter[5] and Ken Voss[6]

[1]*Scripps Institution of Oceanography, University of California, San Diego, California*
[2]*Biospheric Sciences Branch, NASA Goddard Space Flight Center, Greenbelt, Maryland*
[3]*Department of Applied Science, Brookhaven National Laboratory, Upton, New York*
[4]*SAIC General Sciences Corporation, Beltsville, Maryland*
[5]*School of Ocean & Earth Science & Technology, University of Hawaii, Hawaii*
[6]*Physics Department, University of Miami, Florida*

11.0 INTRODUCTION

This chapter is concerned with two types of radiometric measurements essential to verify atmospheric correction algorithms and to calibrate vicariously satellite ocean color sensors. The first type is a photometric measurement of the direct solar beam to determine the optical thickness of the atmosphere. The intensity of the solar beam can be measured directly, or obtained indirectly from measurements of diffuse global upper hemispheric irradiance. The second type is a measurement of the solar aureole and sky radiance distribution using a CCD camera, or a scanning radiometer viewing in and perpendicular to the solar principal plane.

From the two types of measurements, the optical properties of aerosols, highly variable in space and time, can be derived. Because of the high variability, the aerosol properties should be known at the time of satellite overpass. Atmospheric optics measurements, however, are not easy to perform at sea, from a ship or any platform. This complicates the measurement protocols and data analysis. Some instrumentation cannot be deployed at sea, and is limited to island and coastal sites. In the following, measurement protocols are described for radiometers commonly used to measure direct atmospheric transmittance and sky radiance, namely standard sun photometers, fast-rotating shadow-band radiometers, automated sky scanning systems, and CCD cameras. Methods and procedures to analyze and quality control the data are discussed, as well as proper measurement strategies for evaluation of atmospheric correction algorithms and satellite-derived ocean color.

11.1 AUTOMATIC SUN PHOTOMETER AND SKY RADIANCE SCANNING SYSTEMS

The technology of ground-based atmospheric aerosol measurements using sun photometry has changed substantially since Volz (1959) introduced the first hand-held analog instrument almost four decades ago. Modern digital units of laboratory quality and field hardiness collect data more accurately and quickly and are often equipped for onboard processing (Schmid et al., 1997; Ehsani, 1998, Forgan, 1994; and Morys et al., 1998). The method used remains the same, i.e., a detector measures through a spectral filter the extinction of direct beam solar radiation according to the Beer-Lambert-Bouguer law:

$$V(\lambda) = V_o(\lambda)\left(\frac{d_o}{d}\right)^2 \exp\left[-\left(\tau(\lambda)M\right)\right]t_g(\lambda), \quad (11.1)$$

where $V(\lambda)$ is the measured digital voltage, $V_0(\lambda)$ is the extra-terrestrial voltage, M is the optical air mass, $\tau(\lambda)$ is the total optical depth, λ is wavelength, d and d_o are respectively the actual and average earth-sun distances, and $t_g(\lambda)$ is the transmission of absorbing gases. The total optical depth is the sum of the Rayleigh and aerosol optical depth.

The earth-sun distance correction is calculated using the approximation

$$\left(\frac{d_o}{d}\right)^2 = 1 + 0.034\cos\frac{2\boldsymbol{p}\cdot J}{365} \qquad (11.2)$$

where J is the number of the day of the year (Iqbal 1983).

Air mass is a function of the sun zenith angle. Currently, the same value of air mass is used for Rayleigh, ozone, and aerosol factors. Air mass is calculated as

$$M = \left\{\cos\frac{\boldsymbol{pq}_o}{180^o} + 0.15*(93.885 - \boldsymbol{q}_o)^{-1.253}\right\}^{-1}, \quad (11.3)$$

where the sun zenith angle $\boldsymbol{q}_o$ is expressed in degrees.

Sky-scanning spectral radiometers that measure the spectral sky radiance at known angular distances from the sun have expanded the aerosol knowledge base. They provide, through inversion of the sky radiance, aerosol physical properties, such as size distribution, and optical properties, such as the aerosol scattering phase function (Nakajima et al., 1983, 1996; Tanré et al., 1988; Shiobara et al., 1991; Kaufman et al., 1994; Dubovik et al., 2000; and Dubovik and King, 2000). The inversion technique to calculate these aerosol properties requires precise aureole measurements near the solar disk and good stray-light rejection. Historically these systems are cumbersome, not weather hardy and expensive. The CIMEL and PREDE (French and Japanese manufacturers respectively) sun and sky scanning spectral radiometers overcome most of such limitations, providing retrievals of aerosol and water vapor abundance from direct sun measurements, and of aerosol properties from spectral sky radiance measurements. Since the measurements are directional and represent conditions of the total column atmosphere, they are directly applicable to satellite and airborne observations, as well as to studies of atmospheric processes. Owing to a sophisticated tracking system with fast responding motors, the PREDE can be installed onboard a ship, or other moving platform, to monitor aerosol optical properties at sea. In the following, we focus on the CIMEL system, since the measurement protocols are similar for both CIMEL and PREDE systems.

Description

The CIMEL Electronique 318A spectral radiometer, manufactured in Paris, France, is a solar powered, weather hardy, robotically pointed sun and sky spectral radiometer. At each wavelength, this instrument has approximately a 1.2^o field-of-view (full angle) and filtered solar aureole and sky radiance. The 33 cm collimators were designed for 10^{-5} stray-light rejection for measurements of the aureole 3° from the sun. The robot mounted sensor head is pointed at nadir when idle to prevent contamination of the optical windows from rain and foreign particles. The sun/aureole collimator is protected by a quartz window, allowing observation with a ultraviolet enhanced silicon detector with sufficient signal-to-noise for spectral observations between 300 and 1020 nm. The sky collimator has the same 1.2^o field of view, but uses an order of magnitude larger aperture-lens system to improve dynamic range for measuring the sky radiance. The components of the sensor head are sealed from moisture and desiccated to prevent damage to the electrical components and interference filters. Eight ion assisted deposition interference filters are located in a filter wheel rotated by a direct drive stepping motor. A thermistor measures the temperature of the detector, allowing compensation for any temperature dependence in the silicon detector.

A polarization model of the CE-318 is also used in SIMBIOS. This version executes the same measurement protocol as the standard model, but makes additional hourly measurements of polarized sky radiance at 870 nm in the solar principal plane (Table 11.1 and 11.2).

Installation

The installation procedures for the CIMEL instrument are summarized below. More detailed information is available from the AERONET web page (http://aeronet.gsfc.nasa.gov:8080).

The site should have a clear horizon and be representative of the regional aerosol regime. The basic assembly is relatively simple to mount. The cables are labeled clearly and most fit only in one place. Once the robot is assembled, it should be oriented so the zenith motor casing is pointing roughly east (the metal claw to which the sensor head is attached, then points to the west). The round connector end of the data cable should be attached to the sensor head, and the flat connector should be plugged into the white CIMEL control box. Strap the sensor head to the robot metal claw using the silver metal band. Make sure that the face of the sensor head is flush with the edge of the metal claw. Also, ensure that the long axis of the collimator cross-section is perpendicular to the axis of the zenith motor casing and claw. Verify that the robot itself is level. Do not use the embedded

bubble level on top of the robot. Place the supplied bubble level on top of the flat ledge of the central robot tubular body (below the sensor head motor) This should be level in both the N/S and E/W axes. Verify that the CIMEL control box "TIME" and "DATE" are correct, i.e., that they agree with the VITEL transmitter clock. If the Time or Date is wrong, the CIMEL will not find the sun on a "GOSUN" command.

Next, put the CIMEL in manual mode using the white control box display screen. In Manual mode, the main screen reads: "PW MAN SCN VIEW". Do a "PARK" procedure. When "PARK" is complete the sensor head collimator should be pointing down, perpendicular to the ground. Place the bubble level on the top of the metal claw arm and verify that this is level. If not, loosen the zenith bolt's hex nut (below the permanent bubble level on the top of the robot) and level it by rotating the zenith motor casing with your hand. Re-tighten the zenith nut tightly. Important: Perform another "PARK" procedure, or two, and make sure it is in fact level.

Using the right 2 buttons, change the display to read "GOSUN". Select "GO" to initiate. The sensor head should point to the sun. The hole at the top of the collimator should allow the sunlight to illuminate the marker spot at the base of the collimator. When the bright spot is on the mark, the instrument is aligned. If it is off to the left or right, rotate the robot base to align it. After you rotate the robot, you will need to verify that the robot is still level as before. Park the instrument and perform another "GOSUN" to check that the alignment is still good. If not, ensure that the robot is level, and that the sensor head is level when manually parked. One note: when you level the sensor head and do a "GOSUN", repeat this process a few times to be sure of the alignment. The first "GOSUN" after leveling is often not correct, because moving the sensor head while leveling can temporarily offset the robot's zeroing point. Re-parking the sensor and doing a second "GOSUN" should yield a more accurate alignment. Repeat this procedure until the alignment remains accurate and consistent on repetition.

Press "PW" then increment to 4, and place the instrument in "AUTO" mode. The main "AUTO" mode display should read: "PW AUTORUN VIEW". The CIMEL should be left in this mode in order to perform automatic measurement sequences.

The VITEL transmitter has a multi-level menu with "TIME DATE" etc in top level, and sub categories below each top-level item. The exact menu structure varies with software version (2.01,

2.9, and 2.11). Refer to the version most similar to your particular transmitter. One may operate the VITEL display by using the control buttons. To initiate an action, press the "SET-UP" button, then press the "SCROLL" button repeatedly to view the categories in the current menu level. To choose any subcategory, press the "SELECT" button when the desired feature is shown in the display window. To change a parameter use the right 2 buttons "CHANGE" and "ENTER'". At any time, one may return to the previous (higher) menu level by pressing the "SET-UP" button.

Measurement Protocols

The radiometer makes only two basic measurements, either direct solar flux, or sky radiance. Each type of measurement involves several programmed sequences.

Direct sun measurements are made in eight spectral bands distributed between 340 and 1020 nm (440, 670, 870, 940 and 1020 nm are standard). Each measurement requires approximately 10 seconds. A sequence of three such measurements are taken 30 seconds apart creating a triplet observation per wavelength. Triplet observations are made during morning and afternoon Langley calibration sequences and at standard 15-minute intervals in between (Table 15.1). The time variation of clouds is typically much greater than that of aerosols, and therefore significant variation in the triplets may be used to screen cloud contaminated measurements from the data. Variability over the 15-minute interval also allows another check for cloud contamination at a lower frequency.

Sky measurements are performed at 440, 670, 870 and 1020 nm (Table 11.1). A single spectral measurement sequence (Langley sky) is made immediately after the Langley air mass direct sun measurement, with the sensor pointed 20° from the sun. This is used to assess the stability of the Langley plot analysis (O'Neill *et al.* 1984). Two basic sky observation sequences are made, "almucantar" and "principal plane". The objective of these sequences is to retrieve size distribution, phase function and aerosol optical thickness (AOT). This is approached by acquiring aureole and sky radiance observations spanning a large range of scattering angles, relative to the sun's direction, assuming a constant aerosol profile.

An almucantar is a series of measurements taken at the same sun elevation for specified azimuth angles relative to the Sun position. The range of scattering angles decrease as the solar zenith angle decreases, thus almucantar sequences

made at an optical air mass of 2, or more, achieve scattering angles of 120°, or larger. Scattering angles of 120° are typical of many sun-synchronous viewing satellites, and thus a measure of the satellite path radiance is approximated from the ground station. During an almucantar measurement, observations from a single channel are made in a sweep at a constant elevation angle across the solar disk and continue through 360° of azimuth in about 40 seconds (Table 11.2). This is repeated for each channel to complete an almucantar sequence. A direct sun observation is also made during each spectral almucantar sequence.

More than four almucantar sequences are made daily at optical airmasses of 4, 3, 2 and 1.7, both morning and afternoon. An almucantar sequence is also made hourly between 9 AM and 3 PM local solar time for the standard instrument and skipping only the noon almucantar for the polarization instrument.

The standard principal plane sky radiance measurement sequence is similar to the almucantar sequence, but the sensor scans in the principal plane of the sun, and therefore all angular distances from the sun are scattering angles, regardless of solar zenith angle. This measurement pointing sequence begins with a sun observation, moves 6° below the solar disk then sweeps through the sun's principal plane, taking about 30 seconds for each of the four

spectral bands (Table 11.2). Principal plane observations are made hourly when the optical airmass is less than 2 to minimize the variations in radiance due to the change in optical airmass.

Polarization measurements of the sky at 870 nm are an option with this instrument. The sequence is made in the principal plane at 5° increments between zenith angles of –85° and +85°. The configuration of the filter wheel requires that a near-IR polarization sheet be attached to the filter wheel. Three spectrally matched 870 nm filters are positioned in the filter wheel exactly 120° apart. Each angular observation is a measurement of the three polarization filter positions. An observation takes approximately 5 seconds and the entire sequence about 3 minutes. This sequence occurs immediately after the standard measurement sequence in the principal plane.

Data Analysis

We are following the procedures established for the AERONET program (Holben et al, 1998) (Table 11.3). These algorithms impose a processing standardization on all of the data taken in the network, facilitating comparison of spatial and temporal data between instruments.

Table 11.1.   Measurement sequences of the CIMEL Sun/Sky scanning spectral radiometer.

	Spectral Range nm	Target	No. Obs.	Obs. Interval	Application
BASIC DIRECT SUN	340 to 1020	Sun	1 each λ	~ 8 sec. for. 8 λ	AOT, Pw, α
Triplet Observation	340 to 1020	Sun	Three direct sun	3 @ 30 sec. apart, 1 min total	AOT, Pw, α & cloud screening
Standard Measurement Sequence	340 to 1020	Sun	Variable: depends on day length	Ea. 15 min m=2 AM to m=2 PM	AOT, Pw, α
Langley	340 to 1020	Sun	16, am & PM between m 7 & 2	m=7 - 5, incr of.5 m m=5 - 2, incr. of.25	Langley, Cal., AOT, Pw, α
BASIC SKY	440 to 1020	Sky	1 each λ	none	Sky Radiance
Langley sky	440 to 1020	Sky	16 between m 7 & 2	m=7 - 5,.5; m=5- 2,.25	Stability of Lngly Plot
Almucantar	440 to 1020	Sky	72 (Table 2)	>8/day: m= 4, 3, 2, 1.7 hrly 9AM to 3PM	Size Dist. and P(θ), AOT, α
Polarization	870	Sky	42 (Table 2)	hourly m=3 AM to m=3 PM	Size Dist. and P(θ)
Principal Plane	440 to 1020	Sky	42 (Table 2)	hourly m=3 am to m=3 PM	Size Dist. and P(θ) AOT, α

The archival system allows the SIMBIOS community to access either the raw or processed data via internet for examination, analysis and/or reprocessing, as needed, through the AERONET web page: aeronet.gsfc.nasa.gov:8080.

The algorithms, inputs, corrections, and models used in computing the aerosol optical thickness, precipitable water (Pw), spectral irradiance, and sky radiance inversions are referenced in Table 15.3. The algorithms comprise two principal categories; time dependent retrievals such as AOT and Pw, and sky radiance retrievals such as size distribution, asymmetry parameter, single scattering albedo and complex index of refraction. As new and improved approaches and models are accepted within the community the processing may be applied uniformly to the network-wide database.

Sky radiance Inversion Products

Optical properties of the aerosol in the atmospheric column are retrieved by two inversion algorithms: that of Nakajima et al. (1983, 1996) and the new algorithm developed by the AERONET Project (Dubovik and King 2000; Dubovik *et al.* 2000).

a) Inversions by the Nakajima et al.'s (1983, 1996) algorithms

The code inverts sky radiance in two ways:

1. simultaneously at four wavelengths (440; 670; 870 and 1020 nm) in the aureole angular range (scattering angle between 2.8^0 and 40^0 ;
2. separately at each of four wavelengths (440; 670; 870 and 1020 nm) in the whole solar almucantar (scattering angle greater than 2.8^0) - -option "single channel inversion".

The inversion assumptions are that aerosol particles are homogeneous spheres with a fixed index of refraction: n (λ) = 1.45, k(λ) = 0.005. The retrieved variables are: $\dfrac{dV(r)}{d\ln r}$ (in $\mu m^3/\mu m^{-2}$), the volume particle size distribution in range of sizes: 0.057 μm < r < 8.76 μm, the scattering optical thickness at 440,670,870,1020nm, and the phase function at 440, 670, 870 and 1020nm (including an asymmetry parameter).

b) Inversions by the new AERONET code (Dubovik and King 2000; Dubovik et al. 2000)

The code inverts $t_a(\lambda)$ and sky radiances simultaneously at four wavelengths (440; 670; 870 and 1020 nm) in the whole solar almucantar (scattering angles greater than 2.8°). Aerosols are assumed to be homogeneous spheres, but the index of refraction is not fixed.

Table 11.2.   Almucantar and Principal Plane sequences for the standard and polarization instruments.

	Sun	Sky (°)
ALMUCANTAR Azimuth angle relative to sun	0°	6.0, 5.0, 4.5, 4.0, 3.5, 3.0, 2.5, 2.0, -2.0,-2.5, -3.0, -3.5, -4.0, -4.5, -5.0, -6.0, -8.0, -10.0, -12.0, -14.0, -16.0, -18.0, -20.0, -25.0, -30.0, -35.0, -40.0, -45.0, -50.0, -60.0, -70.0, -80.0, -90.0, -100.0, -110.0, -120.0, -130.0, -140.0, -160.0, -180.0 Duplicate above sequence for a complete counter clockwise rotation to –6
PRINCIPAL PLANE: **Standard** Scattering Angle from sun (negative is below the sun)	0°	-6.0, -5.0, -4.5, -4.0, -3.5, -3.0, -2.5, -2.0, 2.0, 2.5, 3.0, 3.5, 4.0, 4.5, 5.0, 6.0, 8.0, 10.0, 12.0, 14.0, 16.0, 18.0, 20.0, 25.0, 30.0, 35.0, 40.0, 45.0, 50.0, 60.0, 70.0, 80.0, 90.0, 100.0, 110.0, 120.0, 130.0, 140.0
PRINCIPAL PLANE: **Polarization** Scattering Angle from sun (negative is in the anti solar direction)	-	-85.0, -80.0, -75, -70, -65.0, -60.0, -55.0, -50.0, -45.0, -40.0, -35.0, -30.0, -25.0, -20.0, -15.0, -10.0, -5.0, 5.0, 10.0, 15.0, 20.0, 25.0, 30.0, 35.0, 40.0, 45.0, 50.0, 55.0, 60.0, 65.0, 70.0, 75.0, 80.0, 85.0

Table 11.3   Procedure of the AERONET Program

Variable, algorithm or correction	Comments	References
Basic Computations		
Rayleigh Optical Depth, τ_r refractive index of air depolarization factor	Input elevation in m	Penndorf, 1957 Edlen, 1966 Young, 1980 Burcholtz, 1995
Solar Zenith Angle, θ_o		Michalsky, 1988
Earth sun distance, d		Iqbal, 1983
Ozone amount, O_3	Table lookup by 5° lat. long.	London et al., 1976
Aerosol optical air mass, m_a		Kasten and Young, 1989
Rayleigh optical air mass, m_r		Kasten and Young, 1989
O_3 optical air mass, m_o		Komhyr et al., 1989
Corrections		
Temperature, T	~0.25%/°C for 1020 nm specific for each inst.	Hamamatsu Inc. and Lab measurements
Water Vapor for 1020 AOT	from Pw retrieval, Lowtran	Kneizys et al, 1988
Rayleigh, all wavelengths	from elevation	
O_3 abs. coef. $\lambda > 350$ nm		Vigroux, 1953
O_3 abs. coef. $\lambda < 350$ nm		Bass and Paur, 1984
Time, t	CIMEL, UTC, DAPS time stamps, ±1 second	Refer to Homepage
Retrievals		
Spectral direct Sun AOT, Langley Plots	Beer's Law	Shaw, 1983
Pw: (a, k, Vo)	Modified Langley	Bruegge et al., 1992; Reagan et al., 1992
Size Dist., Phase function	From spectral sky radiance	Nakajima et al., 1983 Dubovik and King, 2000
Procedures		
Cloud Screening	Thresholds, λ AOT & t	Smirnov et al., 2000
Climatology, Direct Sun	AOT, Pw, Wavelength Exp.	Refer to Homepage
Climatology, Sky	Size Dist., Phase function, g	Refer to Homepage

The retrieved variables are $\dfrac{dV(r)}{d\ln r}$ (in $\mu m^{-3}/\mu m^{-2}$), the volume particle size distribution in the range of sizes 0.05 $\mu m < r < 15$ μm, and the volume concentration, volume mean radius, standard deviation, and effective radius for total (t), fine (f), and coarse (c) modes.

Note that the fine and coarse mode variables can be used only if the retrieved $\dfrac{dV(r)}{\ln r}$ is bi-modal. There is no automatic check for bi-modality. Also retrieved are the real and imaginary parts of the complex refractive index, $m(\lambda) = n(\lambda) - i\, k(\lambda)$, $(1.33 < n(\lambda) < 1.6;\ 0.0005 < k(\lambda) < 0.5)$ at 440,670,870, and 1020nm, the single scattering albedo, and the phase function (including its asymmetry parameter) at 440, 670, 870, and 1020

nm. It is assumed that particles in the range 0.05-0.6 μm are fine mode and those in the range 0.6-15 μm are coarse mode aerosols (Dubovik et al., 2000). This definition is not completely correct in all size distributions. Nevertheless, experience has shown it to hold true in the majority of practical cases.

Quality Control

The AERONET $t_a(\lambda)$ quality assured data are cloud screened following the methodology of Smirnov et al. (2000), and here we present just a brief outline of the procedure. The principal filters used for the cloud screening are based on temporal variability of the $t_a(\lambda)$, with the assumption being that greater temporal variance in t_a is due to the

presence of clouds. The first filter is a check of the variability of the three t_a values measured within a one-minute period. If the difference between minimum and maximum $t_a(\lambda)$ within this one minute interval is greater than 0.02 (for t_a less than 0.667) or 0.03 t_a (for t_a greater than 0.667) then the measurement is identified as cloud contaminated. Then the time series of the remaining $t_a(\lambda)$ are analyzed for the presence of rapid changes or spikes in the data. A filter based on the second derivative of the logarithm of $t_a(\lambda)$ as a function of time is employed to identify rapid variations which are then filtered as observations affected by cloud. Other secondary order cloud screening and data quality checks are also made and these are described in detail in Smirnov et al. (2000). Unscreened data is fully available from the AERONET homepage. Automatic cloud screening of the almucantar and principal plane data is done by checking the distributions of data about the solar disc for symmetry and smoothness.

11.2 SKY RADIANCE DISTRIBUTION CAMERA SYSTEMS

Camera systems for sky radiance distribution are useful to collect the entire hemisphere of sky radiance data in a quick manner. The resulting data images usually contain the sun, so that the measurement geometry can be determined accurately and unambiguously. Also images can be checked for cloud contamination and other measurement artifacts more easily than can be done with data from scanning systems. The limitation of camera systems is that the dynamic range of the whole scene must be contained in each image. Therefore, the camera system must have large dynamic range and there has to be a method of attenuating the direct sunlight before it strikes the imaging optics. To get a complete sky radiance distribution, including the solar aureole, it may be necessary to have an auxiliary system to measure the sky radiance near the sun (Ritter and Voss, 2000).

In addition, a sky radiance system, fitted with polarizers, can measure the Stokes parameters dealing with linear polarization (Voss and Liu, 1997). These additional parameters are useful for investigating the polarization properties of the atmospheric aerosols, and improving the aerosol optical models.

One of the most important areas of the sky radiance distribution to measure is the area near the horizon, opposite the sun, in the principal plane (the plane containing the sun and the zenith direction). This portion of the sky contains information on the large scattering angle portion of the atmospheric aerosol phase function, and is very important for determining the aerosol optical properties relevant to atmospheric correction for ocean color satellites.

The second very important region of the sky is the solar aureole, the region near the sun. Because the aerosol scattering phase function is strongly peaked in the forward direction, information in this region is important in determining the aerosol single scattering albedo. Techniques for converting sky radiance measurements to aerosol properties have been described in Wang and Gordon (1993), Gordon and Zhang (1995) and Zhang and Gordon (1997a, b).

An example of a camera system for sky radiance distribution is described in Voss and Zibordi (1989). The system described has been upgraded, for greater dynamic range, with a cooled CCD array. The basic system consists of a fisheye lens, a spectral/polarization filter changer, and a digital camera. To block direct sunlight from hitting the array, an occulter is manually adjusted to shadow the fish-eye lens. The size of the occulter is approximately $\pm~20^o$ of the almucantar when the sun is at 60° zenith angle; the effect of the occulter is obvious in data images shown in Liu and Voss (1997). Four spectral filters select the wavelength range to be measured. Polarization filters are used to collect 3 planes of polarization in data images. These images can be combined to determine the linear polarization stokes vectors.

Measurement Protocols

Obviously the first order requirement is that the field of view of the camera system be as unobstructed as possible, and that the measurement site be located in an appropriate place with respect to the ships stack exhaust. If the whole field of view cannot be clear (as is usually the case), then one should try for a clear hemisphere, where data between obstructions in the other hemisphere can be used for checking the sky symmetry.

As the desired objective is the aerosol scattering parameters, the sky must also be cloud free. Clouds cause two problems. The first is easy to detect and is the direct effect of having the bright cloud in the scene (in particular on the almucantar or principle plane). Almost any cloud will overwhelm the effect of aerosols in determining the sky radiance. This effect of clouds is usually quite

evident in the sky radiance image. The second problem is the indirect effect of clouds, while not directly causing a problem, shadowing aerosols and reducing the skylight caused by aerosol scattering. This second effect is more difficult to handle and places a more stringent requirement on the state of cloudiness during a measurement sequence. This effect can often be quite visible when the atmospheric aerosol loading is high, causing light beams to be evident in the aerosol layer. For these reasons, measurements with clouds present should be avoided if at all possible.

The maximum scattering angles existing in the sky radiance distribution occur near the horizon in the principle plane opposite the sun. For a given solar zenith angle, the maximum scattering angle is given by adding /2 to the solar zenith angle. Since knowledge of the aerosol phase function at large scattering angles is important for the atmospheric correction process, measurements of the sky radiance distribution should be taken when the sun is at large zenith angles. The optimum angle is a compromise between getting large scattering angles and working too close to the horizon where multiple scattering effects are large (because of long optical paths through the atmosphere). A solar zenith angle of 60^0 has been chosen as optimum, because of these constraints.

Concurrent with the sky radiance measurements, it is important to measure the aerosol optical depth. By combining the aerosol optical depth and sky radiance distribution, the aerosol scattering properties can be determined, together with the single scattering albedo of the aerosols (Wang and Gordon, 1993; Gordon and Zhang, 1995; Zhang and Gordon, 1997a).

Data Analysis Protocols

Data reduction of the sky radiance data is very straightforward, and is described in Voss and Zibordi (1989). Basically with camera images, the data reduction process consists of simple image processing. Each image is multiplied by an absolute calibration factor and by an image that corrects for camera lens roll-off. This last factor is very important with a fisheye lens, as the important portion of the image is near the edge where the roll-off can become very significant. Once the image has been converted to radiometric data, specific areas can be selected for further analysis. In particular the almucantar and principal plane can easily be extracted for use in inversion routines.

Reduction of the sky radiance data to get the polarization properties is slightly more complicated. The current method is described in

Voss and Liu (1997). Basically the Mueller matrix of the camera system is described as interacting with the Stokes vector of the skylight. There are three orientations of a linear polarizer in the system providing three separate Mueller matrices describing the camera system. For each sky direction (a pixel in the camera images), these Mueller matrices and the resultant intensities measured by the camera form a set of simultaneous equations with the unknowns being the sky Stokes vectors. For each pixel, these equations are inverted to obtain the Stokes vector of the skylight. While these images have been evaluated qualitatively (Liu and Voss, 1997), work is currently being done to do more quantitative inversions following the methods of Zhang and Gordon (1997b).

11.3 HAND-HELD SUN PHOTOMETERS

These instruments offer the simplest and most cost-effective means to collect data on aerosol optical thickness at sea. They are based on the measurement of the solar beam intensity, and therefore, the direct atmospheric transmittance. From this transmittance, after proper correction for attenuation by air molecules, the aerosol optical thickness may be obtained (Equation 15.1). The technique is straightforward in principle. It is difficult for an observer to point the photometer at the sun accurately from a moving platform, but this difficulty is obviated with modern-day instruments. The interest of these instruments also resides in the fact that, in most of the oceans, aerosol optical thickness measurements at the time of satellite overpass are sufficient to verify the atmospheric correction of ocean color (Schwindling *et al.* 1998). They allow one to estimate, via the Angstrom coefficient, the "pseudo" phase function of the aerosols (the product of the single-scattering albedo and the phase function), a key atmospheric correction variable.

Many types of sun photometers have been built and are available commercially. In the following, we focus on two instruments, the MicroTops sun photometer, manufactured by Solar Light, Inc., and the SIMBAD radiometer, built by the University of Lille.

The NASA SIMBIOS Program maintains a set of these instruments for use during ocean-color evaluation cruises. The objective is to collect accurate aerosol optical thickness measurements during the ship cruises for comparison with values derived from satellite algorithms.

a) MicroTops

The Solar Light, Inc. MicroTops sun photometer is a hand held radiometer used by many investigators throughout the world. The popularity of MicroTops sun photometers is due to their ease of use, portability, and relatively low cost. The instruments have five channels whose wavelength can be selected by interference filters. In order to follow the specifications given by the World Meteorological Organization (WMO), the wavelengths are typically chosen at 440, 500, 675, 870 nm, with an additional channel at 940 nm to derive integrated water vapor amounts. If an additional sun photometer is available then it is also desirable to make measurements at 380 and 1020 nm.

The MicroTops sun photometers use photodiode detectors coupled with amplifiers and A/D converters. The collimators are mounted in a cast aluminum block with a 2.5^o full field of view. The MicroTops sun photometer has built-in pressure and temperature sensors and allows for a GPS connection to obtain the position and time. A built in microprocessor can calculate the aerosol optical depth, integrated water vapor, and air mass in real time and display these values on a LCD screen. Temperature effects are corrected by taking dark count measurements with the lid covered on startup. Further information on MicroTops sun-photometers can be found in Morys (1998).

b) SIMBAD

The SIMBAD radiometer was designed by the University of Lille to measure both aerosol optical thickness and diffuse marine reflectance, the basic atmospheric correction variables. The radiometric measurements are made in 5 spectral bands centered at 443, 490, 560, 670, and 870 nm. The ocean surface and the sun are viewed sequentially. The same 3° field-of-view optics interference filters, and detectors are used in both ocean- and sun-viewing modes. A different electronic gain, low and high, is used for each mode, respectively. A specific mode allows measurement of the dark current. The optics are fitted with a vertical polarizer to reduce reflected skylight when the instrument is operated in ocean-viewing mode (Fougnie et al., 1999). The polarizer does not affect the sun intensity measurements, because direct solar radiation is not polarized.

Attached to the instrument is a GPS for automatic acquisition of geographic location at the time of measurement. Also acquired automatically are pressure, temperature, and view angles. Frequency of measurements is 10 Hz. In sun-viewing mode, only the highest intensity measured over one second is kept to avoid sun-pointing errors on a moving platform. Data is stored internally and downloaded onto diskette at the end of the day, or cruise. The instrument is powered with batteries, allowing 6 hours of continuous use. In normal use during a cruise (see below), the internal memory and batteries allow for 3 months of operations without downloading data or recharging the batteries.

Installation and Maintenance

The MicroTops and SIMBAD instruments need to be pointed towards the sun manually. The sun is correctly aligned when its image appears in the cross hair on a small screen (MicroTops) or on a target (SIMBAD). After 10-20 minutes of practice the user will become familiar with the pointing procedure and the process will become second nature. It is important to get familiar with this pointing procedure on land as ship based measurements require more skill.

The exterior of the instrument lenses can accumulate salt spray and should be inspected and cleaned if needed. For the open ocean, salt is the primary contaminant. Under these conditions, a lens tissue can be wet with clean (filtered if possible) water or ethanol and used to remove the salt, then a dry lens tissue used to remove remaining water drops.

Faulty electronics pose a potential problem that is not always easy to detect when using MicroTops instruments. In the past it has been found that a leaky capacitor lowered the power and created erratic behavior for the shorter wavelengths where more gain is required. One can also get some idea of the instrument stability by taking numerous measurements with the lid covered. The voltage on all five channels should be less than ± 0.03 mV and the variability will give some idea of the noise present in the photometer. If the values are greater then the unit should be sent back to the manufacturer for repair.

Measurement Protocols

During stable conditions (land or calm seas) pointing the radiometers at the sun is straightforward and most of the measurements will be accurate. Under rough ocean conditions, pointing at the sun can become the major source of uncertainty, with many of the measurements being off the sun. The measurements that are off the sun

will have higher apparent aerosol optical depths, artifacts that bias the average positively. For data acquired under rough sea conditions, repeated measurements of aerosol optical depths are typically distributed in a comet shaped pattern, with a cluster of lower values and a tail extending to higher values. In these cases, the smaller optical depth values are more accurate and the larger values, which are likely due to pointing error, must be removed in post processing. Since many measurements may be discarded in post processing, it is suggested that 25 or more measurements should be made within a short period of time (less than 5 minutes).

In general, the SIMBAD instrument is used alternatively in sun- and ocean-viewing mode. The sun intensity measurements also allow one to compute down-welled solar irradiance accurately in clear sky conditions, or when the sky is partly cloudy (<30%) with the sun not obscured by clouds. The modeled values of solar irradiance are used to normalize water-leaving radiance measurements.

The recommended protocol is to make consecutively one "dark" measurement, three measurements in sun-viewing mode, one "dark" measurement, three measurements in ocean-viewing mode, one "dark" measurement, three measurements in sun-viewing mode, and one "dark" measurement. It requires about 15 minutes to collect a complete data set (ocean, sun, optical zero), including deploying the instrument and logging ancillary data (wind speed, sea state, cloud cover, etc.).

In order to expedite the measurements, the MicroTops averaging time should be set to one and the sampling down to six samples. The shorter sampling periods will speed the measurements and no averaging will improve the chances that at least some of the measurements are accurately pointed at the sun. After making the measurements, post processing is needed to remove the high values that occur from misalignment with the sun. Once the large values have been removed, the remaining values should be averaged which will reduce electronic noise.

Temperature tests have shown that the aerosol optical thickness derived from MicroTops is strongly dependent on the temperature (Porter *et al.* 2000). Being out in the sun for 1-2 minutes can change the instrument's temperature, and thus affect the aerosol optical depth measurement. In order to avoid this effect, the MicroTops should be turned off and on frequently during the measurement period. It is recommended that the MicroTops be shut off and on every 10 seconds

when making measurements, or after every 2 continuous measurements. On the other hand, temperature variation effects are negligible in the SIMBAD measurements.

On several instances we have found condensation to be a problem when radiometers were stored in an air-conditioned room prior to making measurements in the humid marine atmosphere. Condensation may occur outside the SIMBAD radiometer, but can also occur inside the MicroTops (i.e. it is not always possible to wipe it off). To avoid water condensation, the instrument should be placed in the sun to warm to temperatures higher than ambient temperatures prior to making the measurements. It is suggested to leave the instruments in the sun for 15-20 minutes before the measurements. The temperature can be monitored in the MicroTops to ensure enough warming has occurred. This procedure presupposes that the instrument has been calibrated at the elevated temperature level.

For MicroTops the latitude and longitude and time should be set either manually, or by connecting the GPS receiver directly to the radiometer. Using either method, the time can be set to within one second of the correct time. The latitude and longitude can also be stored in the MicroTops for measurements at fixed sites. For SIMBAD the geographic location and time are automatically acquired at the beginning of each acquisition in "dark", sun-viewing, and ocean-viewing modes.

In order to maintain the quality of the aerosol optical thickness measurements, the procedures suggested above should be followed and the radiometers should be calibrated at least twice a year (more frequently if the calibration site is not stable –see Chapter 6). When possible, it is also advisable to make measurements with two instruments. This redundancy will help to determine if any problems are occurring.

Data Analysis

In order to derive aerosol optical thickness measurements, 1) the bad values need to be removed, 2) the air mass should be calculated, and 3) the molecular, ozone, water vapor and trace gas optical depths should be removed.

To remove the bad values, the data should be plotted and large values should be eliminated manually, if they are not part of a systematic trend. Poor pointing artifacts will appear as noise, while real aerosol variations will have a more systematic behavior when plotted as a short time series. This visual inspection and removal of large values

should be done for each channel, and it should not be assumed that removing all bad data points in one channel will remove all bad data for all channels. In this process a final optical depth variability of 20% of the final average value or 0.025 may be permitted when the optical depths are below 0.08. This approach may slightly bias the data to lower values but it will remove the unrealistic larger values that would occur if the data were not filtered.

In the standard processing, the direct atmospheric transmittance $T(\lambda) = exp(-\tau(\lambda)\,m)$ and, thus, the total optical thickness $\tau(\lambda)$ is obtained from the sun intensity (or voltage) V measured by the radiometer and the calibration constant V_0, by solving the Beer-Lambert-Bouguer equation (Eq. 11.1). The protocols used within the SIMBIOS Project to calculate AOT are described below in Sect. 11.5.

11.4 FAST-ROTATING SHADOW-BAND RADIOMETERS

An estimate of τ_a can be made from calibrated measurements of the solar beam irradiance, $E_N(\lambda)$, at normal incidence when there are no clouds in front of the solar disk. Two sun photometer designs are commonly used to measure $E_N(\lambda)$: a narrow-beam detector mechanically pointed at the solar disk and a wide-field-of-view radiometer with a solar occulting apparatus. The first type of sun photometer requires careful angular positioning and can provide additional information about the forward scattering phase functions that help characterize the aerosol constituents. In contrast, a radiometer equipped with an occulting apparatus, known as a shadow-band radiometer, measures the diffuse and global (upper hemispheric) irradiance and computes $E_N(\lambda)$ from the difference between the two. The device gets its name from the hemispherical metal strip that rotates around the detector and blocks the direct solar beam to yield a signal that is from the sky only (after the effect of the arm is included).

The multiple wavelength rotating shadow-band radiometer (Harrison et al., 1994) uses independent interference-filter-photodiode detectors and an automated rotating shadow-band technique to make spatially resolved measurements at seven wavelength pass-bands. The uncertainty of the direct-normal spectral irradiance measurement made with this type of sun photometer is comparable with that made by narrow-beam tracking devices. A significant advantage of the shadow-band technique is that the global and diffuse irradiance measurements can be used to study the solar radiation budgets and the fractional cloud cover at the time of the measurement. The latter capability is particularly important for satellite validation studies. In the SIMBIOS context, direct solar and diffuse sky irradiances are critical terms for correcting down-looking in-water radiometers for self shading (Gordon and Ding (1995).

A marine version of the multiple-wavelength rotating shadow-band radiometer has been developed at the Brookhaven National Laboratory (BNL). The BNL marine version uses a slightly modified version of the detector used for continental applications. It has seven channels: one broadband silicon detector and six ten-nm-wide channels at 415, 500, 610, 660, 870, and 940 nm. Modifications to the detector circuitry used for continental applications are necessary because the response time of the original circuitry is too slow for use on a moving ship. If the response time of the detector is too slow, wave action may cause the orientation of the radiometer to change appreciably during the time the shadow-band is occulting the sun. The rotation of the shadow-band itself must be sufficiently fast for the same reason. The marine version of the shadow-band radiometer is hereafter referred to as the BNL Fast-Rotating, Shadow-band Radiometer (FRSR). Implicit in this terminology is that the FRSR is a multi-filter or "spectral" radiometer.

The response of the silicon cell in the detector used for continental applications is faster than one millisecond, yet the internal preamplifiers have integrating low-noise amplifiers that slow the overall response. The response time of the detector is made faster for marine applications by reducing the magnitude of the low-pass filter capacitors. Laboratory tests do not show additional noise in the measurements as a result of this modification. The processing algorithms, which incorporate pitch, roll and heading measurements, are key to the instrument's ability to derive direct-normal beam irradiance without gimbals and a gyro-stabilized table.

Installation and Maintenance

The installation location of the instrument on a ship must be carefully selected. Ideally, FRSRs should be mounted in an exposed location as high as possible and free of nuisance shadows from other objects. This is often difficult. Radiation measurements on a ship always need to consider

errors from the ubiquitous masts and antennas. A ship's communication antennas have highest vertical priority as do the running lights, and one must be careful of radar beams that can cause severe electronic noise. Once a suitable location has been found and the instrument mounted, the diffuser should be rinsed with distilled water and wiped with a moistened cloth at least once per day. The FRSR is typically mounted as a part of a portable radiation package that includes independent broadband solar and IR radiometers. The glass domes on these radiometers should be rinsed with distilled water and wiped with a moistened cloth.

Calibration is the most essential element of a radiation measurement program. A thorough and on-going calibration process is required before the FRSR can make accurate radiometric measurements at sea. To insure accurate measurements, there are two important elements for FRSR measurement protocol: calibration of the instrument circuitry, which includes temperature stabilization of the detector during measurements, and determination of the extra-terrestrial constants. These elements are discussed in Chapter 6.

Data Analysis

The shadow-band radiometer must properly measure the global and diffuse irradiances from which the direct-beam solar irradiance is derived by the subtraction as

$$E_{sun}(\lambda) = E_s(\lambda) - E_{sky}(\lambda), \qquad (11.4)$$

where $E_{sun}(\lambda)$ is the direct-beam solar incident irradiance projected onto a horizontal plane, $E_s(\lambda)$ is the global irradiance incident on the horizontal plane, and $E_{sky}(\lambda)$ is the diffuse incident irradiance from non-forward scattering. The global irradiance, $E_s(\lambda)$, is measured when the band is out of the field of view and the sensor is exposed to full sunlight. The irradiance normal to the incident solar beam is determined as

$$E_N(\lambda) = E_s(\lambda) \sec\theta_o, \qquad (11.5)$$

A correction for the amount of sky that is blocked by the occulting band is essential for an accurate measurement. An automatic correction for the shadowband is possible through measurement of ``edge'' irradiance as is done with the land-based shadow-band radiometers. The shadow irradiance, $E_{shadow}(\lambda)$, occurs when the sun is completely covered by the shadowband, but a portion of the diffuse irradiance is also blocked. The edge irradiance, $E_{edge}(\lambda)$, is measured when the band is just to one side of the solar disk and provides a good estimate of the global irradiance minus the portion of sky that is blocked by the shadowband at the time it blocks the solar disk. In practice, $E_{edge}(\lambda)$ is selected from two measurements taken when the shadow is on one side or the other of the diffuser. Generally an average is taken, but in some cases in the early morning or late evening only one of the edges is acceptable. It is easy to show that the fully corrected direct solar incident irradiance is

$$E_{sun}(\lambda) = E_{edge}(\lambda) - E_{shadow}(\lambda). \qquad (11.6)$$

With the fast-rotating technique, an advantage of using (15.6) to determine $E_{sun}(\lambda)$ is that the edge and shadow measurements are made in a very short time, which reduces noise significantly, especially on partly cloudy days. Also, if the electronics have a constant bias, the bias is removed by the subtraction. On a moving platform, some smoothing of the data is necessary. It was found that simple averages over a two-minute period (16 sweeps) would reduce the sampling uncertainty by a factor of approximately 4, and yield worst-case measurement uncertainties of about 5 Wm^{-2} for the global values and less than 1 Wm^{2} for the shadow value. For perspective, two minutes is the approximate time for the sun to move by one diameter across the celestial sphere. A discussion and an example of the effectiveness of the two-minute averaging process is shown in Reynolds *et al.* (2000).

The shadow-band theory must be modified for a moving platform when the head might not be on a horizontal plane. Three measurement quantities for each channel are computed from the two-minute mean voltages: the global signal, u'_G, the shadow signal, u'_S, and the edge value, u'_E. The primes indicate the measurement is referenced to the plane of the head, which can be different than a horizontal plane. The two global measurements, u_{G1} and u_{G2}, are combined to produce the best estimate of global voltage, u'_G. The mean shadow voltage is u'_S. The edge value is selected from the two-minute composite sweep using an objective algorithm that accounts shadow width dependence on solar zenith and relative azimuth angles. The objective selection of the edge voltage uses one or a mean of both edge measurements to get the best estimate of u'_E. The voltage due to direct-beam irradiance falling onto the plane of the instrument is given by

$$\mathbf{u}'_H = \mathbf{u}'_E - \mathbf{u}'_S. \qquad (11.7)$$

This equation automatically corrects for the sky that is blocked by the shadow-band and also removes any bias term in the calibration equation. An important point in (15.7) is that the right-hand quantities are measured in a few tenths of a second, while the shadow crosses the diffuser. In such a short time interval the ship attitude changes insignificantly and interference from moving clouds is minimized. The diffuse component of the irradiance signal is computed from

$$\mathbf{u}'_D = \mathbf{u}'_G - \mathbf{u}'_H. \qquad (11.8)$$

As we have stated previously, $\mathbf{u}'_D$ is relatively unaffected by small amounts of platform motion. The exact azimuth and elevation of the solar beam relative to the head must be computed from the following variables measured externally:

$$\{\mathbf{a}_h, \mathbf{q}_h\} = f(\mathbf{a}_S, \mathbf{f}_P, \mathbf{f}_R, \mathbf{a}_r, \mathbf{q}_r) \qquad (11.9)$$

where $\{\mathbf{a}_h, \mathbf{q}_h\}$ are the solar azimuth angle and solar zenith angle relative to the plane of the head, $\mathbf{a}_S$ is the mean heading of the ship in true coordinates, $\mathbf{f}_P$ is the ship mean pitch, and $\mathbf{f}_R$ is the corresponding mean roll over the two-minute period. The relative solar azimuth and zenith angles in geographic coordinates, as seen by the observer, are $\mathbf{a}_r$ and $\mathbf{q}_r$. Equation (6) uses three two-dimensional coordinate transformations in heading, pitch, and roll to shift the solar beam vector to a coordinate system aligned with the FRSR head. The matrix transformation technique is well known and discussed in many textbooks on matrix algebra. Once $\mathbf{a}_h$ and $\mathbf{q}_h$ are known, the calibration table can be consulted and an interpolated correction value, $c(\mathbf{a}_h, \mathbf{q}_h)$, can be derived.

The direct beam intensity on a horizontal plane relative to the instrument, $\mathbf{u}'_H$, is converted to a direct-beam intensity into a plane normal to the solar beam using the relationship

$$\mathbf{u}_N = \frac{\mathbf{u}'_H}{c(\mathbf{a}_h, \mathbf{q}_h)\cos\mathbf{q}_h} \qquad (11.10)$$

The global and horizontal voltages are re-computed for the Earth frame of reference:

$$\mathbf{u}_H = \mathbf{u}_N \cos\mathbf{q}_r \qquad (11.11)$$

$$\mathbf{u}_G = \mathbf{u}_H + \mathbf{u}_D \qquad (11.12)$$

The calibration equation is used to compute E_s, E_{sky}, E_{sun}, and E_N from $\mathbf{u}'_G$, $\mathbf{u}'_D$, $\mathbf{u}'_H$, and $\mathbf{u}'_N$ respectively. From these terms, the Beer-Lambert-Bouguer law (equation 11.1) can be used for estimating the calibration constant or $\mathbf{t}_a(\mathbf{l})$.

Cloud filtering is the most important challenge for FRSR data processing. Because the FRSR operates autonomously, cloud observations are naturally part of the signal that must be processed to obtain $\mathbf{t}$. The cloud filter that is currently used is based on two steps: computing signal statistics over windows of periods of less than two hours and using these statistics to judge the quality of the observation under consideration. If the standard deviation of the observations in a two-hour moving window is less than 0.05, a subjectively defined threshold, and the observation at the center of the window is also less than 0.05, the central observation is accepted. The underpinning of this cloud filtering technique is that $\mathbf{t}$ is relatively constant over a period of two hours, while the cloud signal is highly variable. This approach has proven relatively successful, although improvements in the filter are expected in the future.

11.5 SIMBIOS PROJECT AOT EXTRACTION PROTOCOLS

The SIMBIOS Project is concerned with ocean color satellite sensor intercomparison and merger for biological and interdisciplinary studies of the global oceans. Imagery from different ocean color sensors can now be processed by a single software package using the same algorithms, adjusted by different sensor spectral characteristics, and the same ancillary meteorological and environmental data. This enables cross-comparison and validation of the data derived from satellite sensors and, consequently, creates the continuity of ocean color information in temporal and spatial scales. The next step in this process is the integration of *in situ* obtained ocean and atmospheric parameters to enable cross-validation and further refinement of the ocean color methodology.

Atmospheric correction of satellite radiances and, in particular, estimation of aerosol effects on the upwelling radiance at the top of the atmosphere is one of the most difficult aspects of satellite remote sensing. Merging of aerosol properties obtained from *in situ* observations with these derived by sensor algorithms creates exceptional opportunities to validate and improve the

atmospheric correction. There are many uncertainties associated with *in situ* measurements themselves. They include sun photometer or radiometer calibration and operation problems, inadequate handling by people and cloud contamination. When matching against atmospheric properties obtained by a satellite sensor, additional uncertainties come into play which are caused by different viewing angles by the satellite and surface instruments and by time discrepancies when both instruments acquire their observations. In the case of the atmosphere, these uncertainties are considerable. Therefore, the fine calibration of sun photometers and radiometers is needed as well as the best possible (and uniform from instrument to instrument) correction of obtained measurements. Finally, having multiple observations and from different sun photometers and radiometers is required to cross-validate the quality of *in situ* data, extract measurements of high stability and confidence and compare them against satellite sensor estimates with a larger degree of certainty.

Extraction of in situ AOTs

The Project has recently implemented its own correction strategy for instrument voltages corresponding to AOTs. The approach ensures a uniform AOT processing for all instruments making the AOTs comparable amongst the instruments and between instruments and satellite sensor AOTs derived by means of the atmospheric correction. Also, the method uses a consistent set of tuning variables, such as ancillary data, concurrently applied for the correction of satellite radiances. Therefore, some stages of the satellite and *in situ* data processing are identical, contributing to increasing confidence in the match-ups.

Firstly, separate procedures retrieve sun intensity measurements, V(λ), from individual sun photometers and, in case of the shadow-band radiometer, processed direct-beam irradiances (corresponding to the $I_H(\lambda)$ term from the section 11.4). The following processing is uniform for all instruments, however, of course considers distinct spectral wavelengths used by the sensors. The Beer-Lambert-Bouguer law (equation 11.1) can be written as follows:

$$V(\lambda) = V_0(\lambda) * \left(\frac{d_0}{d}\right)^2 \exp(-M(\theta_o)\, t_R(\lambda))$$
$$* \exp(-M(\theta_o)\, t_o(\lambda)) * \exp(-M(\theta_o)\, t_a(\lambda)) \qquad (11.13)$$

where t_R and t_o are the molecular (Rayleigh) and ozone and aerosol optical thickness, respectively, and the other terms have been previously defined. The equation (11.14) assumes that the signal, $V(\lambda)$, captured by a sun photometer is measured when the instrument is pointing directly into the sun and that gaseous absorption is only due to ozone.

The earth-sun distance adjustment, $(d_0/d)^2$ and air mass, M, are calculated using equations 11.2 and 11.3, respectively. Currently, the same value of air mass is used for Rayleigh, ozone, and aerosol factors.

The desired variable t_a is extracted from equation 11.13 by calculating all other variables. The following estimations of earth and atmospheric parameters to obtain AOT coincide with the SeaWiFS satellite sensor correction, including the choice of meteorological and ozone ancillary data.

Calculations of the Rayleigh optical thickness apply the most contemporary atmospheric pressure readings obtained from the spatial and temporal approximation of daily global pressure maps provided by the National Centers for Environmental Prediction. The Rayleigh optical thickness is extracted as follows:

$$t_R(\lambda) = k_{Ray}(\lambda) * e^{-\frac{A}{7998.9}} * \frac{P}{P_0}, \qquad (11.14)$$

where, k_{Ray} is defined as

$$k_{Ray}(\lambda) = 28773.597886 *$$
$$\left\{1.0e^{-8}\left[8342.13 + \frac{2406030}{130 - \frac{1}{\lambda^2}} + \frac{15997}{38.9 - \frac{1}{\lambda^2}}\right]\right\}^2 *$$
$$\left\{1.0e^{-8}\left[8342.13 + \frac{2406030}{130 - \frac{1}{\lambda^2}} + \frac{15997}{38.9 - \frac{1}{\lambda^2}}\right] + 2\right\}^2 * \frac{1}{\lambda^{-4}}.$$
$$(11.15)$$

where A is the altitude, P is the current atmospheric pressure, and P_0 is the standard atmospheric pressure of 1013.25 hPa (Kasten and Young 1989).

The ozone optical thickness is acquired from spatial and temporal approximation of daily satellite global measurements of ozone amounts. Preferably, ozone data come from Total Ozone Mapping Spectrometer (TOMS). If TOMS data are unavailable, ozone counts from TIROS Operational Vertical Sounder (TOVS) are used. Finally, if TOVS data are missing, ozone climatology files are applied. The ozone optical thickness is calculated from the ozone amount, Dobson, using a scaling factor $k_{oz}(\lambda)$,

$$t_0(\lambda) = k_{oz}(\lambda) * \frac{Dobson}{1000}, \qquad (11.16)$$

where $k_{oz}(\lambda)$ is expressed below for the following spectral bands (Nicolet at al., 1981):

λ = (315, 340, 380, 400, 415, 440, 443, 490, 500, 560, 610, 660, 670, 675, 862, 870, 936, 1020);

k_{oz} (λ) = (1.35, 0, 0.00025, 0.00065, 0.00084, 0.0034, 0.00375, 0.02227, 0.0328, 0.10437, 0.12212, 0.05434, 0.04492, 0.0414, 0.00375, 0.0036, 0, 0).

REFERENCES

Bass, A.M. and R.J. Paur, 1984: The ultraviolet cross-section of ozone:l. *The measurements, in Atmospheric Ozone*, edited by C.S. Zerefos & A. Ghazi, pp. 606-610, Reidel, Dordrecht.

Bruegge, C.T., J.E. Conel, R. O. Green, J.S. Margolis, R.G. Holm, and G. Toon, 1992: Water vapor column abundance retrievals during FIFE. *J.Geophys. Res.*, **97**(D19), 18759-18768.

Burcholtz, A., 1995: Rayleigh-scattering calculations for the terrestrial atmosphere, *Appl. Opt.,* **34**, 2765-2773.

Dubovik, O.and M.D.King,, 2000: A flexible inversion algorithm for retrieval of aerosol optical properties from Sun and sky radiance measurements, *J. Geophys. Res*., (submitted).

Dubovik, O., A.Smirnov, B.N.Holben, M.D.King, Y.J. Kaufman, T.F.Eck, and I.Slutsker, 2000: Accuracy assessments of aerosol optical properties retrieved from AERONET Sun and sky-radiance measurements, *J. Geophys. Res.*, **105**, 9791-9806.

Edlen, B., 1966: The refractive Index of Air, *Meteorol.*, **2**, 71-80.

Ehsani, A. R., J. A. Reagan, and W. H. Erxleben, 1998: Design and performance analysis of an automated 10-channel solar radiometer instrument, *J. Atmos. Ocean. Tech.*, *15*, (in press).

Forgan, B.W., 1994: General method for calibrating Sun photometers, *Applied Optics*, **33**, 4841-4850.

Fougnie, B., R, Frouin, P. Lecomte, and P-Y. Deschamps, 1999: Reduction of skylight reflection effects in the above-water measurement of marine diffuse reflectance. *Applied Optics*, **38**, 3844-3856.

Gordon, H. R., J. W. Brown, and R. H. Evans, 1988: Exact Rayleigh scattering calculations for use with the Nimbus-7 coastal zone color scanner, *Applied Optics*, **27**, 862-871.

Gordon, H.R., and K. Ding, 1992: Self shading of in-water optical instruments. *Limnol. Oceanogr.,* **37**, 491--500.

Gordon, H. R. and T. Zhang, 1995: Columnar aerosol properties over oceans by combining surface and aircraft measurements: simulations. *Applied Optics*, **34**, 5552 – 5555.

Hansen, J. E., and L. D. Travis, 1974: Light scattering in planetary atmospheres. *Space Sci. Rev.*, **16**, 527-610.

Harrison, L. and J. Michalsky, 1994: Objective algorithms for the retrieval of optical depths from ground-based measurements, *Applied Optics*, **33** ,5126-5132.

Harrison, L., J. Michalsky, and J. Berndt, 1994: Automated multi-filter rotating shadow-band radiometer: an instrument for optical depth and radiation measurements, *Applied Optics,* **33,** 5126-5132.

Holben, B.N., T. F.Eck, I.Slutsker, D.Tanre, J.P.Buis, A.Setzer, E.Vermote, J.A.Reagan, Y.Kaufman, T.Nakajima, F.Lavenu, I.Jankowiak, and A.Smirnov 1998: AERONET - A federated instrument network and data archive for aerosol characterization, *Rem. Sens. Environ.*, **66**, 1-16.

Iqbal., M., 1983: *An introduction to Solar Radiation,* Academic, San Diego, Calif., 390 pp.

Kasten F. and A. T. Young, 1989: Revised optical air mass tables an approximation formula, *Applied Optics,* **28**: 4735-4738.

Kaufman, Y.J., A. Gitelson, A. Karnieli, E. Ganor, R.S. Fraser, T. Nakajima, S. Mattoo, B.N. Holben, 1994: 'Size Distribution and Phase Function of Aerosol Particles Retrieved from

Sky Brightness Measurements', *J. Geophys. Res.,* **99**, 10341-10356.

Kneizys, F.X., E.P. Shettle, L.W. Abreu, J.H. Chetwynd, G.P. Anderson, W.O. Gallery, J.E.A. Selby, and S.A. Clough, 1988: Users Guide to LOWTRAN 7, AFGL-TR-88-0177, (NTIS AD A206773), Air Force Geophysics Laboratory, Hanscom Air Force Base, Massachusetts.

Komhyr, W. D., R. D. Grass, and R. K. Leonard, 1989: Dobson Spectrophotometer 83: a standard for total ozone measurements, 1962-1987, *J. Geophys. Res.*, **94,** 9847-9861.

Liu, Y. and K. J. Voss, 1997: Polarized radiance distribution measurements of skylight: II. experiment and data. *Applied Optics*, **36**,8753 - 8764.

London, J., R. D. Bojkov, S. Oltmans, and J. I. Kelley, 1976: Atlas of the global distribution of total ozone July 1957 - June 1967, *NCAR Technical Note 133+STR*, National Center for Atmospheric Research, Boulder, Colorado, 276 pp.

Michalsky, J. J., 1988: The astronomical almanac's algorithm for approximate solar position (1950 - 2050), *Solar Energy*, **40**, 227 - 235.

Morys, M., F.M. Mims III, and S.E. Anderson, 1998: Design, calibration and performance of MICROTOPS II hand-held ozonometer.

Nakajima, T., M. Tanaka and T. Yamauchi, 1983: Retrieval of the optical properties of aerosols from aureole and extinction data. *Applied Optics*, **22**, 2951-2959.

Nakajima, T., G. Tonna, R. Rao, P. Boi, Y. Kaufman, and B. Holben, 1996: Use of sky brightness measurements from ground for remote sensing of particulate polydispersions, *Applied Optics*, **35**, 2672-2686.

Nicolet M., 1981: The solar spectral irradiance and its action in the atmospheric photodissociation processes, Planet. *Space Sci.*, **29**, 951-974.

Penndorf, R., 1957: Tables of the Refractive Index for Standard Air and the Rayleigh Scattering Coefficient for the Spectral Region Between 0.2 and 20.0 Microns and their Application to Atmospheric Opt., *J. Opt. Soc. Am.*, **47**, 176-182.

Porter, J. N., M. Miller, C. Pietras, and C. Motell, 2000: Ship-based sun photometer measurements using MicroTops sun photometers*, J. Ocean. Atmos. Tech*. (in press).

Reagan, J.A., K.J. Thome, and B.M. Herman, 1992: A simple instrument and technique for measuring columnar water vapor via Near-IR differential solar transmission measurements. *IEEE Trans. Geosci. Remote Sensing*, **30**, 825-831.

Reynolds, R.M., M.A. Miller, and M.J. Bartholomew, 2000: Design, Operation, and Calibration of a Shipboard Fast-Rotating Shadow-band Spectral Radiometer, *Jour. Atmos. Ocean. Tech*., (accepted).

Ritter, J. M. and K. J. Voss, 2000: A new instrument to measure the solar aureole from an unstable platform. J. Atmos. Ocean. Tech., in press.

Schmid, B., C. Matzler, A. Heimo and N. Kampfer, 1997: Retrieval of Optical Depth and Particle Size Distribution of Tropospheric and Stratospheric Aerosols by Means of Sun Photometry, *IEEE Trans. on Geosci. and Rem Sens*., **15**, 172-182.

Schwindling, M., P.-Y. Deschamps, and R. Frouin. 1998: Verification of aerosol models for satellite ocean color remote sensing. *J. Geophys. Res.,* 24,919-24,935.

Shaw, G. E., 1983: Sun Photometry, *Bull. Amer. Meteor. Soc.*, **64**, 4-11.

Shiobara, M., T. Hayasaka, T. Nakajima and M. Tanaka, 1991: Aerosol monitoring using a scanning spectral radiometer in Sendai, Japan. *J. Meteorol. Soc. of Japan*, **60**, 57-70.

Smirnov, A., B.N.Holben, T.F.Eck, O.Dubovik, I.Slutsker, 2000: Cloud screening and quality control algorithms for the AERONET data base. *Rem. Sens. Environ*., (accepted).

Tanré, D., C. Devaux, M. Herman and R. Santer, 1988: Radiative properties of desert aerosols by optical ground-based measurements at solar wavelengths. *J. Geophys. Res.*, **93**, 14223-14231.

Tanré, D., C. Deroo, P. Duhaut, M. Herman, J.-J. Morcrette, J. Perbos, and P.-Y. Deschamps,

1990: Description of a computer code to simulate the signal in the solar spectrum: the 5S code. *Int. J. Remote Sensing*, **11**, 659-668.

Young, A.T., 1980: Revised Depolarization Corrections for Atmospheric Extinction, *Applied Optics*, **19**, 3427-3428.

Vigroux, E., 1953: Contribution a l'etude experimentale de l'absorption de l'oxone, *Annales de Phys*., **8**, 709.

Volz, F.E., 1959: Photometer mit Selen-photoelement zurspektralen Messung der Sonnenstrahlung und zer Bestimmung der Wallenlangenabhangigkeit der Dunsttrubung. *Arch. Meteor. Geophys Bioklim.* **B10**, 100-131.

Voss, K. J. and Y. Liu, 1997: Polarized radiance distribution measurements of skylight: I. system description and characterization. *Applied Optics*, **36**, 6083-6094.

Voss, K. J., 1989: Electro-optic camera system for measurement of the underwater radiance distribution. *Optical Engineering*, **28**, 241-247.

Voss, K. J. and G. Zibordi, 1989: Radiometric and geometric calibration of a spectral electro-optic "fisheye" camera radiance distribution system. *J. Atmos. Ocean. Tech*.., **6**, 652-662.

Wang, M. and H. R. Gordon, 1993: Retrieval of the columnar aerosol phase function and single-scattering albedo from sky radiance over the ocean: simulations. *Applied Optics*, **32**,4598 – 4609.

Zhang, T. and H. R. Gordon, 1997a: Columnar aerosol properties over oceans by combining surface and aircraft measurements: sensitivity analysis. *Applied Optics***, 36**, 2650 – 2662.

Zhang, T. and H. R. Gordon, 1997b: Retrieval of elements of the columnar aerosol scattering phase matrix from polarized sky radiance over the ocean: simulations. *Applied Optics,* **36**,7948 – 7959.

Chapter 12

Determination of spectral absorption coefficients of particles, dissolved material and phytoplankton for discrete water samples

[1]B. Greg Mitchell, [2]Annick Bricaud, [3]Kendall Carder, [4]Joan Cleveland, [5]Giovanni Ferrari, [6]Rick Gould, [1]Mati Kahru, [7]Motoaki Kishino, [8]Helmut Maske, [9]Tiffany Moisan, [10]Lisa Moore,[11]Norman Nelson, [12]Dave Phinney, [13]Rick Reynolds, [14]Heidi Sosik, [1]Dariusz Stramski, [5]Stelvio Tassan, [15]Charles Trees, [16]Alan Weidemann, [1]John Wieland and [17]Anthony Vodacek.

[1]*Scripps Institution of Oceanography, Universisity of California San Diego, California*
[2]*Laboratoire de Physique et Chimie Marines, France*
[3]*University of South Florida, Florida*
[4]*Office of Naval Research, Washington , District of Columbia*
[5]*CEC Joint Research Center, Institute for Remote Sensing Applications, Ispra, Italy*
[6]*Naval Research Lab - Stennis Space Center, Mississippi*
[7]*Institute of Physical and Chemical Research, Japan*
[8]*CICESE, Ensenada, Mexico*
[9]*NASA/GSFC Wallops Flight Facility,Virginia*
[10]*Massachusetts Institute of Technology, Massachusetts*
[11]*Bermuda Biological Station, Bermuda*
[12]*Bigelow Laboratory for Ocean Sciences, Maine*
[13]*University of Washington, Washington*
[14]*Woods Hole Oceanographic Institute , Massachussets*
[15]*Center for Hydro-Optics & Remote Sensing, San Diego State University, California*
[16]*Naval Research Lab - Stennis Space Center, Mississippi*
[17]*Carlson Center for Imaging, Rochester Institution of Technology, New York*

12.1 INTRODUCTION

The spectral absorption coefficient is one of the inherent optical properties that influence the reflectance of aquatic systems. Therefore, knowledge of total absorption and its component parts is required to improve our understanding of variability in spectral reflectance estimated with ocean color sensors. Protocols for estimating the volume absorption coefficients for particles, phytoplankton, photosynthetic pigments, de-pigmented particles and soluble material are described. Methods are based on prior literature and results from NASA-sponsored workshops on methodological protocols. Issues, assumptions, and alternative methods are reviewed and recommendations for future research are made. Workshop participants are listed in Table 1.

The absorption coefficient at any point within a natural water body is an inherent property that can be described in terms of the additive contribution of its components:

$$a(\lambda) = a_w(\lambda) + a_p(\lambda) + a_g(\lambda)$$

where w, p, and g refer to water, particles, and soluble components. The particle component may be further decomposed:

$$a_p(\lambda) = a_f(\lambda) + a_d(\lambda) + a_i(\lambda)$$

where f, d and i refer to phytoplankton, de-pigmented and inorganic components. Depth (z) dependence of the coefficients are omitted for brevity. Absorption methods are described for operational estimates of these fractions.

Table 1.   NASA-sponsored workshops participants

Name	Affiliation	Instrument Brought
Scripps Institution of Oceanography Workshop		
Name	Affiliation	Instrument Brought
Lore Ayoub	Lehigh University	
Annick Bricaud	Laboratoire de Physique et Chimie Marines	
Joan Cleveland	Office of Naval Research	HP Diode Array
Giovanni Ferrari	CEC JRC, Institute for Remote Sensing Applications	
Piotr Flatau	University of California San Diego	
Jim Ivey	Naval Research Lab - Stennis Space Center	
Mati Kahru	University of California San Diego	
Motoaki Kishino	Photosynthesis Research Laboratory	
Helmut Maske	CICESE/Ecologia	Elyptica
Greg Mitchell	University of California San Diego	Varian Cary 1 with integrating sphere
Tiffany Moisan	University of California at San Diego	Perkin Elmer λ6 with integrating sphere
Lisa Moore	MIT School of Engineering	
John Morrow	Biospherical Instruments	
Norm Nelson	Bermuda Biological Station for Research	
Jennifer Patch	University of South Florida	Custom built spectral radiometer
Scott Pegau	Oregon State University	AC-9
Rick Reynolds	University of California San Diego	
Heidi Sosik	Woods Hole Oceanographic Institute	Perkin Elmer λ18 with integrating
Dariusz Stramski	University of California San Diego	Kontron Uvikon 860 with integrating sphere
Stelvio Tassan	CEC JRC, Institute for Remote Sensing Applications	
Tony Vodacek	Rochester Institute of Technology	
AlanWeidemann	Naval Research Lab - Stennis Space Center	
John Wieland	University of California at San Diego	
Ron Zaneveld	Oregon State University	
Bigelow Absorption Workshop		
Name	Affiliation	
Rick Gould	Naval Research Lab - Stennis Space Center	ASD Field Spec
Jim Hopkins	Bigelow Laboratory	
Phil Hovey	NOAA, NESDIS	HP Diode Array
Dave Phinney	Bigelow Laboratory	Bausch & Lomb Dual Beam Spec
Charles Trees	San Diego State University/CHORS	Perkin Elmer Lambda 3b
Sara Woodman	Bigelow Laboratory	

To interpret aquatic spectral reflectance and better understand photochemical and photobiological processes in natural waters, it is essential to quantify the contributions of the total absorption coefficients in the ultraviolet (UV) and visible region of the spectrum. The material presented here is based on the evolution of methods starting with articles by Kalle (1938) and Yentsch (1962) on the absorption by soluble and particulate material in the oceans. Laboratory measurements and data analysis protocols are described for separating the total spectral absorption coefficient, $a(\lambda)$, into its components by spectrophotometric measurements on processed samples that have been prepared from filtration of discrete water samples. All filtration methods define operational fractions with assumptions depending on the methodology employed. There has been considerable research to develop robust protocols that provide the most accurate quantitative estimates of various fractions. NASA-sponsored workshops were held at Scripps Institution of Oceanography and Bigelow Laboratory for Ocean Sciences to review absorption protocols, evaluate instrumentation, and define areas of consensus as well as areas of uncertainty that warrant further research. A summary of participants and the instrumentation that was evaluated is provided in Table 1. Recommendations provided here are based on results from the workshops and published literature. In general, recommendations are provided for protocols that have gained broad acceptance by diverse researchers. We also discuss alternative methods, assumptions for various methods, and issues that lead to uncertainties that should be the focus of future research.

12.2 BACKGROUND

The most widely used approach to estimate absorption by particulate matter involves analysis of the particles concentrated on filters (Yentsch, 1957). Absorption of phytoplankton suspensions determined using procedures that capture most of the forward scattered light (Shibata, 1958) can be related to the absorption measured on the filters to make quantitative corrections for the pathlength amplification effect (β) caused by the highly scattering filter medium (Duntley, 1942; Butler, 1962). Kiefer and SooHoo (1982) reported a constant to scale the red peak of chlorophyll absorption for GF/C filter measurements of natural particles to the diffuse absorption coefficients determined on suspensions by Kiefer et al. (1979).
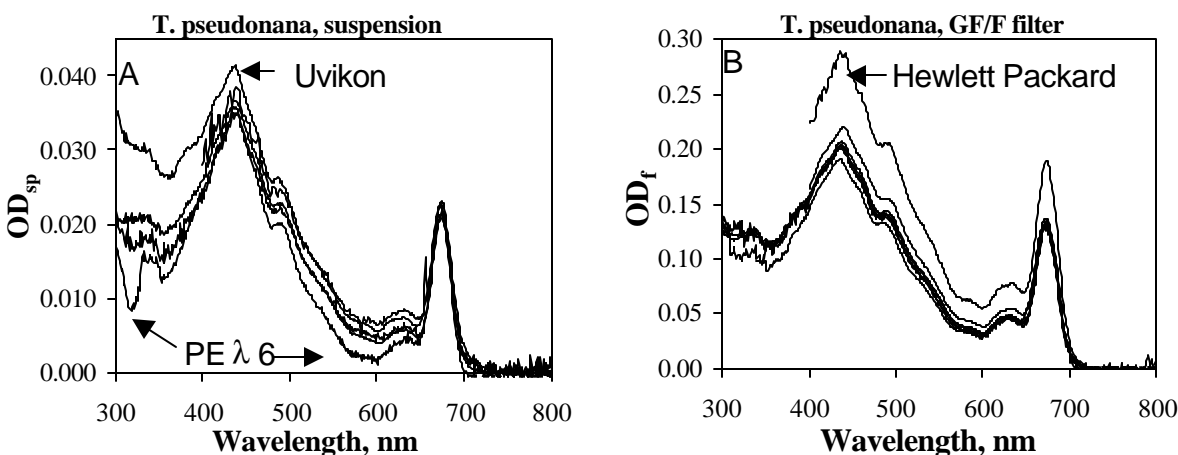

Figure 1. Instrument comparison of optical density (OD) spectra for a culture studied during the Scripps workshop. A. $OD_{sp}(\lambda)$ 300-800 nm for suspensions of *Thalasiosira pseudonana* cultures determined with different spectrophotometers. All units had integrating sphere attachments. Performance in the visible is in good agreement for all instruments except the Perkin Elmer Lambda 6, which had baseline stability problems during the workshop. UV region absorbance is in poor agreement for unknown reasons. The HP unit was not capable of performing below 400 nm. B. $OD_f(\lambda)$ 300-800 nm for *T. pseudonana* cultures on Whatman GF/F™ glass fiber filters determined with various optical geometries. The mean value from 790-800 nm was subtracted as a null value for all spectra. $OD_f(\lambda)$ in the UV agreed better between instruments compared to $OD_{sp}(\lambda)$ determined with integrating sphere systems.

The diffuse absorption coefficient is double the value of the volume absorption coefficient of interest here. Mitchell and Kiefer (1984, 1988a) made direct estimates of volume absorption coefficients for phytoplankton suspensions and absorbance on glass fiber filters with the same particles to develop empirical equations that relate the amplification factor to the glass fiber sample optical density. This procedure is the basis of most methods for determining particle absorption on water samples. Example data for one culture studied at the Scripps workshop are shown in Figure 1.

Field applications of these quantitative estimates of a_p were reported by Mitchell and Kiefer (1988b) and Bricaud and Stramski (1990). More detailed empirical results to correct for path length amplification were reported by Mitchell (1990) for various filter types and diverse cultures ranging from 2 μm coccoid cyanobacteria to 10-20 μm diatoms, chrysophytes and dinoflagellates. Cleveland and Weidemann (1993) and Tassan and Ferrari (1995) found the empirical relationships of Mitchell (1990) were consistent with similar types of phytoplankton, but Moore et al. (1995) reported large differences in the amplification factor for *Synechococcus sp*. (WH8103) and *Prochlorococcus marinus* that were about half the size of the smallest cells studied by Mitchell (1990; see also Table 2). Similar results were obtained by Allali et al. (1997) for natural populations of the Equatorial Pacific dominated by picoplankton. For samples with substantial turbidity due to inorganic matter (coastal, shelf, coccolithophore blooms), artifacts in the estimates can be caused by the large scattering load of the inorganic material; methods to correct for this have been described by Tassan and Ferrari (1995a, 1995b).

Separation of the particle fraction into phytoplankton and other components is of considerable ecological and biogeochemical interest. Early efforts to separate absorbing components for natural particles included treatment with organic solvents, UV radiation, and potassium permanganate (references can be found in Shifrin, 1988, and Bricaud and Stramski, 1990). The most widely used chemical method is based on methanol extraction (Kishino et al. 1985, 1986). A recent method consists of bleaching the phytoplankton pigments by sodium hypochlorite (Tassan and Ferrari, 1995; Ferrari and Tassan, 1999). Spectral fluorescence methods to estimate the fraction of

photosynthetically active absorption, if separate total particulate absorption has been determined, have been reported by Sosik and Mitchell, (1995).

Soluble absorption observations were described by Bricaud et al. (1981) for diverse ocean environments, including oligotrophic and eutrophic regions. Other field reports can be found in the references listed in more recent articles (Carder et al., 1989a, 1989b; Blough et al., 1993; Vodacek et al., 1996; Hoge et al., 1993; Nelson et al., 1998; D'Sa et al., 1999). Estimating the quantitative absorption of soluble material is rather direct, but has limits due to the very small signal for short pathlengths routinely employed (usually 10 cm). A difficult issue is quality control of reference water and specification of an appropriate blank. A summary of average blanks from several cruises is shown in Figure 2.
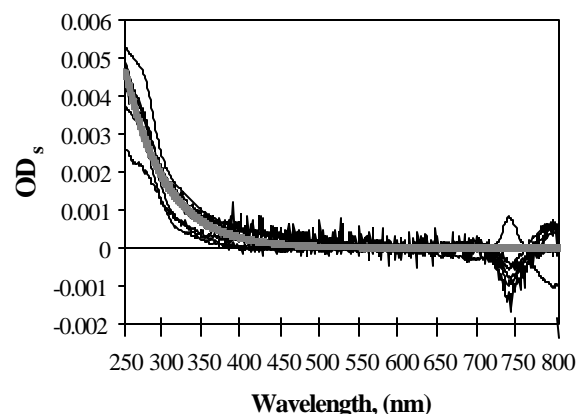
Figure 2. $OD_s(\lambda)$ 250-800 nm spectra for a 0.1m optical path of blank samples prepared by filtering purified water as though it were a sample. Measurements were determined with either Varian Cary 1 or Cary 100 in dual beam mode referenced to purified water. Mean blanks for individual cruises (typically 15-30 total blanks per cruise) are shown as thin lines; the bold line is an exponential fit to the mean for all cruises, where individual cruises were weighted by the relative number of blanks determined. Data collected by Scripps Photobiology Group. For one cruise the instrument baseline noise was > ± 0.0005 which was out of specification for these units. Accurate estimates of $a_g(\lambda)$ require instrumentation with very small baseline noise.

We report recommendations for the determination of absorption coefficients for particulate and soluble matter as defined by operational definitions specified by preparations of water samples. Results of the methods, including separation of particulate and soluble material by filtration methods, partitioning of total particulate absorption into phytoplankton and de-pigmented (detritus), and corrections for various artifacts including scattering and pathlength amplification, will depend on the protocols used for preparation and the methods used for data processing. Recommendations are made based on widely accepted methods and processing procedures. NASA-sponsored workshops have confirmed various aspects of previously reported methods. Significant uncertainty still exists regarding the ideal methods for achieving the most accurate results for various absorption components. Therefore a review of important uncertainties, alternative methods, and recommendations for further research are also included in the Workshop Summary section of this report.

12.3 SAMPLE ACQUISITION

Water samples should be taken using Niskin (or similar) bottles at the site of, and simultaneously with, the surface in-water optical measurements, and at depth increments sufficient to resolve variability within at least the top optical depth. When possible, samples should be acquired at several depths distributed throughout the upper 300m of the water column (or in turbid water, up to seven diffuse attenuation depths, $\ln(E(0)/E(z))=7$), to provide a basis for relating the spectroscopic measurements of absorption to *in situ* profile measurements. Samples should be drawn immediately from the *in situ* sampling bottles into clean sampling bottles using clean Tygon tubing. If Niskin bottles will not be sampled immediately, precautions must be taken to ensure large particles that settle are resuspended. This can be done by transferring all water from the Niskin to a bottle or carboy larger than the total volume of the Niskin so that the entire water sample can be mixed (invert bottle numerous times to mix by turbulence), or by draining a small amount of water from the Niskin and manually inverting the entire Niskin prior to sub-sampling. Sample bottles should be kept cool (ideally near *in situ* temperatures), and dark prior to sample preparations. Preparations should be completed as soon as possible after sampling, but no later than several hours after the vertical profile was acquired.

12.4 PARTICLE ABSORPTION SAMPLE PREPARATION ANALYSIS

For quantitative estimates of particle absorption coefficients, water samples are filtered and absorbance spectra of the filter (OD_f) are estimated for the retained particles using a laboratory spectrophotometer. After measurement, the sample filters are extracted or bleached to remove phytoplankton pigments (Kishino et al., 1985; Tassan and Ferrari 1995a) and the OD_f of the filter is determined again in the spectrophotometer. This yields the de-pigmented absorption component sometimes referred to as detritus or tripton. Depending on the method, this fraction also includes bleached cells, and phycobilipigments which are not extractable in methanol. The raw *OD* data are used to calculate total particulate and de-pigmented absorption coefficients $(a_p \text{ and } a_d)$. The absorption coefficient of phytoplankton (a_f) is then estimated as the difference $a_p - a_d$.

The Whatman GF/F™ filter (which is binder-free and combustible, with a nominal pore size of 0.7 μm) is recommended for particle absorption sampling. This type of filter is also recommended by (JGOFS 1991) for various particulate and pigment analyses. Some authors have reported that particulate material less than 0.7 μm in size will not be retained by the GF/F filter, and that this fraction may contain up to 10-15% of the phytoplankton biomass as measured by chlorophyll concentration. Chavez et al. (1995), however, found no statistical difference between GF/F and 0.2 μm filters for chlorophyll and productivity measurements. Vacuum pressures below ~5 inches of mercury, i.e., ~120 mm Hg, are recommended to reduce the chances of particle breakage. The absorption of the particle fraction with 0.22-0.7 μm diameter can be selectively determined by measuring the GF/F filtrate deposited on a 0.22 μm Millipore cellulose acetate membrane filter (Ferrari and Tassan, 1996).

Filtration volume should be adjusted to keep the samples in the optical density range that is ideal for the pathlength amplification corrections. Glass fiber, cellulose acetate, and other strongly diffusing filters have large scattering coefficients, which increases the optical path length of photons in the measurement beam. Mitchell (1990) studied the effects of variable optical density on the performance of algorithms and recommended that optical densities be in the range 0.05-0.4 for best

performance of empirical algorithms. The optical transparency of the GF/F filter relative to air decreases significantly below 380 nm but many spectrophotometers can still make determinations to 300 nm with these filters. Optical density spectra of the sample filters should be measured as soon as possible, because pigment decomposition may occur (Stramski 1990). If filters must be stored, place the unfolded filters into flat tissue containers designed for liquid nitrogen storage. Liquid nitrogen storage is recommended because alternative freezing methods were shown to have more artifacts in comparison tests (Sosik, 1999). The transparency of the filter also depends on hydration, so all samples must be fully - but not excessively - hydrated for proper performance of analytical procedures and accurate optical corrections.

Sample Filter Preparation

- Collect water samples, and maintain in the dark at or near *in situ* water temperature.
- For each sample, place a GF/F filter onto the filtration rig. Also prepare two blank GF/F filters by soaking them in ~25 ml 0.2 µm filtered water while mounted on the filtration funnel (with valves closed) during the sample filtration.
- Filter samples on GF/F filters under low vacuum (~5 in. Hg) in dim light.
- Filter sufficient volume for proper performance of correction algorithms. For typical field samples collected in the upper 100-150 m appropriate filtration volumes are typically in the range 0.5 – 5 L, depending on abundance of particles. A reasonable volume to filter (Vf, liters) can be estimated if Chl *a* concentration (Chl, µg/l) is known (Vf = 0.4 [Chl]$^{-0.7}$).
- Do not let the preparations run dry during filtration. Turn off the vacuum to each sample as it completes filtering. Immediately place samples on a drop of 0.2 µm filtered water in the appropriate container depending on how they will be stored.
- Record the filter and filtration funnel type, diameter of the area on the filter with the concentrated particles, and volume filtered.
- Run absorption spectra as soon as possible.

Sample Filter Storage

- If samples will be analyzed immediately, store each filter in a labeled petri dish (e.g. Gelman™) snap-top dishes. Ensure proper

hydration of the sample by placing the GF/F filter on a small drop of 0.2 µm filtered seawater. Store dark and refrigerated (~4 deg. C) until analysis.

- If samples will be run more than 24 hours after collection sample filters should be prepared for liquid nitrogen storage. Storage should be done in containers that allow the filter to remain flat, and are specifically designed for liquid nitrogen (e.g. Fisher Histoprep™ tissue capsules). One pair of blank filters for each sample date should be prepared for the subsequent analysis. Samples on liquid nitrogen may be stored for extended periods but analysis as soon as possible is always preferred.
- Non-pressurized liquid nitrogen sample dewars generally retain liquid nitrogen for 2-4 weeks. Pressurized liquid nitrogen dewars can be rented at low cost for extended cruises (4-5 weeks) to keep the sample dewars full. Care must be taken at sea and in return shipping to ensure that the samples are properly frozen. Samples should be shipped in liquid nitrogen dry shippers which can last 2-3 weeks if properly charged and in good condition.
- Air transport of liquid nitrogen dry shippers is approved by International Air Transportation Agreement (IATA 41st Edition Section A800; US Federal Aviation Administration Dangerous Good Bulletin DGAB-98-03; August 25, 1998) but many issues have been reported in clearing customs, or in transport of liquid nitrogen dry shippers via commercial airfreight or as checked baggage. The investigator should contact the carriers in advance and provide the IATA approval and FAA bulletin of liquid nitrogen dry shipper information. If the dry shipper is to be transported as checked baggage, advanced coordination with the airline is strongly recommended to avoid confiscation of samples and delays in return shipment. As checked baggage or freight, the IATA memo, DOT memo, and manufacturer's certificate should be affixed to the dry shipper to minimize potential delays.
- Temporary storage on dry ice can be considered during transport. But maximum duration of dry ice in insulated shipping boxes is several days, so liquid nitrogen dry shippers are recommended.

Sample Filter Preparation for De-pigmented Particle Absorption

After preparing an a_p sample filter and determining OD_f on the spectrophotometer using the standard procedures, the sample should be processed to prepare a de-pigmented sample for determination of a_d.

Methanol Extraction method

- Place the sample and blank filters back onto the filtration system. Treat blank filters exactly as if they were sample filters.
- Add 5-10 ml of 100% methanol to each filter by gently pouring it down the sides of the filter funnel to minimize resuspension of the sample particles. Let stand for 1 minute.
- Filter methanol through, close valves, and add 10-15 ml methanol. Allow sample to stand in methanol for approximately 1 hour. Do not allow the filter to go dry during the extraction period. Time of extraction will vary depending on filter load and species composition on the filter. Place aluminum foil over the filtration cups during extraction to minimize contamination.
- After extraction, turn on the vacuum and draw the methanol through the filter. Rinse the sides of the filter tower twice with small amounts of methanol. Last, rinse the sides of the filter tower three times with ~20 ml of 0.2 μm filtered seawater. Also rinse blanks with filtered seawater after methanol extraction to minimize filter dehydration problems in analysis.
- If the 675 nm absorption peak of the sample is absent, samples can be considered fully extracted.
- Successive short extractions of 10 minutes can sometimes improve the pigment extraction.
- Phycobilins and some eukaryotic pigments will not be extracted by methanol.

Sodium Hypochlorite oxidation method

- *Prepare NaClO solution:*
  For freshwater samples: 0.1% active chlorine in Milli-Q water.
  For marine samples: 0.1% active chlorine in Milli-Q water containing 60 gl^1 Na_2SO_4, to match osmotic pressure of sample cells.
- Determine the solution amount needed to bleach the sample by the empirical expression:

ml of solution (0.1% active chlorine) = 3 OD_f (440).

- Place the sample, particle side up, on the filtration system (closed valves).
- Gently pour the solution down the sides of the filter funnel.
- Let the solution act for 5-10 min time, adding solution to compensate loss through the filter.
- Cover cup with aluminum foil to prevent contamination.
- Rinse the sample by gentle filtration of 50 ml of water (either fresh or salt, depending on sample source).
- Disappearance of the 675 nm peak in the bleached sample, and evidence of concave shape of the OD spectrum about 440 nm, can be considered evidence of complete pigment bleaching.
- If residual pigment absorption remains, repeat NaClO oxidation treatment, as indicated above.
- Treat blank filters in the same way.

Determination of spectral optical density of sample filters

After preparation, the sample filters are scanned in a spectrophotometer. The following procedure is written generically for a dual beam spectrophotometer. Single beam units and a variety of custom-built instruments may be used provided the investigator will invest the extra effort for carefully characterizing the baseline and spectral performance of the instrumentation. Regardless of instrument configuration, care must be taken with respect to maintaining proper knowledge of instrumentation baseline, noise, spectral range, and other characteristics. Due to both large attenuance of sample filters and instrument limitations including dynamic range and spectral performance, there is a wide range of performance between different instruments. Careful selection of instrumentation by the investigator is very important for achieving satisfactory results. Performance of a wide variety of commercial and custom units have been compared and results are discussed in the Workshop Summary section below. In general, research-quality dual beam spectrophotometers had superior performance to various alternative instruments.

With a dual beam spectrophotometer, two reference filter blanks saturated with filtered seawater are used to measure the reference spectrum, and one is left in the reference beam during sample measurements. Most modern spectrophotometers automatically store the

instrument's reference spectrum and recorded sample spectra are automatically corrected. A new instrument reference baseline scan should be measured each time the spectrophotometer is powered and when its configuration has been changed. The baseline should be checked regularly (every 1-2 hours) during extended periods of analysis. Frequency of baseline verification will depend on the performance and stability of individual instrument and should be determined by the investigator prior to executing routine work. Baseline drift, and changes in sorting filters or lamp source can be causes of sample anomalies. Wavelength accuracy should be checked during the analyses (see Spectrophotometer considerations section below).

Analysis Procedure

- Warm up spectrophotometer 30 minutes.
- If using frozen samples, remove filters from container and place in petri dishes on filtered water to ensure hydration. Allow to thaw at least ~5 min; store refrigerated until analysis.
- An instrument-specific sample-mounting device is recommended to hold filters against a quartz glass mounting plate. These mounts should be secure when placed in the sample compartment and hold the sample perpendicular to the illumination beam. In general, these mounts must be fabricated specifically for each different instrument.
- Clean the quartz faceplates of the mounting device with purified water and detergent if needed. Rinse with purified water and ethanol. Dry thoroughly with lint-free laboratory tissues.
- Set the appropriate instrument parameters.
- Mount two pre-soaked and water saturated blank filters (one for sample beam, one for reference beam).
- To test for proper filter hydration, confirm that there is a drop of FSW left on the mounting plate when filter is lifted. With filter on the mounting plate there should be a slight sheen on the top surface of the filter, and a very narrow (~ 1 mm) border of water around the edges of the filter on the quartz plate. Be careful not to have too much water, as the sample may wash away.
- No bubbles should be between the filter and the glass on the sample holder. Test by examining the back of the filter on the mounting plate. There should be a uniform layer of water between the filter and quartz mounting plate. Bubbles will be obvious. If they are present, pick up the filter with forceps, and place back on the plate with a slight dragging of filter across a filtered water drop. Check again. Repeat until no bubbles are present. Adjust amount of filtered water as necessary.
- Mounts that allow both sides of the filter to be in air are an alternative to eliminate the issue of bubbles, but sample hydration is more difficult to maintain.
- Run instrument baseline correction using the two blanks. For most commercial units, this baseline will be automatically subtracted from subsequent scans. Immediately after baseline correction is finished and without touching the filters, run the two blanks as a sample scan to confirm baseline performance within acceptable tolerance over the spectral range of determination. This spectrum should be flat spectrally with baseline noise less than ± 0.005 OD. Save this scan for reference and confirmation of instrument performance. If a spectrally flat baseline cannot be achieved over the spectral range of interest, the stored baseline must be subtracted from subsequent estimates of sample filter $OD_f(\lambda)$. If using a single beam instrument, or instruments run in the single beam mode, it is possible to run a baseline with a blank filter against air; in this case the sample filter will then be run against air, which will avoid the necessity of rehydrating the blank reference filter regularly.
- Remove the blank filter from the quartz glass sample mount, and replace it with a sample filter ensuring proper hydration of sample. Run sample spectrum, save the digital file and record all relevant information.
- The blank reference filter will dry out over time, and must be hydrated regularly. If absorption signal deviates significantly (> $\pm$ 0.02 absorbance) from zero in the infrared (750-800 nm), this often indicates a dry reference or sample filter. If using a quartz plate, check the reference filter after every 5-6 scans, and hydrate as needed. If mounted in air, hydrate blank every scan.
- After determination of particle optical density, samples should be de-pigmented and de-pigmented optical density should be determined as described above.
- Note that methanol-extracted samples and blank filters tend to dry out quickly if the methanol is not thoroughly rinsed from the filters prior to analysis. NaClO oxidized

sample and reference filters should be thoroughly rinsed to extend the spectral range below 400 nm.

12.5 SOLUBLE ABSORPTION SAMPLE PREPARATION AND ANALYSIS

This technique measures the spectral absorption by soluble material (a_g) dissolved in seawater. Seawater samples are collected and particulate material is removed by filtration. The absorption of the filtrate is measured, relative to purified water, using a spectrophotometer. All equipment utilized to prepare soluble absorption samples should minimize contamination by organic or colored material and should protect samples from photo-degradation. Plastic or glass filtration apparatus may be used but the units should have mesh filter supports (e.g. stainless steel or plastic) and not ground glass frits. Glass frits tend to clog over time and change particle retention efficiencies of the units. Amber-colored borosilicate glass bottles are preferred for filtrate collection because they screen ambient light. Prior to each experiment, all filtration and storage bottles should be thoroughly cleaned. For preparations, 0.2 μm membrane filters, (e.g., Nuclepore™ polycarbonate) are recommended. Glass fiber filters are not recommended because of large contamination when tested with purified water. Membrane filters should be pre-soaked in 10% HCl and rinsed copiously with pure water and a small aliquot of sample before preparation. An alternate method for preparing samples allows multiple use of Sterivex sealed filtration cartridges. Use of these cartridges has been described by D'Sa et al. (1999) who used the method to prepare samples delivered to a capillary light guide spectrophotometer for estimating absorption by soluble material. The procedure provides high sensitivity and can be adapted to continuous flow determinations. This new method may prove useful in various applications but has not been applied extensively at this time. Evaluation of the performance of the Sterivex cartridges for sample preparation and light guides for spectroscopy warrant further research but are not discussed further in this report.

Preparation procedures for soluble samples can introduce artifacts so a careful evaluation of the blank is essential. Spectral blanks for soluble absorption must be determined and subtracted from sample spectra. Blanks determined on numerous cruises are presented in Figure 2. For the blanks in Figure 2, the reference water was delivered directly to a pre-cleaned 10 cm quartz cuvette and the baseline was determined from 250-800 nm with Varian Cary 1 or Cary 100 spectrophotometers. The blank was prepared by filtering freshly purified water (Alpha-Q, Milli-Q or Nanopure) with the identical protocol used to prepare samples. The mean value of raw optical density from 590-600 nm was subtracted from the full spectrum as a null absorption correction.

Despite careful consideration of clean techniques, pre-rinse of filters, and sample handling, the purified water blank exhibits significant deviation from the reference below 450 nm. For all cruises, the instrument noise of samples was less than ± 0.0005 optical density units, except for one cruise where the instrument performance was out of specification for baseline noise. Temperature differences between the blank and reference samples lead to the spectral anomalies between 650-800 nm and must be carefully considered in the selection of a null point for soluble absorption determinations. Both reference and sample cells must be maintained at the same temperature if accurate estimates from 650-850 nm are required. For weakly absorbing oceanic samples soluble absorption can be negligible greater than 600 nm and thus 600 nm may be considered a null point. For more strongly absorbing samples the null point should be set at a longer wavelengths and careful consideration of temperature effects in specifying the null point should be made (See Figure 2). These issues are discussed in more detail in the Absorption Workshop Summary below.

Pre-cruise preparations

- Sample bottles (Qorpak™) used to collect sample filtrate need to be thoroughly cleaned in advance to remove any potential organic contaminants. Sequential soaks and rinses in mild detergent, purified water, 10% HCl with final copious rinse in purified water is recommended.
- Rinse plastic caps with 10% HCl, twice with Alpha-Q, then dry at 70^oC for 4-6 hrs.
- Combust bottles with aluminum foil covers at 450^oC for 4-6 hours.
- Fill clean, combusted bottles with fresh Alpha-Q (directly from tap).
- Assemble the combusted bottles and clean caps. Store in the dark.
- These standards are used during cruises to

evaluate the quality of freshly prepared purified water.

Soluble Absorption Sample Preparation, Storage and Analysis

- Wash hands with soap and water to avoid contaminating the samples.
- Use 0.2 μm polycarbonate filters (e.g. Nuclepore or equivalent). Do not use irgalan black stained (low fluorescence background) polycarbonate filters for this preparation. Other membrane filters or Sterivex cartridges may be used, but the investigator must then test for any contamination by the filter and ensure that no artifacts are introduced by the filter type.
- Filtration systems with individual control of vacuum for each sample and direct filtration to clean bottles should be used. See Figure 3 for a diagram of a custom-made soluble absorption filtration assembly that achieves these goals.
- Pre-soak filters for at least 15 minutes in 10% HCl. Rinse filters thoroughly with purified water. Mount filters on funnel and filter ~100 mls of purified water through filter into sample bottles. Shake bottles, rinse inside of caps with bottle rinse, discard water (pour discard over inside of caps to rinse them). Cover filtration cups with aluminum foil until ready to filter sample.
- Collect ~200 ml of seawater sample. For the blank, use purified water drawn directly into 2 clean sample bottle.
- Filter ~75 ml of sample and 1 blank directly into clean bottles at low vacuum (<5 in. Hg). Shake bottles, discard water. Do not allow filters to go dry during sample rinsing.
- Filter ~ 75 ml of sample into bottles. For the blank, filter ~75 ml of purified water. When finished, cap bottles and store until analysis.
- For samples that will be run within 4 hours, store in the dark at room temperature.
- For samples that will be run 4-24 hours later, refrigerate samples in the dark.
- Longer storage is not recommended, as there are artifacts of undocumented magnitude. Several researchers have reported results on frozen samples but no systematic evaluation of freezing artifacts has been reported.
- For refrigerated samples, warm to room temperature before analysis.
- The Qorpak bottles can be re-used at sea. After analysis, thoroughly rinse bottles (and caps) 3x with fresh purified water and store

with 20 ml of 10% HCl. Before re-use, shake well, discard the 10% HCl, and rinse copiously with fresh purified water. Fill the bottle with purified water to be used as the rinse for sample filters.

1. Gelman Filter cup
2. Gelman Filter base/frit holder
3. Rubber stopper
4. PVC 'T' coupling
5. PVC threaded/non-threaded coupling
6. Gelman Filter base canula
7. Anodized aluminum sample bottle receiver w/threads and O-ring
8. PVC ball valve
9. PVC threaded barb
10. O-ring
11. Sample bottle
12. Rubber tubing to vacuum
13. Gelman filter cup frit
14. Silicone tubing
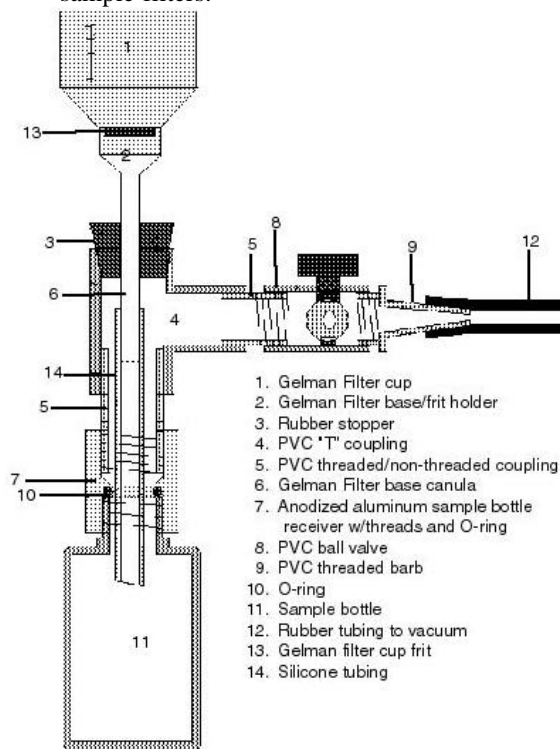
Figure 3. Diagram of filtration apparatus designed to collect clean filtrate directly to a clean sample bottle for determination of soluble absorption coefficients.

Determination of Optical Density of Soluble Absorption Preparations

- If samples have been refrigerated, allow them to warm to room temperature.
- Allow spectrophotometer to warm up for 30 min. Confirm that the optical windows of the spectrophotometer are clean. If necessary, clean with purified water followed by ethanol and dry thoroughly with lint-free laboratory tissues.
- Wash hands with soap and water to avoid contamination
- Between use, 10 cm quartz window spectrophotometer cuvettes should be stored with purified water. For analysis, discard the purified water in the cuvettes, rinse inside and outside of cuvettes 2x with 10% HCl, 2x with ethanol, then rinse inside and outside copiously with purified water. After cleaning, use laboratory tissues when handling the cuvettes,

avoid contact with bare-hands. In particular do not contaminate the optical windows of the cuvette.

- Fill both cuvettes with purified water directly from water preparation system. Use of water stored in containers is not recommended. If purified water is not available at sea, the carefully prepared water in combusted bottles can be used as a reference, but the investigator must document its degradation over time relative to air.

- Carefully dry the cuvettes. Bulk dry with paper towels but dry the quartz optical windows with lint-free laboratory wipes only (e.g. Kimwipes™).

- Inspect cuvettes carefully including visual inspection along the optical path to ensure they are clean. Make sure there are no bubbles, floating dust, or contaminants on the optical windows or in suspension. Looking through the cuvette against a black background can usually identify any problems in the samples. Repeat cleaning and drying procedures as needed for a clean sample.

- Run an air vs. air baseline for the spectrophotometer. Record the digital air baseline. This spectrum should be spectrally flat, with noise less than $\pm\,0.0005$.

- Place one cuvette in spectrophotometer and scan relative to air. Remove and repeat for the second cuvette. Store both spectra noting which file is for the cuvette to be used as reference in subsequent analyses, and which to be used for samples.

- Compare the two pure water vs. air spectra with each other and with a digital library of previous air-water spectra. Ensure that the two cuvettes are well matched optically, and that both conform to tolerance of pure water relative to air. Note anomalies and plan to make any needed corrections during data processing. If anomalies are from poor preparation of the cuvette, repeat the preparation and run new air-water scans.

- Put both cuvettes in the spectrophotometer. Run baseline correction for purified water in both beams. After baseline is complete record the pure water baseline as a sample. This spectrum should be spectrally flat, with magnitude less than $\pm\,0.0007$. Save the digital baseline spectrum. Ensure the baseline is flat and note any anomalies. If baseline is not flat, the spectrum must be used for data processing.

- Remove sample cuvette and discard liquid. Rinse inside of cuvette 3x with ~5-10 ml of

next sample. A copious rinse is desired but sample is often limited. Several vigorously shaken small sample rinses are recommended if volume is extremely limited. The first sample rinse is most important to eliminate all purified water, especially for seawater samples due to refractive index differences between fresh and salt water. Fill cuvette with next sample.

- Dry sample cuvette carefully and inspect as described above to ensure clean sample.

- Place sample cuvette back into spectrophotometer, and run spectrum. Store digital data and record all necessary information.

12.6 DATA PROCESSING

Spectral absorption coefficients in units of m^{-1} are calculated from optical density spectra $OD(\lambda)$ measured using the protocols described above. Subscripts *b, d, f, r, s, sp* and *null* used below are defined as referring to OD for the blank, de-pigmented particles, filter, reference baseline, soluble material, suspension of particles, and null point, respectively. Raw data collected as described above must be processed to provide the absorption coefficients of interest. For simplicity in the following discussion, it is assumed that the baseline reference spectrum $(OD_r(\lambda))$ for either soluble or particulate samples has been automatically compensated in the raw data record through instrument software. If not, it must be corrected in data processing and its omission in the formal equations does not imply that it is not necessary to evaluate this reference baseline and correct for it as required.

For soluble absorption, the calculations are directly proportional to the sample optical density relative to the pure water reference

$$a_g(\lambda) = \frac{2.303}{l}\left[OD_s(\lambda) - OD_b(\lambda)\right], \quad (12.1)$$

where l is the cuvette pathlength (usually 0.1m) OD_s is the soluble preparation absorbance relative to freshly purified water and OD_b is the blank for the preparation. When double beam spectro-photometers are used that produce flat baseline spectra and automatically correct for the pure water reference, the $OD_r(\lambda)$ need not be subtracted since its value is simply zero plus instrumentation noise. If a flat reference spectrum and its noise is subtracted from the sample spectrum, noise is introduced to the result with no change in the basic

spectrum.

There are generally small spectral effects of the filtration and preparation procedure that cause blanks prepared from purified water to have a higher $OD_b(\lambda)$ at short wavelengths compared to purified water drawn directly from the sample system (Figure 2). The value of $OD_b(\lambda)$ for the blank must be subtracted from the raw soluble sample optical density. The $OD_b(\lambda)$ should be determined, recorded and included with the data. It is recommended that the investigator carefully determine these blanks for a cruise or field program for each station, and carry out an evaluation of the stability of this blank for quality control purposes. If the purified water system is performing well and the preparation procedures carefully implemented, the blanks are generally very consistent. In this case it is best to determine a mean spectrum from numerous determinations (e.g. all blanks for a cruise), and then fit a smoothed exponential function to the overall mean. Figure 2 illustrates these results for blanks, prepared from Millipore Alpha-Q, Milli-Q, or Banstead Nanopure water, and determined immediately after preparation for numerous cruises. The OD for the soluble sample and the blank should be set to zero at the selected null point, and then the blank subtracted from the sample. Temperature and salinity effects from 650-750 nm (Pegau et al., 1995) make choice of a null wavelength problematic since it is often not feasible to keep samples and references at identical temperatures. Influence of these effects are evident from ~620-800 nm in the blank spectra shown in Figure 2. The choice of a null point wavelength is discussed in the Workshop Summary section.

For particle absorption determinations, a correction for increased optical pathlength due to scattering by the filter medium is required (Kiefer and SooHoo, 1982; Mitchell and Kiefer 1984, 1988a; Mitchell 1990). The geometric absorption pathlength l_s of the filtered material in suspension is given by

$$l_s = \frac{V}{A}, \qquad (12.2)$$

where V is the volume of water filtered and A is the clearance area of the filter determined by measuring the diameter of the portion of the filter with concentrated particles. Scattering of light within the GF/F filter increases the absorption pathlength. The pathlength amplification parameter was symbolized as β by Kiefer and SooHoo (1982) following the nomenclature of Butler (1962). This symbol should not to be confused with the volume

scattering coefficient $\beta(\theta)$ used in other chapters of this Technical Memorandum. The absorption coefficient of filtered particles must be corrected for pathlength amplification and the equivalent absorption coefficient in m^{-1} in suspension is computed as

$$a_p(\lambda) = \frac{2.303\,A}{\beta V}\left[OD_f(\lambda) - OD_{null}\right]. \qquad (12.3)$$

$OD_f(\lambda)$ is the absorbance of the sample filter measured relative to a fully hydrated blank filter. As with the analysis for soluble absorption, if a spectrophotometer with automatic reference baseline correction is used, and the reference filter blank baseline is flat over the spectral range of interest, $OD_r(\lambda)$ does not need to be subtracted. Spectra of $OD_b(\lambda)$ must be determined, recorded and provided with the sample data. Properly prepared blanks generally have flat spectra relative to the reference baseline filters. If the $OD_b(\lambda)$ is confirmed to be flat, then it is recommended that only a null absorbance is subtracted from the $OD_f(\lambda)$ to compensate for baseline offsets. The investigator must ensure that $OD_b(\lambda)$ is flat if it is not to be subtracted from the raw $OD_f(\lambda)$. To correct for residual offsets in the sample filter relative to the reference, and for scattering artifacts due to particle loading, it is assumed that a null absorption wavelength (OD_{null}) in the infrared can be defined. Previously, investigators have used 750 nm as the null absorption wavelength, but numerous reports indicate this wavelength is too short for many waters. It is recommended that the null wavelength be set at 800 nm (or longer) and the investigator must examine the spectra to evaluate residual absorption structure near the null wavelength. Rather than use a single wavelength (which may be influenced by the instrument noise), a mean OD_f over 10 nm (e.g. 790-800 nm) can be used as the null value to minimize the introduction of noise in the null procedure. This issue is discussed in more detail in the Workshop Summary section.

To correct for the pathlength increases due to multiple scattering in the filter, the prevalent current practice is to estimate β empirically through either a quadratic or power function that may be expressed in the form

$$\beta = \left[C_1 + C_2\left[OD_f(\lambda) - OD_{null}(\lambda)\right]\right]^{-1}, \qquad (12.4a)$$

or

$$\beta = C_0 + C_1\left[OD_f(\lambda) - OD_{null}(\lambda)\right]^{C_2}, \qquad (12.4b)$$

Table 2. Published coefficients for determining pathlength amplification effects. The OD_{sp} derived from Equation 4 for a GF/F filter with $OD_f = 0.2$ is provided for comparison.

Quadratic Functions	Particle Type	C_0	C_1	C_2	OD_{sp} (0.2)
Mitchell (1990)	Mixed Cultures	--	0.392	0.655	0.105
Cleveland & Weidemann (1993)	Mixed Cultures	--	0.378	0.523	0.097
Moore et al. (1995)	*Prochlorococcus marinus*	--	0.291	0.051	0.060
Moore et al. (1995)	*Thalassiosira weissflogii*	--	0.299	0.746	0.090
Moore et al. (1995)	*Synechococcus WH8103*	--	0.304	0.450	0.080
Tassan & Ferrari (1995)	*Scenedesmus obliqus*	--	0.406	0.519	0.102
Nelson et al. (1998)	*Dunaliella tertiolecta*	--	0.437	0.022	0.088
Nelson et al. (1998)	*Phaeodactylum tricornutum*	--	0.294	0.587	0.082
Nelson et al. (1998)	*Synechococcus* WH7803	--	0.277	0.000	0.055
Power Functions					
Mitchell and Kiefer (1988a)	*Dunaliella tertiolecta*	1.3	0.540	-0.467	0.082
Bricaud and Stramski (1990)	Field samples; *D. tertiolecta* Cultures of Mitchell & Kiefer (1988a)	0.0	1.630	-0.220	0.086
Kahru and Mitchell (1998)	Mitchell (1990) data	0.0	1.220	-0.254	0.109
Constant					
Roesler (1998)	Assume β = 2.0	--	--	--	0.100

for quadratic equation or power function fits, respectively. C_1 and C_2 are coefficients of least squares regression fits of measured data. Several recommended coefficients for C_1 and C_2 have been reported in the literature (Table 2).

The best overall performance of the GF/F algorithm evaluated by Mitchell (1990) was achieved when filtered sample density yields $OD_p(670)$ between 0.05 and 0.25 with blue absorption ≤ 0.4. The volume of water filtered for particle absorption measurements should therefore be adjusted accordingly. The various coefficients in Table 2 will predict absorption coefficients that vary by a factor of ~2 but the overall results indicate a much narrower range. For all the coefficients shown in Table 2, the mean $OD_{sp} = 0.087$ when $OD_f = 0.2$; the 95% confidence range is 0.078-0.096. This range is comparable to the estimated precision of the method discussed by Mitchell (1990) where the errors of the method were estimated to be of the order ± 15% for an experiment done carefully with a single filter lot, and perhaps 20-30% considering all aggregated errors of different filter lots, instrumentation, volume filtered, raw optical density, and particle type. The best fit to the data in Mitchell (1990)

results in estimates of OD of suspensions approximately 20-30% higher than values based on the power function coefficients of Mitchell and Kiefer (1988a) determined from a limited study of *D. tertiolecta* (e.g. 28% difference in Table 2 example). Note that results of Bricaud and Stramski (1990) agree within 5% of the results for the Mitchell and Kiefer (1988a) equation because both fits were based on the same *D. tertiolecta* data set. The smallest estimates of OD_{sp} shown in Table 2 correspond to β experiments done for small phytoplankton (*Prochlorococcus, Synechococcus*). There is considerable uncertainty still regarding the influence of particle type, refractive index and size on the β values. The best estimate for β may depend on particle types within a sample that are not known *a priori*. Therefore it is important to report the absorption coefficient estimates, the correction procedure, and the raw data to allow future revisions in the estimates from the original data. Ancillary data including particle size distributions, inorganic sediment mass, flow cytometry and HPLC pigments would be useful to evaluate the ideal correction factors for OD_f. In Case 2 waters, the definition of the null absorption

is more difficult and the investigator may consider the benefits of the transmission-reflectance estimates of particle absorption (Tassan and Ferrari, 1995a). These issues are discussed further in the Workshop Summary section.

For de-pigmented absorption coefficients, $a_d(\lambda)$, one may use a calculation analogous to Equation 3, but where the filter optical density of de-pigmented particles corrected for the reference baseline, is used for OD_f. Generally the same pathlength correction for the de-pigmented samples is applied. The validity of this operational choice of β is difficult to assess because the de-pigmented particles are created operationally from the treatment and therefore true empirical relationships between their absorption on filters compared to suspensions have not be performed. The spectral absorption coefficient for phytoplankton pigments can be computed as the difference between particulate and de-pigmented estimates:

$$a_f(\lambda) = a_p(\lambda) - a_d(\lambda) \qquad (12.5)$$

12.7 ESTIMATION OF PHOTOSYNTHETICALLY ACTIVE ABSORPTION

Methods have been proposed for the estimation of photosynthetically active absorption. Total phytoplankton absorption is attributed primarily to the sum of photosynthetic and photoprotective pigments (e.g. $a_f = a_{ps} + a_{pp}$) Bidigare et al. (1987) reported a method for reconstruction of the phytoplankton absorption from HPLC-determined pigment concentrations and estimates of the mass-specific spectral extinction coefficients of different pigments. HPLC pigment reconstruction was compared to estimates of phytoplankton absorption determined with glass fiber filters for samples from the Sargasso Sea. HPLC reconstruction methods are useful for improving our understanding of the relative contribution of phytoplankton to total absorption, as well as the relative importance of photosynthetic and photoprotective pigments for the phytoplankton fraction. However, issues remain due to the lack of knowledge about the true *in vivo* extinction coefficients of individual pigments, and the uncertainty in the degree of packaging of a polydisperse natural particle assemblage. Estimates of spectral mass extinction coefficients for these methods are provided in Bidigare et al., (1990). The method is useful if pigment-packaging effects are negligible. For this

assumption to hold, both small cells and low pigment per cell volume are required. Compared to directly measured *in vivo* absorption spectra of phytoplankton cultures, the HPLC reconstruction generally over predicts the true value, and results in spectral shapes that are different from *in vivo* estimates (Sosik and Mitchell, 1991; Moisan and Mitchell, 1999). An improvement of Bidigare's method has been proposed by Babin et al. (1996) and applied by Allali et al. (1997) to natural populations of the Equatorial Pacific. It consists of partitioning the measured absorption spectrum into its photosynthetic and non-photosynthetic components using the HPLC information, and thus takes into account the actual degree of packaging for the population.

Fluorescence excitation spectra for chlorophyll *a* have been shown to be a good proxy of the spectral shape of the photosynthetic action spectrum for many phytoplankton types (Neori et al., 1988). Thus, they can represent the relative absorption spectrum of photosynthetically active pigments for some phytoplankton types. Sosik and Mitchell (1995) have proposed a normalization of the fluorescence excitation spectrum to the red peak of absorption for oceanic particulates to estimate absorption by photosynthetically active pigments, $a_{ps}(\lambda)$. They found $a_{ps}(\lambda) \le a_f(\lambda)$, where the difference is attributable to photo-protective pigments in the phytoplankton. Issues related to scaling the relative fluorescence spectrum for cultures to the chlorophyll *a* absorption at the red peak have been discussed further by Johnsen et al., (1994) and Moisan and Mitchell (1999). The method assumes that pigments are equally distributed between the two photosystems (the fluorescence of PSI is undetectable at ambient temperature). This assumption is not valid for phycobiliprotein absorption (Neori et al., 1988) and some other phytoplankton groups (Allali, 1997; M. Babin, unpublished data).

12.8 DATA REPORTING

For purposes of data reporting and archiving, the absorption coefficients will be reported in m^{-1} and computed using the equations summarized above. Uncorrected optical density spectra for the filter samples, blank filter reference, pure water reference, and soluble absorption blank spectra must be recorded and provided so alternative algorithms could be applied to the original data. The pathlength amplification factor and a description of (or reference to) the method and the

procedure for assignment of the null absorption must be reported.

12.9 SUMMARY OF WORKSHOP RESULTS

Two workshops were sponsored by NASA to evaluate different spectrophotometers, previously published literature, and new methods for absorption analyses. The participants in the workshops at Scripps Institution of Oceanography and Bigelow Laboratory for Ocean Sciences are listed in Table 1. Several questions were addressed including comparison of different spectrophotometer systems, evaluation of published methods for determination of β, sample preservation, null absorption wavelength subtraction, de-pigmentation, and other issues. Many of these issues could benefit from further research on advanced protocols.

Spectrophotometer considerations

Various spectrophotometer options exist ranging from commercially available research-quality systems that have scattered transmission and reflectance options to low-cost analytical units, to custom built instruments that may be very simple or quite sophisticated. With appropriate training and knowledge, high quality results may be achieved with diverse spectrophotometers. The investigator must weigh the merits of the flexibility of custom systems with the ease of operation of certain robust analytical or research-quality units. Various instruments that were evaluated during the NASA workshops are listed in Table 1. In terms of baseline noise and stability, spectral precision and range, and ability to measure both filters and suspensions, the top performing spectrophotometers - not surprisingly - were the more expensive commercial research-quality systems. Still, many intermediate cost analytical units performed well throughout the spectral range. However, numerous instruments exhibited problems with baseline noise, spectral range, spectral accuracy and stability. Often several of these problems were found for an instrument. To carry out appropriate work on particle suspensions requires either a high quality scattered transmission accessory or an integrating sphere. For the workshops, the analyses on suspensions were limited to the moderate to expensive commercial systems that had integrating sphere accessories.

Verification of the spectral and quantitative accuracy of the optical density estimates must be carried out by investigators. Commercially available research quality analytical dual beam UV-visible spectrophotometers are recommended for the absorption determinations described here. Many commercial instruments use lines in the mercury lamp to ensure spectral calibration during start up procedures. Still, it is possible for some instruments to develop spectral anomalies during operations including baseline drift, or mechanical mis-alignment of the grating, etc. Therefore it is recommended that investigators have a holmium oxide filter as an independent reference of instrument spectral performance. Periodic checks should be determined by scanning the filter relative to an air-air baseline. Any spectral anomalies found must be corrected. Numerous spectrograph devices and non-commercial spectrophotometers do not have automatic spectral performance adjustment. For such instruments, careful determination of the spectral performance using a holmium oxide filter should be done. If the unit exhibits instabilities, the spectra must be repeated regularly. Since all raw optical density determinations described here are carried out relative to a reference (e.g. blank filter, purified water) proper treatment of the baseline and sample spectra should provide accurate optical density results. To ensure accurate estimates of optical density, absorbing reference standards should be run regularly relative to air with the analytical equipment. Absorption reference filters for different optical densities, and holmium oxide filters can be purchased from manufacturers or scientific optics supply companies to carry out these performance tests.

At the Scripps workshop, several research-quality instruments provided the best overall performance. The Perkin Elmer Lambda 18 was the most consistent in the spectral range from 300-800 nm for all sample types and measurement geometries and is used in comparison to other instruments listed in Table 1. At the Bigelow workshop, the moderately priced Perkin Elmer Lambda 3 was used to compare various units. Scripps workshop results for one culture are shown in Figure 1 as an example of the type of results attained. In general, with proper consideration of instrumental baselines and care in sample preparations, all spectrophotometers that could determine the optical density of suspensions agreed well in the visible within routine analytical error (Figure 1a). This was also true for determinations of cultures or natural particles concentrated on GF/F filters both using standard optics in commercial grating monochromator systems, or

collecting the energy with a scattered transmission accessory or integrating sphere (Figure 1B). When OD_f from 400-700 nm for the traditional dual beam commercial instruments were regressed against each other the slopes of the regression usually were between 0.95 – 1.05 implying minimal difference caused by different instruments. In Figure 4B the slopes for the Cary and the Kontron, relative to the Perkin Elmer Lambda 18 were 0.96 and 0.98, respectively. At the Bigelow workshop, the ASD fiber optics system had a slope of 1.15 relative to the Perkin Elmer Lambda 3.

Optical densities in transmittance mode for GF/F filters were determined at the Scripps workshop for diverse optical geometries including integrating spheres (PE Lambda 18), diffuse transmittance accessory (UVIKON Shibata method), standard optics of pre-sample grating commercial spectrophotometers (Cary 1, Perkin Elmer Lambda 6), diode array with integrating sphere illumination and collection (HP), and sample illumination from broad band light source with spectral dispersion using a post-sample diode array spectrograph (USF). Table 3 summarizes the regression slopes of these diverse optical geometries relative to the Perkin Elmer Lambda 18 integrating sphere estimates. Both the Cary and the Perkin Elmer Lambda 6 with samples placed in the beam of the standard optics path in the sample compartment, as well as the Kontron configured with a proper scattered transmission accessory (Shibata, 1958) resulted in raw OD_f values that were within 5% of the PE Lambda 18 integrating sphere results. These differences for replicate filters prepared individually for each instrument are within the routine methodological uncertainty of replicate filters run on the same instrument. Results in Table 3 indicate that many spectrophotometers, with extremely different optical geometries, can determine raw OD values that are equivalent within methodological uncertainty of the preparations. Results in Table 3 are consistent with the results of Mitchell (1990) that raw OD_f for a filter measured either with standard optics or an integrating sphere were not significantly different.

Large differences among instruments were observed, however, in the baseline noise, spectral range, and transition across instrumentation optical-mechanical wavelengths (e.g. lamp or sorting filter wavelength change positions). These latter performance issues are very important with respect to achieving high quality results, and the investigator should carefully assess the performance of

Table 3   Example of OD_f regression slopes between instruments for replicate GFF filtered samples of *T. weissflogii* analyzed with various spectrophotometers at the Scripps Workshop. Comparisons are relative to OD_f determined with the Perkin Elmer Lambda 18 integrating sphere. Extremely different optical geometries are represented. Data are 400-700 nm after null correction. Other comparisons for different cultures yielded similar results.

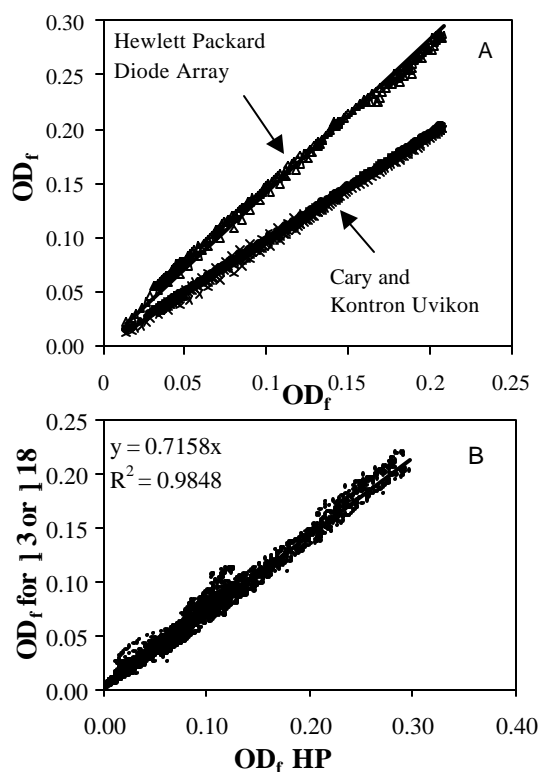| Instrument	Slope	Optical Geometry
Cary	0.98	Standard Optics
Lambda 6	0.95	Standard Optics
UVIKON	0.96	Shibata Optics
USF	1.07	Fiber Diode
HP	1.42	Sphere Diode
Elyptica	0.91	Single Beam

Figure 4.   A.   Linear regression of OD_f values between 400-700 nm for Perkin Elmer Lambda 18, Varian Cary 1 and Kontron. **B.** Merged regression analysis of HP Diode Array unit for various comparisons by SDSU CHORS and Scripps Photobiology Group. Data are for OD_f from 400-700 nm after setting a null point as the mean 790-800 (SIO) or 750 nm (SDSU).

various instruments before choosing the best unit for the work to be achieved. An important generality is that many spectrophotometers, with or without scattered transmission or integrating spheres, provide $OD_f(\lambda)$ within ± 5% for GF/F filters. The investigator must carefully evaluate raw OD_f of a candidate instrument for various filter loading and particle types relative to other units to ensure that the raw data is comparable. One cannot assume all instruments provide a raw OD_f that are equivalent. For example, the ASD unit at the Bigelow Workshop estimated OD_f values 15% higher than the Perkin Elmer Lambda 3.

The Hewlett Packard diode array unit has been confirmed to have raw OD_f that is considerably larger than values determined with more traditional units. The optical design of the Hewlett Packard spectrophotometer requires illumination of the sample in a diffuse flux source from an integrating sphere attachment to achieve results with diffusing materials such as particles on filters. This illumination geometry is significantly different from the collimated beam illumination of pre-sample grating monochromator systems. This difference results in observed optical densities of the diode array system being 35-45% higher than estimates on the same filter samples determined by various dual beam grating monochromator references or single beam units (Figure 4a). The results from comparisons on three different dates with diverse cultures are shown in Figure 4b. We excluded high optical density samples because the relationship became slightly non-linear at OD_f > 0.4. For the Perkin Elmer Lambda 18 and Lambda 3 used as reference instruments for the Scripps and Bigelow workshops, respectively, the Hewlett Packard unit had a consistent offset that is easily predicted with a linear regression for OD_f < 0.35. These results for cultures agree well with previous work comparing many natural field samples (Cleveland, pers. Comm). Based on the regression in Figure 4b we recommend that the investigator multiply OD_f for the Hewlett Packard diode array system by 0.72, after setting the null point in the infrared, to convert to the comparable OD_f for the traditional dual beam scanning monochromator systems. Alternatively, estimates of β can be determined by the investigator if appropriate determinations of suspensions can be done to compare to filtered samples. Another major limitation of the Hewlett Packard diode array unit was that it had a very noisy baseline for glass fiber filters, and could not achieve good results with

these filters below 400 nm or above 750 nm. Noise from 700-750 nm made estimation of the null absorption wavelength more problematic. The advantage of this type of system is that it records a spectrum very rapidly. The sacrifice of data quality for speed is not recommended.

Instrumentation issues imply that an investigator carefully choose an instrument that can perform the analyses of interest. Appropriate, rigorous evaluation should be carried out prior to selection. It is recommended that investigators chose a high quality spectrophotometer that can effectively record raw optical density spectra for filters from 300-850 nm and for soluble samples from 250-850 nm. Systems with variable slit widths are preferred and spectra should be run at a 4 nm bandwidth or smaller. Bandwidth larger than 4 nm will smear the red absorption peak of chlorophyll in $a_p(\lambda)$ determinations. Baseline performance recommendations below are specified for a 4 nm bandwidth. Baseline noise for the glass fiber filters should stay within ± 0.01 over the full spectral range, but performance better than ± 0.005 is strongly recommended.   The units should maintain baseline flatness over time with minimal drift in offset. For soluble absorption, the baseline noise over the full spectral range for 10 cm quartz cuvettes with purified water should be less than ± 0.001 but performance better than ± 0.0005 is strongly recommended. For either preparation, baseline anomalies caused by lamp or sorting filter changes, or other instrumentation effects must be corrected. Automatic baseline corrections for many commercial units do an adequate job. Still, the investigator must carefully evaluate the baseline of all measurements and correct for any residual artifacts. Based on numerous comparisons, the Varian Cary 1 (now called Cary 100) has proven to be a high performing instrument that is moderately priced.   Selection of a unit with comparable performance or better is strongly recommended.

Effective Pathlength Corrections

The methods to determine the pathlength amplification factor based on transmission spectrophotometry of filters and suspensions has been described in detail elsewhere (Mitchell and Kiefer, 1988a; Bricaud and Stramski, 1990; Mitchell, 1990). The recommended approach is to determine the suspension optical density (OD_{sp}) on relatively high transmittance (optically thin) samples to minimize multiple scattering errors (Bricaud et al., 1983; Mitchell and Kiefer, 1988a).

In the following discussion, it is assumed that $OD_p(\lambda)$ has been corrected for the baseline reference and nulled in the infrared. The culture of interest should be filtered at multiple concentrations on different filter preparations to achieve a range of $OD_p(\lambda)$. Scaling of the estimated absorbance of the optically thin suspension (OD_{sp}) is made by multiplying the geometric pathlength for different volumes (l_s) (Equation 12.2) after determining the effective filtration area of the filter (l_sOD_{sp}). The investigator should not measure very high suspension absorbance to match high filter loading for estimates of β as this will cause possible errors in the suspension estimates due to multiple scattering effects (cf. Lohrenz, 1999). For natural populations, measurements on suspensions are in general not feasible due to low particle concentration so pre-concentration is required with possible artifacts such as particle loss, aggregation, etc. A possible alternative, introduced by Allali et al. (1997), is to compare absorption spectra measured on filters to those measured on glass slides (modified FTF technique, see later).

Several ad hoc comparisons of methods have been accomplished by various co-authors on this report, as well as more formal comparisons at the Scripps and Bigelow absorption workshops. In general, the previous results reported by Mitchell and Kiefer (1984; 1988a) that β exhibits variability due to changes in sample OD have been confirmed (e.g. Bricaud and Stramski, 1990; Cleveland and Weidemann, 1993; Tassan and Ferrari, 1995a; Moore et al., 1995). An example plot of OD_{sp} vs. OD_f for *T. pseudonana* for the spectral range 400-700 nm is shown in Figure 5a. Two different volumes of culture were filtered on replicate GF/F filters and the filter OD_f were determined with various spectrophotometers at the Scripps workshop. Published fits corresponding to variable β are also indicated as numbered lines. The Hewlett Packard diode array data fall well outside the data for other instruments. Also, the results for *P. marinus* (reported by Moore et al., 1995) were confirmed at the Scripps workshop (Figure 5b). This result indicating β depends on particle type is not well understood and warrants further research.
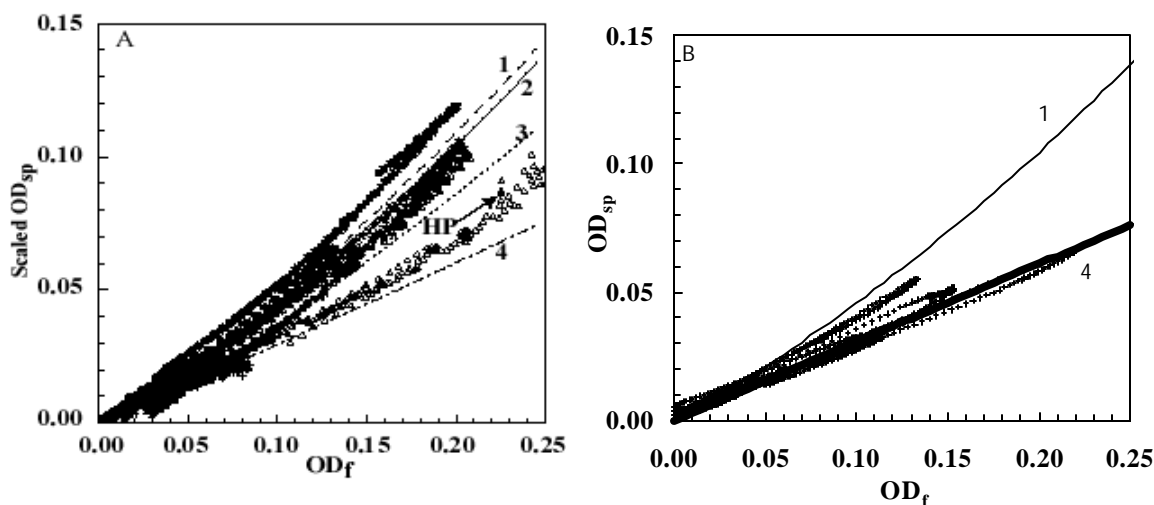

Figure 5. Following the procedures of Mitchell (1990) scaled optical density of suspensions are plotted against GF/F filter optical density to estimate the pathlength amplification factor, β. A. Optical density of the suspension scaled to geometric pathlength (l_sOD_{sp}) for *T. pseudonana* plotted against OD_f for instruments with integrating spheres used at the Scripps Absorption Workshop. Multiple filtration volumes were used to achieve significant range for the raw OD_f values. Numbered lines correspond to published coefficients (1=Mitchell, 1990; 2=Kahru and Mitchell, 1998; 3=Bricaud and Stramski, 1990; 4=Moore et al., 1995). All instruments at the Scripps workshop that could determine OD on both suspensions and filters, except the Hewlett Packard Diode Array unit, produced results similar to those originally reported by Mitchell (1990) for this small (5-6 μm) diatom. Data for the HP system are indicated (see also Figure 4). B. OD comparisons for suspensions and filters for *Prochlorococcus marinus* using the Perkin Elmer Lambda 18 at the Scripps workshop compared to the previously reported relationships for various cultures (line symbols same as panel A). The earlier differences noted by Moore et al. (1995) for *P. marinus* were confirmed during the Scripps workshop. The differences are not understood at this time.

An alternative method based on β being a constant equal to 2.0 is discussed by Roesler (1998). The assumption is that the glass fiber filter method estimates the diffuse absorption of a sample, which is exactly 2 times the volume absorption coefficient (cf. Preisendorfer, 1976). True measurements of the diffuse absorption coefficient of phytoplankton culture suspensions are reported by Kiefer et al., (1979) and it is evident that the chlorophyll-specific absorption coefficients at the red peak of those determinations are approximately 2 times those routinely reported for the volume absorption coefficient (e.g. Mitchell and Kiefer, 1988a; Johnsen et al., 1994; Sosik and Mitchell, 1991; Moisan and Mitchell, 1999). While it would be useful if β could be quantified by a simple constant, the theory of Duntley (1942) and empirical results on the optical dependency of β were confirmed for dyes in diffuse preparations (Butler, 1962) and for phytoplankton on glass fiber and cellulose acetate filters by Mitchell and Kiefer (1988a). This dependency has been found by numerous researchers as summarized in Table 2. The typical measurements in standard spectrophotometers illuminate the sample with a collimated beam, which becomes diffuse as it is transmitted through the filter. However, even the emerging beam is not fully diffuse and this can be demonstrated easily by visualizing a point source of light through a single fully hydrated glass fiber filter. While the point source becomes highly diffused, it is still visible as a distinct source, indicating that the illumination beam is not fully diffuse. Thus, the glass fiber filter does not achieve a measurement of diffuse absorption required to satisfy the optical geometry discussed by Preisendorfer (1976) so the simplification that β = 2.0 does not appear justified on theoretical grounds. However, 2.0 is a reasonable approximation in many cases since according to the Mitchell (1990) relationship, β equals 2.35 and 1.5 when $OD_f(I)$ is equal to 0.05 or 0.4 respectively, the range for optimal algorithm performance. Table 2 shows that for $OD_f(I)$ equal to 0.2, the resulting estimate for the suspension using β = 2.0 is in the middle of various methods recommended in the literature.

Absorption spectra for particles transferred to glass slides

At the Scripps workshop, the method of Allali et al. (1995) was used to estimate absorption coefficients of cultures and seawater samples by freeze transfer of the particles to transparent microscope slides following the protocols of Hewes and Holm-Hansen (1983). This transfer allows determination of OD_f in a non-diffusing preparation to avoid the pathlength amplification. For the filter support, a polysulfone Gelman unit was used (due to clogging, fritted glass supports should be avoided, especially for natural samples). Nuclepore™ 0.2 µm polycarbonate filters were used (0.4 µm filters are also adequate and more convenient for use at sea). Samples were filtered under low vacuum pressure (<5 in. Hg).

Immediately at the end of filtration, the filter was removed from the filtration unit and transferred, particle side down, onto a glass microscope slide (with or without a drop of water). No fixative was used in the preparations at the workshop. The preparation was then frozen by laying the slide (filter on the upper side) on a metal block cooled in liquid nitrogen (it is convenient to use a small-size Dewar container). The temperature of the metal block must be low enough for the filter to become almost immediately "white" with frost. After 10-15 seconds, the slide was removed from the block and the filter was carefully peeled off (when properly frozen, there is some resistance to peeling) and examined by eye to check the efficiency of the transfer. Then a circular cover slip of the same size as the clearance area of the filter was placed on the transferred particles. For most experiments, the Nuclepore™ filter was then put into 90% acetone for chlorophyll extraction to quantify the transfer efficiency of the chlorophyll containing particles. The FTF procedure produced results comparable to the GFF filter method. Performance for a diatom culture was not as good as other cultures, but the results were still quite reasonable (Figure 6a). Other comparisons for cultures of phytoplankton and natural samples are shown in Allali et al., (1995). Diatoms or other larger cells may become crushed by the slide and cover slip preparation in which case release of pigments could lead to reduction of pigment package effects. At the Scripps workshop, results for smaller cells including *Synechococcus*, *Prochlorococcus* and *Emiliania* were better than the results for the diatom. The natural samples concentrated from Scripps Pier also resulted in excellent comparison between the freeze transfer and suspension estimates of absorption (Figure 6b) for wavelengths longer than 350 nm. The reason for larger discrepancies below 375 nm for this preparation is not known.

The transfer of particles from the filter to the slide is a critical step for FTF sample preparation. Visual examination of the filter and slide
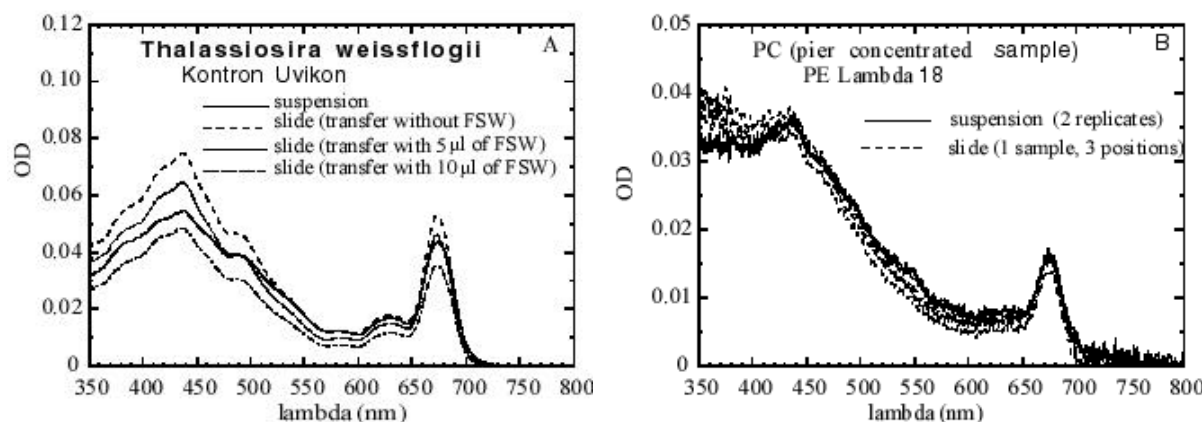
Figure 6. Examples of *OD* determined on a diatom culture and seawater particles transferred to glass slides using the Allali et al. (1995) method and suspensions of the same material determined (using the Perkin Elmer Lambda 18 spectrophotometer or the Kontron Uvikon) at the SIO Absorption Workshop. For these and other cultures (data not shown), the FTF method provides estimates of $a_p(\lambda)$ comparable to those measured on suspensions.

preparation is essential as it gives a quick, albeit qualitative, indication of the success of this operation. The transfer generally appears to be easier and more successful without addition of water to the slide before freezing, except for some species such as diatoms. The additional extraction of the filter and determination of the fraction of total chlorophyll not transferred must be performed for quantitative work. For most of the investigated samples, the technique has given satisfactory results, and the overall uncertainty is similar to that expected for measurements with the GF/F technique because of uncertainty in β. The modified FTF technique is not significantly more time-consuming than the GF/F technique and can provide results that agree well with determinations on suspensions. While filtering on 0.2 µm polycarbonate filters takes longer than GF/F filters, there is no need to reach high optical densities so sample volumes can be reduced. An important limitation remains that methanol or bleach de-pigmentation is feasible but not easily achieved (See Allali et al., 1995) so that it may be more practical to exploit numerical decomposition methods (e.g. Morrow et al., 1989; Bricaud and Stramski, 1990). A more practical issue is that successful determinations of the transmittance of the diffusing particles on the slide require an integrating sphere or scattered transmission accessory for the spectrophotometer. This adds an additional burden of expense and analytical complexity that may make this procedure less amenable to routine applications. Also, as pointed out by Sosik (1999), some artifacts of freezing, particularly in the UV, occur immediately upon freezing. Sufficient issues remain with the FTF method so that the GF/F method is still recommended at this time for most routine work.

Purified water for soluble absorption

At the Scripps workshop, the performance of purified water preparation systems were compared. The units (Millipore Milli-Q and Alpha-Q, and Barnstead Nanopure) all provided similar results in tests relative to air for the spectral range 300-900 nm. Below 300 nm there were small differences (data not shown). These units, or equivalent systems, should be capable of delivering purified water required as a reference for soluble absorption measurements and are recommended as standard equipment for field programs. In many field programs, however, the available feed water is of such an inferior quality that the systems can become overwhelmed and their performance significantly diminished. The experience of the co-authors is that this is a major limitation with respect to knowledge of the pure water baseline. Therefore it is recommended that a set of standard purified water samples be prepared prior to a field deployment and analyzed daily in reference to purified water prepared in the field. Procedures for preparing this standard water are provided in the protocols section. The standard prepared water has been found to deteriorate over time, especially from 250-325 nm, but the magnitude of the observed increase in optical density relative to freshly purified water is much smaller than the magnitude of the potentially dramatic degradation in the output of pure water systems. Therefore, routine determination of the reference standard can assist in quality control of, or serve as an alternative source

to, low quality output from a purified water system. Given the issues regarding frequent failure of pure water systems during fieldwork, the investigator must routinely record a spectrum of the purified reference water used for analysis relative to air. This procedure provides an absolute check for the quality of the purified water and could serve as the basis for making corrections. Further work on the UV absorption of pure water should be carried out to extend our knowledge of pure water in the visible and infrared reported by Pope and Fry (1997). See also a recent recommendation for UV-Visible absorption coefficients for pure water (Fry, 2000).

Null point normalization of particle absorption measurements

The accurate determination of particulate light absorption requires some procedure to correct measured absorption coefficients for errors, which arise from scattering losses within the measurement system. Both soluble and particulate absorption methods require adjustment of the spectrum at a null point. The most common approaches begin by identifying a spectral region where sample absorption can be assumed negligible, which allows an initial assessment of the scattering error for a limited portion of the spectrum. For measurements

of absorption by aquatic particles, this "null point" wavelength is usually taken from a spectral region in the near-infrared typically 750 nm to 800 nm for the correction of spectrophotometric measurements of water sample preparations.

Differences in light absorption and scattering properties among individual filters used for sample filtration are one source of variability. The optical properties of blank GF/F filters can vary significantly between individual filters (up to 0.05 OD), presumably as a result of differences inherent in the manufacturing process. While differences in blank OD are noted, the spectrum of two blank filters relative to each other is essentially flat. Different glass fiber filter types have different transmittances (Mitchell and Kiefer, 1988a) and there are variations between manufacturing lots of the same filter type (Mitchell, 1990). The relative degree of water saturation between baseline and sample filters may also lead to differences in the measured $OD_f(\lambda)$ of sample filters so proper hydration of samples is an essential part of the protocol. Pre-soaking filters in filtered seawater 1-2 hrs before use can lead to less variability between individual filters (Bricaud and Stramski 1990). Blanks used as references must be adequately soaked and remain hydrated during analyses.

The choice of a null point in the infrared originates primarily from the assumption that absorption by phytoplankton cells is negligible in this wavelength region. For *T. pseudonana* raw OD values measured at 750 nm relative to a
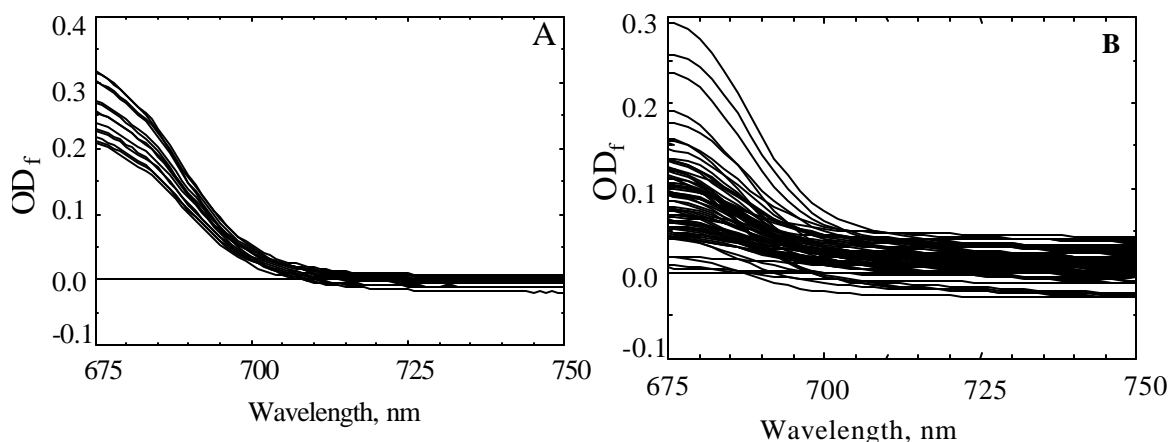
Figure 7. A. Raw OD_f 675-750 for a culture of *T. pseudonana*. B. Raw OD_f 675-750 for seawater samples. The mean value $OD_f(750)$ for *T. pseudonana* is not significantly different from 0.0, but the mean $OD_f(750)$ for seawater samples is significantly greater than 0.0 (p < 0.001). This suggests the possibility of true absorption at 750 nm that may result in an absolute error in routine application of a null value and/or significant scattering with unknown spectral dependency. Scattering error may have spectral dependency

leading to either positive or negative errors depending on the particle types and the spectral range of interest. Routine selection of a null wavelength in the infrared contributes error that is not well quantified.

pre-soaked and hydrated filter varied from -0.019 to 0.01. The mean value of -0.0016 (15 measurements) is not significantly different from zero (Figure 7a). These results suggest that phytoplankton have negligible absorption in the near infrared, and introduce minimal scattering error when collected on GF/F filters for absorption measurements. However, there are examples, especially in the presence of suspended sediment loads, that significant absorption for field samples is still present at 750 nm. Minerals may exhibit significant absorption in the near infrared (e.g. Bukata et al. 1995). Figure 7b illustrates examples of optical density spectra for natural particle assemblages from Case 1 waters of the California Current collected on glass fiber filters. In contrast to the culture, the field data indicate that the measured optical density signal in the infrared is frequently positive, with mean values significantly greater than zero implying that scattering by the particles on the filter contribute to this non-zero raw optical density. The magnitude of $OD(750)$ is not trivial. Despite the careful baseline treatment and efforts to minimize filter-to-filter variability in these measurements, this rather systematic tendency towards positive values of OD in the infrared for field samples is difficult to interpret if only transmittance measurements are determined because it is not possible to distinguish true absorption from scattering error. The transmittance-reflectance method can improve on this uncertainty (Tassan and Ferrari, 1995a).

The error in estimating absorbance from OD using a near-IR null point will depend on the relative magnitude of absorption to scattering at the null point. Subtracting out true absorption introduces an absolute error equal to the true absorption at the null wavelength. Spectral dependence of scattering can introduce positive or negative bias at shorter wavelengths depending on the size of the particles and their refractive index. For particles greater than several microns, the spectral dependence of scattered losses will be nearly flat, so small errors may be expected. If the scattering is dominated by small particles, the errors can be greater, and their relative magnitude difficult to assess *a priori* without detailed knowledge of the size and refractive index. Since natural particle size distributions and refractive indices can vary substantially, these factors can introduce errors of uncertain magnitude. Still, at least for Case 1 waters and many Case 2 waters, the errors from using a null absorption correction will be smaller than if no null absorption is used.

For soluble absorption, temperature differences between the reference water and sample can lead to strong spectral absorption features (Pegau and Zaneveld, 1993). These absorption bands are strongest in the range 650 - 750nm but appear to have harmonics both shorter and longer so that choice of a null point is an important consideration. To avoid temperature effects, sample and blank should be maintained at the same temperature. It is often difficult in practice to ensure temperature equivalence in which case care must be taken regarding the wavelength for setting a null point for soluble absorption analysis. If strong temperature residuals are in the spectra, one must inspect the data to determine an appropriate wavelength range to use as a null point. In many clear open ocean waters, the $OD_s(l)$ values greater than 600 nm are typically not significantly different from the baseline, so it is feasible to utilize a shorter wavelength null point in these situations (Mitchell et al., 1998). However, more turbid lake, bay and coastal waters have large soluble absorption into the near IR. Figure 2 illustrates that the magnitude of the temperature effects for pure water blanks determined for various cruises is typically ± 0.001 OD for a 0.1 m pathlength. While this may seem to be a small analytical uncertainty, it corresponds to a_g ± 0.02 – similar to the magnitude of pure water 400-500 nm, or phytoplankton absorption at the red peak for chlorophyll of 1 μg/L. Situations where the reference was both colder and warmer than the sample are shown in Figure 2. It is evident that for these samples, the region near 600 nm is a preferred null wavelength compared to any choice between 600-800 nm. When soluble absorption values are large, the relative effects of temperature are smaller, and one may be able to choose a null point greater than 600 nm. The performance of some spectrophotometers diminishes at longer wavelengths in the infrared, especially for particulate samples. The investigator must carefully inspect baseline, blank and sample spectra to determine an appropriate wavelength for null assignment. The final choice will introduce some uncertainty and error in the derived absorption coefficients, which leads to the requirements of reporting raw data for $OD_s(l)$, blanks, and purified water vs. air.

De-Pigmented Particle Absorption

Material collected on glass-fiber filters includes phytoplankton and other particles, including bacteria, microzooplankton, organic detritus (e.g. dead organisms, phytodetritus, and marine snow), and inorganic particles (sand, dust, coccoliths, etc.). Separation of the total particulate absorption coefficient as measured on glass-fiber filters (a_p) into phytoplankton (a_f) and non-phytoplankton or "detrital" (a_d) components is an important pre-condition for using these absorption data to validate ocean color satellite products, including pigment biomass indexes and primary productivity. Early efforts to separate absorbing components in natural samples included treatment with organic solvents, UV radiation, and potassium permanganate (references can be found in Shifrin, 1988, and Bricaud and Stramski, 1990).

Methods to partition a_p into its components can be grouped by methodology. Chemical techniques extract or bleach the more labile pigments on the filter, leaving refractory absorbing material behind. The treated filter is scanned again to retrieve a_d, which is then subtracted from a_p to yield a_f (e.g., Kishino et al., 1985, Tassan and Ferrari 1995a). Statistical techniques to decompose total particulate absorption spectra into these two components have been proposed (e.g., Morrow et al., 1989, Bricaud and Stramski 1990, Cleveland and Perry 1994). Mathematical methods are not truly independent since they are typically validated using the results of chemical separation methods. Microspectrophotometric observations of individual particles to estimate each component directly (e.g., Iturriaga et al., 1988; Iturriaga and Siegel 1989), are time consuming and therefore not amenable to routine estimates, but of great value in understanding the details of particle absorption within a sample. Reconstruction of spectra from the concentration of HPLC-determined phytoplankton pigments (e.g., Bidigare et al., 1990) can be used but this method does not directly result in an estimate of non-phytoplankton (detrital) absorption. At the Scripps workshop, an intercomparison of the most commonly used chemical partitioning methods, were evaluated to assess differences and to provide recommendations for common procedures.

Chemical methods are the most widely used as they have the advantages of requiring no specialized equipment (e.g. microspectrophotometer) or assumptions about the spectral nature of component absorption (as is the case in some mathematical methods or HPLC reconstruction). It must be stressed at this point that definitions resulting from partitioning of the total particulate absorption coefficient using chemical or mathematical techniques are purely operational, as any extraction or bleaching technique does not purely select for (or against) phytoplankton pigments. Any non-phytoplankton pigments extracted or bleached in a chemical method would thus result in an overestimation of a_f, while any phytoplankton pigments left on the filter after treatment would result in an overestimation of a_d. Mathematical methods also involve various assumptions leading to un-quantified uncertainties. The a_d spectrum generally has a monotonically increasing absorption with decreasing wavelength usually with a slight exponential form that is flatter than soluble absorption. Since the goal is generally to get an estimate of phytoplankton absorption, if there is a residual chl *a* absorption peak in the red near 675 nm the extraction process should be repeated until the peak disappears. Bleaching of the organic pigments can also be accomplished for situations with difficult to extract pigments including phycobilins or other chemically polar pigments that do not extract well in methanol. Variations of this method include use of hot or boiling methanol and varying extraction times. Use of hot methanol has risks due to flammability, and volatility. If this process is used, extra precautions must be taken.

Extractive methods such as methanol are fundamentally different in action from sodium hypochlorite (NaClO) used to bleach, rather than extract, phytoplankton pigments. Bleaching involves placing a small amount of 0.1% active chlorine solution onto the filter, then rinsing with water. The NaClO oxidizes the pigment molecules, making their light absorption negligible. Water rinses then remove the excess NaClO, whose absorption is negligible above 400 nm but increases steeply below that wavelength. This method was found to be effective in situations where methanol cannot be used, as on cellulose membranes such as the 0.22 micron Millipore filter, or on phycobilins. Also this procedure can be adapted for use with particulate suspensions.

Several chemical methods for extracting pigments from marine particles collected on glass-fiber filters were compared. Test samples included pure cultures of *Thalassiosira weissflogii* (a diatom), *Dunaliella tertiolecta* (a chlorophyte), *Synechococcus* strain WH7805 (a cyanobacterium), and an offshore sample with mixed population including large diatoms. Hot and cold absolute

methanol treatments had similar results for extraction times ranging from 1 to 30 minutes. Methanol and methanol + water treatments failed to extract phycobilins from WH7805 (Figure 8). Bleach (NaClO) treatments succeeded in rapidly removing phycobilin and other pigment absorption but in some cultures and field samples an artifact resembling 'detritus' absorption was also produced in the wavelength range below 400 nm. Independent studies conducted outside the Scripps workshop were consistent with these results.
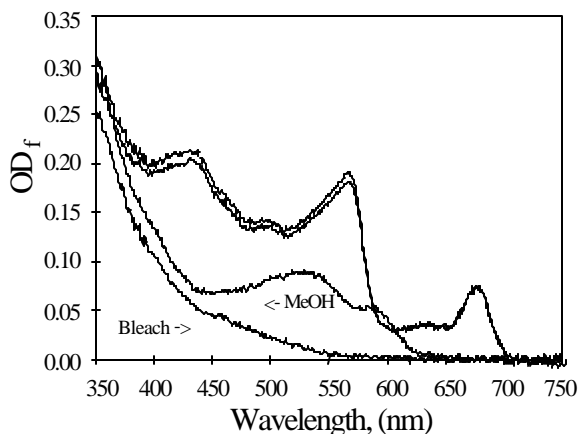

Figure 8. $OD_f(\lambda)$ spectra 350-750 determined at the Scripps Workshop for *Synechococcus sp.* compared to methanol extraction and NaClO oxidation de-pigmentation. OD_f values were set to zero at 750 nm. Phycobiliproteins of the cyano-bacterium do not extract in methanol. Adequate rinsing of the NaClO bleach allows extension of this method below 400 nm.

Neither methanol extraction nor NaClO oxidation provide ideal means of separating particulate absorption into 'algal' and 'detrital' components. In both cases the action of the chemical agents is not well understood, and in many cases is quite different. The decision to apply either the bleaching or methanol extraction method will depend on the situation. For example, for inland waters where either cyanobacteria or chlorophytes are dominant, the bleaching technique will be preferable because of the presence of phycobilins and of extraction resistant algae (e.g. Porra 1990). In coastal oceanic waters the methanol technique will be preferable because results will be comparable to previously published results, and there is no particular advantage to using bleach. In open-ocean samples (e.g. the Sargasso Sea) absorption by phycobilins is small but present in some particulate absorption samples and in methanol-extracted filters (N.B. Nelson unpubl. data). The methanol technique will provide results

which are comparable to earlier studies, but with errors due to incomplete extraction and wavelength shifts in the phycobilin absorption bands.

Modifications of the bleaching procedure based on the results at the Scripps workshop and subsequent work at CEC JRC Ispra (Ferrari and Tassan, 1999) and Bermuda Biological Station has permitted better control of the treatment. In the wavelength range from 400 to 750 nm the agreement between pigment absorption spectra obtained by methanol extraction and NaClO bleaching is generally good. With some phytoplankton types bleaching yields a detritus-like absorption in the 350-400 nm interval higher than that obtained by methanol extraction. This is likely an artifact caused by NaClO-induced reactions, but could also be due to incomplete rinsing of the residual sodium hypochlorite. NaClO bleaching is effective with a very large variety of phytoplankton types (in fact no resistant type has been found so far), including the water-soluble pigments of the cyanobacteria that are poorly extracted by methanol.

All techniques include uncertainties and assumptions not considered in the present studies. For example, resuspension and redistribution of particles from filters when solutions are added may have some effect on the absorption of the sample. Also, changes in the size or shape of the particles on the filter may be induced by the chemical treatments, changing their scattering properties and possibly changing the package effects and β. Finally, it is well known that these techniques do not merely remove the absorption by the primary phytoplankton chlorophylls, carotenoids (and phycobilins in the case of the NaClO technique), but they may also remove absorption by other pigments such as flavins, cytochromes, breakdown products (e.g. phaeophytins and phaeophorbides) and animal pigments. These considerations should be taken into account when interpreting results of chemical separation methods.

Transmission-Reflectance (T-R) Method

Backscattering of light by particles represents an error source for absorption measurements carried out by the routine light-transmission technique (T), leading to an overestimate of the true sample absorption. These errors are partially compensated for OD_f determined in T-mode by subtracting the OD_{null} at a wavelength assumed to have negligible absorption. But as discussed above such assumptions regarding a null point choice may lead to errors of uncertain magnitude. The

backscattering loss, and its spectral dependence depends on the particle size distribution as well as on the type of material (through the refraction index). For medium-to-large phytoplankton cells (3 μm) spectral dependence of scattering is small 300 – 800 nm, but is more significant for small cells (prochlorophytes, heterotrophic bacteria), fine organic detritus and inorganic suspended sediment. Large backscattering is frequently observed with algal species containing inorganic material (e.g. coccolithophores).
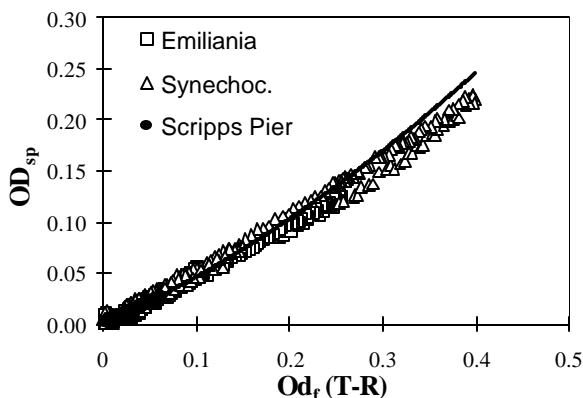

Figure 9. Comparison of the absorbance 400-700 nm for suspensions and filter pads using the T-R method of Tassan and Ferrari (1995) for cultures and concentrated pier water during the SIO Absorption Workshop. Note the coherence of the data compared to Figure 5A. Consideration of both transmittance and reflectance in development of corrections for glass fiber filters can improve methods, especially when particle scattering introduces large errors associated with assignment of a near-IR null point.

A modification of the current light-transmission method that corrects for backscattering was described by Tassan and Ferrari (1995). This technique combines light-transmission (T) and light-reflection (R) measurements, carried out using an integrating sphere attached to the dual-beam spectrophotometer. The data analysis is performed by a theoretical model that eliminates the effect of light backscattering by the particles. The conversion of the optical density of the sample filter measured by the T-R method, into the equivalent optical density of the particle suspension is obtained by means of an empirical correlation that is determined comparing the scattering-free pigment optical densities of particles in suspension and retained on the filter. Because of the risk of NaClO-induced artifacts absorbing below 400 nm, only the $OD(\lambda)$ portion above 440

nm is analyzed for the determination of the correlation (Tassan and Ferrari, 1998). At the Scripps workshop, the global error of the T-R method was comparable to the error yielded by the simpler T method. Subsequent modifications of the T-R experimental routine (Tassan and Ferrari, 1998; Ferrari and Tassan, 1999) yielded a significant reduction of the experimental error. The T-R method is particularly suited for applications to samples containing highly scattering particles that are commonly found in Case 2 waters. Figure 9 illustrates the results for a β relationship using Scripps Pier water with a considerable amount of light-scattering detritus. The T-R method, being more complicated than the T method, is affected by a larger number of error sources that must be considered. Also, since the method requires a high quality spectrophotometer with integrating sphere attachment that is more costly and difficult to maintain during many field campaigns, this method does not yet have the widespread use of the simple T method. Still, to the extent feasible, more investigators should evaluate the advantages of the T-R methods.

12.9 CONCLUSIONS

Spectral absorption and backscattering govern the reflectance of the ocean. In principle, it is trivial to determine absorption coefficients at hyperspectral resolution on water samples with accuracies of 20-30% after appropriate preparation and attention to optical analysis and data processing. Such data is strongly recommended in support of ocean color science to allow a better understanding of ocean reflectance, and for various photochemical and photobiological applications. Standard protocols for determining the absorption by different fractions in seawater are described. Laboratory comparisons of different instruments and procedures at two NASA-sponsored workshops have led to several important conclusions regarding the methods and a set of simple analytical protocols that should ensure consistent data quality if properly implemented.

The demonstration that raw $OD_f(\lambda)$ of replicate samples for many instruments with diverse optical geometries were within 5% (Table 3) implies that investigators can determine raw data that is essentially equivalent using very different configurations. However, some instruments provide significantly different results (e.g. the HP diode array) and the investigator must evaluate raw data of any instrument prior to quantitative work.

A trivial linear transform can convert raw OD_f determined with the HP diode array system to the equivalent optical density of standard spectrophotometers (Figure 4b). More uncertainty is associated with application of the pathlength amplification factor (β) since it may be dependent on particle type that is not known *a priori*. At this time, it is not feasible to accomplish a full error analysis for natural particle assemblages because most studies of β have been carried out on cultures that may not adequately represent the diversity of all particle types of interest. Corrections for β published in the literature generally agree within 20-30%, with the most significant difference reported for *Prochlorococcus* (Table 2). The workshops confirmed previously reported OD-dependence of β, as well as the divergence of β for very small phytoplankton (*Prochlorococcus*) compared to large phytoplankton. The cause of the difference in β for *Prochlorococcus* is still not understood, and may be related to errors in spectral scattering that are not compensated via the null point normalization, differences in the interaction between scattering and absorption within the glass fiber filter or other unresolved issues with the methods.

Soluble absorption estimates are rather simple, but there are serious practical considerations related to creation of appropriate reference water in the field, baseline stability and noise, and assignment of a null value. Long-term storage of samples remains an issue that has been given relatively little attention and no systematic studies have been done on artifacts caused by storage for soluble absorption. To achieve satisfactory results, we recommend that the investigator use a high quality commercial spectrophotometer that achieves specific performance criteria outlined above for the particle and soluble baseline noise, stability, spectral bandwidth, and spectral range. These criteria are trivial to test during instrument demonstrations provided by manufacturers and should be given very high priority in selecting the best unit for the work. All water sample preparations should be analyzed as soon as possible due to artifacts caused by long-term storage.

ACKNOWLEDGEMENTS

REFERENCES

Allali, K., 1997: Variabilité des coefficients d'absorption spécifique du phytoplancton et des pigments photosynthétiques. Aspects méthodologiques et application à des espèces en culture et aux populations naturelles (Pacifique équatorial et Méditerranée) 92 pp

Allali, K., A. Bricaud, M. Babin, A. Morel, and P. Chang, 1995: A new method for measuring spectral absorption coefficients of marine particulates. *Limnology and Oceanography.* **40,** 1,526-1,523

Allali, K., A. Bricaud, and H. Claustre, 1997: Spatial variations in the chlorophyll-specific absorption coefficients of phytoplankton and photosynthetically active pigments in the Equatorial Pacific. *Journal of Geophysical Research.* **102,** 12,413-12,423

Babin, M., A. Morel, H. Claustre, A. Bricaud, Z. Kolber, and P.G. Falkowski, 1996: Nitrogen- and irradiance-dependent variations of the maximum quantum yield of carbon fixation in eutrophic, mesotrophic and oligotrophic marine systems. *Deep-Sea Research I.* **43,** 1,241-1,272

Bidigare, R.R., M.E. Ondrusek, J.H. Morrow, and D. Kiefer, 1990: *In vivo* absorption properties of algal pigments. SPIE, Ocean Optics X. **1302**: 290-302

Bidigare, R.R., R.C. Smith, K.S. Baker, and J. Marra, 1987: Oceanic primary production estimates from measurements of spectral irradiance and pigment concentrations. *Global Biogeochemical Cycles.* **1,** 171-186

Blough, N.V., O.C. Zafiriou, and J. Bonilla, 1993: Optical absorption spectra of waters from the Orinoco River outflow: terrestrial input of colored organic matter to the Caribbean. *Journal of Geophysical Research.* **98,** 2,271-2,278

Bricaud, A., A. Morel, and L. Prieur, 1981: Absorption by dissolved organic matter of the sea (yellow substance) in the UV and visible domains. *Limnology and Oceanography.* **26,** 43-53.

Briaud, A, 1983: Optical efficiency factors of some phytoplankters. *Limnology and Oceanography.* **28,** 816-832

Bricaud, A., and D. Stramski, 1990: Spectral absorption coefficients of living phytoplankton and non-algal biogenous matter: A comparison between the Peru upwelling area and the Sargasso Sea. *Limnology and Oceanography.* **35,** 562-582

Bukata, R.P., J.H. Jerome, K.Y. Kondratyev, and D.V. Pozdnyakov, 1995: Optical properties and remote sensing of inland and coastal waters 362

Butler, W.L., 1962: Absorption of light by turbid materials. *Journal of the Optical Society of America.* **52,** 292-299

Carder, K.L., S.K. Hawes, K.S. Baker, R.C. Smith, and R.G. Steward, 1989: Remote sensing algorithms for discriminating marine humus from chlorophyll. *Limnology and Oceanography.*

Carder, K.L., R.G. Steward, G.R. Harvey, and P.B. Ortner, 1989: Marine humic and fulvic acids: Their effects on remote sensing of ocean chlorophyll. *Limnology and Oceanography.* **34,** 68-81

Chavez, F.P., K.R. Buck, R.R. Bidigare, D.M. Karl, D. Hebel, M. Latasa, L. Campbell, and J. Newton, 1995: On the chlorophyll *a* retention properties of glass-fiber GF/F filters. *Limnology and Oceanography.* **40(2),** 428-433

Cleveland, J.S., and M.J. Perry, 1994: A model for partitioning particulate absorption into phytoplanktonic and detrital components. *Deep-Sea Research.* **41,** 197-221

Cleveland, J.S., and A.D. Weidemann, 1993: Quantifying absorption by aquatic particles: A multiple scattering correctionfor glass-fiber filters. *Limnology and Oceanography.* **38,** 1321-1327

D'Sa, E.J., and S.E. Lohrenz, 1999: Theoretical treatment of fluorescence detection by a dual-fiber-optic sensor with consideration of sampling variability and package effects associated with particles. *Appl.Opt.* **38,** 2,524-2,535

D'Sa, E.J., R.G. Steward, A. Vodacek, N.V. Blough, and D. Phinney, 1999: Determining optical absorption of colored dissolved organic matter in seawater with a liquid capillary waveguide. *Limnology and Oceanography.* **44,** 1,142-1,148

Duntley, S.Q., 1942: The optical properties of diffusing materials. *Journal of the Optical Society of America.* **32,** 61-70

Ferrari, G.M., and S. Tassan, 1996: Use of the 0.22 μm Millipore membrane for light-transmission measurements of aquatic particles. *Journal of Plankton Research.* **18,** 1,261-1,267

Ferrari, G.M, 1999: A method for removal of light absorption by phytoplankton pigments using chemical oxidation. *Journal of Phycology.* **35,** 1,090-1,098

Fry, E.S., 2000: Visible and near-ultraviolet absorption spectrum of liquid water: comments. *Applied Optics.* **39,** 2,743-2,744

Hewes, C.D., and O. Holm-Hansen, 1983: A method for recovering nanoplankton from filters for identification with the microscope: The filter-transfer-freeze (FTF) technique. *Limnology and Oceanography.* **28,** 389-394

Hoge, F.E., A. Vodacek, and N.V. Blough, 1993: Inherent optical properties of the ocean: retrieval of the absorption coefficient of chromophoric dissolved organic matter from fluorescence measurements. *Limnology and Oceanography.* **38,** 1394-1402

Iturriaga, R., and D.A. Siegel, 1989: Microphotometric characterization of phytoplankton and detrital absorption properties in the Sargasso Sea. *Limnology and Oceanography.* **34,** 1,706-1,726

Johnsen, G., N.B. Nelson, R.V.M. Jovine, and B.B. Prézelin, 1994: Chromoprotein- and pigment-dependent modeling of spectral light absorption of two dinoflagellates, *Prorocentrum minimum* and *Heterocapsa pygmaea. Mar Ecol Prog Ser.* **114,** 245-258

Joint Global Ocean Flux Study, 1991: JGOFS Core Measurements Protocol. *JGOFS Report #6, Scientific Committee on Oceanic Research.* 40

Kahru, M., and B.G. Mitchell, 1998: Spectral reflectance and absorption of a massive red tide off Southern California. *Journal of Geophysical Research.* **103,** 21,601-21,609

Kalle, K., 1938: Zum problem der meerwasserfarbe. *Ann.Hydr.u.martim.Meterol.* **66,** 1.S.55-

Kiefer, D.A., R.J. Olson, and W.H. Wilson, 1979: Reflectance spectroscopy of marine phytoplankton. Part 1. Optical properties as related to age and growth rate. *Limnology and Oceanography.* **24,** 664-672

Kiefer, D.A., and J.B. SooHoo, 1982: Spectral absorption by marine particles of coastal waters of Baja California. *Limnology and Oceanography.* **27,** 492-499

Kishino, M., N. Okami, M. Takahashi, and S. Ichimura, 1986: Light utilization efficiency and quantum yield of phytoplankton in a thermally stratified sea. *Limnology and Oceanography.* **31,** 557-566

Kishino, M., N. Takahashi, N. Okami, and S. Ichimura, 1985: Estimation of the spectral absorption coefficients of phytoplankton in the sea. *Bulletin of Marine Science.* **37,** 634-642

Lohrenz, S.E., 2000: A novel theoretical approach to correct for pathlength amplification and variable sampling loading in measurements of particulate spectral absorption by the quantitative filter technique. *Journal of Plankton Research.* **22,** 639-657

Mitchell, B.G. 1990: Algorithms for determining the absorption coefficient of aquatic particulates using the quantitative filter technique (QFT).*Ocean Optics X.* 137-148

Mitchell, B.G., M. Kahru, and P.J. Flatau, 1998: Estimation of spectral values for the mean cosine of the upper ocean. SPIE, Ocean Optics XIV. CD-ROM.

Mitchell, B.G., and D.A. Kiefer 1984: Determination of absorption and fluorescence excitation spectra for phytoplankton.*Marine phytoplankton and productivity.* **8,** 157-169

Mitchell, B.G., 1988a: Chlorophyll *a* specific absorption and fluorescence excitation spectra for light-limited phytoplankton. *Deep-Sea Research I.* **35,** 639-663

Mitchell, B.G.,, 1988b: Variability in pigment specific particulate fluorescence and absorption spectra in the northeastern Pacific Ocean. *Deep-Sea Research I.* **35,** 665-689

Moisan, T.A., and B.G. Mitchell, 1999: Photophysiological acclimation of *Phaeocystis antarctica* Karsten under PAR Light Limitation. *Limnology and Oceanography.* **44,** 247-258

Moore, L.R., R. Goericke, and S.W. Chisholm, 1995: Comparative physiology of *Synechococcus* and *Prochlorococcus*: influence of light and temperature on growth, pigments, fluorescence and absorptive properties. *Marine Ecology Progress Series.* **116,** 259-275

Morrow, J.H., W.S. Chamberlain, and D.A. Kiefer, 1989: A two-component description of spectral absorption by marine particles. *Limnology and Oceanography.* **34,** 1,500-1,509

Nelson, N.B., D.A. Siegel, and A.F. Michaels, 1998: Seasonal dynamics of colored dissolved material in the Sargasso Sea. *Deep-Sea Research.* **45,** 931-957

Neori, A., M. Vernet, O. Holm-Hansen, and F.T. Haxo, 1988: Comparison of chlorophyll far-red and red fluorescence excitation spectra with photosynthetic oxygen action spectra for photosystem II in algae. *Marine Ecology Progress Series.* **44,** 297-302

Peacock, T.G., K.L. Carder, P.G. Coble, and Z.P. Lee, 1994: Long-path spectometer for measuring Gelbstoff absorption in clear waters. *EOS Transactions American Geophysical Union (Supplement).* **75,** 22-22

Pegau, W.S., J.S. Cleveland, W. Doss, C.D. Kennedy, R.A. Maffione, J.L. Mueller, R. Stone, C.C. Trees, A.D. Weidemann, W. Wells, et al. 1995: A comparison of methods for measurement of the absorption coefficient in natural waters. *Journal of Geophysical Research.* **100,** 13,201-13,220

Pegau, W.S., and J.R.V. Zaneveld, 1993: Temperature-dependent absorption of water in the red and near infrared portions of the

spectrum. *Limnology and Oceanography.* **38,** 188-192

Piskozub, J., and D. Stramski, 2000: The use of scattering error in absorption measurement for estimating the scattering phase function of marine phytoplankton. Ocean Optics XV.

Pope, R.M., and E.S. Fry, 1997: Absorption Spectrum (380-700 nm) of Pure Water: II. Integrating Cavity Measurements. *Applied Optics.* **36,** 8,710-8,723

Preisendorfer, R.W., 1961: Application of radiative transfer theory to light measurements in the sea. International Union of Geodesy and Geophysics & International Association of Oceanography. **10**: 83-91

Preisendorfer, R.W., 1976: Hydrologic optics 1. Introduction 2. Foundations 3. Solutions 4. Imbeddings 5. Properties 6. Surfaces 1450

Roesler, C.S., 1998: Theoretical and experimental approaches to improve the accuracy of particulate absorption coefficients derived from the quantitative filter technique. *Limnology and Oceanography.* **43,** 1,649-1,660

Shibata, K., 1958: Spectrophotometry of intact biological materials. Absolute and relative measurments of their transmission, reflection and absorption spectra. *Journal of Biochemistry.* **45,** 599-623

Shifrin, K.S., 1988: Physical optics of ocean water 285

Sosik, H.M., 1999: Storage of marine particulate samples for light-absorption measurements. *Limnology and Oceanography.* **44,** 1,139-1,141

Sosik, H.M., and B.G. Mitchell, 1991: Absorption, fluorescence and quantum yield for growth in nitrogen limited *Dunaliella tertiolecta.* *Limnology and Oceanography.* **36,** 910-921.

Sosik, H.M., 1995: Light absorption by phytoplankton, photosynthetic pigments, and

detritus in the California Current System. *Deep-Sea Research I.* **42,** 1,717-1,748

Stramski, D., 1990: Artifacts in measuring absorption spectra of phytoplankton collected on a filter. *Limnology and Oceanography.* **35,** 1,804-1,809

Tassan, S. and G.M. Ferrari, 1995a: An alternative approach to absorption measurements of aquatic particles retained on filters. *Limnology and Oceanography.* **40,** 1,358-1,368

Tassan, S.,, 1995b: Proposal for the measurement of backward and total scattering by mineral particles suspended in water. *Applied Optics.* **34,** 8,345-8,353

Tassan, S.,, 1998: Measurement of the light absorption by aquatic particulates retained on filters: determination of the optical pathlength amplification by the "Transmittance-Reflectance" method. *Journal of Plankton Research.* **20,** 1,699-1,709

Tassan, S.,, 2000: A sensitivity analysis of the "Transmittance-Reflectance" method for measuring light absorption by aquatic particles retained on filters (Unpublished)

Tassan, S., G.M. Ferrari, A. Bricaud, and M. Babin, 2000: Variability of the amplification factor of light absorption by filter-retained aquatic particles in the coastal environment. *Journal of Plankton Research.* **22,** 659-668

Vodacek, A., N.V. Blough, M.D. DeGrandpre, E.T. Peltzer, and R.K. Nelson, 1996: Seasonal variation of CDOM and DOC in the Middle Atlantic Bight: Terrestrial inputs and photooxidation. *Limnology and Oceanography.* **42,** 674-686

Yentsch, C.S., 1957: A non-extractive method for the quantitative estimation of chlorophyll in algal cultures. *Nature.* **179,** 1302-1304

Yentsch, C.S.,, 1962: Measurement of visible light absorption by particulate matter in the ocean. *Limnology and Oceanography.* **7,** 207-217

Chapter 13

HPLC Phytoplankton Pigments: Sampling, Laboratory Methods, and Quality Assurance Procedures

Robert R. Bidigare[1] and Charles C. Trees[2]

[1] *Department of Oceanography, University of Hawaii, Hawaii*
[2]*Center for Hydro-Optics and Remote Sensing, San Diego State University, California*

13.1 INTRODUCTION

Marine phytoplankton utilize chlorophyll *a* as their major light harvesting pigment for photosynthesis. Other accessory pigment compounds, such as chlorophylls *b* and *c*, carotenoids and phycobiliproteins, also play a significant role in photosynthesis by extending the organism's optical collection window, thereby improving absorption efficiencies and adaptation capabilities. The important chlorophyll degradation products found in the aquatic environment are the chlorophyllides, phaeophorbides, and phaeophytins. The presence, or absence, of the various photosynthetic pigments is used to separate the major algal groups, and to map the chemotaxonomic composition of phytoplankton in the oceans.

The unique optical properties of chlorophyll *a* have been used to develop spectrophotometric (Jeffrey and Humphrey 1975) and fluorometric (Holm-Hansen et al. 1965) measurement techniques. With the commercial availability of fluorometers for routine measurements of chlorophyll *a*, this pigment became a universal parameter in biological oceanography for estimating phytoplankton biomass and productivity. These optical methods can significantly under- or overestimate chlorophyll *a* concentrations, because of the overlap of the absorption and fluorescence bands of co-occurring chlorophylls *b* and *c*, chlorophyll degradation products, and accessory pigments (Trees et al. 1985; Smith et al. 1987; Hoepffner and Sathyendranath 1992; Bianchi et al. 1995; Tester et al. 1995).

The application of HPLC to phytoplankton pigment analysis has lowered the uncertainty for measuring chlorophyll *a* and pheopigments, as well as the accessory pigments, since compounds are physically separated and individually quantified. HPLC has provided oceanographers with a powerful tool for studying the processes affecting the phytoplankton pigment pool. Pigment distribution is useful for quantitative assessment of phytoplankton community composition and zooplankton grazing activity.

For low uncertainty determinations of chlorophylls *a*, *b*, and *c*, chlorophyll degradation products, and carotenoid pigments, HPLC techniques are recommended. It should be noted, however, that the reverse-phase C_{18} HPLC method recommended by the Scientific Committee on Oceanographic Research (SCOR) (Wright et al. 1991) is not capable of separating monovinyl chlorophyll *a* from divinyl chlorophyll *a*, nor monovinyl chlorophyll *b* from divinyl chlorophyll *b*. This method, therefore, only provides estimates of total chlorophyll *a* and total chlorophyll *b* concentrations, respectively. Protocols for optically resolving monovinyl chlorophyll *a* and divinyl chlorophyll *a* are given below.

Divinyl chlorophyll *a*, the major photosynthetic pigment found in *Prochlorococcus,* accounts for 10-60% of the total chlorophyll *a* in subtropical and tropical oceanic waters (Goericke and Repeta 1993, Letelier et al 1993, Andersen et al. 1996, Bidigare and Ondrusek 1996, and Gibb et al. 2000). Divinyl chlorophyll *a* is spectrally different from *normal* (monovinyl) chlorophyll *a* and its presence results in a significant overestimation of total chlorophyll *a* concentration as determined by the conventional HPLC methods (Goericke and Repeta 1993, Letelier et al. 1993, and Latasa et al. 1996). To avoid these errors, it is recommended that monovinyl and divinyl chlorophyll *a* be spectrally resolved, or chromatographically separated, in order to obtain an unbiased determination of total chlorophyll *a* (that is, total chlorophyll *a* equals divinyl chlorophyll *a* plus monovinyl chlorophyll *a*) for the purpose of ground-truthing satellite ocean color algorithms and imagery. These co-eluting

chlorophyll species can be resolved spectrally following C_{18} HPLC chromatography (Wright et al. 1991) and quantified using dichromatic equations at 436 and 450 nm (Latasa et al. 1996). Alternatively, these two chlorophyll species can be separated chromatographically and individually quantified using the C_8 HPLC technique described by Goericke and Repeta (1993). (C_{18} and C_8 designate column-packing materials used in HPLC.)

These protocols specified below for HPLC pigment analyses follow closely those prescribed in the *JGOFS Core Measurement Protocols* (UNESCO 1994). Both sets of protocols include:

1. Use of Whatman GF/F glass fiber filters, approximately 0.7 μm pore size;
2. Extraction in aqueous acetone; and
3. Calibration with authenticated standards.

The present protocols differ from the JGOFS protocols in one critical respect. Absorption of light in seawater, or any other medium, is a volumetric process, even though the volume absorption coefficient may vary with the density of the medium. For ocean color and optical analyses, therefore, the concentrations in seawater of all phytoplankton pigments shall be expressed in units of mass per unit volume of seawater, usually either in μg L^{-1}, or mg m^{-3}. This differs from the JGOFS protocols, which specify that concentrations in seawater of all phytoplankton pigments should be expressed in ng kg^{-1}.

In addition to HPLC analyses, it is recommended that the standard fluorometric methodology used for measuring chlorophylls and pheopigments (Yentsch and Menzel 1963, Holm-Hansen et al. 1965, and Strickland and Parson 1972) also be applied to the same extracted pigment samples used for HPLC analysis. Protocols for fluorometric measurements of chlorophyll *a* and pheopigments are given here in Chapter 21. For a more in depth review of guidelines for measuring phytoplankton pigments in oceanography see Jeffrey et al. (1997)

13.2 SAMPLING PROTOCOLS FOR PHYTOPLANKTON PIGMENTS

Water Samples

Water samples should be taken using Niskin bottles at the site of, and simultaneously with, the surface in-water upwelled radiance and reflectance measurements, and at depth increments sufficient to resolve variability within at least the top optical depth. The K (λ,z), profiles over this layer will be used to compute optically weighted, near-surface pigment concentration for bio-optical algorithm development (Gordon and Clark 1980).

When possible, samples should be acquired at several depths distributed throughout the upper 200 m of the water column [or in turbid water, up to seven diffuse attenuation depths, $\ln((E(\lambda,0)/E(\lambda,z))=7]$, to provide a basis for relating fluorescence signals to pigment mass concentration.

Samples should be filtered as soon as possible after collection. If processing must be delayed (>1 hr), hold samples on ice or at 4°C and protected from exposure to light. Use opaque sample bottles, because even brief exposure to light during sampling and/or storage might alter pigment values.

Filtration

Whatman GF/F glass fiber filters, approximately 0.7 μm pore size, are preferred for removing phytoplankton from water. The glass fibers assist in breaking the cells during grinding, accommodate larger sample volumes, and do not form precipitate forms after acidification. Inert membrane filters, such as polyester filters, may be used when size fraction filtration is required, although it is recommended to also filter a replicate sample through a GF/F to determine the total concentration (summing the various size fractionated concentrations will not produce an accurate estimate of the total, because of the potential for cell disruption during filtration). Twenty-five mm diameter GF/F glass fiber filters should be used with vacuum (7-8 inches of mercury) or positive pressure (1-2 psi). Positive pressure filtration is recommended, because it filters larger volumes of water at reduced filtration times. The only problem with vacuum filtration is that unobservable air leaks may occur around the filtration holder, and as a result the pressure gradient across the filter is much less than what is indicated on the vacuum gauge. When positive filtration is used, any leakage around the filter holder results in observable dripping water.

There has been an ongoing discussion on filter types and retention efficiencies for natural samples. Phinney and Yentsch (1985) showed the inadequacy of GF/F filters for retaining chlorophyll *a* in oligotrophic waters, as did Dickson and Wheeler (1993) for samples from the North Pacific. In response to Dickson and Wheeler (1993), Chavez et al. (1995) compared samples collected in the Pacific Ocean using GF/F and 0.2 μm membrane filters with small filtered volumes (100-

540 mL). Their results showed a very close agreement between the two filter types with GF/F filters having only a slightly positive 5% bias.

Filtration volume can directly affect the retention efficiency for GF/F filters. Particles can be retained by filters through a variety of ways such as filter sieving, filter adsorption, electrostatic and van der Waals attractions, etc. (see the review by Brock 1983). It is known that Whatman GF/F filters can retain particles much smaller than their rated pore size. With Nuclepore filters, when water flows through the pores, streamlines are formed that can align small particles longitudinally (cell diameter becomes important with these filters). Generally, at small volumes (100-300 mL) filter adsorption, and electrostatic and van der Waals attractions are important, whereas at larger volumes (> 2,000 mL) sieving dominates. This has been tested in oligotrophic waters off Hawaii in which small (< 500 mL) and large volumes (> 2-4 liters) retained similar amounts of chlorophyll a, whereas intermediate volumes had lower concentrations. During several cruises off the Hawaiian Islands, differences in retention efficiencies were found for GF/F filters to be a function of sample volume; large sample volumes (2 and 4 liters) retained about 18% more chlorophyll a than replicate 1 liter samples.

Filtration volumes are usually limited by the concentration of particles present in each sample. For HPLC analysis it is important to filter as large of volume as possible so as to accurately measure most of the major pigments. A qualitative check to determine whether a large enough volume has been filtered is to count the number of accessory pigments (chlorophylls b, c_1, c_2, c_3, and carotenoids) quantified, excluding chlorophyll degradation products (Trees et al. 2000). Most algal groups (excluding phycobiliprotein-containing groups) contain at least *four* HPLC-measurable accessory pigments (see Jeffrey et al. 1997). Therefore, pigment samples that do not meet this minimum accessory pigment requirement may have detection limit problems related to low signal-to-noise ratios for the HPLC detectors and/or insufficient concentration techniques (e.g. low filtration volumes). It is recommended that generally the following volumes be filtered for these water types: 3-4 liters for oligotrophic, 1-2 liters for mesotrophic, and 0.5-1 liter eutrophic waters.

It is recommended that seawater samples not be pre-filtered to remove large zooplankton and particles, because this might result in the exclusion of pigment-containing colonial and chain-forming phytoplankton, e.g., diatoms and *Trichodesmium* sp. Large zooplankton can be removed following filtration using forceps.

Sample Handling and Storage

Samples should be filtered as quickly as possible after collection and stored immediately in liquid nitrogen. Liquid nitrogen is the best method for storing samples with minimum degradation for short, as well as, longer storage times (e.g. 1 year). Placing samples in liquid nitrogen also assists in pigment extraction by weakening the cell wall and membrane during this rapid temperature change. Ultra-cold freezers (-90°C) can be used for storage, although they have not been tested for longer than 60 days (Jeffrey et al. 1997). Conventional deep freezers should not be used for storing samples more than 20 hours before transferring them to an ultra-cold freezer, or liquid nitrogen. Again, storage of samples in liquid nitrogen immediately after filtration is the preferred method.

Samples should be folded in half with the filtered halves facing in. This eliminates problems of rubbing particles off the filter during placement in sample containers and storage. The easiest and least expensive sample container is aluminum foil. Cut small pieces of heavy duty aluminum foil into approximately 4 cm squares. Fold this in half and using a fine-point permanent marker write a short sample identifier (e.g. first letter of the cruise and a sequential numbering scheme) on the foil. Writing on the folded foil, prior to placement of the filter, alleviates problems of puncturing the foil with the marking pen, as well as improving the legibility of the sample identifier. Take the folded filter and place it in the aluminum foil. Fold the three open sides to form an envelope that is only slightly larger than the folded filter (~3 cm x 1.5 cm). This protocol will minimize the size requirement of the storage container. Cryogenic tubes or HistoPrep tissue capsules can be used, although they require a larger storage space and unless reused, are expensive as compared to aluminum foil. Information regarding sample identification should be logged in a laboratory notebook.

13.3 LABORATORY METHODS FOR HPLC PHYTOPLANKTON PIGMENT ANALYSIS

Internal Standard and Solvent Preparation.

In addition to daily calibration of the HPLC system with external standards, an internal standard (canthaxanthin) should be used to determine the

extraction volume. The internal standard should be added to the sample prior to extraction and used to correct for the addition of GF/F filter-retained seawater and sample volume changes during extraction. When new external and internal standards are prepared they should be verified against previous standards and a standard reference solution if available. An internal standard with an HPLC peak removed from those of all the pigments, canthaxanthin, is added at a fixed concentration to the HPLC-grade acetone solvent used to extract the pigments from the filtered samples (20.2.2 below). A sample of canthaxanthin spiked acetone solvent is injected into the HPLC system and its peak area A_{STD}^{Cantha} is recorded to provide a baseline internal standard for monitoring the solvent concentration in each extracted sample.

Extraction

Filters are removed from the liquid nitrogen, briefly thawed (~1 min), and placed in glass centrifuge tubes for extraction in acetone. Three mL HPLC-grade acetone is added to each tube, followed by the addition of a fixed volume of internal standard (typically 50 µL canthaxanthin in acetone). Alternatively, canthaxanthin spiked HPLC-grade acetone solvent may be prepared in advance, in a batch large enough for all samples, and 3 mL is added to each tube in a single step. Since GF/F filters retain a significant amount of seawater following filtration (ca. 0.2 mL per 25 mm filter), the final acetone concentration in the pigment extracts is ~ 94% (acetone:water, vol:vol); by measuring the canthaxanthin peak area A_{Sample}^{Cantha} for each sample, the ratio $A_{STD}^{Cantha}/A_{Sample}^{Cantha}$ may be used to adjust for sample to sample variations in the acetone:water ratio. Samples are disrupted by sonication in darkness at $0^{o}C$ and allowed to extract at -20°C for 24 h. Alternatively, the cells can be mechanically disrupted using a glass/Teflon tissue grinder. The ease at which the pigments are removed from the cells varies considerably with different phytoplankton. In all cases, freezing the sample filters in liquid nitrogen improves extraction efficiency. Prior to analysis, pigment extracts are vortexed and centrifuged to minimize cellular debris. To remove fine glass fiber and cellular debris from the extract, as well as enhance the life expectancy of the HPLC column, filter the extract through 13mm PTFE (polytetrafluoroethylene) membrane syringe filters (0.2 µm pore size).

Apparatus

The HPLC system consists of solvent pumps, sample injector, guard and analytical columns, absorption (and fluorescence) detector, and a computer. A temperature-controlled autosampler is optional, but highly recommended, to chill the samples chilled prior to injection and to reduce uncertainties during sample preparation and injection. A variety of companies manufacture HPLC systems (e.g. Beckman, ThermoQuest, Waters Associates). For a review of hardware and software requirements for measuring chlorophylls and their degradation products, as well as carotenoids, see Jeffrey et al. (1997).

HPLC Eluants and Gradient Programs

There are currently two recognized HPLC methods for separating chlorophylls, chlorophyll derivatives and taxonomically important carotenoids.

The first method, which is recommended by SCOR and proposed by Wright et al. (1991), separates more than 50 chlorophylls, carotenoids, and their derivatives using a ternary gradient system. This HPLC method is described in detail in section *20.2.4*. Briefly, pigments are separated on a Spherisorb ODS-2 C_{18} column using a three solvent gradient system [Solvent A: 80:20 methanol: 0.5 M ammonium acetate (v/v); Solvent B: 90:10 acetonitrile: water (v/v); Solvent C: ethyl acetate] at a flow rate of 1 mL min^{-1}. The separation of the various pigments requires about 30 minutes. Prior to injection, 1 mL of the aqueous acetone pigment extract is diluted with 0.3 mL HPLC-grade water to increase the affinity of pigments for the column during the loading step. This results in sharper peaks, allowing greater loading than can be obtained with undiluted samples. This method does not separate monovinyl and divinyl chlorophylls *a* and *b*. The presence of divinyl chlorophylls *a* and *b*, can cause errors if they are not separated either physically on the column, or by a channels ratio method from the monovinyl forms. Latasa et al. (1996) showed that the use of a single response factor (only for monovinyl chlorophyll *a*) could result in a 15-25% overestimation of total chlorophyll *a* concentration if divinyl chlorophyll *a* was present in significant concentrations. Although monovinyl and divinyl chlorophyll *a* co-elute, each compound absorbs differently at 436 nm and 450 nm and it is therefore possible to deconvolve the absorption signals due to these pigments (Latasa et al. 1996).

The second method, which physically separates the monvinyl and divinyl chlorophylls *a* and *b*, chlorophyll derivatives and carotenoids, is that of Goericke and Repeta (1993). Pigments are separated on a C_8 column using a linear binary solvent gradient using the following solvents: Solvent A: 75:25 methanol: 0.5 N ammonium acetate (v/v) and Solvent B: methanol. This method is not recommended under the present protocols, and it will not be discussed further.

Determination of Algal Chlorophyll and Carotenoid Pigments by HPLC (Wright et al. 1991):

a. Equipment and reagents:

1. *Reagents*: HPLC grade acetone (for pigment extraction); HPLC-grade water, methanol, acetonitrile and ethyl acetate; 0.5 M ammonium acetate aq. (pH = 7.2); and BHT.
2. *High-pressure injector valve* equipped with a 200 μL sample loop.
3. *Guard-column* (50 x 4.6 mm, ODS-2 Spherisorb C_{18} packing material, 5 μm particle size) for extending life of primary column.
4. *Reverse-phase HPLC column* with endcapping (250 x 4.6 mm, 5 μm particle size, ODS-2 Spherisorb C_{18} column).
5. *Variable wavelength or filter absorbance detector* with low volume flowthrough cell. Detection wavelengths are 436 and 450 nm.
6. *Data recording device*: strip chart recorder or, preferably, an electronic integrator or computer equipped with hardware and software for chromatographic data analysis.
7. *Glass syringe (500 mL) or HPLC autosampler.*
8. *HPLC Solvent*: solvent A (80:20, v:v; methanol:0.5 M ammonium acetate aq., pH=7.2; 0.01% BHT, w:v), solvent B (87.5:12.5, v:v; acetonitrile:water; 0.01% BHT, w:v) and solvent C (ethyl acetate). Use HPLC-grade solvents. Measure volumes before mixing. Filter solvents through a solvent resistant 0.4 μm filter before use and degas with helium.
9. *Calibration standards*: Chlorophylls *a* and *b* and β, β-carotene can be purchased from Sigma Chemical Co. (St. Louis, MO 63178, USA). Other pigment standards

can purchased from the International Agency for [14]C Determination, VKI Water Quality Institute, Agern Allé 11, DK-2970 HØrsholm, Denmark. The concentration of all standards should be determined using a monochromator-based spectrophotometer in the appropriate solvents prior to calibration of the HPLC system (see Latasa et al. 1999). The recommended extinction coefficients for the various phytoplankton pigments can be found in Appendix E of Jeffrey et al. (1997). Absorbance is measured in a 1 cm cuvette at the appropriate wavelength (usually at λ_{max}) and 750 nm (to correct for light scattering).

Concentrations of the standards are calculated as follows:

$$C^i_{STD} = \frac{10^6 g[A^i(\lambda^i_{max}) - A^i(750)]}{b g E^i_{1cm}}. \qquad (13\text{-}1)$$

where C^i_{STD} is the concentration (μg L^{-1}) of the standard for pigment *i*, $A^i(\lambda^i_{max})$ and $A^i(750)$ are absorbances at λ^i_{max} and 750 nm, respectively, b is the pathlength of the cuvette (cm), and E^i_{1cm} is the weight-specific absorption coefficient (L g^{-1} cm^{-1}) of pigment *i*. Values for λ^i_{max} and E^i_{1cm} are given in Appendix E of Jeffrey et al. (1997). Standards stored under nitrogen in the dark at -20°C are stable for about one month.

b. Procedure:

1. Set up and equilibrate the HPLC system with eluant A at a flow rate of 1 mL min^{-1}.
2. Calibrate the HPLC system using working standards prepared, on the day of use, by diluting the primary standard with the appropriate solvent (Jeffrey et al. 1997, Appendix E). Prepare at least 5 concentrations (μg L^{-1}) of working standards for each pigment spanning the concentration range appropriate for the samples to be analyzed.
3. For each working standard, mix 1000 μL with 300 λL of distilled water, shake, and equilibrate for 5 min prior to injection (diluting the standards and sample extracts with water increases the affinity of pigments for the column in the loading step, resulting in an improved separation of the more polar pigments). Rinse the sample syringe twice

with 300 µL of the diluted working standard and draw 500 µL of the working standard into the syringe for injection. Place the syringe in the injector valve, overfilling the 200 µL sample loop 2.5-fold. To check for possible interferences in the extraction solvent and/or filter, prepare a blank by extracting a glass fiber filter in 90% acetone, mixing 1000 µL of the 90% acetone filter extract and 300 µL distilled water, and injecting the mixture onto the HPLC system. For each pigment i, plot absorbance peak areas (arbitrary system units) against working standard pigment masses (concentrations multiplied by injection volume). The HPLC system response factor F^i (area μg^{-1}) for pigment i is calculated as the slope of the regression of the peak areas of the parent pigment (plus areas of peaks for structurally-related isomers if present) against the pigment masses of the injected working standards (µg). Structurally related isomers (e.g. chlorophyll a allomer) contribute to the absorption signal of the standards and disregarding them will result in the over-estimation of analytes in sample extracts (Bidigare 1991).

4. Prepare pigment samples for injection by mixing a 1000 µL portion of the aqueous acetone pigment extract and 300 µL distilled water, shake, and equilibrate for 5 min prior to injection. Inject the sample onto the HPLC column.

5. Following injection of the sample onto the HPLC system, use a gradient program to optimize the separation of chlorophyll and carotenoid pigments. The system described in Table 13.1 has been modified from the Wright et al. (1991) method to assure elution of the most hydrophobic pigments. Degas the solvent system with helium during analysis.

6. Peak identities are routinely determined by comparing the retention times of sample peaks with those of pure standards. Peak identities can be confirmed spectrophotometrically by collecting eluting peaks from the column outlet (or directly with an on-line diode array spectrophotometer). Absorption maxima for the various phytoplankton pigments can be found in Part IV of Jeffrey et al. (1997).

7. Calculate individual pigment concentrations as

$$C_{Sample}^{i} = \frac{A_{Sample}^{i} \cdot V_{Extracted} \cdot A_{STD}^{Cantha}}{V_{Injected} \cdot F^{i} \cdot V_{Sample} \cdot A_{Sample}^{Cantha}}. \qquad (13\text{-}2)$$

where C_{Sample}^{i} is the individual pigment concentration (µg L^{-1}), A_{Sample}^{i} is the area of individual pigment peak for a sample injection, $V_{Extracted}$ is the volume extracted (mL, to nearest 0.1 mL), $V_{Injected}$ is the volume injected (mL, measured to the nearest 0.001 mL), V_{Sample} is the sample volume filtered (L, measured to the nearest 0.001 L), and the other coefficients are defined above.

8. This method is designed for the separation of chlorophyll and carotenoid pigments, however, it is also capable of separating the major chlorophyll breakdown products.

9. The precision of the HPLC method was assessed by performing triplicate injections of a mixture of phytoplankton and plant extracts, and coefficients of variation (standard deviation/mean x 100%) ranged from 0.6 to 6.0%. The use of an appropriate internal standard will increase precision.

13.4 QUALITY ASSURANCE PROCEDURES

Quality assurance (QA) procedures outlined here should be routinely employed to insure accurate, precise and representative results. A selected number of samples should be analyzed in duplicate (or triplicate) to assess representativeness and uncertainty in the method and instrumentation. Some fortified samples should be analyzed as part of the QA effort. Fortified samples are prepared in duplicate by spiking a sample with known quantities of the analytes of interest at concentrations within the range expected in the samples. Fortified samples are used to assess the method's uncertainty in the presence of a typical sample matrix. In addition, system and spiked blanks should be routinely analyzed. A system blank consists of a filter, reagents, and the glassware and hardware utilized in the analytical scheme. The system blank is quantified under identical instrumental conditions as the samples and is analyzed by appropriate quantitative methods.

The system blank may not contain any of the analytes of interest above the MDL (see below) or corrective action is taken. A spiked blank is defined as a system blank plus an authentic external standard containing the analytes of interest. Each set of samples should be accompanied by a spiked blank and is quantified under the same instrumental conditions as the samples.

Table 13.1   HPLC solvent programs (after Wright et al. 1991)

Time (min)	Flow Rate (mL min^{-1})	%A	%B	%C	Conditions
A. Analysis Protocol					
0.0	1.0	100	0	0	Injection
2.0	1.0	0	100	0	Linear gradient
2.6	1.0	0	90	10	Linear gradient
13.6	1.0	0	65	35	Linear gradient
18.0	1.0	0	31	69	Linear gradient
23.0	1.0	0	31	69	Hold
25.0	1.0	0	100	0	Linear gradient
26.0	1.0	100	0	0	Linear gradient
34.0	1.0	100	0	0	Hold
B. Shutdown Protocol					
0	1.0	100	0	0	Analysis complete
3.0	1.0	0	100	0	Linear gradient
6.0	1.0	0	0	100	Linear gradient
16.0	1.0	0	0	100	Washing
17.0	1.0	0	0	100	Shutdown

In multi-ship/investigator studies, replicate samples should be collected and archived for future intercalibration checks. If desired, the method detection limit (MDL) for the analytes of interest can be determined by seven replicate standard injections (Glaser et al. 1981). The standard deviation of the seven replicate measurements is calculated and the MDL is computed as

$$MDL = t\left(N\text{-}1, 1\text{-}\boldsymbol{a} = 0.99\right) * S_c. \qquad (13\text{-}3)$$

where $t\left(N\text{-}1, 1\text{-}\boldsymbol{a} = 0.99\right)$ is the student's t value for a one-tailed test at the 99% confidence level with N-1 degrees of freedom and S_c is the standard deviation of the seven replicate analyses.

REFERENCES

Andersen, R.A., R.R. Bidigare, M.D. Keller, and M. Latasa, 1996: A comparison of HPLC pigment signatures and electron microscopic observations for oligotrophic waters of the North Atlantic and Pacific Oceans. *Deep-Sea Res. II*, **43** ,517-537.

Bianchi, T. S., C. Lambert, and D. C. Biggs. 1995: Distribution of chlorophyll *a* and pheopigments in the northwestern Gulf of Mexico: a comparison between fluorometric and high-performance liquid chromatography measurements. *Bull. Mar. Science* **56** ,25-32.

Bidigare, R.R., 1991: Analysis of algal chlorophylls and carotenoids. In: *Marine Particles: Analysis and Characterization*, D.C. Hurd and D.W. Spencer, Eds., Am. Geophys. Union, Washington, DC, 119-123.

Bidigare, R.R., and M.E. Ondrusek, 1996: Spatial and temporal variability of phytoplankton pigment distributions in the central equatorial Pacific Ocean. *Deep-Sea Res. II*, **43**, 809-833.

Brock, T.D., 1983: *Membrane filtration: a user's guide and reference manual*. Science Tech., Madison, WI, 381 pp.

Chavez, F., K.R. Buck, R.R. Bidigare, D.M. Karl, D. Hebel, M. Latasa, L. Campbell, and J. Newton, 1995: On the chlorophyll *a* retention properties of glass-fiber GF/F filters. *Limnol. Oceanogr.*, **40**, 428-433.

Dickson, M.-L., and P.A. Wheller, 1993: Chlorophyll *a* concentrations in the North Pacific: Does a latitudinal gradient exist? *Limnol. Oceanogr.*, **38**, 1813-1818.

Gibb, S.W, R.G. Barlow, D.G. Cummings, N.W. Rees, C.C. Trees, P. Holligan and D. Suggett, 2000: Surface phytoplankton pigment distribution in the Atlantic: an assessment of basin scale variability between 50°N and 50°S. Progress in Oceanography (in press).

Glaser, J.A., D.L. Foerst, G.D. McKee, S.A. Quave, and W.L. Budde, 1981: Trace analyses for wastewaters. *Environ. Sci. Technol.,* **15**, 1426-1435.

Goericke, R., and D.J. Repeta, 1993: Chlorophylls *a* and *b* and divinyl chlorophylls and in the open subtropical North Atlantic Ocean. *Mar. Ecol. Prog. Ser.*, 10, 307-313.

Gordon, H.R., and D.K. Clark, 1980: Remote sensing optical properties of a stratified ocean: an improved interpretation. *Appl. Optics*, **19,** 3,428-3,430.

Hoepffner, N., and S. Sathyendranath, 1992: Bio-optical characteristics of coastal waters: absorption spectra of phytoplankton and pigment distribution in the western North Atlantic. *Limnol. Oceanogr.* **37**,1660-1679.

Holm-Hansen, O., C.J. Lorenzen, R.W. Holmes, and J.D.H. Strickland, 1965: Fluorometric determination of chlorophyll. *J. du Cons. Intl. Pour l'Expl. de la Mer.,***30**, 3-15.

Jeffrey, S.W., and G.F. Humphrey, 1975: New spectrophotometric equations for determining chlorophylls *a*, *b*, c_1 and c_2 in higher plants, algae and natural phytoplankton. *Biochem. Physiol. Pflanzen*, **167**, 191-194.

Jeffrey, S.W., R.F.C. Mantoura, and S.W. Wright (eds.), 1997: *Phytoplankton Pigments in Oceanography*, Monographs on Oceanographic Methodology, UNESCO, 661 pp.

Latasa, M., R. R. Bidigare, M. E. Ondrusek, and M. C. Kennicutt II, 1996: HPLC analysis of algal pigments: A comparison exercise among laboratories and recommendations for improved analytical performance. *Mar. Chem.*, **5**_1_, 315-324.

Latasa, M., R. R. Bidigare, M. E. Ondrusek, and M. C. Kennicutt II, 1999: On the measurement of pigment concentrations by monochromator and diode-array spectrophotometers. *Mar. Chem.,* **66**, 253-254.

Letelier, R.M., R.R. Bidigare, D.V. Hebel, M.E. Ondrusek, C.D. Winn, and D.M. Karl, 1993: Temporal variability of phytoplankton community structure at the U.S.-JGOFS time-series Station ALOHA ($22^0$45'N, 158^0W) based on HPLC pigment analysis. *Limnol. Oceanogr.*, **38**, 1,420-1,437.

Phinney, D.A., C.S. Yentsch, 1985: A novel phytoplankton chlorophyll technique: Toward automated analysis. *J. Plankton Res.*, **7**, 633-642.

Smith, R. C., R. R. Bidigare, B. B. Prezelin, K. S. Baker, and J. M. Brooks, 1987: Optical characterization of primary productivity across a coastal front. *Mar. Biol.* **96**, 575-591.

Strickland, J.D.H., and T.R. Parsons, 1972: *A Practical Handbook of Sea Water Analysis,* Fisheries Research Board of Canada, 310 pp.

Tester, P. A., M. E. Geesey, C. Guo, H. W. Paerl, and D. F. Millie, 1995: Evaluating phytoplankton dynamics in the Newport River estuary (North Caroline, USA) by HPLC-derived pigment profiles. *Mar. Ecol. Prog. Ser.* **124**, 237-245.

Trees, C.C., M.C. Kennicutt II, and J.M. Brooks, 1985: Errors associated with the standard fluorometric determination of chlorophylls and pheopigments. *Mar. Chem.*, **17**, 1-12.

Trees, C.C., D.K. Clark, R.R. Bidigare, M.E. Ondrusek, and J.L. Mueller, 2000: Accessory pigments versus chlorophyll *a* concentrations within the euphotic zone: a ubiquitous relationship. *Limnol. Oceanogr.* (in press).

UNESCO, 1994: Protocols for the Joint Global Ocean Flux Study (JGOFS) Core Measurements, Manual and Guides 29, 170pp.

Wright, S.W., S.W. Jeffrey, R.F.C. Mantoura, C.A. Llewellyn, T. Bjornland, D. Repeta, and N. Welschmeyer, 1991: Improved HPLC method for the analysis of chlorophylls and carotenoids from marine phytoplankton. *Mar. Ecol. Prog. Ser.,* **77**, 183-196.

Yentsch, C.S., and D.W. Menzel, 1963: A method for the determination of phytoplankton, chlorophyll, and phaeophytin by fluorescence. *Deep-Sea Res.,* **10**, 221-231.

Chapter 14

Fluorometric Chlorophyll *a*: Sampling, Laboratory Methods, and Data Analysis Protocols

Charles C. Trees[1], Robert R. Bidigare[2], David M. Karl[2] and Laurie Van Heukelem[3]

[1]*Center for Hydro-Optics & Remote Sensing, San Diego State University, California*
[2] *Department of Oceanography, University of Hawaii, Hawaii*
[3]*Horn Point Laboratory, University of Maryland Center for Environmental Science, Horn Point, Maryland*

14.1 INTRODUCTION

In addition to HPLC analyses, it is recommended that the standard fluorometric methodology used for measuring chlorophylls and pheopigments also be applied to (i) the same extracted pigment samples used for HPLC analysis, and (ii) additional independent samples. Analysis of fluorometric chlorophyll *a* concentration is a far simpler procedure than HPLC analysis, especially at sea. On a given research cruise, therefore, it is economically feasible to acquire and process many more fluorometric than HPLC samples and to statistically relate fluorometric and HPLC chlorophyll a concentrations using linear regression analysis. This additional analysis will also enable a direct link to the historical bio-optical algorithms and database development during the CZCS validation experiments.

Protocols for fluorometric determination of the concentrations of chlorophyll and pheopigments were developed initially by Yentsch and Menzel (1963) and Holm-Hansen et al. (1965), and are described in detail by Strickland and Parsons (1972). Holm-Hansen et al. (1965) and Strickland and Parsons (1972) used first principles of fluorescence spectroscopy to derive these fluorometric equations. The equation proposed by Yentsch and Menzel (1963) is only indirectly linked to first principles, through debatable assumptions, and its use is not recommended. Although these measurements have been shown to contain errors as compared to HPLC determinations (Trees et al. 1985; Smith et al. 1987; Hoepffner and Sathyendranath 1992; Bianchi et al. 1995; Tester et al. 1995), the CZCS phytoplankton pigment concentration algorithms were based on them entirely. The SeaWiFS protocols for this analysis will be those given in Strickland and Parsons (1972) as updated by this protocol.

Pigment databases generally show a log-normal distribution, which is consistent with that proposed by Campbell (1995) for bio-optical properties. Therefore, it is appropriate to perform log-linear regressions on HPLC determined total chlorophyll *a* (chlorophyllide *a*, chlorophyll *a* epimer, chlorophyll *a* allomer, monovinyl chlorophyll *a* and divinyl chlorophyll *a*) and fluorometrically determined chlorophyll, using model I regressions. Standard Model I regressions were selected because HPLC determined total chlorophyll *a* concentrations are to be predicted from fluorometrically determined chlorophyll [Model I regressions are appropriate for both predictions and determining functional relationships, whereas Model II regressions should not be used to predict values of y given x (page 543, Sokal and Rohlf, 1995)]. Examples of regression models predicting log HPLC total chlorophyll *a* (following Chapter 20 HPLC protocols) from log fluorometric chlorophyll *a* for three cruises in different geographic areas are shown in Figures. 14.1, 14.2, and 14.3. There are statistically significant differences, although for the Gulf of California (GoCal November 1996, Figure 14.3) there seems to be a reasonably good agreement. One to one ratios have been found for other geographic areas, although it can have a seasonal cycle within each area. Therefore, the offset between HPLC total chlorophyll *a* and fluorometric chlorophyll must be determined for a selected number of samples for each cruise, so that a scaling factor can be applied to other fluorometric samples, if necessary.

Absorption of light in seawater, or any other medium, is a volumetric process, even though the volume absorption coefficient may vary with the density of the medium. For ocean color and optical analyses, therefore, the concentration of chlorophyll a shall be expressed in units of mass per unit volume of seawater, either in $\mu g\ L^{-1}$, or mg m^{-3}.

This differs from the JGOFS protocols, which specify that concentrations in seawater of chlorophyll a and pheopigments should be expressed in $\mu g \, kg^{-1}$.

14.2 SAMPLING ACQUISITION AND STORAGE

Water samples should be taken using Niskin bottles or equivalents at the site of, and simultaneously with, the surface in-water upwelled radiance and reflectance measurements, and at depth increments sufficient to resolve variability within at least the top optical depth.
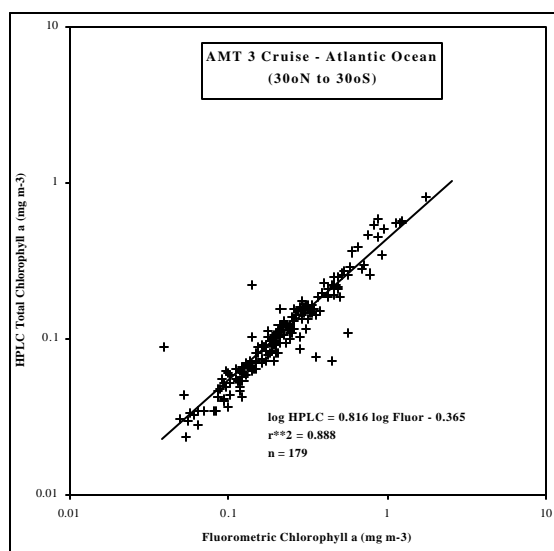
Figure 14.1 Comparisons between fluorometrically determined chlorophyll and HPLC determined total chlorophyll *a* (chlorophyllide *a*, chlorophyll *a* epimer, chlorophyll *a* allomer, monovinyl chlorophyll *a*, and divinyl chlorophyll *a*) from samples collected during Atlantic Meridional Transect 3 cruise (30°N to 30°S, October 1996).

The K(z), profiles over this layer will be used to compute optically weighted, near-surface pigment concentration for bio-optical algorithm development (Gordon and Clark 1980). When possible, samples should be acquired at several depths distributed throughout the upper 200 m of the water column [or in turbid water, up to seven diffuse attenuation depths, $\ln((E(0)/E(z))=7]$, to provide a basis for relating fluorescence signals to pigment mass concentration.

Samples should be filtered as soon as possible after collection. If processing must be delayed (>1 hr), hold samples on ice or at 4°C and protected

from exposure to light. For periods longer than several hours, the samples should be stored in liquid nitrogen. Use opaque sample bottles, because even brief exposure to light during sampling and/or storage might alter pigment values.
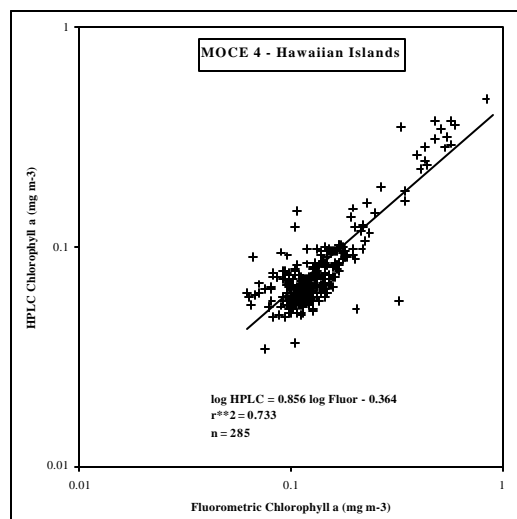
Figure 14.2 Same as Figure 14.1 for data collected during the Marine Optical Characterization Experiment (MOCE) 4 cruise.
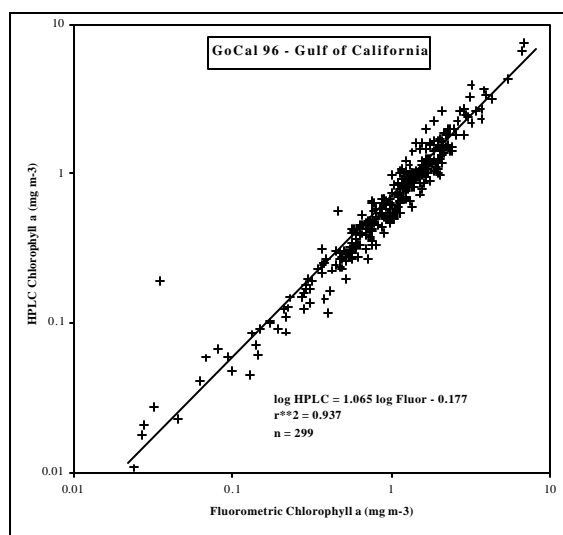
Figure 14.3 Same as Figure 14.1 for data collected during the Gulf of California cruise (Gulf of California, November 1996).

Filtration

Whatman GF/F glass fiber filters, approximately 0.7 μm pore size, are preferred for removing phytoplankton from water. The glass fibers assist in breaking the cells during grinding

and no precipitate forms after acidification. Inert membrane filters, such as polyester filters, may be used when size fraction filtration is required. In addition, it is also recommended to filter a replicate sample through a GF/F to determine the total concentration (summing the various size fractionated concentrations may not produce an accurate estimate of the total, because of the potential for cell disruption during filtration). Twenty-five mm diameter GF/F glass fiber filters should be used with a vacuum or positive pressure with a pressure differential equivalent to 180-200 mm of mercury. Large filtration volumes are not required, because of the increased sensitivity of the fluorescence measurement.

There has been an ongoing discussion on filter types and retention efficiencies for natural samples. Phinney & Yentsch (1985) showed the inadequacy of GF/F filters for retaining chlorophyll a in oligotrophic waters, as did Dickson and Wheeler (1993) for samples from the North Pacific. In response to Dickson and Wheeler (1993), Chavez et al. (1995) compared samples collected in the Pacific Ocean using GF/F and 0.2 μm membrane filters with small filtered volumes (100-540 mL). Their results for small volumes showed a very close agreement between the two filter types with GF/F filters having only a slightly positive 5% bias.

Filtration volume can directly affect the retention efficiency for GF/F filters. Particles can be retained by filters through a variety of ways, such as filter sieving, filter adsorption, electrostatic and van der Waals attractions (Brock, 1983). It is known that Whatman GF/F filters can retain particles much smaller than their rated pore size. With Nuclepore filters, when water flows through the pores, streamlines are formed that can align small particles longitudinally (cell diameter becomes important with these filters). Generally, at small volumes (100-300 mL) filter adsorption, and electrostatic and van der Waals attractions are important, whereas at larger volumes (> 2,000 mL) sieving dominates. This has been tested in oligotrophic waters off Hawaii in which small (< 500 mL) and large volumes (> 2-4 liters) retained similar amounts of chlorophyll a, whereas intermediate volumes had lower concentrations. As a general rule, it is recommended that the following volumes be filtered for these water types: 0.5-1.0

liter for oligotrophic, 0.2-0.5 liter for mesotrophic, and 0.1 liter and less for eutrophic water.

It is recommended that seawater samples not be pre-filtered to remove large zooplankton and particles as this might result in the exclusion of pigment-containing colonial and chain-forming phytoplankton, e.g., diatoms and *Trichodesmium* sp. Large zooplankton should be removed following filtration using forceps.

Sample Handling, and Storage

Samples should be filtered as quickly as possible after collection and stored immediately in liquid nitrogen. Liquid nitrogen is the best method for storing samples with minimum degradation for short, as well as, longer storage times (e.g. 1 year). Placing samples in liquid nitrogen also assists in pigment extraction by weakening the cell wall and membrane during this rapid temperature change. Ultra-cold freezers (-90°C) can be used for storage, although they have not been tested for longer than 60 days (Jeffrey et al. 1997). Conventional deep freezers should not be used for storing samples more than 20 hours before transferring them to an ultra-cold freezer, or liquid nitrogen. Again, storage of samples in liquid nitrogen immediately after filtration is the preferred method. The addition of $MgCO_3$ at the end of the filtration process to stabilize chlorophyll has not been used for many years as a routine oceanographic method, because of the uncertainty in pigment absorption by $MgCO_3$.

If samples are to be stored for any length of time prior to fluorometric analysis, they should be folded in half with the filtered halves facing in. This eliminates problems of rubbing particles off the filter during placement in sample containers and storage. The easiest and least expensive sample container is aluminum foil. Cut small pieces of heavy-duty aluminum foil into approximately 4 cm squares. Fold this in half and using a fine-point permanent marker write a short sample identifier (e.g. first letter of the cruise and a sequential numbering scheme) on the foil. Writing on the folded foil, prior to placement of the filter, alleviates problems of puncturing the foil with the marking pen, as well as improving the legibility of the sample identifier. Take the folded filter and place it in the aluminum foil. Fold the three open

sides to form an envelope that is only slightly larger than the folded filter (~3cm x 1.5cm).

This protocol will minimize the size requirement of the storage container. Cryogenic tubes, or HistoPrep tissue capsules, can be used, although they require a larger storage space, and unless reused, are more expensive than aluminum foil. If fluorometric analysis is to be done soon after collection, it is still recommended to place the samples in liquid nitrogen to assist in pigment extraction and then place them immediately in chilled 90% acetone.

Recordkeeping

Information regarding sample identification should be logged in a laboratory notebook with the analyst's initials. For each filter sample record the sample identifier (as written on the sample container), station number for the cruise, water volume filtered (V_{FILT}) in mL, and depth of the water sample, together with the date, time, latitude, and longitude of the bottle cast during which the sample was acquired.

14.2 LABORATORY METHODS FOR FLUOROMETRIC DETERMINATION OF CHL. *a* AND PHEOPIGMENT CONCENTRATIONS

Chlorophyll and pheopigments can be determined using either a Turner Designs (or Sequoia) fluorometers equipped with the standard light sources and Corning excitation and emission filters, following the manufacture's recommendation for measuring extracted chlorophyll. The fluorometric instrument should be warmed-up for at least 30 to 45 minutes prior to making measurements. Because of the acidification requirement for the standard fluorometric method (Holm-Hansen et al., 1965), differences in excitation and emission wavelength bands between fluorometers can produce uncertainties (Trees et al., 1985). The sensitivity of an instrument to differentiate between chlorophyll and pheopigment, which is a function of the excitation wavelength, is measured during calibration of the fluorometer

and is called the tau factor (τ). Saijo and Nishizawa (1969) have shown that τ can vary from 1 to 11.5, depending upon the excitation wavelength (410-440 nm). A comparison between Turner Designs analog (Model 10-005R) and Turner Designs digital (Model 10-AU-005, Black) fluorometers showed statistically significant differences for 42 oceanic samples (slope = 1.06), even though both were calibrated with exactly the same standards (Figure 14.4). Obviously, there were some differences in the excitation bands for the two fluorometers.

Fluorometer Calibrations

Bench fluorometers used to measure concentrations of extracted chlorophyll and pheopigments should be calibrated using authentic chlorophyll *a* standards as prescribed in the HPLC Protocols. Chlorophyll *a* can be purchased from Sigma Chemical Co. (St. Louis, MO 63178, USA). The concentration of the standard, in the appropriate solvent, must be determined using a monochromator-based spectrophotometer prior to calibration of the fluorometer. The recommended extinction coefficient for chlorophyll *a* in several solvents can be found in Appendix E of Jeffrey et al. (1997). Absorbance is measured in a 1 cm cuvette at the peak wavelength λ_{max} and 750 nm (to correct for light scattering). The bandwidth of the spectrophotometer should be between 0.5 and 2 μm with the standard concentration beign such that the absorbance value ranges between 0.08 to 1.0 optical density. Concentration of the standard is calculated as follows:

$$C_{STD} = \frac{10^6[A(\lambda_{max}) - A(750)]}{b \ x \ E_{1cm}}, \qquad (14.1)$$

where C_{STD} is the concentration (μg L^{-1}) of the chlorophyll *a* standard, $A(\lambda_{max})$ and $A(750)$ are absorbances at λ_{max} and 750 nm, b is the pathlength of cuvette (cm), and E_{1cm} is the specific absorption coefficient (L g^{-1} cm^{-1}) of chlorophyll *a* in 90% acetone. For 90% acetone E_{1cm} =87.67 L g^{-1} cm^{-1}, and for 100% acetone E_{1cm} =88.15 L g^{-1} cm^{-1}, when applied to the absorption measured at the peak wavelength λ_{max} (Jeffrey et al 1997, Appendix E). The peak wavelength λ_{max} must be determined by inspection of the measured spectrum, because its shift results from interactions

between the particular solvent and pigment compounds measured. Standards stored under nitrogen in the dark at -20^oC are stable for about one month. If the fluorometer has been shipped for a cruise, or if it has been unused for several weeks, it is strongly recommended that it be recalibrated with an authentic chlorophyll *a* standard. The use of solid standards, like those provided by Turner Designs and others, can only provide a check for instrumental drift. They cannot be used as primary pigment standards. The stock chlorophyll *a* standard, with its concentration measured on a spectrophotometer as described above, should be diluted using calibrated gas-tight syringes, and Class A volumetric pipettes and flasks. The minimum number of dilutions of the stock standard for calibrating a fluorometer depends on whether it is a digital model (Turner Designs 10-AU-005), or it is an analog model with a mechanical mode (e.g. Turner Designs 10-005) for changing sensitivity. A minimum of 5 dilutions is required for calibrating a digital fluorometer. Fluorometers with a variety of door settings, such as the Turner Designs Model 10-005, must be calibrated for each door setting using at least three standard concentrations per door. The diluted standard pigment concentrations used in calibrating the fluorometer must bracket the range of concentrations found in the samples being analyzed.
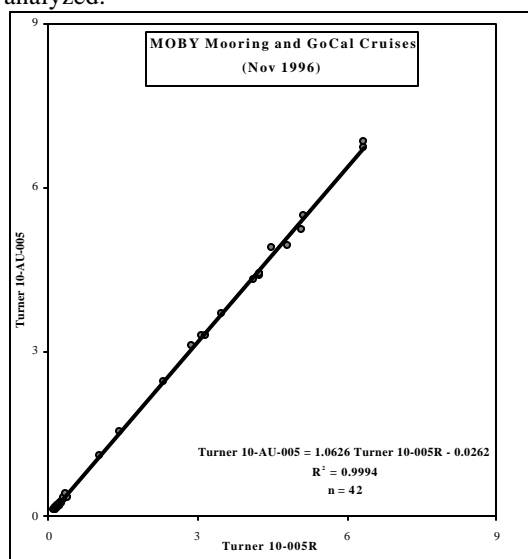
Figure 14.4   Comparison of fluorometrically determined chlorophyll a using the VisLab Turner Fluorometer (10-005R) and the Moss Landing Marine Laboratory Turner Fluorometer (10-AU-005). Samples were analyzed from a MOBY Nov 96 cruise and a Gulf of California cruise (Mueller, Nov 96).

Each diluted chlorophyll *a* standard is placed in the fluorometer and the signal (F_b) is recorded, after waiting a short period of time (60 seconds) for it to stabilize.   The standard is removed and diluted HCL acid (2 drops of 5%, or 1 drop of 10%) is added and mixed within the test tube. The tube is then placed back into the fluorometer, and after stabilization, the acidified fluorescence signal (F_a) is recorded.   Following acidification of the chlorophyll *a* standard, the fluorescence signal stabilizes relatively quickly. This is not the case for natural samples that contain a mixture of pigment compounds, however, and stabilization time may vary from sample to sample. Stabilization time has to be the same for both pigment standards and for natural samples. To minimize this source of uncertainty, and to standardize this measurement technique, it is recommended that both acidified natural sample and acidified pigment standards be allowed to react with the acid for one minute prior to recording the acidified fluorescence signal (F_a). Two drops of 5% v/v hydrochloric acid is added to each of the pigment standards and natural samples. Once the acid is added, the sample in the test tube should be mixed by inverting the tube several times, using parafilm as a stopper. All fluorometric measurements for both pigment standards and natural samples should be carried out at room temperature.   A 90% acetone blank (Blk_b) and a acidified acetone blank (Blk_a) should also be measured. Generally, the acidified blank (Blk_a) has been found to be equal to the non-acidified blank (Blk_b).   The   fluorometer's   sensitivity   to pheopigments, τ, is calculated as

$$\boldsymbol{t} = \frac{F_b - Blk_b}{F_a - Blk_a}, \tag{14.2}$$

and is averaged over all concentrations of the chlorophyll *a* standard. For the mechanical door model fluorometers, data from the higher gain door settings will often become noisy and computed τ values will begin to decrease. These data should be excluded from the average. The fluorometer's response factor, F_R (μg L^{-1} per fluorescence signal) is determined as the slope of the simple linear regression equation

$$C_{STD} = F_R \left(F_b - Blk_b \right), \tag{14.3}$$

calculated for the sample of diluted concentrations of the pigment standard, and forcing a zero intercept. With a digital fluorometer, the regression analysis is applied to the data from the entire 5, or more, concentrations and a single F_R factor is

determined for the instrument. With a mechanical fluorometer, the regression is applied to the data from the 3, or more, concentrations of the standard, and a separate F_R factor is determined, for each door setting. As a means of monitoring an instrument's performance, F_R factors from successive calibrations should be charted as functions of time. These quality control graphs should be retained with the data analysis logbooks to document the quality of each data set for which that fluorometer is used.

Solvent Preparation.

It is recommended that 90% acetone (v/v) be used to extract pigments for the fluorometric analysis. Richard and Thompson (1952) were the first to propose 90% acetone as a solvent to extract pigments from marine phytoplankton. Their results indicated improved extraction efficiencies, as well as minimizing the activity of the naturally-occurring chlorophyllase enzyme, which degrades the pigment. With a graduated cylinder, make up 90% acetone by first pouring in the distilled water, followed by 100% acetone. Using volumetric pipettes, or auto-pipettes, accurately measure 8 to 10 mls of 90% acetone and place it in a centrifuge tube. Record this volume as V_{EXT}. A number of such tubes containing acetone are then stored in a freezer and individually removed as filter samples are collected. Pre-chilling the solvent in this way reduces the possibility of temperature induced pigment degradation.

Extraction

Filters are removed from liquid nitrogen and placed in the chilled centrifuge tubes for extraction in V_{EXT} mL of 90% acetone. Samples are disrupted by sonication and allowed to extract at 0^oC for 24 h. Alternatively, the cells can be mechanically disrupted using a glass/Teflon tissue grinder and allowed to extract at 0^oC for 24 h. If after disrupting the cells, it is necessary to rinse the tissue grinder, or mortar and pestle, then a known volume of 90% acetone, measured using a Class A volumetric pipette, should be used. The ease at which the pigments are removed from the cells varies considerably with different phytoplankton. In all cases, freezing the sample filters in liquid nitrogen improves extraction efficiency. Prior to analysis, pigment extracts are swirled into a vortex to remove particles from the sides of the tube, and then centrifuged to minimize cellular debris.

Measurement

Following the same measurement procedure described above, under *Fluorometer Calibration*, each extracted sample is placed in the fluorometer and its non-acidified and acidified responses, Fb and Fa, are measured and recorded. The concentration of chlorophyll [Chl] (μg L^{-1}) in the sample is calculated as

$$[Chl] = (F_b - F_a - Blk_b + Blk_a)\frac{t}{t-1}F_R\frac{V_{EXT}}{V_{FILT}}, \quad (14.4)$$

and pheopigments concentration [Pheo] (μg L^{-1}) as

$$[Pheo] = \{(F_a - Blk_a)t - (F_b - Blk_b)\}\frac{t}{t-1}F_R\frac{V_{EXT}}{V_{FILT}}, \quad (14.5)$$

where volumes extracted V_{EXT} and filtered V_{FILT} are in mL. Pheopigment concentrations determined using the standard fluorometric method of Holm-Hansen et al. (1965) have not been reported in published articles for many years. This is based on the fact that (i) there is always a residual amount of pheopigments in all natural samples (Smith and Baker, 1978; 25% of the summed chlorophyll plus pheopigment), (ii) pheopigment concentrations are overestimated in the presence of chlorophyll *b* (Lorenzen and Jeffrey, 1980; Vernet and Lorenzen, 1987), and (iii) HPLC measured pheopigments, generally contribute very little to the chlorophyll *a* pigment pool (e.g., Hallegraeff, 1981; Everitt et al., 1990; and Bricaud et al., 1995). Trees et al. (2000) assembled an extensive HPLC pigment database (5,617 samples) extending over a decade of sampling and analysis, and includes a variety of environments ranging from freshwater to marine, oligotrophic to eutrophic, and tropical to polar, and found that the average pheopigment to chlorophyll *a* ratio was only 0.037. This global scale result emphasizes the problems associated with estimating pheopigments using the standard fluorometric method.

14.3 *In Situ* CHLOROPHYLL a FLUORESCENCE PROFILES

An *in situ* fluorometer should be employed to measure a continuous profile of chlorophyll fluorescence. The fluorometer should be mounted

on the same underwater package as the water sampler, ideally together with a CTD, transmissometer and other IOP sensors. In some cases it may be desirable to also include a radiometer on this package, if shading effects associated with the package and/or ship are not significant.

In situ fluorometers produce nearly continuous profiles of artificially stimulated fluorescence. Fluorometer data (in volts) should be corrected by subtracting an offset, determined by shading the instrument on deck. These unscaled fluorescence responses are adequate to provide guidance in K-profile analysis and interpretation.

To produce vertical continuous profiles of pigment concentration, HPLC-derived pigment concentrations from water samples taken at discrete depths may be interpolated, with the aid of *in situ* fluorescence profiles. These *fluorescence interpolated* profiles should then be used with $K_d(z,\lambda)$ profiles to compute optically weighted pigment concentration over the top attenuation length (Gordon and Clark 1980).

The A/D channel used to acquire and record signal voltages from the *in situ* fluorometer must be calibrated, and its temperature-dependent response to known voltage inputs characterized. The range dependent A/D bias coefficients should be determined at approximately 5^0 C intervals over the range from $0\text{-}25^0$ C to characterize the temperature sensitivity of the data acquisition system.

Zero fluorescence offsets should be measured on deck before and after each cast; the optical windows should be shaded to avoid contamination of the zero offset value by ambient light. Before each cast, the fluorometer windows should be cleaned following the manufacturer's instructions.

14.4 PROTOCOL STATUS AND FUTURE DIRECTIONS FOR RESEARCH

In order to minimize interferences caused by the overlapping excitation and emission wavebands of chlorophylls *a, b, c* and pheopigments, Turner Designs (Sunnyvale, CA) recently introduced the multi-spectral fluorometer TD-700. This instrument was recently beta-tested using samples collected at the US JGOFS Hawaii Ocean Time-series Station ALOHA (22.75^0N, 158^0W). An annual set of monthly pigment samples (0-200 m) was analyzed by HPLC using the protocols described in Chapter 20. Extracts were subsequently diluted and analyzed with the TD-700. Model I regression

analyses, which summarize these results are given below (pigment concentrations are expressed as ng L-1).

HPLC Chl a = 0.80[TD-700 Chl a] + 25.98 (r^2 = 0.916),

HPLC Chl b = 0.80[TD-700 Chl b] + 11.74 (r^2 = 0.843),

HPLC Chl c = 1.21[TD-700 Chl c] + 3.40 (r^2 = 0.867).

It is interesting noteworthy that the TD-700 did not detect pheopigments in any of the samples analyzed.

REFERENCES

Bianchi, T. S., C. Lambert, and D. C. Biggs. 1995: Distribution of chlorophyll *a* and pheopigments in the northwestern Gulf of Mexico: a comparison between fluorometric and high-performance liquid chromatography measurements. *Bull. Mar. Science,* **56,** 25-32.

Brock, T.D., 1983: *Membrane filtration: a user's guide and reference manual*. Science Tech., Madison, WI, 381 pp.

Campbell, J.W. 1995: The lognormal distribution as a model for bio-optical variability in the sea. J. Geophys Res., **100**, 13237-13254.

Chavez, F., K.R. Buck, R.R. Bidigare, D.M. Karl, D. Hebel, M. Latasa, L. Campbell, and J. Newton, 1995: On the chlorophyll *a* retention properties of glass-fiber GF/F filters. *Limnol. Oceanogr.*, **40**, 428-433.

Dickson, M.-L., and P.A. Weeller, 1993: Chlorophyll *a* concentrations in the North Pacific: Does a latitudinal gradient exist? *Limnol. Oceanogr.*, **38**, 1813-1818.

Gordon, H.R., and D.K. Clark, 1980: Remote sensing optical properties of a stratified ocean: an improved interpretation. *Appl. Optics*, **19**, 3,428--3,430.

Hoepffner, N., and S. Sathyendranath. 1992: Bio-optical characteristics of coastal waters: absorption spectra of phytoplankton and pigment distribution in the western North Atlantic. *Limnol. Oceanogr.* **37:** 1660-1679.

Holm-Hansen, O., C.J. Lorenzen, R.W. Holmes, and J.D.H. Strickland, 1965: Fluorometric determination of chlorophyll. *J. du Cons. Intl. Pour l'Expl. de la Mer.,***30**, 3-15.

Jeffrey, S.W., R.F.C. Mantoura, and S.W. Wright (eds.), 1997: *Phytoplankton Pigments in Oceanography*, Monographs on Oceanographic Methodology, UNESCO, 661 pp.

Lorenzen, C.J. and S.W. Jeffrey. 1980: *Determination of Chlorophyll in Seawater.* UNESCO Technical Papers in Marine Science, Vol. **35**, UNESCO, 20 pp.

Phinney, D.A. and C.S. Yentsch, 1985: A novel phytoplankton chlorophyll technique: Toward automated analysis. *J. Plankton Res.*, **7**, 633-642.

Richards, F.A. and T.G. Thompson. 1952: The estimation and characterization of plankton populations by pigment analysis. II. A spectrophotometric method for the estimation of plankton pigments. *J. Mar. Res.*, **11**, 156-172.

Saijo, Y. and S. Nishizawa. 1969: Excitation spectra in the fluorometric determination of chlorophyll a and phaeophytin *a*. *Mar Biol*,. **2**, 135-136.

Smith, R. C., and K. S. Baker. 1978: The bio-optical state of ocean waters and remote sensing. *Limnol. Oceanogr.*, **23**, 247-259.

Smith, R. C., R. R. Bidigare, B. B. Prezelin, K. S. Baker, and J. M. Brooks. 1987: Optical characterization of primary productivity across a coastal front. *Mar. Biol.* **96:** 575-591.

Strickland, J.D.H., and T.R. Parsons, 1972: *A Practical Handbook of Sea Water Analysis,* Fisheries Research Board of Canada, 310 pp.

Tester, P. A., M. E. Geesey, C. Guo, H. W. Paerl, and D. F. Millie, 1995: Evaluating phytoplankton dynamics in the Newport River estuary (North Caroline, USA) by HPLC-derived pigment profiles. *Mar. Ecol. Prog. Ser.* **124,** 237-245.

Trees, C.C., D.K. Clark, R.R. Bidigare, M.E. Ondrusek, and J.L. Mueller. 2000: Accessory pigments versus chlorophyll *a* concentrations within the euphotic zone: a ubiquitous relationship. Limnol Oceanogr. (in press).

Trees, C.C., M.C. Kennicutt II, and J.M. Brooks, 1985: Errors associated with the standard fluorometric determination of chlorophylls and pheopigments. *Mar. Chem.*, **17**, 1-12.

Vernet, M., and C. J. Lorenzen. 1987: The presence of chlorophyll b and the estimation of pheopigments in marine phytoplankton. J. Plankton Re*s.*, **9**, 255-265.

Yentsch, C.S., and D.W. Menzel, 1963: A method for the determination of phytoplankton, chlorophyll, and phaeophytin by fluorescence. *Deep-Sea Res.,* **10**, 221-231.

Chapter 15

SeaBASS Data Protocols and Policy

P. Jeremy Werdell[1], Sean Bailey[1] and Giulietta S. Fargion[3]

[1]Science System and Applications Inc., Lanham, Maryland
[2]Future Tech Corporation, Greenbelt, Maryland
[3]SAIC General Sciences Corporation, Beltsville, Maryland

15.1 INTRODUCTION

The SeaWiFS Project developed the SeaWiFS Bio-optical Archive and Storage System (SeaBASS) to be a local repository for *in situ* optical and pigment data products regularly used in a variety of scientific analyses. Information on the original SeaBASS design is provided in the SeaWiFS Technical Report Series, (Hooker et al. 1994). The system has since been expanded to contain data sets collected by participants of the SIMBIOS Project (NASA Research Announcement 1996 and 1999). A detailed description of the SeaBASS system is available via the World Wide Web at http://seabass.gsfc.nasa.gov.

Both the SeaWiFS and SIMBIOS Projects use *in situ* bio-optical data for the validation of SeaWiFS and other (e.g. OCTS, POLDER) satellite data products, and for the development of new ocean chlorophyll algorithms. In addition SeaBASS supports international protocol workshops, data merger studies, and time series studies. Archived data include measurements of water-leaving radiance, chlorophyll-a, and other related optical and pigment parameters. When available, additional oceanographic data (e.g. water temperature, salinity, total suspended particulate matter (SPM), and chromatic dissolved organic matter (CDOM) and atmospheric data (e.g. aerosol optical thickness (AOT) are also archived in SeaBASS. Data are collected by a number of different instrument packages, such as profilers, buoys, and above-water measurement devices, on a variety of platforms, including ships, moorings, and drifters. The contents of SeaBASS are made readily available to SIMBIOS and MODIS Science Team Members and to other approved individuals on a case by case basis (e.g. members of other ocean color instrument teams, volunteer-contributing researchers, etc.). Access to the database and data archive is available to authorized users via the World Wide Web (WWW).

As SIMBIOS US Science Team members are contractually obligated to provide data to SeaBASS, the volume of archived data is rapidly increasing (McClain and Fargion, 1999a and 1999b). With the launch of MODIS, as well as a number of present and upcoming international missions (e.g. GLI, POLDER-2, MERIS, OCI, OCM, etc.), the use of SeaBASS data archive is expected to increase dramatically as these missions begin to require validation data.

15.2 SeaBASS DATA FORMAT

SeaBASS presently contains over 10,000 bio-optical data files, encompassing more than 400 separate experiments. In addition, its historical pigment database holds over 300,000 records of phytoplankton pigment data. To account for the continuous growth of the data archive, the Project believed it essential to develop efficient data ingestion and storage techniques. Such ingestion procedures and protocols were designed to be as straightforward and effortless as possible on the part of the contributing investigators, while still offering a useful format for internal analysis efforts. The Project considered the following to be the most important in the design of the system:

1. simple data format, easily read and updated,
2. global portability across multiple computer platforms; and
3. Web accessible data holdings.

As a result, SeaBASS supports standard, flat (two-dimensional) ASCII text files, which are easily managed from any computer platform and by most programming languages. The architecture of a SeaBASS data file is simple: data are presented in columns (delimited by spaces, tabs, or commas) and preceded by a series of predefined metadata headers. The headers provide descriptive information on the data file, such as date, time, location, investigators, column names and units,

and additional ancillary information. Several examples of SeaBASS data files are available online at: http://seabass.gsfc.nasa.gov/seabass _submit.html. Appendix B provides a detailed description of the SeaBASS file format.

15.3 SeaBASS ARCHITECTURE

SeaBASS contains two separate but linked entities, a data archive and a relational database. The data archive consists of series of sub-directories organized by affiliation, experiment, and cruise. Each cruise has additional subdirectories containing the *in situ* data sets, associated documentation, and calibration files associated with that cruise. Authorized users may peruse the directory tree via the SeaBASS web page.

Presently, the database consists of a single table with numerous columns to store metadata information. Each row in the table contains the name of the data file and all of the header information provided in that file. Hence, data files meeting pre-defined criteria may be located by performing simple keyword searches on the metadata. Authorized users may search the database using the SeaBASS web server at http://seabass.gsfc.nasa.gov/dataordering.html

The web-based interface allows (1) simple keyword searches of the headers 'affiliations', 'investigators', 'experiment', 'cruise', 'data_type' and 'fields', (2) the application of user defined date, time, latitude, and longitude ranges, and (3) advanced keyword searches of all of the metadata information via a user-written query. Data files meeting applied search conditions may be viewed via the World Wide Web or compressed and downloaded to an FTP (File Transfer Protocol) site.

Redesign of the SeaBASS database began in Spring 2000, and is expected to be operational in Winter 2000. Changes to the database will include:

- an increase in the number of tables to improve data normalization and database performance,
- a reconfiguration of the system to take advantage of multiple computer processors and increased physical storage space,
- the utilization of stored procedures and applications for internal SIMBIOS Project Office accounting activities, and
- the ability to ingest bio-optical and pigment data into tables within the database. The latter will allow specific data values to be extracted by performing simple keyword searches on the metadata or by applying range conditions (e.g. waveband, depth, etc.) on the data tables.

15.4 DATA QUALITY

To assist with the standardization of SeaBASS data files, the Project developed feedback software and protocols to evaluate the format of submitted data files. The primary component of the software is known as FCHECK. FCHECK consists of a PERL (Practical Extraction and Report Language) script with connections to several look-up tables and UNIX mail handling utilities. Data contributors, using any computer platform, may test a data file for compatibility with the SeaBASS format by electronically mailing the file to fcheck@seabass.gsfc.nasa.gov. Upon receipt of the file, FCHECK parses the data and metadata and compares it to the required SeaBASS format. Results of this analysis are electronically mailed to the contributor and to the SeaBASS Administrator. This format analysis requires little to no intervention on behalf of the Administrator and has proven to reduce considerably the amount of processing time needed for both the Administrator and contributor. Additional information on FCHECK is available online at http://seabass.gsfc.nasa.gov/fcheck_desc.html.

Once data are prepared for archival, the contributor uploads the data files, calibration files, and supporting documentation to SeaBASS via File Transfer Protocol (FTP). The Administrator then collects the files and evaluates the data set. The following requirements need to be met: (1) data files must be organized in the proper SeaBASS format (i.e. FCHECK does not report any errors), (2) supporting documentation and calibration files must be included in the submission, and (3) the documentation and calibration files must match those listed in the 'documents' and 'calibration_files' headers in each data file.

Additionally, the documentation and calibration files are inspected for completeness. At a minimum, the Project requires that documentation include a cruise report or station log (with ancillary information such as date, time, location coordinates, water depth, sea and sky states, observations, and notes) and an instrument report (with information such as instruments used, processing methods, equations, and references). The Project encourages the contributor to include additional documentation, such as digital photographs of sea and sky states. Calibration files must include calibration coefficients and the date each instrument was calibrated. Once the data set has passed visual inspection, the Administrator archives the data files and ingests the appropriate information into the database. At this point, the

new data become available online to the Science Team.

15.5 ACCESS POLICY AND USERS

The policy applies to data submitted to the NASA SIMBIOS Project at GSFC for inclusion in the calibration and validation data collection. This policy supercedes the SeaWiFS Project 1991 policy (Appendix A in Hooker et. al., 1993). The SIMBIOS investigators must, at a minimum, comply with SIMBIOS data policy, although the Project encourages a more open policy.

Ocean color algorithm development is severely observation limited. As such, rapid turnaround and access to field data are essential to advance the state of the art. Data obtained under SIMBIOS NRA-99 contracts must be submitted no later than six months from the date of collection. International SIMBIOS Science Team and researchers involved in other ocean color missions (i.e., POLDER, GLI, MODIS, MERIS, etc.) are encouraged to provide their data as well, in order to foster collaboration.

For a period of three years following data collection, access to the digital data will be limited to SIMBIOS Science Team members and other approved users as agreed upon by the SIMBIOS Project and data providers. The SIMBIOS Project will grant access to the international science team members on a case by case basis according to ongoing collaboration tasks. Other investigators from the ocean color community will be able to query information about the data (i.e., parameters, locations, dates and investigators), but will not have access to the data itself. Instead, if they are interested in the data, they will be referred to the provider. After the third year anniversary of data collection, the data will change from a "restricted" to an "open" status and will be distributed by National Oceanographic Data Center (NODC). Some special data sets for algorithm development will be made available to the research community without restrictions with the approval of the SIMBIOS Science Team.

Prior to the three-year data collection anniversary, users of data will be required to provide proper credit and acknowledgment of the provider. Citation should also be made of the data archive. The provider(s) shall have the right to be a named co-author. Users of data are encouraged to discuss relevant findings with the provider early in the research. The user is required to give all providers of the data being used a copy of any manuscript resulting from use of the data prior to initial submission for publication, thus providing the data provider an opportunity to comment on the paper. All users and providers are required to report to SeaBASS administration possible data errors or mislabels found in the database.

A major purpose of the SeaBASS database is to facilitate comparisons between *in situ* observations (regionally, temporally, by technique, by investigator, etc.), as well as between *in situ* and remotely sensed observations. Updates and corrections to submitted data sets are encouraged. Records will be maintained of updates and corrections and a summary of new and updated data will be posted online. It is the provider's responsibility that the current data in the archive will be identical to the data used in the provider's most recent publications or current research. At the end of each SIMBIOS contract, a final data resubmission, or a written certification of data quality, from the provider is mandatory.

After receiving the final data, the SIMBIOS Project will forward the data at the appropriate time to NODC for open distribution. A courtesy citation, naming the provider and the funding agency, will accompany the data. The SIMBIOS Project will not be held responsible for any data errors or misuse. Data copyright is retained by the US Government.

To afford continued rapid submission of data sets, the SeaBASS web server has been configured as a password protected system. Additionally, the web server and SeaBASS software log all user activity. This information is available to contributing investigators.

REFERENCES

Hooker, S.B., C.R. McClain, J.K. Firestone, T.L. Westphal, E-n. Yeh, and Y. Ge, 1994: The SeaWiFS Bio-Optical Archive and Storage System (SeaBASS), Part 1. *NASA Tech. Memo. 104566, Vol. 20*, S.B. Hooker and E.R. Firestone, Eds., NASA Goddard Space Flight Center, Greenbelt, Maryland, 40 pp.

McClain, C.R. and G.S. Fargion, 1999: SIMBIOS Project 1998 Annual Report, *NASA Tech. Memo*. 1999-208645, NASA Goddard Space Flight Center, Greenbelt, Maryland, 105 pp.

McClain, C.R. and G.S. Fargion, 1999: SIMBIOS Project 1999 Annual Report, *NASA Tech. Memo*. 1999-209486, NASA Goddard Space Flight Center, Greenbelt, Maryland, 128 pp.

Appendix A

Characteristics of Satellite Ocean Color Sensors: Past, Present and Future

James L. Mueller[1] and Giulietta S. Fargion[2]

[1]*Center for Hydro-Optics and Remote Sensing, San Diego State University, California*
[2]*SAIC General Sciences Corporation, Beltsville, Maryland*

This appendix summarizes the essential operational characteristics of ocean color sensors of the past, present and future. Table A.1 lists general characteristics of past and presently operating ocean color sensors, including for each the satellite platform, country and agency, operational time period (actual or planned), orbit characteristics, spatial resolution at nadir, swath width, and tilt capabilities. Table A.2 lists the same information for ocean color sensors currently planned for launch and operation in the future. Table A.3 lists the center wavelength, spectral bandwidth (FWHM) and noise equivalent radiance resolution (NEΔL) for the ocean color bands of each of the sensors listed in Tables A.1 and A.2. Many of these sensors have additional bands, not listed here, addressing data requirements in terrestrial or atmospheric sciences. The information in these tables was updated from that published in IOCCG (1998). The sensor band data in Table A.3 should be used to expand Table 4.1 when specifying *in situ* instrument characteristics needed to support algorithm development and validation related to any of the other sensors, in addition to SeaWiFS, which fall within the SIMBIOS purview.

REFERENCES

IOCCG 1998: Minimum Requirements for an Operational, Ocean Colour Sensor for the Open Ocean. *Reports of the International Ocean-Colour Coordinating Group, No. 1.* IOCCG, Dartmouth, Canada, 46pp.

Table A2.   Characteristics of future ocean-color sensors.

	GLI	POLDER-2	MODIS-PM
Platform	ADEOS2	ADEOS–2	EOS–PM1
Agency	NASDA	CNES	NASA
Country	Japan	France	USA
Operation Start	Nov. 2001	Nov 2001	Dec. 2000
Orbital Inclination	98.6	98.6	98.2
Equatorial Crossing Time (h)	10:30	10:30	13:30
Altitude (km)	803	803	705
Resolution at Nadir (km)	1/0.25	6 x 7	1
Swath (km)	1600	2400	2330
Tilt (degrees)	±20	Variable	No
Direct Link	UHF/X-band	X-band	X-band
Recorded	X-band	X-band	X-band
Solar Calibration	Yes	No	Yes
Lunar Calibration	No	No	Yes
Lamp Calibration	Yes	No	Yes

Table A1. Characteristics of past and present ocean-color sensors.

Sensor	CZCS	OCTS	POLDER	MOS	SeaWiFS	OCM	OCI	OSMI	MODIS-AM	MISR	MERIS
Platform	Nimbus-7	ADEOS-1	ADEOS-1	IRS-P3	OrbView-2	IRS-P4	ROCSAT	KOMPSAT	EOS-AM1	EOS-AM1	Envisat
Agency	NASA	NASDA	CNES	DLR	OSC/NASA	ISRO	Taiwan	KARI	NASA	NASA	ESA
Country	USA	Japan	France	Germany/India	USA	India	Taiwan	Korea	USA	USA	Europe
Operation Start	Oct. 1978	Aug. 1996	Aug. 1996	Mar. 1996	Sep. 1997	Nov. 98	Feb. 1999	Jul. 1999	Dec. 1999	Dec. 1999	Mar. 2002
Operation End	Jun. 1986	Jun. 1997	Jun. 1997								
Orbital Inclination	99.3	98.6	98.6	98.7	98.2	98.3	35	98.13	98.2	98.2	98.5
Equatorial Crossing Time (h)	12:00	10:41	10:41	10:30	12:00	12:00	09:00/15:00	10:50	10:30	10:30	10:00
Altitude (km)	955	804.6	804.6	817	705	720	600	685	705	705	800
Resolution at Nadir (km)	0.825	0.7	6 x 7	0.5	1.1	0.36	0.8	0.85	1	0.25	1.2/0.3
Swath (km)	1566	1400	2400	200	2800	1420	704	800	2330	360	1150
Tilt (degrees)	±20	±20	Variable	No	±20	±20	No	No	No	Variable	No
Direct Link	No	UHF/X-band	X-band	S-band	L-band	X-band	S-band	X-band	X-band	No	X-band
Recorded	Yes	X-band	X-band	None	S-band	Yes	None	Yes	X-band	X-band	X-band
Solar Calibration	No	Yes	No	Yes	Yes	Yes	—	Yes	Yes	No	Yes
Lunar Calibration	No	No	No	No	Yes	No	—	No	Yes	Yes	No
Lamp Calibration	Yes	Yes	No	Yes	No	Yes	—	No	Yes	No	No

Table A3. Summary of the spectral bands used for ocean-color applications. Center λ (nm), Bandpass (FWHM, nm), NEΔL (W m^{-2} sr^{-1} µm^{-1}).

CZCS Center λ	FWHM	NEΔL	**OCTS** Center λ	FWHM	NEΔL	**POLDER** Center λ	FWHM	NEΔL	**MOS** Center λ	FWHM	NEΔL	**SeaWiFS** Center λ	FWHM	NEΔL
443	20	0.208	412	20	0.186	443	20	0.138	408	10	0.192	412	20	0.092
520	20	0.173	443	20	0.109	490	20	0.147	443	10	0.124	443	20	0.077
550	20	0.166	490	20	0.089	565	20	0.088	485	10	0.148	490	20	0.056
670	20	0.094	520	20	0.121	670	20	0.063	520	10	0.141	510	20	0.049
750	100	0.040	565	20	0.091	763	10	0.090	570	10	0.150	555	20	0.043
			670	20	0.037	765	40	0.086	615	10	0.105	670	20	0.031
			765	40	0.057	865	40	0.034	650	10	0.141	765	40	0.019
			865	40	0.031	910	20	0.045	685	10	0.088	865	40	0.015
									750	10	0.102			
									815	10	0.034			
									870	10	0.033			

MISR Center λ	FWHM	NEΔL	**MODIS** Center λ	FWHM	NEΔL	**MERIS** Center λ	FWHM	NEΔL	**OCI** Center λ	FWHM	NEΔL	**OSMI** Center λ	FWHM	NEΔL
446	41	0.063	412	15	0.048	412.5	10	0.026	443	20	–	443	20	–
557	27	0.061	443	10	0.032	442.5	10	0.025	490	20	–	490	20	–
672	20	0.050	488	10	0.025	490	10	0.022	510	20	–	510	20	–
867	39	0.031	531	10	0.018	510	10	0.019	555	20	–	555	20	–
			551	10	0.019	560	10	0.016	670	20	–	670	20	–
			667	10	0.008	620	10	0.014	865	40	–	865	40	–
			678	10	0.007	665	10	0.013						
			748	10	0.009	681	7.5	0.014						
			870	15	0.006	709	9	0.011						
			469 *	20	0.145	779	14	0.008						
			555 *	20	0.127	870	20	0.007						
			645 **	50	0.170	890	10	0.011						
			858 **	35	0.123	900	10	0.010						

GLI Center λ	FWHM	NEΔL	**OCM** Center λ	FWHM	NEΔL	**POLDER-2** Center λ	FWHM	NEΔL	**S–GLI** Center λ	FWHM	NEΔL	
380	10	0.076	412	20	0.26	443	20	0.138	412	10	0.081	
400	10	0.051	443	20	0.22	490	20	0.147	443	10	0.067	
412	10	0.045	490	20	0.17	565	20	0.088	490	10	0.054	
443	10	0.054	510	20	0.17	670	20	0.063	520	20	0.052	* Spatial resolution 0.5 km
460	10	0.055	555	20	0.15	763	10	0.090	565	20	0.029	**Spatial resolution 0.25 km
490	10	0.027	670	20	0.10	765	40	0.086	625	20	0.021	(others: 1 km)
520	10	0.044	765	40	0.05	865	40	0.034	680	20	0.012	
545	10	0.044	865	40	0.08	910	20	0.045	710	20	0.007	
565	10	0.018							749	20	0.009	
625	10	0.017							865	20	0.006	
666	10	0.015										
680	10	0.014										
710	10	0.012										
749	10	0.010										
865	20	0.007										

Appendix B

SeaBASS Data File Format

P. Jeremy Werdell[1], Sean Bailey[1] and Giulietta S. Fargion[3]

[1]*Science System and Applications Inc., Lanham, Maryland*
[2]*Future Tech Corporation, Greenbelt, Maryland*
[3]*SAIC General Sciences Corporation, Beltsville, Maryland*

SeaBASS HEADERS

Each header begins with a '/' and every data file opens with 'begin_header'. The headers are then listed in any order, as long as the list ends with 'end_header'. A value of 'NA' (not available or applicable) is assigned to any header where information cannot be provided. Data files with missing headers will not be accepted for submission to SeaBASS. A description of each follows.

'Data_file_name' simply provides the name of the data file. 'Affiliations', 'investigators', and 'contact' provide information on the contributing researchers. The primary investigator is listed first, followed by any associate investigators. Commas separate multiple entries, and white spaces and apostrophes are not allowed. 'Contact' is the electronic mail address of the contributor. 'Experiment', 'cruise', and 'station' record information on the long-term experiment (if available), the specific cruise, and the station within the cruise. For each of the latter, an entry of 'SIMBIOS' is not permitted. 'Documents' refers to cruise reports, logs, and associated documentation that provide additional information about the experiment or cruise. 'Calibration_files' points to additional file(s) that contain the coefficients and techniques used to calibrate the instruments used in data collection. The files referred to by 'documents' and 'calibration_files' must accompany the data files at the time of submission.

'Data_status' describes the condition of the data file, accepting values of preliminary, update, and final. 'Preliminary' is used when the data are submitted for the first time and the investigator intends to analyze the data further. 'Update' indicates the data are being resubmitted and informs the Project that an additional resubmission will occur in the future. 'Final' is used when the investigator has no intention of revisiting the data set. 'Data_type' describes the general collection method of the data. Accepted values include: 'cast' for vertical profiles (e.g. optical packages, CTD); 'flow_thru for continuous data (e.g. underway flow through systems); 'above_water' for above surface radiometry data (e.g. ASD, SIMBAD); 'sunphoto' for sunphotometry data (e.g. MicroTops, PREDE); 'mooring' for moored data and buoy data; 'drifter' for drifter and drogue data; 'scan' for discrete hyperspectral measurements (e.g., absorption spectra); and 'pigment' for laboratory measured pigment data (fluorometry, spectrophotometry, HPLC). 'North_latitude', 'south_latitude', 'east_long itue', 'west_longitude', 'start_date', 'end_date', 'start_time', and 'end_time' provide information on the location, date, and time data were collected. Each entry should be the extreme value for the entire data file. For example, 'north_latitude' refers to the coordinate furthest north data in the file were collected. 'Start_time' and 'end_time' refer to the earliest and latest time-of-day data in the file were collected. The latter do not refer to the time data collection began and data collection ceased, respectively. Latitude and longitude are listed in decimal degrees, with coordinates north of the equator or east of the Prime Meridian set positive and south of the equator or west of the Prime Meridian set negative. Dates have the format 'YYYYMMDD'. Times have the format 'HH:MM:SS' and are listed in Greenwich Mean Time (GMT).

'Cloud_percent', 'wave_height', 'wind_speed', 'secchi_depth'', 'measurement_depth', and 'water_depth' provide ancillary information about the station, when available. 'Wave_height' and 'water_depth' have units of meters and 'wind_speed' has units of meters per second. A value for 'measurement_depth' is included when the file contain data collected at a discrete depth (e.g., bottle samples or buoy/moored radiometers).

'Fields' names each of the columns of *in situ* data presented below the headers. Each entry describes the data in a one column, and every column must have an entry. 'Units' provides the units for each column of data. Every value in 'fields' must also have an equivalent entry in

'units'. 'Missing' refers to a null value used as a placeholder for any missing data point. Each row of data must contain the same number of columns as defined in the 'fields' header. 'Delimiter' indicates how the columns of data are delimited. Accepted delimiters include tabs, spaces, and commas, but only one delimiter is permitted per data file. Finally, if the investigators wish to include additional comments about the data file, they may do in the within the header boundaries. Lines of comments begin with a '!' and may include any and all text characters and white space. Comment comments include addition ancillary information about the data file, sea and sky states, difficulties encountered during data collection, methods of data collection, instruments used, and a description of nonstandard SeaBASS field name included in the data file. A list and description of the SeaBASS metadata headers is available online at http://seabass.gsfc.nasa.gov/seabass_header.html. This list is updated regularly.

development of the expanded version of the SeaBASS database, a standard set of case-insensitive field names and units has been adopted. While the list of standardized field names is reasonably comprehensive, it cannot account for all the possible data types one might wish to provide to the SeaBASS archive. If a data type to be submitted to SeaBASS does not fall under one of the predefined standard field names, the investigator may still include the data. Note that the standardized set is updated as the need arises (e.g. a data parameter is commonly submitted or queried). Non-standard data will be archived, however, the data values will not be ingested into the online database. The data will be retrievable, but only with the original archived file, not as a separate dataset. A list of the standardized field names and units is available online at http://seabass.gsfc.nasa.gov/cgi-bin/stdfields.cgi. This list is updated regularly (Table 1B).

FIELD NAMES AND UNITS

In an effort to ensure compatibility within the SeaBASS data archive, and to facilitate the

Table 1B. SeaBASS Standardized Fieldnames and Units as of June 2000. (###.# = wavelength).

Fieldname	Units	Description
a###.#	1/m	Total absorption coefficient
aaer###.#	1/m	Absorption coefficient of atmospheric aerosols
ad###.#	1/m	Absorption coefficient of detrius
adg###.#	1/m	Absorption coefficient of detrital+gelbstoff
ag###.#	1/m	Absorption coefficient of CDOM
altitude	m	Altitude (above sea level)
am	unitless	Airmass (calculable from time/position)
angstrom	unitless	Angstrom exponent
AOT###.#	unitless	Aerosol optical thickness
ap###.#	1/m	Absorption coefficient of particles
aph###.#	1/m	Absorption coefficient of phytoplankton
a*ph###.#	1/m	Chl a-specific aph
At	degreesC	Air temperature
bb###.#	1/m	Backscatter
bincount	none	Number of records averaged into a bin
bp###.#	1/m	Particle scattering coefficient
c###.#	1/m	Beam attenuation coefficient
cloud	%	Percent cloud cover
cond	mmho/cm	Conductivity
depth	m	Depth of measurement
Ed###.#	uW/cm^2/nm	Downwelling irradiance
EdGND	volts	Dark current values for Ed sensor
Epar	uE/cm^2/s	Profiled Photosynthetic Available Radiation

Es###.#	uW/cm^2/nm	Downwelling irradiance above the surface
EsGND	volts	Dark current values for Es sensor
Eu###.#	uW/cm^2/nm	Upwelling irradiance
EuGND	volts	Dark current values for Eu sensor
F0###.#	uW/cm^2/nm	Extraterrestrial Solar irradiance
Kd###.#	1/m	Diffuse attenuation coefficient for downwelling irradiance
Kl###.#	1/m	Diffuse attenuation coefficient for upwelling radiance
Knf###.#	1/m	Diffuse attenuation coefficient for natural fluorescence of chl a
Kpar	1/m	Diffuse attenuation coefficient for PAR
Ku###.#	1/m	Diffuse attenuation coefficient for upwelling irradiance
Lsky###.#	uW/cm^2/nm/sr	Sky radiance
Lt###.#	uW/cm^2/nm/sr	Total water radiance
Lu###.#	uW/cm^2/nm/sr	Upwelling radiance
LuGND	volts	Dark current values for Lu sensor
Lw###.#	uW/cm^2/nm/sr	Water leaving radiance
Lwn###.#	uW/cm^2/nm/sr	Normalized water leaving radiance (Nlw=Lw * Fo/Es)
natf	nE/m^2/sr/s	natural fluorescence of chl a
Oz	dobson	Column Ozone
PAR	uE/cm^2/s	Photosynthetic Available Radiation measured at the sea surface
pitch	degrees	Instrument pitch
PP	mgC/mgchla/hr	Primary Productivity
pressure	dbar	Water Pressure
pressure_atm	mbar	Atmospheric pressure
Q###.#	sr	Eu/Lu (equal to Pi in diffuse water)
quality	none	Data quality flag...arbitrary analyst specific value
R###.#	unitless	Irradiance reflectance (Re=Eu/Ed)
RelAz	degrees	Sensor azimuth angle, relative to the solar plane (for above water radiometers)
Rl###.#	1/sr	Radiance reflectance (Rl=Lu/Ed)
roll	degrees	Instrument roll
Rpi###.#	unitless	Radiance reflectance with PI
Rrs###.#	1/sr	Remote sensing reflectance (Rrs=Lw/Ed)
sal	PSU	Salinity
sample	none	Sample Number
SenZ	degrees	Sensor zenith angle (for above water radiometers)
sigmaT	kg/m3	Density - 1000kg/m3
SN	none	Instrument serial number - should be in documents...
SST	degreesC	Sea Surface Temperature
stimf	volts	Stimulated fluorescence of chl a
SZ	m	Secchi disk depth
SZA	degrees	Solar zenith angle (calculable from time/position)
tilt	degrees	Instrument tilt
trans	%	Precent transmission
SPM	g/L	Total Suspended Particulate Material
volfilt	L	Volume Filtered
wavelength	nm	Wavelength of measurement
windspeed	m/s	Wind Speed
Wt	degreesC	Water temperature
Wvp	mm	Water vapor
Pigments		
Allo	mg/m^3	Alloxanthin

Anth	mg/m^3	HPLC Antheraxanthin
Asta	mg/m^3	HPLC Astaxanthin
At	degreesC	Air temperature
beta-beta-Car	mg/m^3	HPLC Beta,beta-Carotene
beta-eta-Car	mg/m^3	HPLC Beta,eta-Carotene
beta-psi-Car	mg/m^3	HPLC Beta,psi-Carotene
But-fuco	mg/m^3	HPLC 19'-Butaonoyloxyfucoxanthin
Cantha	mg/m^3	HPLC Canthaxanthin
CHL	mg/m^3	Fluoresence/spectrophotometric derived chlorophyll a
Chl_a	mg/m^3	HPLC Chlorophyll a
Chl_b	mg/m^3	HPLC Chlorophyll b
Chl_c	mg/m^3	HPLC Chlorophyll c
Chlide_a	mg/m^3	HPLC Chlorophyllide a
Chlide_b	mg/m^3	HPLC Chlorophyllide b
Croco	mg/m^3	HPLC Crocoxanthin
Diadchr	mg/m^3	HPLC Diadinochrome
Diadino	mg/m^3	HPLC Diadinoxanthin
Diato	mg/m^3	HPLC Diatoxanthin
Dino	mg/m^3	HPLC Dinoxanthin
DV_Chl_a	mg/m^3	HPLC Divinyl Chorophyll a
DV_Chl_b	mg/m^3	HPLC Divinyl Chorophyll b
Echin	mg/m^3	HPLC Echinenone
Et-8-carot	mg/m^3	HPLC Ethyl-apo-8'-carotene
Et-chlide_a	mg/m^3	HPLC Ethyl Chlorophyllide a
Et-chlide_b	mg/m^3	HPLC Ethyl Chlorophyllide b
eta-eta-Car	mg/m^3	HPLC Eta-eta-Carotene
Fuco	mg/m^3	HPLC Fucoxanthin
Hex-fuco	mg/m^3	HPLC 19'-Hexanoyloxyfucoxanthin
Lut	mg/m^3	HPLC Lutein
Lyco	mg/m^3	HPLC Lycopene
Me-chlide_a	mg/m^3	HPLC Methyl Chlorophyllide a
Me-chlide_b	mg/m^3	HPLC Methyl Chlorophyllide b
Mg_DVP	mg/m^3	HPLC Mg 2,4 divinyl pheoporphyrin a5 monomethyl ester
Monado	mg/m^3	HPLC Monadoxanthin
Neo	mg/m^3	HPLC Neoxanthin
P-457	mg/m^3	HPLC P-457
Perid	mg/m^3	HPLC Peridinin
PHAEO	mg/m^3	Pheaopigment
Phide_a	mg/m^3	HPLC Pheophorbide a
Phide_b	mg/m^3	HPLC Pheophorbide b
Phide_c	mg/m^3	HPLC Pheophorbide c
Phythl-chl_c	mg/m^3	HPLC Phytylated Chlorophyll c
Phytin_a	mg/m^3	HPLC Pheophytin a
Phytin_b	mg/m^3	HPLC Pheophytin b
Phytin_c	mg/m^3	HPLC Pheophytin c
Pras	mg/m^3	HPLC Prasinoxanthin
Pyrophytin_a	mg/m^3	HPLC Pyropheophytin a
Pyrophytin_b	mg/m^3	HPLC Pyropheophytin b
Pyrophytin_c	mg/m^3	HPLC Pyropheophytin c
Siphn	mg/m^3	HPLC Siphonein
Siphx	mg/m^3	HPLC Siphonaxanthin
Tpg	mg/m^3	Total (sum of all) pigments

Vauch	mg/m^3	HPLC Vaucheriaxanthin-ester
Viola	mg/m^3	HPLC Violaxanthin
Zea	mg/m^3	HPLC Zeaxanthin
Time, Location		
date	yyyymmdd	Sample date
day	dd	Sample Day
hour	hh	Sample Hour
jd	jjj	Sample Julian Day (Day of Year)
lat	degrees	Sample Latitude
lon	degrees	Sample Longitude
minute	mn	Sample Minute
month	mo	Sample Month
second	ss	Sample Second
station	none	Sample Station
time	hh:mm:ss	Sample time
year	yyyy	Sample Year

An example of an optical cast data file:

```
/begin_header
/investigators=John_Smith,Mary_Johnson
/affiliations=MBARI,State_University
/contact=jsmith@mbari.org,mary@state.edu
/experiment=TAO_Moorings
/cruise=TAO_Moorings_97
/station=341
/data_file_name=n97f341b.txt
/documents=README.txt
/calibration_files=ocp14a.cal
/data_type=cast
/data_status=preliminary
/start_date=19971215
/end_date=19971215
/start_time=21:15:39[GMT]
/end_time=21:19:30[GMT]
/north_latitude=-0.016[DEG]
/south_latitude=-0.016[DEG]
/east_longitude=-170.02[DEG]
/west_longitude=-170.02[DEG]
/cloud_percent=10.0
/measurement_depth=NA
/secchi_depth=15
/water_depth=225
/wave_height=0.5
/wind_speed=5
!
!       COMMENTS
!
/missing=-999
/delimiter=space
/fields=depth,Lu412.2,Lu443.4,Lu489.7,Ed412.5,Ed443.1,Ed489.8,Ed510.0
/units=m,uW/cm^2/nm/sr,uW/cm^2/nm/sr,uW/cm^2/nm/sr,uW/cm^2/nm,uW/cm^2/nm,uW/cm^2/nm
/end_header@
```

1.0 1.244184 1.066594 0.852400 65.430025 65.883773 71.745284
2.0 1.299710 1.113997 0.884608 58.041549 59.823693 66.357239
3.0 1.298214 1.113140 0.886502 51.693890 51.255351 57.233860

An example of a pigment data file:

/begin_header
/investigators=John_Smith,Mary_Johnson
/affiliations=Goddard_Space_Flight_Center,State_University
/contact=jsmith@simbios.gsfc.nasa.gov,mary@state.edu
/experiment=AMT
/cruise=AMT07
/station=14
/data_file_name=A07OD014.SHO
/documents=A7OPSLOG.TXT
/calibration_files=MVD009I.CAL,OCP004O.CAL
/data_type=pigment
/data_status=preliminary
/start_date=19981016
/end_date=19981020
/start_time=12:11:08[GMT]
/end_time=15:25:45[GMT]
/north_latitude=36.1234[DEG]
/south_latitude=31.8823[DEG]
/east_longitude=-51.2363[DEG]
/west_longitude=-55.1125[DEG]
/cloud_percent=NA
/measurement_depth=NA
/secchi_depth=NA
/water_depth=NA
/wave_height=NA
/wind_speed=NA
!
!   COMMENTS
!
/missing=-999
/delimiter=space
/fields=date,time,station,lat,lon,depth,CHL
/units=yyyymmdd,hh:mm:ss,none,degrees,degrees,m,mg/m^3
/end_header@
19981016 14:33:22 st001 32.3234 -53.1624 0.5 0.32
19981017 13:01:56 st002 33.1122 -53.1276 0.5 0.33
19981018 15:25:45 st003 36.1234 -51.2363 0.5 0.45
19981019 12:11:08 st004 31.8823 -55.1125 0.5 0.22
19981020 14:13:14 st005 34.2341 -52.3545 0.5 0.11

GLOSSARY

A/D	Analog-to-Digital
ALSCAT	ALPHA and Scattering Meter (Note: the symbol α corresponds to $c(\lambda)$, the beam attenuation coefficient, in present usage.)
AOL	Airborne Oceanographic Lidar
ARGOS	Not an acronym: the name given to the data collection and location system on NOAA Operational Satellites
ASCII	American Standard Code for Information Inter- change
AMT	Atlantic Meridional Transect
AMT-3	The Third AMT Cruise
AMT-5	The Fifth AMT Cruise
AMT-6	The Sixth AMT Cruise
AMT-7	The Seventh AMT Cruise
AVHRR	Advanced Very High Resolution Radiometer
AVIRIS	Advanced Visible and Infrared Imaging Spectrometer
BSI	Biospherical Instruments, Inc.
CDOM	Colored Dissolved Organic Material
CERT	Calibration Evaluation and Radiometric Testing
CHN	Carbon, Hydrogen, and Nitrogen
CTD	Conductivity, Temperature, and Depth
CW	Continuous Wave
CZCS	Coastal Zone Color Scanner
DAS	Data Acquisition Sequence
DIW	Distilled Water
DOC	Dissolved Organic Carbon
DOM	Dissolved Organic Matter
DUT	Device Under Test
DVM	Digital Voltmeter
ER-2	Earth Resources-2, a research aircraft
FEL	Not an acronym; a type of standard lamp for irradiance and radiance calibration
FOV	Field-of-View
FWHM	Full-Width at Half-Maximum
GAC	Global Area Coverage
GASM	General Angle Scattering Meter
GF/F	Not an acronym; a specific type of glass fiber filter manufactured by Whatman
GMT	Greenwich Mean Time
GOES	Geostationary Operational Environmental Satellite
GPIB	General Purpose Interface Bus
GPS	Global Positioning System
GSFC	Goddard Space Flight Center
HPLC	High Performance Liquid Chromatography
IAPSO	International Association for the Physical Sciences of the Ocean
ICES	International Council on Exploration of the Seas
IFOV	Instantaneous field-of-view

IOP	Inherent Optical Properties
IR	Infrared
JGOFS	Joint Global Ocean Flux Study
MARS	Multispectral Airborne Radiometer System
MER	Marine Environmental Radiometer
MERIS	Marine Environment Research Imaging Spectroradiometer (French)
MOS	Moderate Resolution Imaging Spectrometer
NAS	National Academy of Science
NASA	National Aeronautics and Space Administration
NASIC	NASA Aircraft/Satellite Instrument Calibration
NESDIS	National Environmental Satellite Data Information Service
NIST	National Institute of Standards and Technology
NOAA	National Oceanic and Atmospheric Administration
NOARL	Naval Oceanographic and Atmospheric Research Laboratory
OCTS	Ocean Color and Temperature Sensor (Japanese)
OCS-5002	Optical Calibration Source
OFFI	Optical Free-Fall Instrument
OMP-8	Not an acronym; a type of marine anti-biofouling compound
OSFI	Optical Surface Floating Instrument
PAR	Photosynthetically Available Radiation
POC	Particulate Organic Carbon
POLDER	Polarization and Directionality of the Earth Reflectance (French)
PON	Particulate Organic Nitrogen
PSU	Practical Salinity Units
PTFE	Polytetrafluoroethylene, commonly known by the trade name Teflon
QED	Quantum Efficient Device
ROSIS	Remote Ocean Sensing Imaging Spectrometer, also known as the Reflecting Optics System Imaging Spectrometer (German)
ROV	Remotely Operated Vehicle
ROW	Reverse Osmosis Water
SCOR	Scientific Committee on Oceanographic Research
SeaWiFS	Sea-viewing Wide Field-of-view Sensor
SIRREX	SeaWiFS Intercalibration Round-Robin Experiment
SIRREX-7	The Seventh SIRREX
SNR	Signal-to-Noise Ratio
SPM	Suspended Particulate Material
SPO	SeaWiFS Project Office
SPSWG	SeaWiFS Prelaunch Science Working Group
SQM	SeaWiFS Quality Monitor
SQM-II	Secondgeneration SQM
SST	Sea Surface Temperature
TS	Temperature-Salinity
TIROS	Television Infrared Observation Satellite
TMS	Total Suspended Material
UNESCO	United Nations Educational, Scientific, and Cultural Organizations
UPS	Un-interruptable Power Supply
UV	Ultraviolet

UVB	Ultraviolet-B
WMO	World Meteorological Organization
YES	Yankee Environmental Systems, Inc.